The Gran Sasso National Laboratory

The INFN Gran Sasso National Laboratory (LNGS) is the largest underground laboratory in the world for experiments in particle and astroparticle physics. It is one of four INFN national laboratories and it is a worldwide facility used by scientists (presently 900 in number) from 24 countries.

Its location is near the town of L'Aquila, about 120 km from Rome. The underground facilities are located on a side of the ten kilometres long freeway tunnel crossing the Gran Sasso d'Italia Mountain. They consist of three large experimental halls, each about 100 m long, 20 m wide and 15 m high and service tunnels for a total volume of about 180,000 cubic metres.

The average 1400 m rock coverage gives a reduction factor of one million in the cosmic ray flux; moreover, the neutron flux is thousand times less than on the surface, thanks to the smallness of the Uranium and Thorium content of the dolomite rocks of the mountain.

The headquarters and the support facilities including the general electric and safety service, library and meeting halls, canteen, computing and networking services, mechanical, electronic and chemical shops, low radioactivity service, assembly halls, offices and administration department are located on the surface.

The mission of the Laboratory is to host experiments that require a low background environment in the field of astroparticle physics and nuclear astrophysics and other disciplines that can profit of its characteristics and of its infrastructures.

The geographical location (inside the National Park of Gran Sasso - Monti della Laga) and the special operating conditions (underground, near a highway tunnel and in close proximity to a large water basin) demand that special attention is paid to the safety and environmental aspects of the activities.

Main research topics of the present scientific programme are: neutrino physics with neutrinos naturally produced in the Sun and in Supernova explosion and neutrino oscillations with a beam from CERN (CNGS program), search for neutrino mass in neutrinoless double beta decays, dark matter search, nuclear reactions of astrophysical interest.
Let me summarize the activity of the main research lines in 2008.

One of the major commitments of the Gran Sasso laboratory in the next five years will be the search of τ neutrino appearance on the artificial μ neutrino beam built at CERN in Geneva, main aim of the CERN Neutrinos to Gran Sasso (CNGS) project. The beam, directed through the Earth crust to Gran Sasso at 732 km distance, sent neutrinos for short periods during 2006 and 2007 and has been delivered for a substantial part of the year in 2008.

The OPERA experiment is designed for the direct observation of τ neutrinos resulting from oscillations of the μ neutrino of the beam. This search requires both micrometer scale resolution, obtained with modern emulsion techniques and large (kton) sensitive mass obtained here with 150,000 bricks consisting in Pb sheets interleaved by emulsion layers. A very important event in 2008 was the completion of the OPERA detector with the all the bricks.

ICARUS is a general-purpose detector, with a broad physics programme, based on the novel concept of the liquid Argon time-projection chamber. During 2008 the needed infrastructure has been completed and the commissioning of the cryogenic plant has started. The detector will be ready for operation in 2009.

Solar neutrino physics is one of the traditional research sectors of the laboratory. After the glorious life of GALLEX and GNO, the focus is now on Borexino, which is dedicated mainly

to the measurement of the Be line component of the solar neutrino spectrum. The experiment started the data taking in May 2007 and continued to take data regularly during all 2008, publishing the first results.

The detection of low energy neutrinos from the gravitational collapse of galactic objects is the major purpose of the LVD (Large Volume Detector) experiment. The experiment is continuosly monitoring the Galaxy with its 1000 tons of liquid scintillator and represents also an original monitor of the CNGS neutrino beam. LVD participates to the Supernovae Early Warning System of detectors.

Elementary particles are different from their antiparticles because their charges - not only the electric one, but all of them - are opposite. The standard model assumes that neutrinos have only one charge, the lepton number. But, if this charge is not conserved, neutrinos and antineutrinos can be two states of the same particle. In this case well-specified nuclides would decay through the neutrino-less double beta channel. The Laboratory hosts today experiments searching for these very rare decays, employing different and complementary techniques, and is preparing new important activities.

CUORICINO, which employs TeO_2 bolometers for a total of 42 kg and started taking data data in 2003, has been the most sensitive running experiment up to 2008.

In this field the Laboratory approved two new experiments representing the state of the art: GERDA, planning to employ 500 kg of enriched ^{76}Ge, and CUORE, bringing the CUORICINO technique to a mass of more than 400 kg of TeO_2 bolometers. The works for the installation of these experiments are in progress, and are already in the final installation phase for GERDA.

From astronomical observations, we know that most of the matter in the Universe is not made of nuclei and electrons as normal matter. It is called dark matter, because it does not emit light, and its nature is unknown. Its likely constituents, elementary particles that interact only very weakly with the rest, are called WIMPs. The search for WIMPs is very difficult and requires a very low background environment and the development of advanced background reduction techniques. The search is going on in many experiments worldwide. At Gran Sasso several experiments, using different techniques, are active and new experiments have been approved and started operating.

DAMA/LIBRA employs NaI crystals to detect the WIMPs by means of the flash of light produced in the detector by a Iodine nucleus recoiling after having been hit by a WIMP, a very rare phenomenon. To distinguish these events from the background, DAMA searches for an annual modulation of the rate, a behaviour that has several aspects that are peculiar of the searched effect and not of the main backgrounds. With its about 100 kg sensitive mass DAMA was the only experiment world wide sensitive to the annual modulation signature. After the conclusion of the experiment, results were published showing a signal of annual modulation.

The larger experiment LIBRA, with 250 kg sensitive mass, started taking data in 2003 and in 2008 a new result has been published confirming the signal of annual modulation.
This result is exciting and constitutes the touchstone for other experiments.

CRESST searches for WIMPs with a cryogenic technique, looking for a very tiny temperature increase in the detector, due to the energy deposited by nuclei hit by the WIMPs. Activity of the new CRESST2 $CaWO_2$ detector has continued.

Two new dark matter experiments, WARP and XENON are active underground. They are based on the simultaneous detection of the ionization and scintillation signals in, respectively, liquid argon and liquid xenon. WARP and XENON performed interesting measurements underground with a 2.3 l and a 10 l prototype, respectively. In 2008 the WARP Collaboration continued the installation of the 100 litres experiment and the Xenon Collaboration continued the modification of their apparatus to host a 50 litres experiment. Both experiments should produce new exciting data in 2009.

The solar models are based on data and extrapolations; in particular the thermonuclear cross sections of the involved reactions are not measured in the relevant energy range but rather extrapolated from higher energies. The direct measurements are made very difficult by the very low values of the cross sections. Using the 400 kV accelerator, LUNA continued its activity for the measurements of the cross section of nuclear reaction of astrophysical interest.

The main activity of the theory group, staff and visitor scientists, has been focused on various aspects of astroparticle physics, including solar and Supernova neutrinos, massive neutrinos, ultra high energy cosmic rays, topological defects and relativistic astrophysics. Important activity took place also in particle phenomenology and computer simulations of Lattice Field Theories.

Intense programs of Training and Outreach are being carried out in the last years. About the Outreach in 2008, let me put the emphasis here on the inauguration of the new Museum of Physics and Astrophysics in Teramo and on the continuation of the Gran Sasso–Princeton Summer School for Abruzzo Region secondary school students. About the Training, it is worth mentioning the new Agreement in 2008 between INFN-LNGS and Abruzzo Region, giving in the next year: 22 fellowships to young graduate and undergraduate people of this region; a new e-learning training program; the realization of an advanced station for chemical-physical analysis; outreach activities for secondary school students and teachers and the realization of an Astroparticle Physics Center for training of young researchers.

The Gran Sasso laboratory is recognized by Europe as a large scientific infrastructure. An EU contract is involving LNGS as one of the leader paricipants in the Integrated Infrastructure Initiative (I3) called ILIAS within Framework Program 6 (contract RII3-CT-2003-505818).
The main goal of ILIAS (Integrated Large Infrastructures for Astroparticle Physics) is to pull together all of Europe's leading infrastructures in Astroparticle Physics to produce a focused, coherent and integrated project to improve the existing infrastructures and their operation as well as to organise and structure the scientific community to prepare the best infrastructures for the future. This EU program is terminating now, but a new project (ILIAS-next) is in preparation to continue these activities within the Framework Program 7.

Assergi, April 3 2009

The Director of the Laboratory
Prof. Eugenio Coccia

BOREXINO. Solar Neutrino Physics

Borexino collaboration

G. Bellini[a], J. Benziger[c], S. Bonetti[a], M. Buizza Avanzini[a], B. Caccianiga[a], L. Cadonati[t], F.P. Calaprice[d], C. Carraro[i], A. Chavarria[d], F. Dalnoki-Veress[d], D. D'Angelo[h], H. de Kerret[o], A. Derbin[u], A. Etenko[s], K. Fomenko[m], D. Franco[a], C. Galbiati[d], S. Gazzana[b], M.G. Giammarchi[a], M. Goeger-Neff[h], A. Goretti[d], C. Grieb[n], S. Hardy[n], A. Ianni,[b], A.M. Ianni[d], M. Joyce[n], V. Kobychev[v], G. Korga[b], D. Kryn[o], M. Laubenstein[b], M. Leung[d], T. Lewke[h], E. Litvinovich[s], B. Loer[d], P. Lombardi[a], L. Ludhova[a], I. Machulin[s], S. Manecki[m], W. Maneschg[j], G. Manuzio[i], F. Masetti[g], K. McCarty[d], Q. Meindl[h], E. Meroni[a], L. Miramonti[a], M. Misiaszek[q], D. Montanari[b], V. Muratova[u], L. Oberauer[h], M. Obolensky[o], F. Ortica[g], M. Pallavicini[i], L. Papp[b], L. Perasso[a], S. Perasso[i], A. Pocar[d], R.S. Raghavan[n], G. Ranucci[a], A. Razeto[b], P. Risso[i], A. Romani[g], D. Rountree[n], A. Sabelnikov[s], R. Saldanha[d], C. Salvo[i], S. Schönert[j], H. Simgen[j], M. Skorokhvatov[s], O. Smirnov[m], A. Sotnikov[m], S. Sukhotin[s], Y. Suvorov[s], R. Tartaglia,[b], G. Testera[i], D. Vignaud[o], B. Vogelaar[n], F. von Feilitzsch[h], M. Wojcik[q], M. Wurm[h], O. Zaimidoroga[m], S. Zavatarelli[i], G. Zuzel[j]

[a]Dip. di Fisica dell'Università and Infn Milano - Italy
[b]Laboratori Nazionali del Gras Sasso, Assergi (Aq) - Italy
[c]Dept. of Chemical Engineering, Princeton University - NJ USA
[d]Dept. of Physics, Princeton University - NJ USA
[g]Dip. di Chimica dell'Università and Infn Perugia - Italy
[h]Dept. of Physics, Technische Universität München - Germany
[i]Dip. di Fisica dell'Università and Infn Genova - Italy
[j]Max Planck Inst. für Kernphysik, Heidelberg - Germany
[m]Joint Institute for Nuclear Research Dubna - Russia
[n]Dept. of Physics, Virginia Polytechnic Institute - VA USA
[o]Laboratoire de AstroParticule et Cosmologie, Paris - France
[q]Institute of Physics, Jagellonian University, Kracow - Poland
[s]RRC Kurchatov Institute, Moscow - Russia
[t]Dept. of Physics, University of Massachusetts, Amherst - MA USA
[u]St. Petersburg Nuclear Physics Institute, Gatchina, Russia
[v]Kiev Institute for Nuclear Research, Kiev, Ukraine

Abstract

Borexino is a solar neutrino detector located in the Hall C of LNGS. After the complete installation of the apparatus, the data taking started in May 2007 and led to the first real time measurement of ^{7}Be solar neutrinos and the first experimental evidence of the matter/vacuum transition in solar neutrino oscillations. We summarize here the status of the project and briefly outline the essentials of the Be-7 measurement as well as the first observation of the B-8 solar neutrino spectrum below 5 MeV. We also discuss the perspectives for future measurements.

1 Introduction

Solar neutrino physics is a topic that originally started from the perspective of studying the basic working principle of the core of the Sun, nuclear fusion reactions producing energy and emitting neutrinos.

The pioneer Davis experiment [1] was the first one to measure (with radiochemical methods) solar neutrinos as predicted by theoretical models and to detect a significant deficit in the predicted flux. New experiments were performed starting from the end of the 80's, both in radiochemical mode [2, 3, 4] and in real-time mode [5, 6] while the most widely accepted model of the Sun evolved into what is now known as the Standard Solar Model [7].

As a general statement, real-time experiments have been performed with large water Cerenkov detectors with an energy threshold of about 5 MeV, mainly due to natural radioactivity. This implies that only $\sim$0.001% of the total neutrino flux has been observed in real time prior to 2007.

The issue of directly measuring low energy solar neutrinos has been the subject of an intensive research study carried out in the frame of the Borexino development and starting from the very beginning of the 90's. Borexino [10] is a real time experiment to study sub-MeV solar neutrinos having as the main experimental goal the detection of the 0.862 MeV ^{7} Be solar neutrino line through the neutrino-electron elastic scattering reaction $\nu e \rightarrow \nu e$. The maximum energy of the recoiling electron is 664 KeV and the experimental design threshold is of 50 keV while the analysis threshold is 200 keV. The detection reaction is observed in a large mass (100 tons fiducial volume) of well shielded liquid scintillator.

The prediction of the ^{7}Be solar flux depends both on the Standard Solar Model and the value of the parameters of the LMA solution of neutrino oscillations [8] [9]. The Borexino experimental program makes it possible to specifically test this prediction in a direct way as well as opening up the unexplored territory of real time sub-MeV solar neutrino spectroscopy.

The main problem of an experiment with such a low energy threshold is the background coming from natural sources such as cosmic rays or radioactivity. This problem has been addressed by means of an intense R&D program focused on low radioactivity materials and purification techniques. This effort was complemented by a comparably thorough research in the field of detection and measurement of very low radioactivity levels [11]. As a part of this program, a prototype of the Borexino detector, called Counting Test Facility [12], was built and operated at LNGS to demonstrate very low radioactive contamination levels (10^{-16} g/g of U-238 equivalent or less [13]) in a ton scale scintillator detector.

This research and development culminated into the construction, filling and operation of the full-scale Borexino detector. The experimental data taking in the final configuration begun in May 2007.

2 The Borexino Detector

Borexino [14] is an unsegmented scintillation detector featuring 300 tonnes of well shielded liquid ultrapure scintillator viewed by 2200 photomultipliers (fig. 1). The detector core is a transparent spherical vessel (Nylon Sphere, 100μm thick), 8.5 m of diameter, filled with 300 tonnes of liquid scintillator and surrounded by 1000 tonnes of high-purity buffer liquid. The scintillator mixture is PC and PPO (1.5 g/l) as a fluor, while the buffer liquid consists of PC alone (with the addition of DMP as light quencher). The photomultipliers are supported by a Stainless Steel Sphere, which also separates the inner part of the detector from the external shielding, provided by 2400 tonnes of pure water (water buffer).An additional containment vessel (Nylon film Radon barrier) is interposed between the Scintillator Nylon Sphere and the photomultipliers, with the goal of reducing Radon diffusion towards the internal part of the detector.

The outer water shield is instrumented with 200 outward-pointing photomultipliers serving as a veto for penetrating muons, the only significant remaining cosmic ray background at the Gran Sasso depth (about 3500 meters of water equivalent). The innermost 2200 photomultipliers are divided into a set of 1800 photomultipliers equipped with light cones (so that they see light only from the Nylon Sphere region) and a set of 400 PMT's without light cones, sensitive to light originated in the whole Stainless Steel Sphere volume. This design greatly increases the capability of the system to identify muons crossing the PC buffer (and not the scintillator).

The BOREXINO design is based on the concept of a graded shield of progressively lower intrinsic radioactivity as one approaches the sensitive volume of the detector; this culminates in the use of 200 tonnes of the low background scintillator to shield the 100 tonnes innermost Fiducial Volume. In these conditions, the ultimate background will be dominated by the intrinsic contamination of the scintillator, while all backgrounds from the construction materials and external shieldings will be negligible.

BOREXINO also features several external systems and conceived to purify the experimental fluids (water, nitrogen and scintillator) used by the experiment.

3 Status of the project

The Borexino filling started in January 2007, with scintillator displacing the purified water from inside the detector volumes. Data taking started and the detector was completely filled and operational by May 2007.

The radiopurity of the detector has been found in general to be better than the specifications. In particular, among the best radioactivity levels found during the data taking:

1. C-14 contamination of the scintillator was found to be at $\sim 2 \times 10^{-18}$ ^{14}C/^{12}C.

2. The general level of Th-232 contamination - as measured by means of $^{212}Bi/^{212}Po$ delayed coincidences was found to be at $\sim 6 \times 10^{-18}$ g/g.

3. The U-238 family contamination - assessed by studying the $^{214}Bi/^{214}Po$ delayed coincidence rate, was measured to be less than 7×10^{-18} g/g.

4. Kr-85 contamination, of considerable importance due to the spectral shape similar to the one of the signal searched for was found (by means of the ^{85m}Rb decay and the related β/γ tagging) to be at the level of less than 35 count/day in the 100 tons fiducial volume.

This general level of radiopurity, together with the use of mild cuts and the α/β discrimination technique has allowed a sensitive study of the Be-7 solar signal inside the 100 tons of fiducial volume and the first observation of the B-8 spectrum below 5 MeV.

During the year 2008, an intensive calibration campaign was carried out by using radioactive sources located in the fiducial volume, including C-14 and Rn-222 sources, an Am-Be neutron source and a few gamma sources.

4 Measurement of Be-7 solar neutrinos

While we refer the interested reader to the published papers for the detailed description of the analysis, fig. 2 shows a spectrum of the singles rate obtained after analysis cuts (including veto of external muons, Radon-related activity and Po-210 subtraction) in the Borexino fiducial volume.

The Be-7 flux was determined by fitting the experimental distribution to the light yield, to the Be-7 interaction rate and to the other contributions shown in the figure. Neutrinos from Be-7 are visible in the electron recoil spectrum by means of the Compton-like shoulder generated by $\nu e^- \rightarrow \nu e^-$ scattering (fig. 2).

The systematic error was dominated by the knowledge of the fiducial mass and the detector response function, since the detector calibration was not yet carried out at that time. The published measurement of $49 \pm 3_{stat} \pm 4_{syst}$ counts/(day·100 ton) has to be compared to the expected (high-metallicity) Standard Solar Model without oscillations of 74 ± 4 or to the expected number of 48 ± 4 when LMA oscillations of solar neutrinos are taken into account [9].

This analysis was made during the first 192 live days of the detector and prior to the calibration.

5 Observation of the B-8 solar signal below 5 MeV

Further accumulation of data prior to the calibration (246 days) allowed to observe the more rare B-8 solar neutrino component, which is important because the solar model with MSW-LMA solution predicts that electron neutrino survival probability is dominated by vacuum oscillations at low energies and by resonant matter-enhanced oscillations (taking place in the Sun) at higher (E>5 MeV) energies. In Borexino this component can be studied down to 2.8 MeV electron energy, lower than the previously considered 5 MeV. Again, we refer the interested reader to the relevant paper and show only the observed B-8 spectrum in fig. 3.

The combination of the Be-7 and B-8 measurements constitute the first evidence of solar neutrinos obtained with scintillation techniques in the same experiment. It allows for

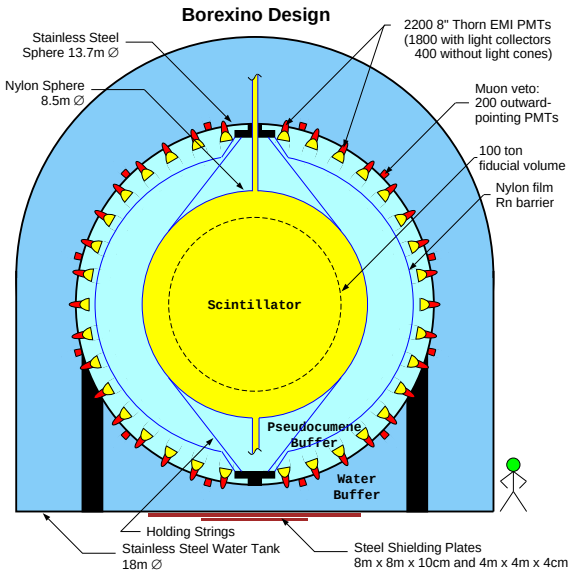

Figure 1: Schematic view of the Borexino detector.

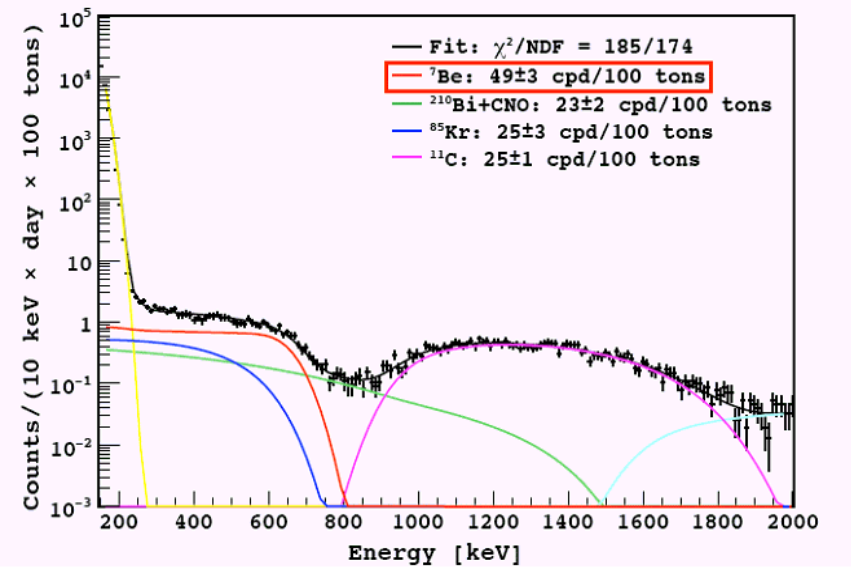

Figure 2: The observed Borexino spectrum after cuts, showing the shoulder due to solar Be-7 neutrino events (red line). The other main fit components in this energy region are also shown.

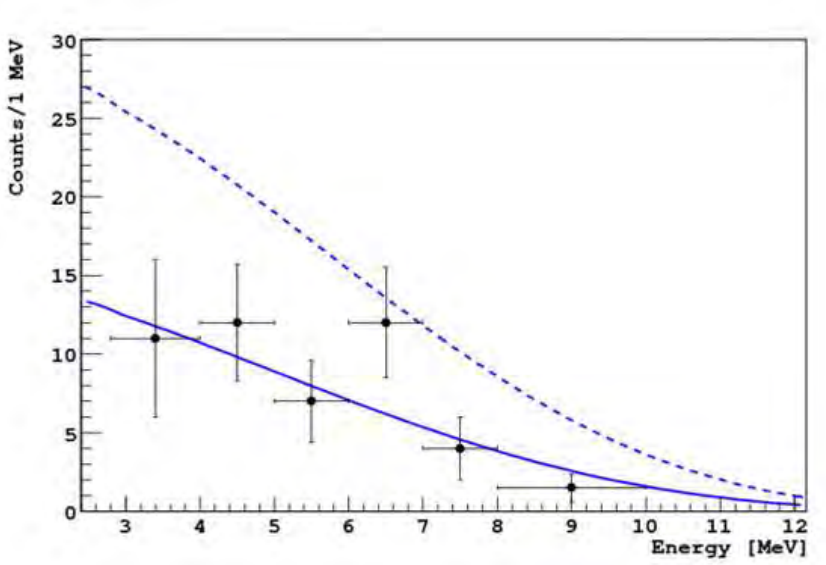

Figure 3: Spectrum of B-8 in Borexino after analysis cuts The dashed line correspond to the non-oscillation hypotesis, while the continuous line is the LMA-MSW (high-metallicity) solution of the solar neutrino problem.

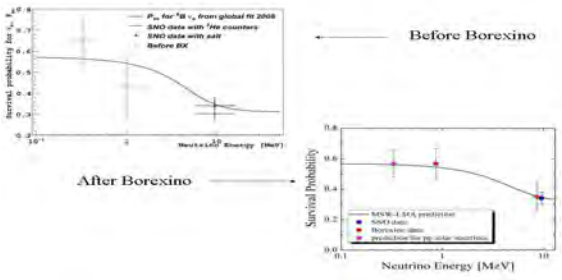

Figure 4: The survival probability as a function of energy for electron neutrinos as a function of energy.

the first time to observe the matter-to-vacuum transition of the electron neutrino survival probability, as shown in fig. 4.

6 Future perspectives

The Borexino experimental program is continuing with the goal of improving the understanding of the detector and reducing the error on the Be-7 measurement.

In addition, the following additional physics topics are being considered for the future investigation, depending on the background conditions and on the refinement of the ongoing analysis:

1. Reduce the background in the region above the Be-7 shoulder, to the goal of measuring the CNO solar neutrinos and possibly the pep component as well.
2. Search for terrestrial antineutrino interactions.
3. Study the very low energy part of the spectrum to the goal of looking for pp neutrinos.
4. Watch for neutrino bursts from Supernovae events.

In addition, neutrino source calibrations (with a ^{51}Cr source) are being considered, both to the goal of a final calibration and to the study of neutrino magnetic moment.

7 List of articles published in year 2008

1. C. Arpesella et al., *First real time detection of ^{7}Be solar neutrinos by Borexino*, Phys. Lett. B 658 (2008) 101.
2. C. Arpesella et al., *Direct Measurement of the ^{7}Be Solar Neutrino Flux with 192 Days of Borexino Data*, Phys. Rev. Lett. 101 (2008) 091302.
3. G. Bellini et al., *Measurement of the solar ^{8}B neutrino flux with 246 live days of Borexino and observation of the MSW vacuum-matter transition*, arXiv:0808.2868.

References

[1] R. Davis, Nobel Prize Lecture 2002.

[2] W. Hampel et al., Phys. Lett. B 447 (1999) 127.

[3] J.N. Abdurashitov et al., Phys. Rev. Lett. 83 (1999) 4686.

[4] M. Altmann et al., Phys. Lett. B 616 (2005) 174.

[5] S. Fukuda et al., Phys. Rev. Lett. 86 (2001) 5651; Phys. Lett. B 539 (2002) 179.

[6] Q.R. Ahmad et al., Phys. Rev. Lett. 87 (2001) 071301.

[7] J.N. Bahcall and M.H. Pinsonneault, Phys. Rev. Lett. 92 (2004) 121301.

[8] J.N. Bahcall et al., JHEP 0408 (2004) 016.

[9] G.L. Fogli et al., Progr. Nucl. Phys., 57 (2006) 742.

[10] G. Alimonti et al., Astroparticle Physics 16 (2002) 205.

[11] C. Arpesella et al., Astroparticle Physics 18 (2002) 1.

[12] G. Alimonti et al., Nucl. Instr. & Methods A406 (1998) 411.

[13] G. Alimonti et al., Astroparticle Physics 8 (1998) 141.

[14] G. Alimonti et al., Nucl. Instr. & Methods A600 (2009) 568.

COBRA

V. Bocarov[a], P. Cermak[a], O. Civitarese[b], J. Dawson[c], A. Fauler[d], M. Fiederle[d], A. Garson[e], C. Gößling[f], H. Gastrich[f], E. Hamann[d], M. Heine[g], B. Janutta[g], M. Junker[h], T. Köttig[f], H. Krawczynski[e], Q. Li[e], J. Martin[e], D. Münstermann[f], T. Neddermann[f], S. Rajek[f], C. Reeve[c], K. Schreiner[f], O. Schulz[f], F. Simkovic[i], J. Suhonen[j], I. Stekl[a], K. Zuber[g,*]

[a] *Czech Technical University in Prague* - Czech Republic
[b] *University of La Plata* - Argentina
[c] *University of Sussex* - UK
[d] *Freiburg Materials Research Center - Germany*
[e] *Washington University in St. Louis* - USA
[f] *Technische Universität Dortmund* - Germany
[g] *Technische Universität Dresden* - Germany
[h] *Laboratori Nazionali del Gran Sasso* - Italy
[i] *Comenius University in Bratislava* - Slovakia
[j] *University of Jyvaskyla* - Finnland
([*] Spokesperson)

Abstract

The aim of COBRA is to search for neutrinoless double beta decay events in a large array of Cadmium Zinc Telluride (CZT) semiconductor detectors. As a semiconductor, CZT offers the low radioactivity levels and good energy resolution required for a rare decay search, with the added advantage that it can be operated at room temperature. It contains a number of double beta decay candidates, the most promising of which is ^{116}Cd , having a high Q-value (2.8 MeV) above many of the possible background contributions from natural radioactivity. Currently, a prototype apparatus is being established in LNGS to investigate the major experimental issues of operating CZT detectors in low background mode, whilst additional studies into the detector technology are proceeding in surface laboratories.

1 Introduction

Over the last 10 years various neutrino experiments have proved that neutrinos oscillate between flavour states and therefore have a non-vanishing rest mass. However, as neutrino oscillation experiments probe the difference between neutrino mass states, the absolute

mass scale is still unknown. Another important unknown is the fundamental nature of the neutrino which could be either Dirac or Majorana. A golden channel for answering both the question of neutrino nature and neutrino mass is neutrinoless double beta decay. The COBRA experiment aims to provide answers to these fundamental questions by searching for these rare decays of especially ^{116}Cd in a large array of Cadmium Zinc Telluride (CZT) semiconductor detectors. However, various other isotopes and decay modes of Cd, Te and Zn isotopes can be explored. An extensive discussion of the double beta decay modes detectable with COBRA is given in the LNGS Annual Report 2006.

2 R&D Activities

Currently the experiment is in an R&D phase, operating a prototype low-background apparatus in the LNGS laboratory in order to investigate the instrumentation and background issues critical to the rare decay search. Studies into detector properties, especially pixelated CZT detectors, are being performed simultaneously at a number of member institutions. Details of the experimental set-up and recent progress are given in this section.

2.1 Low Background Prototype

A prototype COBRA setup, capable of handling sixty-four 1 cm^3 CZT crystals is being installed in LNGS. This array will provide valuable information on the background levels of various components of the set-up and will be used to test and design methods of instrumentation and construction that would also be applicable to a larger array. It will also allow studies using coincidences among the detectors and its potential to reduce background, as double beta decay is considered to be a single detector event.

Currently the crystals used in the low background experiment are 1 cm×1 cm×1 cm CZT semiconductor detectors, each of mass ∼6.5 g, provided by eV-PRODUCTS. The detectors are mounted in layers of 4×4 crystals, held in a Delrin support. The detectors are surrounded by 10 cm of pure copper shielding and 20 cm of low radioactivity lead. Supply of bias voltages and signal readout occurs via low-diameter coaxial cable and copper traces on Kapton foils which feed through this shielding. The custom built preamplifier electronics are ∼25 cm from the crystals. This apparatus is all mounted inside a copper Faraday cage, surrounded by 7 cm of borated polyethylene to shield the apparatus from neutrons. Location in the Gran Sasso laboratory provides a further ∼3500 mwe of shielding against cosmic ray sources.

One of the major outcomes of the background investigation was that the dominant sources of radioactive background are the red passivation coating on the detector crystals itself and radon in the lab atmosphere. First of all, at this point it became obvious that further installation of detectors with red passivation is useful. Thus, the completion of the array was interrupted and instead 4 CZT crystals passivated with a new colourless coating, specially provided by the manufacturer, were installed. In parallel the collaboration decided to remove the red paint on all crystals and replace it with a commercially available clear passivation. For testing, four detectors were stripped of the red passiva-

tion and re-coated with the new alternative. Evaluation of the re-coated detectors showed good performance and stability, no degradation was measurable. The detectors were installed in the LNGS underground setup alongside the previously described test-layer in December of 2008. As a side activity a new, reliable, non-permanent and low-background compatible detector connection system was developed and applied to the above mentioned detectors to gain more stable data taking. As one of the results the noise threshold could be reduced from about 100 keV down to 30 keV.

To address the issue of radon an automatic Nitrogen flushing system has been installed, using radon free nitrogen to eliminate air and therefore radon from the experimental setup. The first data taken with this system looked very promising, motivating a further upgrade of the flushing system in the fall of 2008.

The combined effect of the activities showed a dramatic improvement in background (see Fig. 1). A reduction of almost an order of magnitude is obtained in the spectrum.

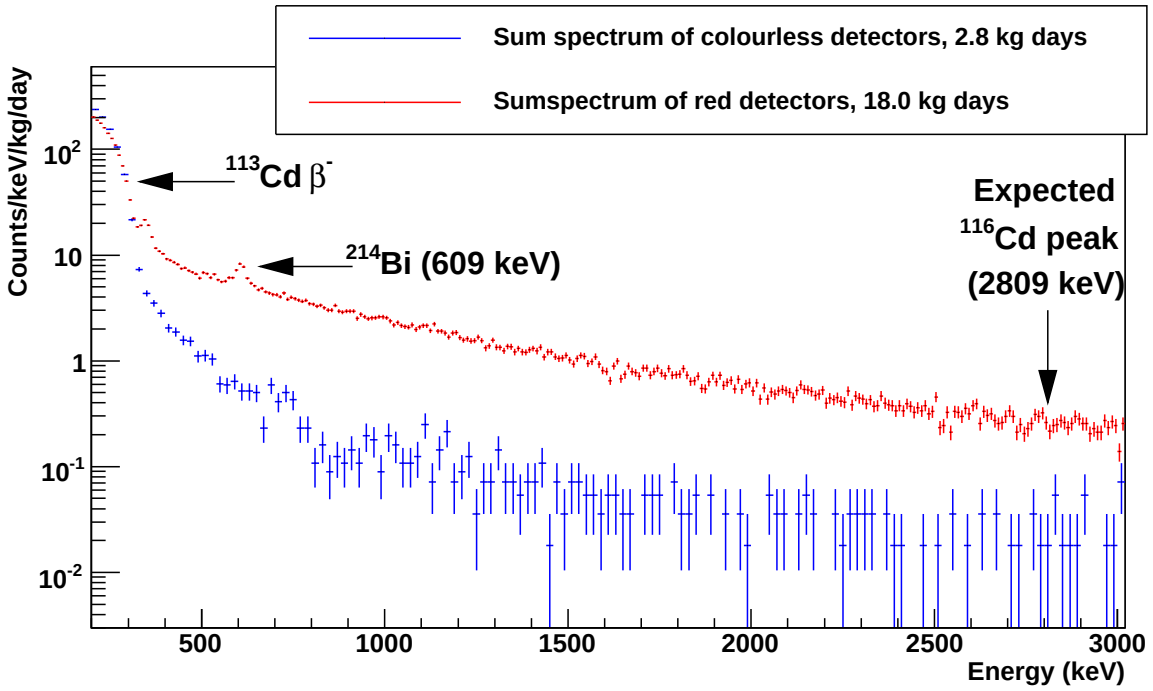

Figure 1: Summed spectra obtained with the old setup of red-painted crystals and with the new setup featuring clear-painted detectors and the new detector connection scheme.

2.2 Analysis

Physics results based on a 4 detector array used before with an exposure of 4.34 kg days have been published in [2]. With the first full layer of 16 detectors more than 18 kg· days of data have been accumulated and were evaluated in two ways. The high statistics of the ^{113}Cd decay allows for about a dozen independent measurements of this decay. For the first time ever a statistical significant sample of half-life measurements of the order 10^{16} years have been obtained (Fig. 2). In addition, single detector events were explored for double beta signals using a maximum likelihood fit procedure as described in the Annual

Report 2007. A search was performed for rare decays of all the double beta candidate isotopes in CdZnTe that produce peaks above 500 keV.

The detailed analysis of the 4-fold forbidden non-unique ^{113}Cd decay resulted in a half-life of $T_{1/2} = 8.00 \pm 0.11(stat.) \pm 0.24(sys.) \times 10^{15}$ years. A fit to the spectrum revealed a Q-value of $322 \pm 0.3(stat.) \pm 0.9(sys.)$ keV, the most precise value ever obtained. A comparison with calculated spectral shape [3] shows a worse result than fitting a 3-fold forbidden unique decay (Fig. 3), which has also been observed by [4]. For details of the analysis see [5] .

A comparison of the new preliminary neutrinoless double beta decay results with the one published in [2] and [6] is summarised in table 1. As can be seen various limits are improved by an order of magnitude and more, several half-life limits are now beyond 10^{20} years.

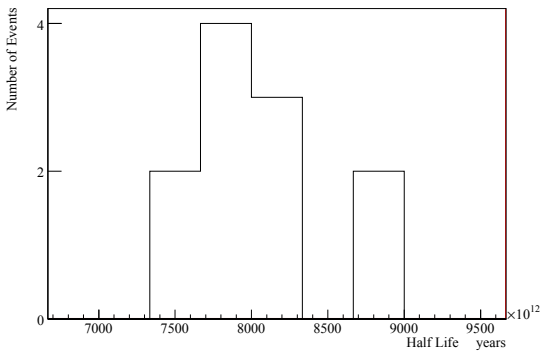

Figure 2: Histogram of individual ^{113}Cd half-lives obtained for each detector. The spread reflects the potential variations in Cd content due to insufficient knowledge of Zn-content, mass, background and other paramters.

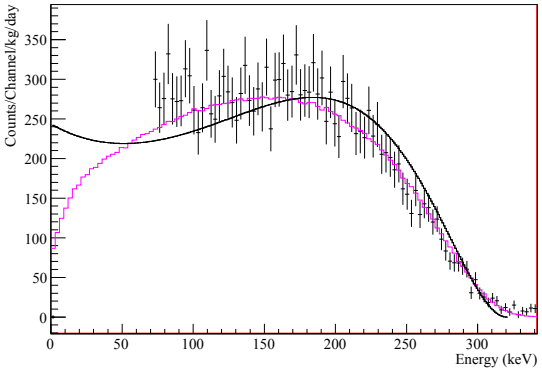

Figure 3: Comparison of spectral shapes based on calucations of [3] (black) and a 6th order polynomial (purple) often used to describe 3-fold forbidden decays with the data astonishingly shows a better agreement with the latter.

2.3 Pixellated Detector Studies

The development of pixellated detectors offers the possibility of enhancing the performance of COBRA in two key areas; (i) background suppression, and (ii) providing a unique signal for double beta decay. It is the different characters of beta, alpha and gamma-radiation compared to that of double beta decay, within the CZT material, which provides the potential for event identification, as discussed in more detail in the Annual Report 2007. The basic result is that a pixel size between 50-500 μm seems appropriate, which must be optimised between number of readout channels and background reduction.

In the meantime various detectors have been built. Based on 2x2x0.5 cm^3 crystals, one with 1024 pixels, resulting in a pixel size of 625 μm and also one with 100x100 pixels

Isotope	Decay	$T_{1/2}$ limit (years)	
		4-detector	First layer
$\beta^-\beta^-$ decays			
^{116}Cd	to g.s	3.1×10^{19}	9.4×10^{19}
^{130}Te	to g.s	9.9×10^{19}	5.0×10^{20}
^{130}Te	to 536 keV	3.7×10^{19}	3.5×10^{20}
^{116}Cd	to 1294 keV	4.9×10^{18}	5.0×10^{19}
^{116}Cd	to 1757 keV	9.1×10^{18}	4.2×10^{19}
^{114}Cd	to g.s	-	2.0×10^{20}
$\beta^+\beta^+$ decays			
^{64}Zn	$0\nu\beta^+$EC to g.s.	2.8×10^{17}	3.3×10^{17}
^{64}Zn	0νECEC to g.s.	1.2×10^{17}	7.4×10^{18}
^{120}Te	0νECEC to g.s.	2.7×10^{15}	2.4×10^{16}
^{120}Te	0νECEC to 1171keV	9.7×10^{15}	1.8×10^{16}
^{106}Cd	$0\nu\beta^+\beta^+$ to g.s.	4.5×10^{17}	2.7×10^{18}
^{106}Cd	0νECEC to g.s.	5.7×10^{16}	1.6×10^{17}
^{106}Cd	$0\nu\beta^+\beta^+$ to 512keV	1.8×10^{17}	9.4×10^{17}

Table 1: Comparison of obtained 90% confidence limits with the original prototype of 4 detectors as published in [2] together with preliminary limits from the first layer of the 64 array.

corresponding to 200 μm have been made. Work is now concentrated on the readout and preparation for installing such a device underground.

In addition, COBRA was provided with a CdTe TimePix detector. It is a CdTe detector (1 mm thickness, 256×256 pixel matrix, 55 μm pitch, dimension $1.4\times1.4\,cm^2$) bump-bonded on a readout ASIC developed by the Medipix collaboration in CERN. Within each pixel of this device an analog circuitry and a digital counter are integrated. The TimePix device, operated in Time Over Threshold (TOT) mode, can use the counter as a Wilkinson type ADC offering spectroscopic capabilities in each individual pixel.

The main effort was to perform an initial characterization and calibration of the CdTe detector and its comparison with a silicon detector of similar type. For the per-pixel calibration process X-ray fluorescence peaks in the range of 6 to 20 keV and 60 keV peak from ^{241}Am were used. Some test measurements with the calibrated TimePix were performed in order to get acquainted with the typical response of the detector to different types of particles. As an example figure 4 shows the typical response to α-radiation. This snapshot was chosen from a background measurement, i.e. no radioactive sources were used.

3 Conclusions

The COBRA experiment aims to search for neutrinoless double beta decay of ^{116}Cd with CZT semiconductors. An array of 16 detectors was successfully running for about a year at

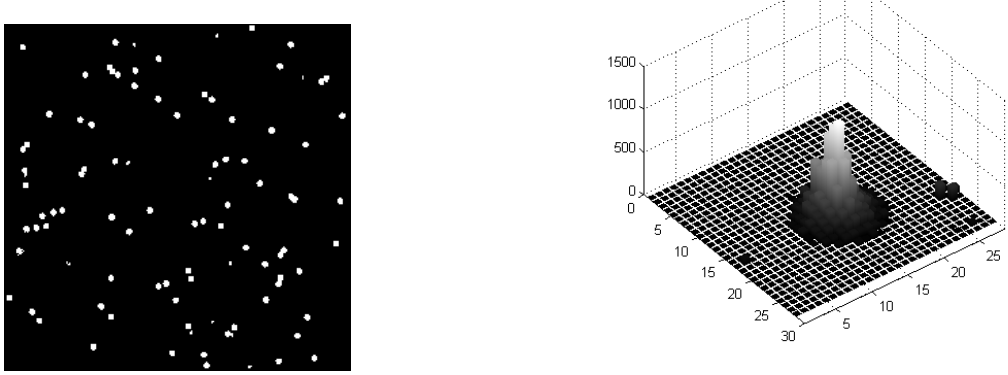

Figure 4: Typical response to alpha particles - large clusters of round shape (left) and 3D view of single cluster (right).

LNGS. The array provided interesting results on ^{113}Cd beta decay and also half-life limits for several neutrinoless double beta decay modes beyond 10^{20} yrs. Improvements on the set-up lead to reduction of background by about an order of magnitude more or less over the whole energy range. New detector layers are operating now to explore potential other background components. The work on pixellated detectors continues and first detectors with sub-mm are at hand and are operational. Various particle types have been identified showing the potential of the method and first pixel detectors will be installed underground in 2009.

4 List of Publications

1. *An Investigation into the 113-Cd Beta Decay Spectrum using a CdZnTe Array* J. V. Dawson *et al.*, Nucl. Phys. A 818, 264 (2009)
2. *An Investigation on Cooling of CZT Co-Planar Grid Detectors*, J. V. Dawson *et al.*, Nucl. Inst. Meth. A 599, 209 (2009)

References

[1] K. Zuber, *Physics Letters B* **519** (2001) 1

[2] T. Bloxham et al., *Phys. Rev. C* **76** (2007) 025501

[3] M. T. Mustonen and J. Suhonen, *Phys. Lett. B* **657** (2007) 38

[4] P. Belli et al., *Phys. Rev. C* **76** (2007) 064603

[5] J.V. Dawson et al., *Nucl. Phys. A* **818** (2009) 264

[6] H. Kiel, D. Muenstermann and K. Zuber, *Nucl. Phys. A* **723** (2003) 499

CRESST. Dark Matter Search

G. Angloher [a], I. Bavikina [a], M. Bauer [e], A. Bento [a], A. Brown [b], C. Bucci [d], C. Ciemniak [c], C. Coppi [c], F. von Feilitzsch [c], D. Hauff [a], S. Henry [b], P. Huff [a], J. Imber [b], S. Ingleby [b], C. Isaila [c], J. Jochum [e], M. Kiefer [a], M. Kimmerle [e], H. Kraus [b], T. Lachenmaier [c], J.C. Lanfranchi [c], R. Lang [a], V. Mikhailik [b], E. Pantic [a], F. Petricca [a], S. Pfister [c], W. Potzel [c], F. Pröbst [a], S. Roth [c], C. Rottler [e], K. Schäffner [a], J. Schmaler [a], S. Scholl [e], W. Seidel [a, +], L. Stodolsky [a], A. J. B. Tolhurst [b], I. Usherov-Marshak [e], W. Westphal [c],

[a] *MPI für Physik, Föhringer Ring 6, 80805 Munich, Germany*
[b] *University of Oxford, Department of Physics, Oxford OX1 3RH, U.K.*
[c] *Technische Universität München, Physik Department, D-85747 Garching, Germany*
[d] *Laboratori Nazionali del Gran Sasso, I-67010 Assergi, Italy*
[e] *Eberhard-Karls-Universität Tübingen, D-72076 Tübingen, Germany*
[+] *Spokesperson E-mail address: seidel@mppmu.mpg.de*
[*] *present address: University of Warwick, Coventry CV4 7AL, U.K.*

Abstract

The aim of CRESST (**C**ryogenic **R**are **E**vent **S**earch with **S**uper"-con"-ducting **T**hermometers) is to search for particle Dark Matter and to contribute to the elucidation of its nature. The experiment is located at the 'Laboratori Nazionali del Gran Sasso' (LNGS), Italy, and it uses low background cryogenic detectors with superconducting phase transition thermometers for the direct detection of WIMP-nucleus scattering events.

1 The Dark Matter Problem

The search for Dark Matter and the understanding of its nature is of central interest for particle physics, astronomy and cosmology. There is strong evidence for its existence on all scales, ranging from dwarf galaxies, through spiral galaxies like our own, to large scale structures. The history of the universe is difficult to reconstruct without Dark Matter, be it Big Bang Nucleosynthesis or structure formation.

Particle physics provides a well motivated candidate with the lightest SUSY-particle, the "neutralino". Generically, such particles are called WIMPs (Weakly Interacting Massive Particles). WIMPs are expected to interact with ordinary matter by elastic scattering on nuclei. All direct detection schemes have focused on this possibility.

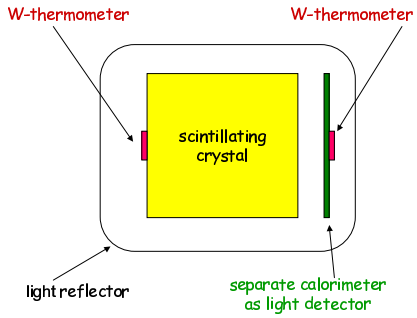

Figure 1: Schematic representation of the detector for simultaneous phonon and light measurement. It consists of two separate cryogenic detectors enclosed in a highly reflective housing, read out by tungsten superconducting phase-transition thermometers. This concept allows a very efficient discrimination of the searched nuclear recoil signals from the dominant radioactive β- and γ-backgrounds.

Conventional methods for direct detection rely on the ionization or scintillation caused by the recoiling nucleus. This leads to certain limitations connected with the low ionization or scintillation efficiency of the slow recoil nuclei. The cryogenic detectors developed for the first phase of CRESST (CRESST-I) measure the deposited energy calorimetrically, independent of ionization, and allow a detection of much smaller recoil energies. When the cryogenic measurement of the deposited energy is combined with a measurement of scintillation light an extremely efficient discrimination of the nuclear recoil signals from radioactive background signals can be obtained. This type of detectors is beeing used in the upcomingphase CRESST-II.

2 Detection Principle

The low-temperature calorimeters consist of a target crystal with an extremely sensitive superconducting phase transition thermometer on its surface. A weak thermal coupling to a heat bath restores again the equilibrium temperature after an interaction. The thermometer is made of a tungsten film evaporated onto the target crystal. Its temperature is stabilised within the transition from the superconducting to the normal conducting state, which

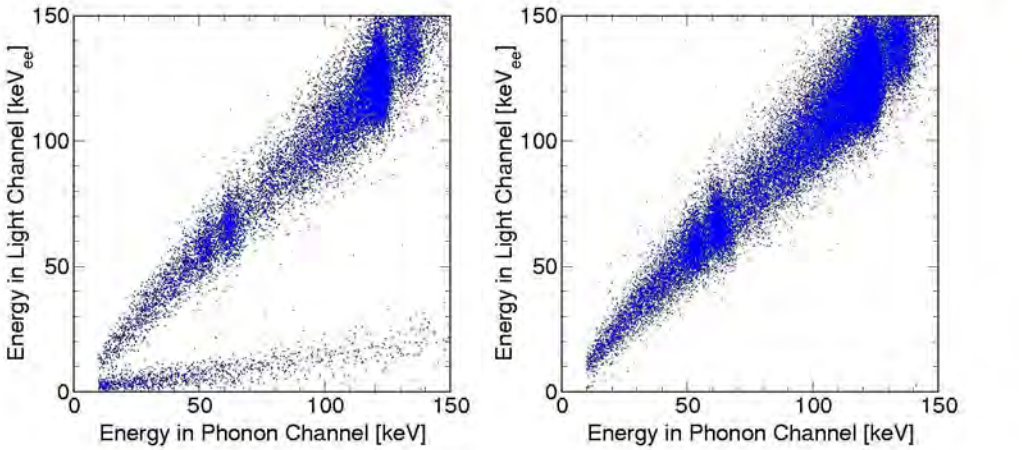

Figure 2: Coincident detection of phonons and scintillation light with a $CaWO_4$ detector. Left: The upper band of events is due to irradiation of the $CaWO_4$ crystal with electrons and gammas, whereas the lower band with lower light yield, is from nuclear recoils caused by a neutron source. Right: Removing the neutron source confirms that there is no leakage of ionising events into the nuclear recoil region.

occurs at temperatures of about 10 mK. A typical width of the transition is about 1 mK. A small temperature rise e.g.from a WIMP–nucleus scattering event (typically some μK), leads to an increase of resistance, which is measured with a SQUID (**S**uperconducting **Qu**antum **I**nterference **D**evice). For the first phase of CRESST, which ended in 2001, 262 g sapphire detectors had been developed at MPI. These detectors provided an excellent energy resolution of 133 eV at 6 keV and a very low energy threshold of 600 eV.

In the second phase, CRESST-II, we are using 300 g scintillating $CaWO_4$ target crystals. The scintillating crystal is equipped with a superconducting tungsten phase-transition thermometer for the detection of the phonons created by a particle interaction in the scintillating crystal. A small fraction of $\sim$ 1% of the deposited energy is emitted as scintillation light, which is measured with a separate cryogenic detector, optimised for light detection. Fig. 2 shows a scheme of this composite detector.

Starting with a proof-of-principle experiment in 1998, the technique of simultaneous measurement of phonons and scintillation light has been developed within the CRESST collaboration with the aim of dark matter detection. The important advantage of this technique is that it offers an extremely efficient suppression of the radioactive background down to very low recoil energies of about 10 keV. While the phonon signal measures the deposited

energy, the amplitude of the corresponding light signal depends on the type of interaction. Nuclear recoils, such as WIMP or neutron scattering events, emit substantially less scintillation light than fully ionising interactions, e.g. γ or β interactions, do. As the overwhelming part of the background consists of β and γ interactions, this phonon/light technique provides a very effective method of background suppression. Fig. 2 illustrates this detection method.

Compared with the alternative approach of simultaneous measurement of phonons and charge in a semiconductor crystal, which is applied in the experiments CDMS-II and Edelweiss-II, the method developed for CRESST-II has the important advantage that it does not suffer from dead layers at the surface. A reduced charge collection for ionising events occurring close to the surface in semiconducting crystals may lead to a false identification of low energetic γ's and β's as nuclear recoils. The result in Fig. 2, which was obtained with a gamma and beta source, confirms that the suppression also works for low-energy electrons impinging onto the crystal surface.

3 The CRESST Setup in Gran Sasso

The central part of the CRESST installation at Gran Sasso is the cryostat, sketched in Fig. 3. The low temperature which is generated in the mixing chamber of the dilution refrigerator is transferred into the radio-pure cold box, via a 1.5 m long cold finger. The cold finger is protected by thermal radiation shields, all fabricated of low-background copper. The detectors are mounted inside the cold box at the end of the cold finger. Two internal cold shields consisting of low-level lead are attached to the mixing chamber and to a thermal radiation shield at liquid N_2 temperature, respectively, in order to block any line-of-sight from the non-radio-pure parts of the dilution refrigerator to the detectors inside the cold box. The design completely avoids potentially contaminated cryogenic liquids inside the cold box.

An extensive passive shielding of low-background copper and lead surrounds the cold box and serves to shield radioactivity from the surrounding rock. The entire shielding is enclosed inside a gas-tight radon box that is flushed with boil of N_2 gas and maintained at a small overpressure. Special care was taken to minimise above-ground exposure of the construction materials of the cold box and the shielding to cosmic rays, in order to avoid activation.

This setup has been upgraded for the experimental program of CRESST-II, to allow the operation of 33 phonon/light detector modules. The upgrade included the installation of a 66-channel SQUID readout in the existing cryostat, a system for the integration of the 33 detectors in the cold box, the

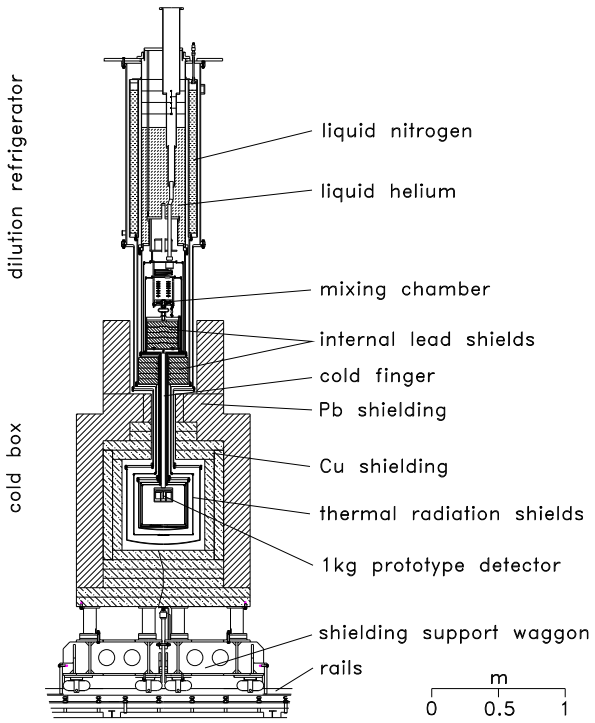

Figure 3: Layout of the CRESST ^{3}He/^{4}He dilution refrigerator and low background cold box with its shielding.

installation of a passive neutron shield, a muon veto, and a new multichannel electronics and DAQ. The cryostat with the upgraded shielding is shown schematically in Fig. 4. In this upgrade the institute was responsible for the neutron shield, the wiring of the cryostat from the mixing chamber down to the detectors, the detector integration system and the DAQ. The upgrade began in 2004 after a 52-day run with two 300 g prototype phonon/light detector modules in the old setup. With this short run a competitive sensitivity of 1.6×10^{-6} pb for the WIMP nucleon scattering cross section was reached despite the absence of any neutron shield.

4 Results

After completion of the upgrade, nine detector modules were mounted in October 2006. Fig. 4 shows the mounted detectors before closing the cold box. An extended commissioning run followed the cool down in November

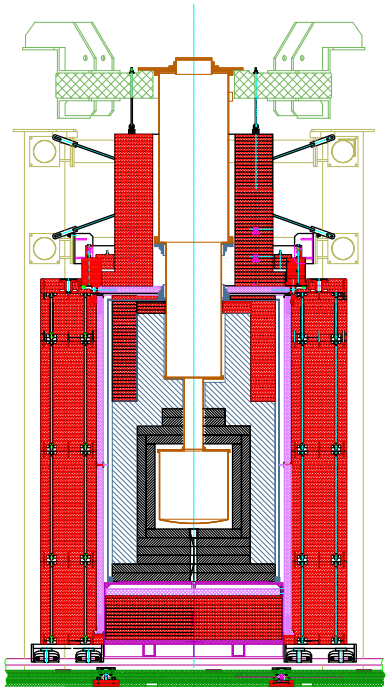

Figure 4: Dilution refrigerator and low background cold box with its shielding upgraded for CRESST-II. The gas tight radon box enclosing the Cu (shown in grey) and Pb (blue) shielding will be completely covered by a plastic scintillator μ-veto (pink) and 50 cm of polyethylen (red).

2006. A number of issues with the biasing electronics and SQUID system had to be settled during this commissioning run. A series of modifications has finally improved the interferences originally seen in the light detectors to an acceptable level. Seven phonon channels were working perfectly, delivering sub keV energy resolutions. Due to problems with some light detectors and SQUID channels, only three complete modules were working. Towards the end of this commissioning run, the 50 kg days of dark matter data shown in Fig. 4 were collected with two detector modules. Form-factor effects effectively limit the energy transfer to the heavy tungsten nuclei in elastic WIMP nucleus scattering to energies below 40 keV for all WIMP masses. In the energy region below 40 keV and above the background separation threshold of 11 keV, three tungsten recoil events were observed in the data of Fig. 4. The light signal, which varies with the recoiling nucleus, can be used to determine which nucleus, in a compound material like $CaWO_4$, is recoiling. This

Figure 5: Detector modules mounted at the end of the cold finger, before closing the cold box in October 2006. The spring suspended platform provides additional vibration decoupling of the detectors from the cryostat. The mounting system was fabricated by the MPI workshop from low background, low heat leak Cu and low background CuSn2 springs.

would have significant consequences in verifying a possible positive dark matter signal. For these reasons it is important to understand the light output (or 'quenching factor') and the CRESST collaboration has undertaken a series of investigations of light emission with different projectiles and particles. An interesting and simple explanation of the pattern of results was found by means of the assumption that the light output is simply proportional to the length of the light-producing track (and not the energy for example). In addition it was noted that this assumption leads to a simple model for the intrinsic fluctuations in light output at low energy. These turn out to be rather large and could be of significance in limiting noble gas detector projects.

If we attribute all tungsten recoils below the black lines in Fig. 4 to WIMP interactions, we can set the upper limit for the WIMP scattering cross-section shown in Fig. 4. The minimum of the curve is at about 5.5×10^{-7} pb, which is about a factor of 3 improvement over the previous run in 2004 before the upgrade. To get interferences likely caused by the multi channel SQUID electronics under control, our collaboration partner at Oxford made a strong effort to build a replacement for that part of the commercial SQUID

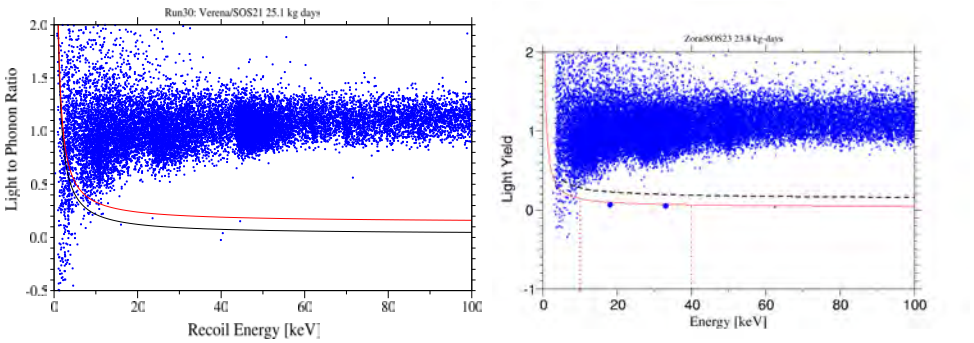

Figure 6: Low energy event distribution measured with two 300g $CaWO_4$ detector modules during the commissioning run. The vertical axis represents the light yield expressed as the ratio (energy from the light channel/energy from the phonon channel), the horizontal axis is the total energy measured by the phonon channel. Below the red curve 90% of all nuclear recoils, and below the black curve 90% of the tungsten recoils are expected.

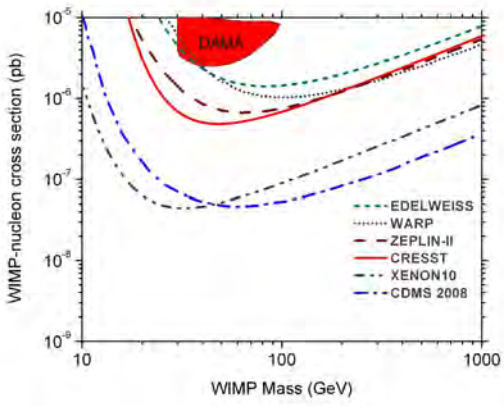

Figure 7: Spin independent or coherent scattering cross section exclusion limit derived from the 50 kg days of data of Fig. 4, collected with two detector modules during the commission run. For comparison the limits from other experiments and the range predicted by Supersymmetry are also shown.

electronics, which was very likely the origin of the interference problems in the commissioning run. A new set of detectors has been fabricated at MPI, and 16 detectors were installed in spring 2008. With some of them, design variations have been implemented to address the question of the origin of our very small residual background observed in the commissioning run. The best design of this run will be implemented in the 2009 run. With this run we hope to increase the recorded data volume by a factor of 10. This could allow us to reach a sensitivity for the scattering cross section below 10^{-7} pb and touch the region favoured by a larger class of Supersymmetric model predictions.

5 Publications

- Commissioning Run of the CRESST-II Dark Matter Search, The CRESST Collaboration, G. Angloher et al., arxiv:0809.1829
- Glued CaWO4 detectors for the CRESST-II experiment, Michael Kiefer et al., Optical Materials , CryoScint 2008, Edited by: DiStefano, Petricca (2008) , arxiv:0809.4975v2
- Some Practical Applications of Dark Matter Research, L. Stodolsky, CISNP 2008, 0810.4446
- Limits on WIMP dark matter using scintillating CaWO cryogenic detectors with active background suppression, G.Angloher et al. Journal of Astroparticle Physics 23 , 325-339 (2005)
- Detection of Natural Alpha Decay of Tungsten, C. Cozzini et al. Phys. Rev. C 70 (2004)
- CRESST-II: dark matter search with scintillating absorbers, G. Angloher et al. NIM A Vol. 520 Nos. 1-3
- Light detector development for CRESST-II, F. Petricca et al. , NIM A Vol. 520 Nos. 1-3

CUORICINO and CUORE

F. Alessandria[g], E. Andreotti[e], R. Ardito[j], C. Arnaboldi[h,i], F. T. Avignone III[w], M. Balata[d], I. Bandac[w], M. Barucci[a], J.W. Beeman[p], F. Bellini[k,l], B. Berger[p], C. Brofferio[h,i], A. Bryant[p,q], C. Bucci[d], X. Cai[y], S. Capelli[h,i], L. Carbone[i], M. Carrettoni[h,i], M. Clemenza[h,i], C. Cosmelli[k,l], O. Cremonesi[i], R.J. Creswick[w], I. Dafinei[l], A. Debiasi[f], M.P. Decowski[p,q], M.M. Deninno[m], A. de Waard[o], S. Di Domizio[b,c], M.J, Dolinski[s,q], L. Ejzak[x], R. Faccini[k,l], D. Fang[y], H.A. Farach[w], E. Ferri[h,i], F. Ferroni[k,l], E. Fiorini[h,i], L. Foggetta[e], S.J. Freedman[p,q], C. Gargiulo[l], A. Giachero[i], L. Gironi[h,i], A. Giuliani[e], P. Gorla[d], E. Guardincerri[c], T.D. Gutierrez[v], E. E. Haller[p,r], K.M. Heeger[x], H.Z. Huang[u], R. Kadel[p], K. Kazkaz[s], S. Kraft[h,i], G. Keppel[f], L.Kogler[p,q], Yu.G.Kolomensky[p,q], X. Liu[u], E. Longo[k,l], Y. Ma[y], C. Maiano[h,i], G. Maier[j], R.H. Maruyama[x], C. Martinez[w], M. Martinez[i,n], L. Mizouni[w], N. Moggi[m], S. Morganti[l], S. Nisi[d], C. Nones[e], E. B. Norman[s,t], A. Nucciotti[h,i], M. Olcese[c], F. Orio[k,l], D. Orlandi[d], P. Ottonello[b,c], M. Pallavicini[b,c], V. Palmieri[f], M. Pavan[h,i], L. Pattavina[h,i], M. Pedretti[s], G. Pessina[i], S. Pirro[i], E. Previtali[i], V. Rampazzo[f], F. Rimondi[m], L. Risegari[a], C. Rosenfeld[w], C. Rusconi[e], C. Salvioni[e], S. Sangiorgio[x], D. Schaeffer[h,i], N.D. Scielzo[s], M. Sisti[h,i], A. R. Smith[p], E. Tatananni[d] W. Tian[y], C. Tomei[d], D. Torazza[b,c], S. Trentalange[u], G. Ventura[a], M. Vignati[k,l], H. Wang[y], C. Whitten Jr[u], N. Xu[p], L. Zanotti[h,i] C. Zarra[d], and S. Zucchelli[m]

[a] Dip. di Fisica dell'Università di Firenze e Sez. INFN di Firenze - Italy
[b] Dip. di Fisica dell'Università di Genova - Italy
[c] Sez. di Genova dell'INFN, Genova - Italy
[d] Laboratori Nazionali del Gran Sasso, I-67010, Assergi (L'Aquila) - Italy

[e] Dip. di Fis. e Mat. dell'Univ. dell'Insubria e Sez. INFN di Milano - Italy
[f] Laboratori Nazionali di Legnaro, Legnaro (Padova) - Italy
[g] INFN - Sez. di Milano, Milano - Italy
[h] Dip. di Fisica dell'Università di Milano-Bicocca e Sez. INFN di Mi-Bicocca - Italy
[i] INFN - Sez. di Milano Bicocca, Milano - Italy
[j] Dip. di Ingegneria Strutturale del Politecnico di Milano - Italy
[k] Dip. di Fisica dell'Università di Roma La Sapienza e Sez. INFN di Roma - Italy
[l] Sez. INFN di Roma, Roma - Italy
[m] Dip. di Fisica dell'Università di Bologna e Sez.INFN di Bologna - Italy
[n] Lab. de Fisica Nuclear y Altas Energias, Univ. de Zaragoza - Spain
[o] Kamerling Onnes Laboratory, Leiden university - Netherland
[p] Lawrence Berkeley National Lab., Berkeley - USA
[q] Dept. of Physics, Univ. of California, Berkeley - USA
[r] Dept. of Materials Sc. and Engin., Univ. of California, Berkeley - USA
[s] Lawrence Livermore National Laboratory, Livermore, California - USA
[t] Dept. of Nuclear Engineering, Univ. of California, Berkeley - USA
[u] Dep. of Physics and Astronomy, University of California, Los Angeles - USA
[v] California Polytechnic State Univ., San Luis Obispo - USA
[w] Dept.of Phys. and Astron., Univ. of South Carolina, Columbia, South Carolina - USA
[x] Univ. of Wisconsin, Madison, Wisconsin - USA
[y] Shanghai Institute of Applied Physics, Shanghai, China

Abstract

We present a report on the most relevant activities carried out during 2008 in the framework of the CUORE experiment at LNGS.

1 Introduction

The recent discoveries and measurements of atmospheric and solar neutrino oscillations have shown that there exist scenarios in which the effective Majorana mass of the electron neutrino could be larger than 0.05 eV. Recent developments in detector technology make the observation of $\beta\beta(0\nu)$ decay at this scale now feasible. The CUORICINO experiment [**?**], built in 2002, employed a large cryogenic array of TeO_2 bolometers containing the $\beta\beta$ parent isotope (^{130}Te) to search for this decay. Concluded in June 2008 CUORICINO has reported a negative signal (a fraction of the total collected statistic has still to be analyzed) defining an upper bound on the Majorana mass of neutrino of about 200-700 meV. Besides being on of the more sensitive $\beta\beta(0\nu)$ experiments of the last years, CUORICINO was a crucial test of the CUORE concept. CUORE [**?**] is a bolometric experiment aiming at the search of neutrinoless double beta decay of ^{130}Te with a sensitivity on the Majorana neutrino effective mass of the order of 20-30 meV. The CUORE detector will consist of an array of 988 TeO_2 bolometers arranged in a cylindrical configuration of 19 towers of 52 5×5×5 cm^3 crystals each.

2 CUORICINO and the Three Towers

CUORICINO data taking was stopped at the end of June 2008. The analyzed statistics accounts for 15 kg(^{130}Te) y and refers to the data collected until August 2007. The last ten months of data taking are still waiting to be analyzed and include the period during which muon veto and new DAQ prototype were installed. The detector was dismounted in July 2008. A part of its building elements (crystals and thermistors) was used in the preparation of "Three Towers Test" (see later) while the remaining TeO_2 crystals were safely stored underground under controlled athmosphere. The last four months of data taking were carried out with a cosmic ray veto (muon counter) and were mainly dedicated to evaluate the muon contribution to the measured background. Preliminary results (when extrapolated by means of Monte Carlo simulations to the CUORE geometry) suggest that such a contribution is well below the target background level for CUORE and imply that a muon veto will not be needed in CUORE. In the same period, a prototype of the CUORE DAQ was also installed and operated in order to manage both the bolometric inputs and the muon counter. A complete reprocessing of the CUORICINO data is now foreseen with the aim of optimizing data processing taking into account the full evolution of the measurement. The digital filtering technique used for pulse amplitude and pulse shape analysis (noise rejection and pile-up treatment) were in fact optimized during the experiment. This optimized procedure will now be applied to the whole CUORICINO data sample aiming at an improvement of data quality and at a better control of systematics. The relevant physical processes sought by the experiment will be studied using the final statistics: neutrinoless and two neutrino double beta decay, background sources identification, evaluation of the muon contribution to background and validation of MonteCarlo results. This will be moreover a unique occasion to test the new analysis tools that are currently under development for CUORE.

The background level and the development of new methods for its reduction have been so far the subject of deep studies and have lead to a background model according to which most of our background is due to radioactive contributions originating from the surface of the crystals and of the Cu supporting structure. Details of this model have been already presented to the LNGS SC in the past. Dedicated tests have demonstrated our ability in reducing the contribution from the TeO_2 crystal surface to levels below the aimed sensitivity of CUORE by means of a proper surface processing based on an acid attack followed by a lapping process with ultrapure pads and SiO_2 powders. Our baseline for the Cu structure is instead based on a complex recipe developed at LNL and consisting of a sequence of mechanical, electro-chemical, chemical and plasma treatment (TECM) of the copper surface. Only ICPMS and medium sensitivity measurements (Si detectors) of the surface contamination of Cu samples have been so far carried out. A final test aiming at measuring with a bolometric detector and a reasonably high statistics the actual background level in detectors processed with the TECM recipe has been decided by the CUORE Collaboration in June and is now under preparation. It consists of three independent arrays of 12 detectors (Three Towers) in which the crystals have all been processed with the CUORE recipe while the Cu supporting structures have been processed with different methods: 1) TECM recipe, 2) EC processing with ultrapure certified materials and 3) wrapping with Polyethylene films (PW). The comparison between

Figure 1: The three towers.

the different towers will indicate the best method besides guaranteeing a reference value (the PW method has been already applied a number of times in the past in the framework of our R&D program). The three tower test will be carried out in Hall A in the same cryostat which hosted CUORICINO. The building elements of the three towers are almost ready and data taking is foreseen to start in march 2009. Some crystals have been equipped with NTD thermistors characterized by a new geometry. We expect therefore also relevant technical results crucial for fixing the final design of the CUORE thermistors.

3 CUORE

The process of construction of CUORE was already discussed in the LNGS Annual Report of year 2007 [**?**]. Here we summarize the 2008 achievements with regards to the most important activities.

Figure 2: CUORE hut.

3.1 Hut

The design of the building for the CUORE experimental setup was already completed during 2007. Details of its structure have been optimized during the present year and the first phase of its construction (steel work) was just suspended in June 2008 in order to wait for the installation of the CUORE cryostat Main Support Platform (MSP). In the meanwhile details of the needed services and a complete design of the CUORE clean room have been fixed. MSP order has been placed, after a careful analysis of the seismic study, in September 2008. The estimated time for material procurement and structure construction is abour 2 months so that MSP delivery and installation is foreseen for the first week of December. Steel work and hut walls completion is evolving independently (stairs were just installed last week) but roof completion will be only possible after MSP installation and will be carried out at the beginning of 2009. Technical specifications for hut services and CUORE clean room are presently being fixed in order to obtain INFN tender approval by mid December. Taking into account usual development for public tenders both installations are foreseen for summer 2009.

3.2 Cryostat

Cryogenics is one of the most complex items of the CUORE setup. Besides the challenge of developing an effective, low noise, liquid-free, low radioactivity system for operating a massive detector at very low temperatures it involves in fact a number of separately designed parts (wiring, suspension, cold lead shields, calibration, cooling and damping system) which require a detailed integration job. During 2008 the public tender for the cryostat fabrication has been successfully completed. The company which will contruct it has been selected (SIMIC) and the order has been placed. The construction will start beginning of 2009 after fixing all the details of the cryostat design and all the interfaces between the cryostat and the various systems which interfere with it. In order to start the construction, the final drawings will be issued in early 2009 as well. At the same time a special effort has been made to perform the seismic analysis of the cryostat inner

structure and its mechanical connection to the main support plate. Dedicated tests on the cryostat construction materials have been started and some are already completed. In particular the residual heat leak of the procured NOSV copper has been characterized at low temperature at Univeristy and INFN of Milano Bicocca and preliminarly found to be negligible.

Progresses have been obtained also on the various cryogenic systems integrated in the Cryostat:

- Detector Calibration System (DCS): In 2008 the Universiy of Wisconsin (UW) completed the conceptual design of the DCS. This includes the mechanical design, the thermal analysis, and motion control and monitoring. The design was reviewed and approved in a collaboration design review in November 2008, and parts of the system are now being prototyped and tested at UW. Montecarlo simulations have been carried out by LLNL and UW to optimize the calibration procedure and calibration time. Background simulations are underway in Milano Bicocca. The calibration, cryostat, and integration groups are continuing to work together very closely for the detailed integration of the DCS into the CUORE experimental setup. An extensive cooldown and motion test of the full-size DCS is planned in late 2009 as part of the cryostat commissioning.

- Pulse Tubes: one of the CUORE Pulse Tubes, which will provide the 40K and 4K cooling stages, is being tested and characterized at the Milano Bicocca low temperature laboratory.

- Detector and Lead Shield Suspensions: The design has been completed and the 1:1 model construction is in progress. The mechanical strength at low temperature of the Kevlar part of the suspensions have been measured in Milano (LASA).

- Upper Wiring System (UWS): Tests have been carried out at low temperature in Florence to find the best thermalization stage design. The final design is being completed. The order for the needed amount of Nb-Ti wires has been already placed while the completion of the wire chains (with all needed connectors) has been moved to 2009.

- Still Lead Shield: A preliminary design of the Still temperature lead shield has been developed in Milano. A first finite elements analysis have been carried out.

- Dilution Unit (DU) and Fast Cooling System (FCS): Work is in progress at Leiden-cryogenics for the construction of the DU. A large effort has been devoted to the R&D of a powerful cryogen-free DU. Presently the silver heat exchanger have been made out of the silver powder essayed in Milano and LNGS for radiopurity. The Gas Handling System is completed and the Pulse Tubes have been delivered. A thermal design of the Fast Cooling System has been studied in collaboration with the Milano Group and the GM coolers are going to be delivered soon.

- Movement Tools and Assembly Procedure: The Bologna group is designing the tools for opening and closing the cryostat. While the Milano Group together with the

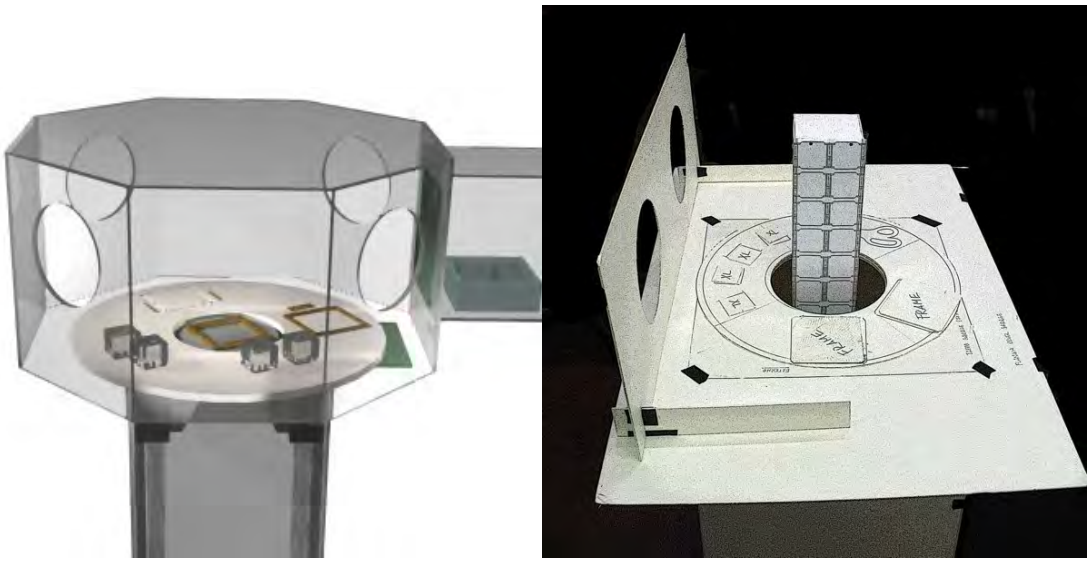

Figure 3: Every special glove box required for the assembly line of the CUORE towers has been preliminary designed 3D with CAD and then studied with 1:1 Laminil^{TM} model and the real elevator and rotation system.

Experiment Integrator in Roma and the Berkeley group is defining the Cryostat Assembly Procedure.

3.3 Detector and assembly

The design of the detector is in charge of the Single Module Development WG (SMD) which has defined the details of the single bolometer structure (absorber, thermistor and heater). The design and test of the CUORE towers (from its mechanical structure, to the read-out wires, to the assembly procedures and tools) are the responsibilities of the Assembly WG (CAW). The SMD design follows the experience of CUORICINO and has produced a baseline prototype detector used in the past for a number of bolometric tests carried out both in Como and LNGS. The performance of such a detector is therefore well known and guarantees a good performance and level of reproducibility. The activity carried out in the past year mainly involves the monitoring of the NTD production process (Ge irradiation and thermistor structure) through a series of bolometric calibration runs carried out in Como and at LNGS. The baseline thermistor structure is now fixed, and consists in the so-called "wrap-around" geometry. Another interesting structure, which could lead to higher signal-to-noise ratio, is however the so-called "flat-pack" geometry which would imply a simplified preparation process. A supplementary investigation is required. It will be performed in the framework of the three-tower run whose results will determine the final choice. The program of neutron irradiation of the Germanium samples selected for the CUORE thermistors (and the respective checks on the irradiation level) are still continuing. For what concerns heaters, we have so far selected 2/3 of the total amount needed for CUORE.

Important steps towards the definition of the final design of the CUORE detector have been achieved. The activities accomplished during year 2008 have been characterized by a

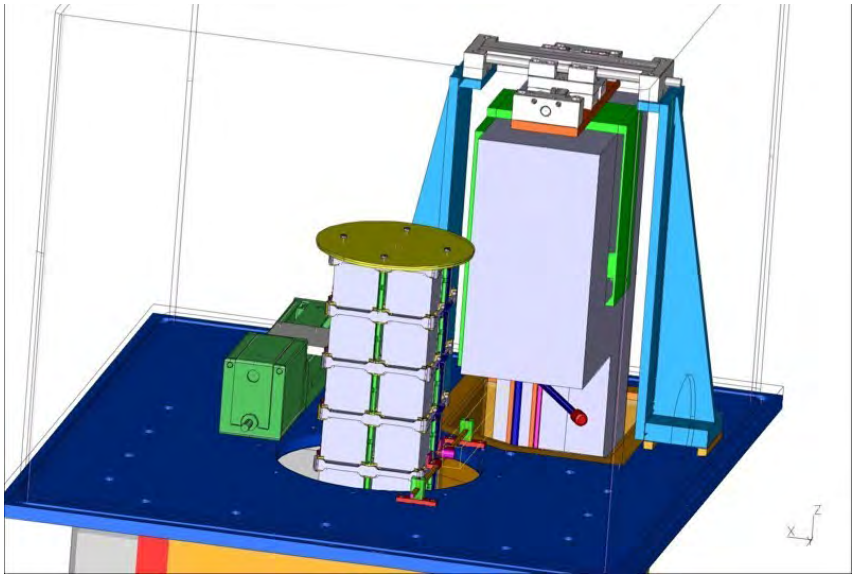

Figure 4: The CAD design of the bonding glove box has been tested with 1:1 Laminil^{TM} model.

series of fundamental tests and checks on the detector design summarized in the following:

- Mechanical tolerances. The statistical distribution around the mean of the more crucial parameters of the CUORE single tower structure, achieved by different factories in the production of Cu frames and columns, PTFE spacers and crystals, have been collected. The change in this statistical distribution after the different cleaning procedures of the Cu parts has then been studied. These data will be used to validate the CUORE parts production and to make the fine-tuning corrections to the mechanical drawing dimensions and tolerances, before going into the real CUORE structure production, to be started at the beginning of 2009.

- Detector wiring. The material to be used for the detector readout from crystals to cryostat mixing chamber was forcedly changed with respect to the original design, because the already tested Cu-Mylar ribbons were no more available on the market. We started therefore a campaign on different substrates, choosing at the end a PEN-Cu bi-layer, that was tested from the radioactivity point of view and from electric characteristics. The final layout will be fixed at the beginning of 2009 and will then go into production.

- Wire bonding. The "custom made" bonding machine was studied and realized by the selected company, which delivered it in Gran Sasso at the end of July 2008. A series of tests on ribbon prototypes and chips were carried out in order to better understanding the characteristics and difficulties of bonding with a vertical bonding machine. The next step, on its way in these days in Rome, is the full integration of the bonding machine inside a special glove box, and the optimization of the latter one to guarantee an easy procedure for the operator.

- Thermistor and heater gluing. Feasibility studies for a total automatic system for

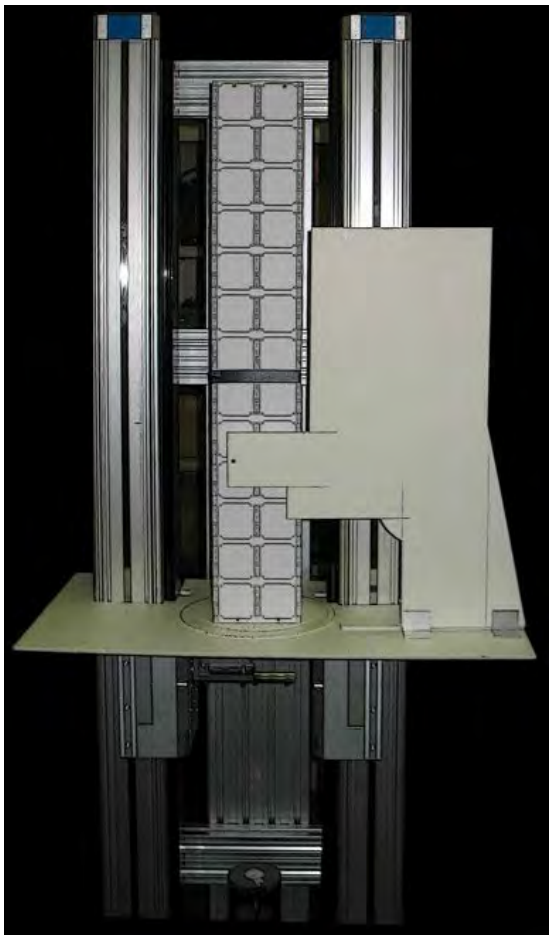

Figure 5: The real garage and rotation hardware.

thermistor and heater gluing on crystal has been accomplished. Due to economical restrictions, the gluing system will be probably only semi-automatic. Studies in this sense are going on and will come to an end (the gluing system) around june 2009.

- Assembly glove boxes. Several parallel studies on the different special glove boxes needed for the assembly line in the "zero contact" philosophy adopted for CUORE are presently being carried out. Some of them are depicted in the following figures (figures **??**, **??** and**??**). One of the most relevant part for the assembly line (a kind of elevator) was designed and constructed and the special glove boxes will be ordered before spring 2009.

- Rn emanation. In order to exclude the risk of recontamination of the surfaces of Cu pieces during assembly, measurements of Rn emanation of all the tools, materials and ancillary structures, that will be in the same glove box as the CUORE tower, will be done. A special equipment for this specific study has been constructed and used to check for emanation from the complex elevator structure, with satisfactory results (figure **??**).

A relevant task, in strict connection with the assembly, is the storage of all the detector

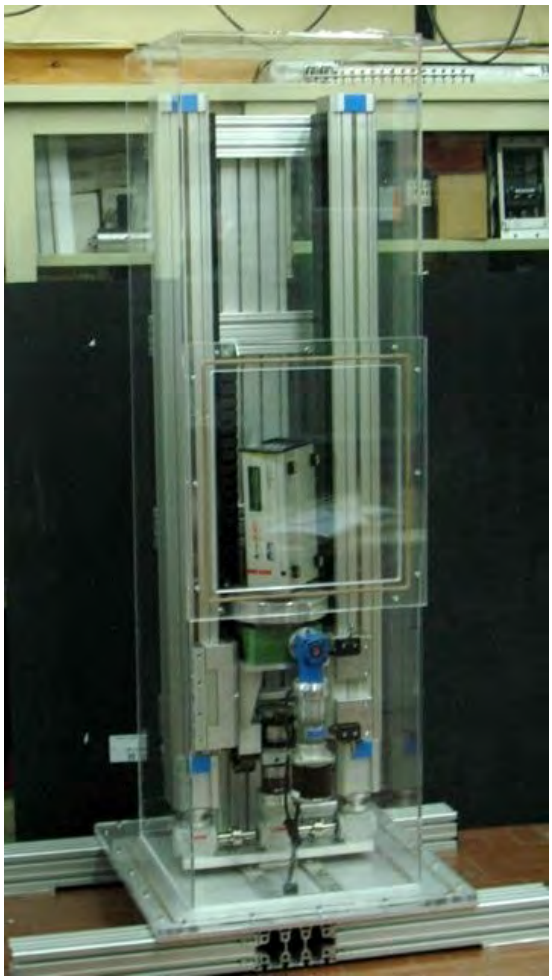

Figure 6: The tower elevator and rotation system have been enclosed in an air-tight plexiglass box and then checked for Rn emanation using a Rn-meter put in place of a real tower. No signal has been observed.

parts (after cleaning) and the related software implementation to govern the in/out fluxes during delivery and assembly, on a time schedule of several years. Special storage in clean room environments will be tested at the beginning of 2009 while, as mentioned above, the database software is already partially in use for the part strictly related to crystals productions, delivery and stocking.

3.4 Radioactivity

Main tasks of the radioactivity WG are the Copper procurement, production and cleaning for all the needed setup parts and the validation of all needed materials and procedures from a radioactive point of view.

3.4.1 Copper production and cleaning

The copper frames which hold the CUORE crystals have a complicated design which should respect strict mechanical tolerances in order to stack without causing cryogenic touches or electrical shorts of the corresponding tower. Moreover the frame surface roughness must be reduced at minimum in order to minimize the area of possible contaminant implantation and to give more effectiveness to the following cleaning procedure. For these reasons, machining by EDM (Electrical Discharge Machining) was chosen for the frame production. A quality check of the EDM produced frames by different companies has been performed at the beginning of 2008, by checking the mechanical tolerances with a dedicated probe at INFN-Genova workshop. The same checks performed on the frames produced by EDM by INFN-LNL workshop showed a much better agreement with the project requirements. As a result INFN-LNL workshop has been chosen for the entire CUORE frame production. In order to be able to machine all 300 frames within CUORE time schedule, a new EDM machine will be acquired by LNL workshop, which allows a semi-automated processing that enables overnight working. As settled by INFN executive commitee, a one-year-old EDM machine will be transferred from INFN-Padova workshop to INFN-LNL and upgraded in order to be able to produce CUORE frames. The LNL workshop should be ready to start the processing in early 2009. A contract between INFN-Milano Bicocca and a metrological laboratory at the Engineering Department of Padova University, signed in 2008, will allow a much easier logistics of the tolerance checks on the CUORE frame production. The other copper pieces making the CUORE tower (columns, wire trays, plates,...) will be machined by INFN- Milano Bicocca workshop. This decision was taken in order to limit costs and to have a higher control on the production, therefore an higher quality both form the mechanical and the cleanliness points of view. To make this possible and compatible with the available manpower, a small EDM machine will be acquired by the workshop in early 2009. During 2008 a quality check of the surface cleaning procedure of the copper frames has also been performed. Each of the four steps of the surface cleaning process has been separetely applied to one or more frames; after that the mechanical tolerances of the frames have been measured once more by the sameprobe. In this way some weak points of the cleaning process with respect to surface uniformity have been localized and corrected. In the meanwhile all details of the CUORE detector mounting structure and the CUORE cryostat have been finalized. Therefore it has been possible to inventory all copper starting material missing to produce all the needed pieces. For this reason a new order to the same company who delivered the first half of the copper plates needed for CUORE has been prepared and the delivery is foreseen in early 2009.

3.4.2 Material selection/cleaning and procedure validation

A lot of activities involving Radioactivity aspects of needed materials for the CUORE setup were started during 2008. They are briefly here summarized.

Crystal validation. The year 2008 was dedicated to the start of large scale production of TeO_2 crystals needed for CUORE. At this purpose specific manufacturing conditions were implemented at the crystals production centre in Jiading, compliant with CUORE requirements, with a special concern for radio-purity and production traceability. The

	K [ppb]	Pt [ppb]	Pb [ppb]	Bi [ppb]	Th [ppb]	U [ppb]	Cs137 [mBq/kg]	Co60 [mBq/kg]	method	laboratory
H_2O (a)	<10	-	0.03	-	0.0015	0.002	-	-	ICP-MS	LNGS
H_2O (b)	<10	-	0.11	-	<0.001	<0.001	-	-	ICP-MS	LNGS
HNO_3	<100	<0.100	1.9	14	<0.010	<0.010	-	-	ICP-MS	LNGS
HCl	<100	0.38	3.1	0.085	<0.001	<0.010	-	-	ICP-MS	LNGS
NH_4OH	<100	0.21	2	2.6	<0.001	<0.010	-	-	ICP-MS	LNGS
PE bags	<10	<0.001	<0.001	<0.001	<0.001	<0.001	-	-	ICP-MS	LNGS
SiO_2	<5000	<1	<10	<0.5	<0.5	<0.5	-	-	ICP-MS	LNGS
SiO_2	(1.3±0.5)E2				<0.16	<1.2	<0.17	<0.1	HPGe	LNGS
H_2O (a)	-	<0.003	<0.1	0.663	<0.001	<0.001	-	-	ICP-MS	SINAP
HNO_3	-	1.723	1.674	7.474	<0.001	<0.001	-	-	ICP-MS	SINAP
HCl	-	7.797	9.2	12.86	<0.001	<0.001	-	-	ICP-MS	SINAP
NH_4OH	-	<0.003	<0.1	0.991	<0.001	<0.001	-	-	ICP-MS	SINAP

Figure 7: Radio-purity of materials used for TeO_2 crystals production in 2008. Samples (a) and (b) were taken respectively from Kunshan Jincheng Chemical facility and the clean room at Jiading. Sample PE bags refers to polyethylene bags used for the preparation of SiO2 slurry used for TeO_2 crystals final polishing.

reliability of these conditions was subject to periodical controls focused on the technological environment, the radio-purity of reactants, cleaning liquids, consumables and ancillaries. Handling, storage and shipment of materials, intermediary products and of crystals - ready to use - were also subject of periodical controls. In addition to dedicated areas for the production of TeO_2 powder, crystal growth and surface processing, described in our previous report, a new technological area dedicated to raw mechanical processing of CUORE crystals was completed in 2008 at the crystals production centre in Jiading. Each production step from TeO_2 powder synthesis to the shipment of crystals ready to use was allowed only upon written conformity report made by INFN experts in radio-contamination prevention procedures. The results of radio-purity analysis made on reactants, cleaning liquids, consumables and ancillaries used for TeO_2 crystals production in 2008 are given in Table 1 (figure **??**). Samples (a) and (b) refer respectively to the ultrapure water used at Kunshan Jincheng Chemical facility for the chemical synthesis and successive drying of TeO_2 powder and ultrapure water used in the clean room at Jiading for the surface processing of TeO_2 crystals. Sample PE bags refers to polyethylene bags used for the preparation of SiO2 slurry used for TeO_2 crystals final polishing. Different values obtained by SINAP and LNGS for heavy metal contamination must be due to possible contamination of samples during transport. Measurements made at LNGS are more reliable due to the special care taken in preparing the vials in which reagent samples were transported in view of cross-check ICP-MS measurement.

Table 2 (figure **??**) gives the results of ICP-MS radio-purity analysis made on raw materials (metallic Tellurium) and intermediary products (different TeO_2 powders). Cross-check measurements were systematically made in Italy at LNGS and in China at SINAP. Some of these materials were also subject to HPGe measurements reported in Table 3. The results of radio-purity measurements performed in different laboratories and using

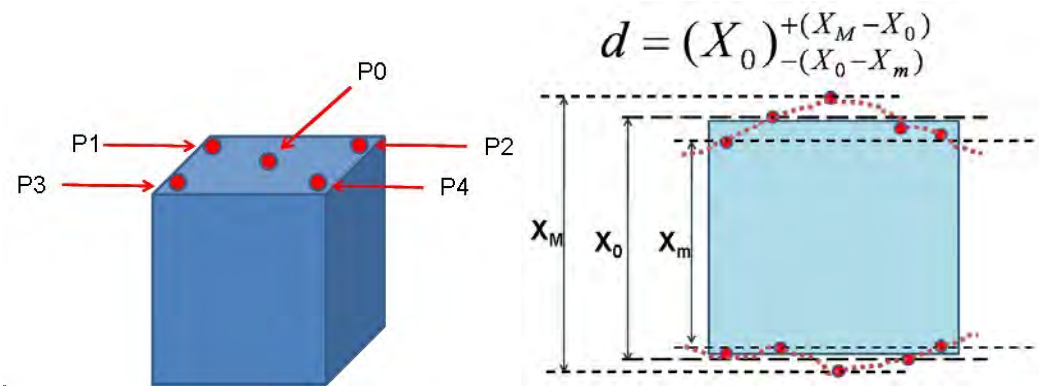

Figure 8: Measurement protocol and definition of crystals dimension on one direction and corresponding tolerances. Left: positioning of the five touch points measured on each crystals face with the bench micrometer. Right: definition of crystals dimension and tolerances. The real shape of two opposite crystal faces is exaggeratedly represented by dashed, red lines

different methods are in a good agreement and in most cases are within CUORE specifications. In the case of batch no. 2 of metallic Tellurium for which a high ^{40}K contamination was measured, it was decided to continue the production process where it was expected a purification of the material during the chemical synthesis of TeO_2 powder. The results of measurements performed on resulting TeO_2 powder confirmed this hypothesis showing a ^{40}K concentration within CUORE specification limits (data reported in Tables 2 and 3). Crystals produced in 2008 underwent the final surface processing in the clean room following a protocol essentially based on a general precautionary principle: any tool or material entering into direct contact with crystals surface, no matter for how much time, carries with it a certain level of radio-contamination risk that is proportional to the level of exposure. The protocol, defined with the twofold purpose of refining crystal dimensions and cleaning crystal surface, takes into account the mutual conditioning of these two targets. The crystal shape, dimensions and crystallographic orientation of faces are brought very close to their nominal values during the raw mechanical processing performed outside the clean room. Inside the clean room the possibility to modify these parameters is quite reduced due to very strict operation conditions aimed at avoiding any radio-contamination risk. Dimensions are directly measured only once in the clean room, before etching. Afterwards, the crystal is only weighed after each procedure: etching and successive polishing of each face. The modification of dimension following each of these manufacturing steps is calculated correspondingly. The dimension measurement protocol at crystals reception in the clean room as well as the definition of crystal dimensions and tolerances are described in figure **??**. The measurement, performed with a digital bench micrometer is also aimed at checking the conformity with planarity specifications needed for CUORE (<10). The results of planarity measurements made on the 2 hard faces (<100>) and 4 soft faces (<001>) of the 63 crystals produced in 2008 are given in figure **??**. The dimensions of these crystals are given in figure **??**. The slightly larger mean value of crystal dimension on the hard <100> direction is due to the difficult polishing of the corresponding (hard) faces.

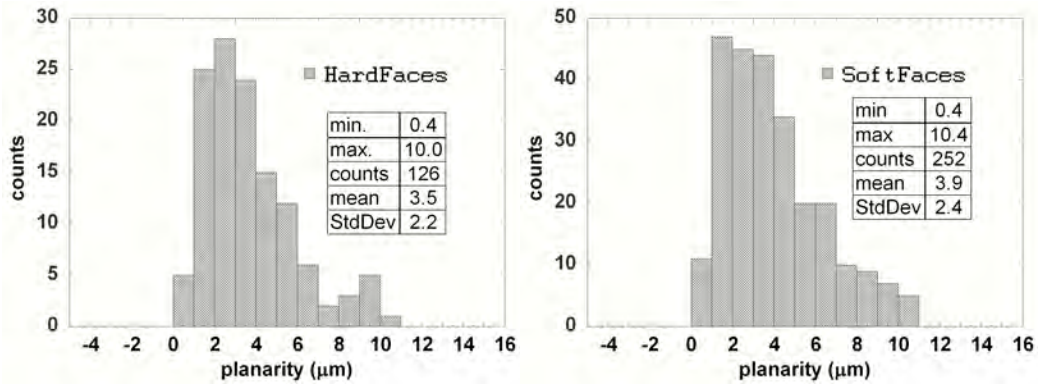

Figure 9: Planarities of hard (<100>) and soft (<001> and <00-1>) faces of the 63 TeO_2 crystals produced in 2008

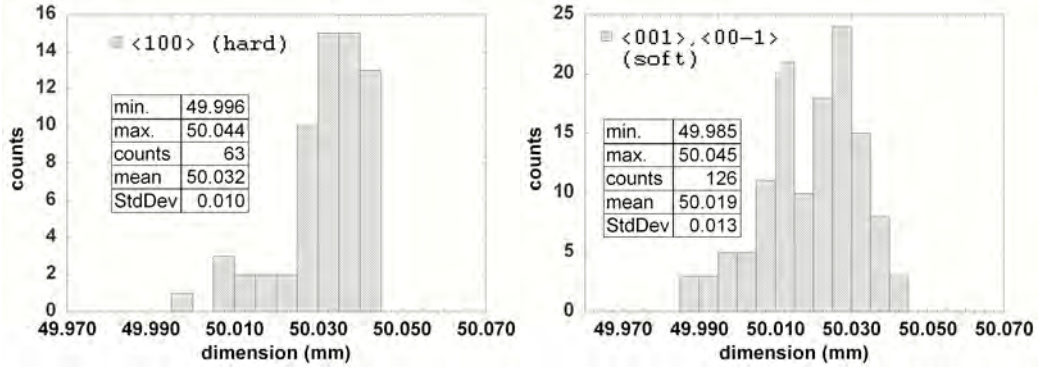

Figure 10: Dimensions the 63 TeO_2 crystals produced in 2008. Left: crystals dimensions on the <100> (hard) direction. Right: crystals dimensions on the <001> and <00-1> (soft) directions

As already mentioned, the final mechanical processing has also the purpose of deep cleaning of crystal surfaces, possibly contaminated during the raw mechanical processing (cutting, shaping, grinding and lapping). The cleaning process is made in two steps, first by chemical etching and second by polishing. The polishing is also made in order to smooth out the crystal faces, possibly damaged by chemical etching. The targeted number of atomic layers to be taken away by these two procedures is of the order of 104 in order to make sure that all impurity atoms adsorbed on crystal face and further difused in the bulk of it are washed away. As figure **??** shows, the mean depth of the crystal layer washed away by chemical etching of 63 crystals produced in 2008 is 13.5 microns and the least value of this width is 10.2 microns which makes more than 105 atomic layers for a constant lattice of the order of few ·Angstrom (TeO_2 lattice constants: a=4.8088 ·A, c=7.6038 ·A).

The surface cleaning process is further consolidated by the polishing procedure. As figure **??** shows, approximately other 105 atomic layers are taken away by polishing. Relatively large spread of the polishing depth is due to the fact that polishing is not only a surface cleaning process. Besides the purpose of taking away the surface layer possibly contaminated with radioactive isotopes, the polishing has also the aim of bringing the

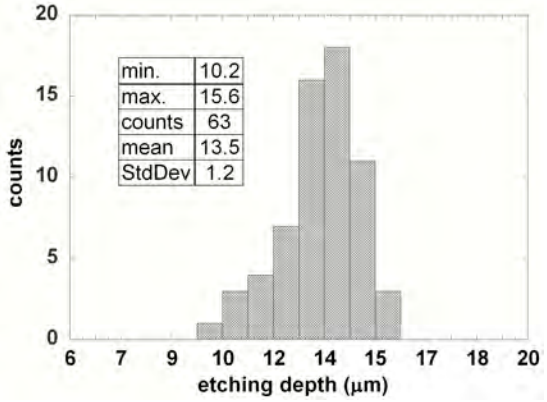

Figure 11: Width of chemically etched layer on the surface of 63 crystals produced in 2008

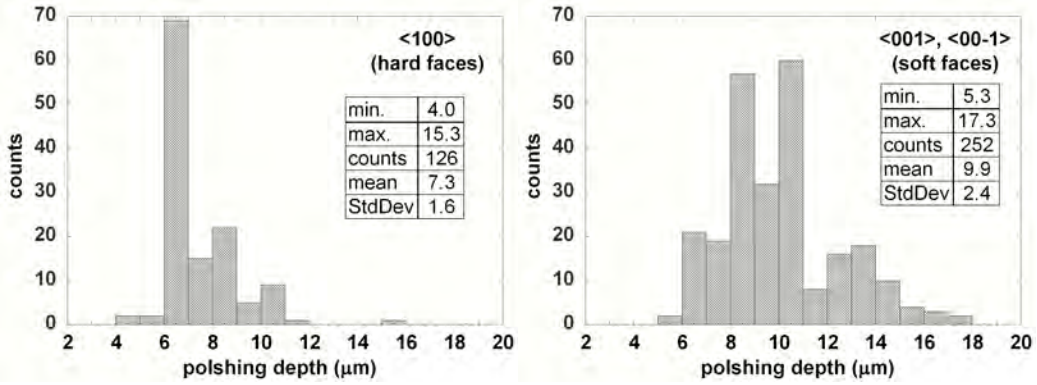

Figure 12: Width of mechanically polished layer on the surface of 63 crystals produced in 2008

crystal dimensions as close as possible to the nominal values and improve the surface quality by removing possible extended defects induced by chemical etching.

Though hard and soft faces are easily distinguishable by an expert operator, very strict rules were defined in order to avoid bad processing of crystal faces. Crystals are delivered to the clean room with one of the hard faces facing up and all operation in the clean room (ultrasound washing, chemical etching and mechanical polishing) are made to track the crystallographic orientation of the crystal faces. Special care is taken in order to avoid any contamination risk during the operations in the clean room. The polishing slurry is made by adding ultrapure water directly in the powder bags (PE bags in Table 1, figure **??**) and mixing the slurry in situ. Once the crystals have been etched, they come into direct touch only with the following materials / parts: ultra clean gloves, ultra pure water, polishing slurry, polishing pads, cleaned and conditioned polyethylene sheets, vacuum plastic bag. At the end of clean room operation, crystals are packed and barcode labeled in a triple vacuum package and further stored by groups of six crystals in polyethylene vacuum boxes. 63 crystals aimed to be used for CUORE0 have been grown, processed in Jiading and shipped in 2008 to LNGS following the production plan agreed between CUORE Collaboration and SICCAS. The whole production process as

Figure 13: Delivery to LNGS of TeO_2 crystals transported by sea. Left: polyethylene vacuum boxes containing 59 crystals. Right: crystals in their triple polyethylene vacuum bags

well as shipment procedure was supervised by INFN specialist and made in agreement with strict protocols stipulated in the contracts between SICCAS and INFN and SICCAS and LBNL. Four crystals were shipped by air and are currently subject of a cryogenic test aimed at measuring their bolometric characteristics and possibly extract information on their surface radio-purity. The remaining 59 crystals were shipped by sea in order to avoid cosmogenic contamination. This first batch of 63 crystals will be paid by LBNL. Figs. 6 and 7 are photos taken during the delivery at LNGS of 59 crystals shipped by sea and their storage in the dedicated PSA area (Permanent Storage Area). The production of 500 crystals ordered by INFN is currently on the way. A total of 360 crystals are foreseen to be delivered at LNGS within the end of the year 2009.

NTD thermistors. One of the most important aspects that was investigated during 2008 was the actual contribution to the CUORE background produced by the surface contamination of NTD thermistors. The data reported in literature were contradictory and not well specified. A germanium slab whose surface was processed in the same ways as NTD germanium was produced at Lawrence Berkeley Laboratory and was measured at Milano Bicocca with Silicon Surface Barrier detectors. The main issue was to evaluate the possible alpha contamination on surfaces mainly related with ^{210}Pb . To evaluate also the possible background produced by the gold deposition, one of the surfaces was completely plated. Results indicate clearly that present productions of NTDs don't release substantial contamination on germanium surfaces. Scaling the obtained results respect to the final dimension of NTD thermistors that will be used for detectors read out the total contribution to the CUORE background produced by the sensor will be negligible. Special care must be devoted to maintain the actual quality for the final production.

Radon. Radon diffusion and radon implantation on material surfaces directly facing the detector can be considered one of the most critical aspects for the detector assembly and storage. A specially dedicated measurement was implemented at Milano Bicocca in order to evaluate the radon sticking factor on material surfaces. A sealed box with a high concentration of radon (300 kBq/m3 of 222Rn) was constructed and samples of copper, TeO_2 and Si were exposed to the high contaminated atmosphere. Relevant results can be summarized as follows: a clear diffusion inside the material was observed, two different

Figure 14: Storage of TeO_2 crystals at LNGS. Left: crystals as arrived (in their triple polyethylene bags) are stored inside vacuum boxes. Right: vacuum boxes containing crystals are stored in N2 fluxed cupboard in the Permanent Storage Area (PSA)

diffusion profiles were estimated, and indication of possible degraded alpha contribution at the energy of the neutrinoless double beta decay was identified. The obtained information can be used in order to minimize possible radon contamination during the assembly and the installation of the CUORE detector.

Copper cleaning. Copper surface treatments are one of the most critical procedures of CUORE. As demonstrated by the results of CUORICINO and of a series of test measurements carried out in our hall C facility at LNGS, contaminations present on copper surfaces can give one of the most important contributions to the background produced by degraded alpha. LNL activity was directed to optimize the various procedure on copper cleaning: the setup was configured to clean frames, bars, plates and discs that can be installed in the CUORE detector. At the same time, different cleaning procedures based on the use of radio-pure chemicals were implemented at LNGS. Measurements with Silicon surface barrier detectors was done in order to identify the best approach. Though showing small differences in the residual contaminations, most cleaned samples indicated a background compatible with the intrinsic detectors background. To overcome this limit a special dedicated bolometric run was programmed in Hall A at LNGS. Three towers made with the same type of copper but cleaned in different ways were designed: the comparison between their backgrounds will indicate the final choice for the CUORE cleaning procedures. Selected approaches are: complete TECM (Tumbler plus Electrochemical plus Chemical plus Magnetron) LNL cleaning; a more simple cleaning procedure developed at Gran Sasso and based on electrochemical treatments plus chemical with ultrapure materials; a very simple copper surface cleaning with final surfaces completely wrapped

Te batch	Part Type	BC	contaminant concentration (ppb)								laboratory
			K	Ag	Au	Pt	Pb	Bi	Th	U	
1	Te metal	10001	<5000			<1	650	220	<0.2	<0.2	LNGS
	Te metal	10001	<5000			<1	350	140	<0.2	<0.2	LNGS
	Te metal	10001	<10000	1200±200	<1000	<1000	700±200	200±30	<4	<1	SINAP
	TeO2 RD	20001	<5000			6	32	25	<0.2	<0.2	LNGS
	TeO2 RD	20001	<5000	<1	<50	<50	320±40	<30	<4	<1	SINAP
	TeO2 RC	30001	<5000	<1	<50	<50	<200	<30	<4	<1	SINAP
	TeO2 RC	30001	<5000			250	29	19	<0.2	<0.2	LNGS
	TeO2 RC	30001	<5000			16	84	18	≈0.3	<0.2	LNGS
	TeO2 UPD	40001	<10000			<15	<2000	51	<0.2	<0.2	LNGS
	TeO2 UPD	40001	<5000	<1.5	<1	3.1±0.1	<900	43±5	<0.2	<0.6	SINAP
	TeO2 UPC	50001	<10000			93	<2000	77	<0.2	<0.2	LNGS
	TeO2 UPC	50001	<5000	<1.5	<1	48±12	<100	67±10	<0.2	<0.2	SINAP
2	Te metal	10002	41000			<1	1080	800	<0.2	<0.2	LNGS
	Te metal	10002	31000			<1	1000	780	<0.2	<0.2	
	Te metal	10002	28000 ±8000	1100±200	<1000	<1000	1000 ±100	800±100	<4	<1	SINAP
	TeO2 RD	20002	<5000			<50	10	40	<0.2	<0.2	LNGS
	TeO2 RD	20002	<5000	1.1±0.2	1.9±0.2	1.3±0.3	<100	36.6±1.2	0.16±0.04	0.09±0.01	SINAP
	TeO2 RC	30002	<5000			<50	27	37	<0.2	<0.2	LNGS
	TeO2 RC	30002	<5000	1.5±0.7	2.2±0.3	4.9±0.1	<400	39.6±0.6	0.20±0.02	0.12±0.02	SINAP
	TeO2 UPD	40002	<5000	<1.5	<1	9.5±1.0	<130	47±10	<2	<0.7	SINAP
	TeO2 UPD	40002	<10000			<10	<500	22	<0.2	<0.2	LNGS
	TeO2 UPC	50002	<10000			70	<500	22	<0.2	<0.2	LNGS
	TeO2 UPC	50002	<5000	<1.5	<1	32±1.7	<130	35±1	<2	<0.7	SINAP
3	Te metal	10003	<5000			<1	600	700	<0.2	<0.2	LNGS
	Te metal	10003	<5000	434±10	<10	<1	<600	173±10	<2	<0.7	SINAP
	TeO2 RD	20003		<2	<3	4±1	<200	20	<2	<0.5	SINAP
	TeO2 RD	20003	<10000			<10	55	10	<0.2	<0.2	LNGS
	TeO2 RC	30003		<2	<3	45±8	<250±30	27±5	<2	<0.5	SINAP
	TeO2 RC	30003	<10000			750	<20	11	<0.2	<0.2	LNGS
	TeO2 UPD	40003	<5000	<2	<2	8±1	<100	73±16	<1	<1	SINAP
	TeO2 UPD	40003	<5000			7	<100	40	<0.2	<0.2	LNGS
	TeO2 UPC	50003	<5000	<2	<2	9±1	<100	125±133	<1	<1	SINAP
	TeO2 UPC	50003	<5000			7	<100	31	<0.2	<0.2	LNGS

Figure 15: ICP-MS measurements performed at LNGS and SINAP on all raw materials and intermediary products used for the production of TeO_2 crystals for CUORE in 2008

with PET film. As mentioned above, the detector is presently under construction and will be installed in the Hall A cryostat before the end of 2008. Preliminary results will be ready by spring 2009.

Packaging. Before starting of the mass production of all CUORE parts, a definition of the packaging and storage approach is mandatory. In the framework of the radioactivity WG a strong effort was dedicated to define the best solution for the package system dedicated to crystals and copper parts. After a long validation process, the use of a packaging system specifically developed for food conservation was finally selected. CUORE samples will be therefore enclosed in a multiple set of evacuated plastic bags. Measured plastic bags were found very clean from a radioactivity point of view. A very low radon permeability was measured and the use of three nested bags (for clean room reasons) practically guarantee the complete separation between the inner and the outer part of the package. Test were also carried out on the stability of the prepared packages. Stable vacuum levels

Te batch	Part Type	contaminant concentration mBq/kg								contaminant concentration g/g					
		Th-232		U-238		U	K40	Cs	Co 60	Th-232		U-238		U 235	K40
		Ra 228	Th 228	Ra 226	Pa 234	235		137		Ra 228	Th 228	Ra 226	Pa 234		
1	Te	<0.76	<0.25	<0.90	<270	<4.9	64±12	1.8	<0.36	<1.9E-10	<6.2E-11	<7.3E-11	<2.2E-8	<8.7E-9	(2.1±0.4)E-6
		<1.1	<0.75	<0.92	<46	<5.0	76±10	1.4±0.3	<0.15	<2.7E-10	<1.8E-10	<7.5E-11	<3.7E-9	<8.8E-9	(2.4±0.3)E-6
	TeO2 RD	<0.51	<0.57	<0.79	<15	<1.5	<2.7	<0.21	<0.28	<1.3E-10	<1.4E-10	<6.4E-11	1E-09	<2.7E-9	<8.6E-8
2	Te						1900 ±200								(6.0±0.7)E-5
	TeO2 RD	<0.36	0.30 ± 0.13	<0.46	28	0.31	2.5± 1.0	<0.14	<0.16	<8.8E-11	(7.4± 3.3)E-11	4E-11	2E-09	5E-10	(7.9± 3.2)E-8
3	Te	<0.67	<0.73	<0.50	15	<5.3	64±8	2.5±0.4	<0.21	<1.7E-10	<1.8E-10	<4.0E-11	<1.3E-9	9E-09	(2.1±0.3)E-6

Figure 16: HPGe measurements performed at LNGS on raw metallic Tellurium and resulting TeO_2 powder used for the production of TeO_2 crystals for CUORE in 2008

were observed over very long time (months) without any degradation.

3.4.3 Electronics

The CUORE Electronic System consists of many parts, the design of most of which is based on the experience of the pilot experiment CUORICINO. Space occupation of the CUORE front-end will be smaller by about a factor close to 3 with respect to the CUORICINO set-up, thanks to the optimization of the electronic components. In addition the part of the front-end that takes care the programming of all the necessary parameters, mastered by the acquisition system, will be implemented by the last generation of microcontroller based on the ARM core, featuring a great flexibility at a low cost. The present status of the front-end and the next progress of the development are given.

- The preamplifier has been designed and prototyped at Milano-Bicocca. A preproduction has been made at USC, in USA. It is a differential voltage sensitive preamplifier. The differential JFETs at its input has been selected based on a semi-custom process. The JFETs are already available for the full production, fully supported with INFN funds. The main very-front board will consist of 6 channels each including a preamplifier, a second stage, a detector biasing network, the detector load resistors, a number of secondary features, the glue logic and the remotely-programmable interface, ARM-microcontroller based. The prototype/preproduction board is foreseen within the first half of 2009.

- The antialiasing filter consist in a board that contain 12 6-poles Thomson, or Bessel, active filters having each 4 independent programmable frequencies. It was prototyped by the group of Genova, following the design from Milano-Bicocca. This board will be validated, to enter in the pre-production phase, within the first half of 2009.

- 2 switching power supplies for the remote (48 V) supply voltage of the Electronic System are already available, supported by INFN. Another pair of modules will be provided by USC within the first half of 2009.

- Some test switching low noise module for the pre-regulated (48 V => +/-12 V and 48 V => +/- 5 V) supply voltage are available.

3.4.4 DAQ

The CUORE Data Acquisition and Slow control systems are basically completely designed in their most relevant parts. Most of the software has been written. In order to test and validate the new system, the collaboration has decided to upgrade both the system in the Hall C setup in 2007 and the one in use in CUORICINO in early 2008. As mentioned above the last period of CUORICINO data collection was carried out by means of this CUORE DAQ prototype. A complete test of the DAQ system and data analysis tools will be therefore one of the most relevant outcomes of the CUORICINO data reprocessing. The complete procurement of the CUORE DAQ system is foreseen later in the experiment time schedule.

3.5 CUORE-0

CUORE-0 is a single CUORE tower to be installed and operated in the existing dilution refrigerator placed in the hall A of the Gran Sasso Laboratory. This refrigerator has been housing Cuoricino until June 2008. CUORE-0 is foreseen to be ready to take data from January 2010. CUORE-0 motivations are manifold and can be summarized as follows:

- test of the CUORE assembly chain and procedure.
- high statistics test of crucial components of the estimated CUORE background.
- test of the bolometric behavior of the detectors.
- test of the CUORE Data Acquisition.
- test of the CUORE analysis tools.

Being the first operating CUORE tower, prepared and assembled according to the same protocols and tools, CUORE-0 development and preparation strictly follows the evolution of the CUORE project. The time schedule of each item anticipates however the mass production of CUORE and serves as a general test of it. The following is a summary of its present status item by item:

Crystals. Test samples of the pre-production have been delivered in November 2008 and a validation run has started in December 2008 in hall C at LNGS. Presently, the run is going on. Preliminary analysis seems to show that the specifications of the crystals are met, both from the radio-purity and bolometric point of views. All the CUORE-0 crystals have been delivered and stored at LNGS in February 2009.

Heaters. All the CUORE-0 heaters have been produced and characterized. Their cleaning procedure is approximately defined: organic solvent (ethanol or aceton) in PTFE container in ultrasound bath. Cleaning and packaging will be performed within June 30st, 2009.

Thermistors. The CUORE-0 thermistors will be prepared (90 samples) after a final test to define their geometry, to be completed within the end of March, 2009. The production

is foreseen to end in July 2009. A sampling characterization will be then performed in Como and Florence. They will be subsequently cleaned, packed and delivered to LNGS.

Tower-Cryostat interface. The same suspension used in Cuoricino and in the three-tower test will be used in CUORE-0, with small modifications.

Cu part production and cleaning. The drawings of the pieces common to CUORE (regarding the tower) and the specific parts for CUORE-0 are complete. The various workshops and companies involved in the production have been identified. Copper cleaning will start in LNL in June 2009, in parallel with part of the piece production. The cleaned pieces should be ready in October 2009, when the Cu parts are required for assembly.

PTFE blocks. The contract for production was issued. The parts will be ready and cleaned within October 2009, when required for assembly.

Wiring. In spite of the large difference between the CUORE cryostat and the hall A cryostat, the wiring structure of CUORE-0 will be kept as similar as possible to that of CUORE. The wiring both at the tower and at the cryostat level has been designed and part of the components ordered. Within June 2009, the wiring components will be ready to be cleaned and installed.

Assembly. There are critical items not fully defined, for example the thermistor / heater gluing procedure. This is at the moment the most delicate issue of the assembly chain. However, the assemble line is scheduled to be prepared for test and training within September 2009, and for actual assembly within November 2009.

Final operation. The tower of CUORE-0 will assembled in December 2009 and installed in the hall A LNGS cryostat within January 2010. February and March 2010 will be devoted to cool-down and detector optimisation. Data taking is foreseen for April 2010.

4 List of 2008 Publications

1. C. Arnaboldi et al., Physical Review C, 78 (2008) 035502
2. M. Pavan et al., Europhysics Journal A 36 (2008) 159
3. M. Pedretti, International Journal of Modern Physics A, 23 (2008) 3395
4. M. Pedretti et al., Journal of Low Temperature Physics, 151 (2008) 841
5. P. Gorla, Journal of Low Temperature Physics 151 (2008) 607
6. A. Nucciotti et al., Journal of Low Temperature Physics 151 (2008) 662
7. A. Arnaboldi and G. Pessina, Journal of Low Temperature Physics 151 (2008) 662
8. M. Barucci et al., Cryogenics 48 (2008) 166-168
9. I.C. Bandac (for the CUORE collaboration), J.Phys.Conf.Ser.110 (2008) 082001
10. A. Giuliani (for the CUORE collaboration), J.Phys.Conf.Ser.120 (2008) 052051
11. C. Brofferio (for the CUORE collaboration), J.Phys.Conf.Ser.136 (2008) 022034

References

[1] C. Arnaboldi et at., Phys. Lett. B 584 (2004) 260 C. Arnaboldi et al., Phys. Rev. Lett. 95 (2005) 14501 C. Arnaboldi et al., Phys. Rev. C, 78, 035502 (2008)

[2] C. Arnaboldi et al., NIM A518 (2004) 775, C. Arnaboldi et al. Astroparticle Physics 20 (2003) 91-110

[3] CUORE Collaboration, LNGS Annual Report 2006.

[4] CUORE Collaboration, LNGS Annual Report 2006.

DAMA. Dark Matter Search

Collaboration:

P. Belli[a], R. Bernabei[a,@], A. Bussolotti[a,*], F. Montecchia[a], F. Nozzoli[a], A. d'Angelo[b], F. Cappella[b], A. Incicchitti[b], A. Mattei[b,*], D. Prosperi[b], M. Cini[c], R. Cerulli[c], C.J. Dai[d], H.L. He[d], H.H. Kuang[d], J.M. Ma[d], X.H. Ma[d], X.D. Sheng[d], Z.P. Ye[d,e], R.G. Wang[d], Y.J. Zhang[d]

in neutron measurements: M.Angelone[f], P.Batistoni[f], M.Pillon[f]

in some by-product results and small scale experiments: R.S. Boiko[g], V.B. Brudanin[h], F.A. Danevich[i], S. d'Angelo[a], A.E. Dossovitskiy[j], B.V. Grinyov[k], V.I. Goriletsky[k], V.V. Kobychev[i], G.P. Kovtun[l], B.N. Kropivyansky[i], M. Laubenstein[c], A.L. Mikhlin[j], V.M. Mokina[i], L.L. Nagornaya[k], P.G. Nagornyi[g] S.S. Nagorny[i], S. Nisi[c] D.V. Poda[i], R.B. Podvujanyuk[i], A. P. Shcherban[l], O.G. Shkulkova[i], D. A. Solopikhin[l], A.V. Tolmachev[m], V.I. Tretyak[i], I.A. Tupitsyna[k], V. D. Virich[l], R.P. Yavetskiy[m], S.S. Yurchenko[i], I.M. Vyshnevskyi[i]

in some studies on $\beta^+\beta^+$, EC/β^+, EC/EC decay modes (under the joint Indo-Italian DST-MAE project): P.K. Raina[n], A.K. Singh[n], P.K. Rath[n], A. Shukla[n]

[a]Dip. di Fisica, Università "Tor Vergata" and INFN-Roma Tor Vergata, Roma, Italy.
[b]Dip. di Fisica, Università di Roma "La Sapienza" and INFN-Roma, 00185 Roma, Italy.
[c]Laboratorio Nazionale del Gran Sasso, INFN, 67010 Assergi (Aq), Italy.
[d]IHEP, Chinese Academy, P.O. Box 918/3, Beijing 100039, China.
[e]Physics Dept, Jing Gangshan University 343009, Jiangxi, China.
[f]ENEA - C. R. Frascati, P.O. Box 65, 00044 Frascati, Italy.
[g]Chemical Dept., Kiev National Taras Shevchenko University, Kiev, Ukraine.
[h]Joint Institute for Nuclear Research,141980 Dubna, Russia.
[i]Institute for Nuclear Research, 252650 Kiev, Ukraine.
[j]Joint stock company NeoChem,117647 Mosckow, Russia.
[k] Institute for Scintillation Materials, 61001 Kharkiv, Ukraine.
[l]National Science Center Kharkiv Institute of Phys. and Tech., Kharkiv, Ukraine.
[m] Institute for Single Crystals, 61001 Kharkov, Ukraine.
[n]Indian Institute of Technology, Kharagpur, India.

@ Spokesperson
* technical staff

Abstract

DAMA is an observatory for rare processes and it is operative deep underground at the Gran Sasso National Laboratory of the I.N.F.N. (LNGS). The main experimental set-ups are: i) DAMA/NaI ($\simeq$ 100 kg of highly radiopure NaI(Tl)), which completed its data taking on July 2002, while various data analyses have continued; ii) DAMA/LXe ($\simeq$ 6.5 kg liquid Kr-free Xenon enriched either in ^{129}Xe or in ^{136}Xe); iii) DAMA/R&D, devoted to tests on prototypes and to small scale experiments, mainly on the investigations of double beta decay modes in various isotopes; iv) the second generation DAMA/LIBRA set-up ($\simeq$ 250 kg highly radiopure NaI(Tl)) in operation since March 2003; v) the low background DAMA/Ge detector mainly devoted to sample measurements. In some measurements on rare processes the low-background Germanium detectors of the LNGS facility are also used. Moreover, a third generation R&D is in progress towards a possible 1 ton set-up, DAMA proposed in 1996. In the following main arguments on the activity developed during 2008 are summarized.

1 DAMA/NaI

The highly radio-pure DAMA/NaI set-up [1, 2, 3, 4] has been a pioneer Dark Matter experiment of suitable exposed mass, sensitivity and stability of the running conditions, taking data at LNGS over seven annual cycles. The data taking has been completed on July 2002 and results are still produced by various kinds of studies.

The main aim of DAMA/NaI has been the investigation of the presence of Dark Matter (DM) particles in the galactic halo by exploiting the DM model independent annual modulation signature (see refs. [1, 2, 3, 4, 5, 6, 7, 8, 9, 10, 11, 12, 13, 14] and the 2008 publication list), originally suggested by [15, 16] in the middle of 80's. In addition, profiting from its low-background features and from the high collected exposure, several results have been achieved both on Dark Matter particle investigations with other approaches and on several other rare processes [17, 18, 19, 20, 21, 22, 23, 24, 25, 26].

The DAMA/NaI set-up has pointed out the presence of an annual modulation in the *single-hit* residual rate in the lowest energy interval (2 – 6) keV, which satisfies the many peculiarities of a DM particle induced effect. The presence of DM particles in our Galaxy is supported at 6.3 σ C.L. over seven annual cycles (total exposure: 107731 kg $\times$ day; see refs. [2, 3, 4, 5, 6, 7, 8, 9, 10, 11, 12, 13, 14] and in the 2008 publication list). No systematic effects or side reactions able to account for the observed effect (that is able to account for the whole observed modulation amplitude and to contemporaneously satisfy all the many peculiarities of the signature) have been found or suggested by anyone over more than a decade.

This result is model-independent and gives experimental evidence for the presence of DM particles in the galactic halo. At present, apart from DAMA/LIBRA, no other experiment is sensitive to such a DM model independent signature and using the same target material and procedures (mass, radiopurity, full control of the stability, etc.); thus, no other activity is available whose result can directly be compared in a model independent way with the one by DAMA/NaI.

On the basis of the obtained 6.3 σ C.L. model-independent result, corollary investigations can also be pursued on the nature of the DM particle candidate. This latter investigation is instead model-dependent and – considering the large uncertainties which exist on the astrophysical, nuclear and particle physics assumptions and on the theoretical and experimental parameters needed in the calculations – has no general meaning (as it is also the case of exclusion plots and of the DM particle parameters evaluated in indirect detection activities).

For simplicity, the results of the corollary analyses are presented in terms of allowed volumes/regions obtained as superposition of the configurations at given C.L. for the considered model frameworks (see e.g. ref. [3, 4, 12, 13, 14] and the 2008 publication list); thus, each one accounts for a large set of best fit values. The results briefly summarized here and the several other ones available in literature are not exhaustive at all of the many scenarios possible at present level of knowledge.

For the case of WIMP class candidates[1], it has been considered so far – in some of the many possible astrophysical, nuclear and particle physics frameworks – low (of order of few GeV) and high mass (up to many hundreds of GeV) candidates interacting with ordinary matter via: i) mixed SI&SD coupling; ii) dominant SI coupling; iii) dominant SD coupling; iv) preferred SI inelastic scattering. A detailed discussion on the volumes/regions allowed by the DAMA/NaI data for some WIMP candidates in some given model frameworks can be found in ref. [3, 4]. This analysis has also been extended in ref. [13] by including the possible effect of the presence of a non thermalized DM particle component in the dark halo due to the Sagittarius Dwarf Elliptical Galaxy, SagDEG. The effect of other possible non-thermalized substructures will be addressed in future.

Among the related theoretical works we just remind for the neutralino case ref. [27]. Moreover, among the many other possibilities which exist, considering the existing literature, we remind just the Light Dark Matter particles or particles in the MeV scale, the light ($\simeq$ keV mass) bosonic candidate (either with pseudoscalar or with scalar axion-like coupling), the sneutrino in various SUSY scenarios, the Kaluza Klein particles from theories with extra dimensions, the electron-interacting DM, the mirror matter, the heavy neutrinos, the keV scale sterile neutrino, the axino, the gravitino, the moduli fields, the majorons, the familons, the self-interacting dark matter particles, the elementary black holes such as e.g. the Daemons, etc., and in principle whatever particle with suitable characteristics, even not yet foreseen by theories.

Obviously candidates which give part or all the signal in electromagnetic channels can be detected in DAMA/NaI (and DAMA/LIBRA, see later), but are lost in activities applying rejection procedures of the electromagnetic contribution to the counting rate (such as e.g. Cdms, Edelweiss, Cresst, Warp, Xenon10, etc.).

We remind that various corollary analyses, considering some of the many possible astrophysical, nuclear and particle Physics scenarios, have been analysed by DAMA itself [12, 3, 4, 13, 28, 29, 30], while several others are also available in literature, such as e.g. refs. [31, 32, 33, 34, 35, 36, 37, 38, 39, 40, 41, 42, 43, 44, 45, 46, 47, 48, 49, 50, 51].

During 2008 three main topics have been published:

[1]It is worth noting that, to this class belong many particles having a phenomenology similar, but not identical. Each one has its own peculiarities as regards the interaction.

- the effect of the channeling effect of low energy ions along the crystallographic axes and planes of NaI(Tl) crystals. This effect implies a more complex evaluation of the luminosity yield for low energy recoiling Na and I ions.

- the DM candidate particles – foreseen by some extensions of the Standard Model – which have a dominant coupling with the lepton sector of the ordinary matter. Thus, these candidates can be directly detected only through their interaction with electrons.

- the light Dark Matter candidates with sub-GeV mass provided by some extensions of the Standard Model.

The first two items have already been addressed in the LNGS activity report 2007 and will not discussed again here, while in the following just the third item will be summarized.

1.1 Investigation on light Dark Matter

Some extensions of the Standard Model provide Dark Matter (DM) candidate particles with sub-GeV mass; in the following these candidates will be indicated as Light Dark Matter (LDM).

LDM particles have been considered for example in Warm Dark Matter scenarios such as e.g. keV-scale sterile neutrino, axino or gravitino. In addition, MeV-scale particles (e.g. axino, gravitino, heavy neutrinos, moduli fields from string theories, *Elko* fermions) have been proposed as DM particles and as possible source of 511 keV gamma's from the Galactic center, due either to DM annihilation or to decay in the bulge. Moreover, also supersymmetric models exist where the Lightest Supersymmetric Particle naturally has a MeV-scale mass and the other phenomenological properties, required to generate the 511 keV gammas in the galactic bulge. A wide literature is available on all these candidates, see e.g. references quoted in the devoted paper in the 2008 publication list.

Since the kinetic energy of LDM particles in the galactic halo does not exceed hundreds eV, the elastic scattering of such LDM particles both on electrons and on nuclei yields energy releases well below the energy thresholds of the detectors used in the field of DM direct detection. Thus, this prevents the exploitation of the elastic scattering as detection approach for these candidates, while the inelastic process is the only possible exploitable one for the direct detection of LDM.

The following process is, therefore, considered for detection (see Fig. 1): the LDM candidate (hereafter named ν_H with mass m_H and 4-momentum k_μ) interacts with the ordinary matter target, T, with mass m_T and 4-momentum p_μ. The target T can be either an atomic nucleus or an atomic electron depending on the nature of the ν_H particle interaction. As a result of the interaction a lighter particle is produced (hereafter ν_L with mass $m_L < m_H$ and 4-momentum k'_μ) and the target recoils with an energy E_R, which can be detectable by suitable detectors. The lighter particle ν_L is neutral and it is required that it interacts very weakly with ordinary matter; thus, the ν_L particle escapes the detector. In particular, the ν_L particle can also be another DM halo component (dominant or sub-dominant with respect to the ν_H one), or it can simply be a Standard Model particle.

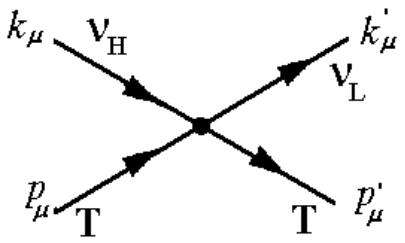

Figure 1: Inelastic scattering process considered for the detection of the Light Dark Matter candidate. The 4-momenta are defined in the laboratory frame. The target T can be either an atomic nucleus or an atomic electron.

Since $m_H > m_L$, it is important to require that the lifetime of the possible decay of the ν_H particle is longer than the age of the Universe. We also note that the detection process of Fig. 1 also offers a possible (unavoidable) decay channel of ν_H into ν_L and $T\bar{T}$ pair if $m_H > m_L + 2m_T$. Finally, due to the presence of the ν_L particle in the final state, the LDM can be either a boson or a fermion.

Assuming the target at rest before the scattering and the non-relativistic nature of the LDM particle and defining $\Delta = m_H - m_L$ the mass splitting of the ν_H-ν_L particle system, the recoil energy of the target for the process of Fig. 1 can be evaluated.

In order to offer to the reader just a view of the detectability of LDM particles, Fig.2 shows some examples of the configurations in the plane Δ vs m_H (shaded areas).

The interaction rate of the LDM particle with the target T for the studied process can be evaluated (see the paper in the 2008 publication list for details) and the expected signal is given by the sum of two contributions: one independent on the time and the other one dependent on the time through $cos(\omega(t - t_0))$, where $\omega = 2\pi/T$ with T= 1 year and with relative amplitude depending on the adopted scenario.

As regards the interaction with atomic electrons, after the interaction the final state can have – beyond the ν_L particle – either a prompt electron and an ionized atom or an excited atom plus possible X-rays/Auger electrons. Therefore, the process produces X-rays and electrons of relatively low energy, which are mostly contained with efficiency $\simeq 1$ in a detector of a suitable size.

Considering the case of a crystal detector target (as e.g. the NaI(Tl)), the possible channeling effect [29] has also to be taken into account. The detection of a nuclear recoil of kinetic energy, E_R, is, in particular, related to the response function $\frac{dN_T}{dE_{det}}(E_{det}|E_R)$ [29], where E_{det} is the released energy in keV electron equivalent. Thus, finally, as for the electron interacting LDM, the expected differential rate is given by the sum of two contributions: $\frac{dR_T}{dE} = S_0 + S_m \cdot cos\omega(t - t_0)$, where S_0 and S_m are the unmodulated and the modulated part of the expected differential counting rate, respectively.

In NaI(Tl) detectors, both Na and I nuclei ($\eta_{Na} = \eta_I \simeq 4 \times 10^{24}$ kg^{-1}) can contribute to the detection of LDM. Therefore, the total expected counting rate is given by the sum of two contributions, arising from the two nuclei species (T = Na, I). Generally, the target cross section σ can be a function of v, depending on the peculiarity of the particle interaction. In the following, we adopt a widely considered approximation for the

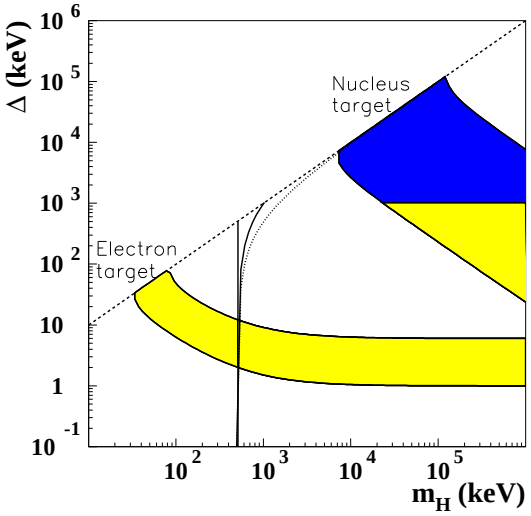

Figure 2: Examples of configurations in the plane Δ vs m_H (shaded areas); they correspond to released energies in NaI(Tl) within the energy interval 1-6 keV electron equivalent. The upper area is due to LDM interaction on Na and I nuclear targets, while the lower area to LDM interaction on electron target. The dashed line ($m_H = \Delta$) marks the case where ν_L is a massless particle or also a very light particle. The configurations characterized by $\Delta \geq 2m_e$ (dark area) are of interest for the positron annihilation line from the galactic center through the decay: $\nu_H \to \nu_L e^+ e^-$. The thresholds of the possible annihilation processes: $\nu_H \bar{\nu}_H \to e^+ e^-$ (solid vertical line at $m_H = 511$ keV); $\nu_H \bar{\nu}_L \to e^+ e^-$ (solid curve); $\nu_L \bar{\nu}_H \to e^+ e^-$ (solid curve); $\nu_L \bar{\nu}_L \to e^+ e^-$ (dotted curve) are shown.

non-relativistic case:

$$\sigma v \simeq a + b v^2 \ . \tag{1}$$

There a and b are constant and depend on the peculiarity of the particle interaction with the target T; they will be considered as free parameters in the description of the process. In order to deal the direct detection process with more usual parameters, the cross sections $\sigma_0 = \frac{a}{v_0}$ and $\sigma_m = b v_0$ will be used as free parameters; they are related to the a and b parameters rescaled with the Dark Matter local velocity, v_0. The cross section parameters σ_0 and σ_m for Na and I are related with some model dependent scaling laws; in particular the two illustrative cases of coherent ($\sigma^{coh} \simeq \frac{\sigma^{Na}}{A^2_{Na}} \simeq \frac{\sigma^I}{A^2_I}$) and incoherent ($\sigma^{inc} \simeq \sigma^{Na} \simeq \sigma^I$) nuclear scaling laws have been investigated. As template purpose, in Fig. 3, the expected energy distributions of the unmodulated/modulated part of the differential rate in NaI(Tl) are shown for interactions of LDM with $m_H = 100$ MeV on the target nuclei in some different cases. It is worthwhile to note that similar behaviors can also be obtained by using other choices of the halo model, quenching factors and values of the masses of the involved particles in the interaction.

In the following corollary analyses, the same dark halo models and related parameters given in table VI of ref. [3] have been considered. However, although a large number of self-consistent galactic halo models has been considered, still many other possibilities exist.

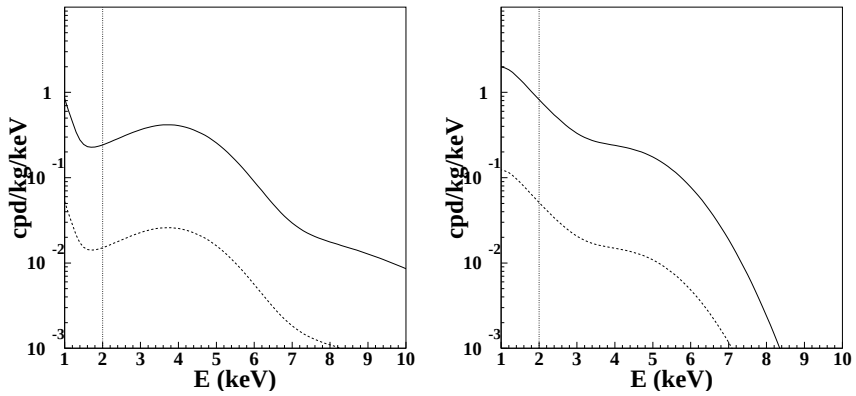

Figure 3: Examples of the energy distributions of the unmodulated (solid) and of the modulated (dotted) parts of the expected differential rate in NaI(Tl) for interactions of LDM with $m_H = 100$ MeV on the target nuclei. *Left:* case of coherent cross section scaling laws; here $\Delta = 4.8$ MeV and $\xi\sigma_0^{coh} \ll \xi\sigma_m^{coh} \simeq 2 \times 10^{-6}$ pb. *Right:* case of incoherent cross section scaling laws; here $\Delta = 0.95$ MeV and $\xi\sigma_0^{inc} \ll \xi\sigma_m^{inc} \simeq 20 \times 10^{-3}$ pb. The A5 halo model (a NFW halo model with local velocity equal to 220 km/s and density equal to the maximum value, see ref. [3, 4]) has been considered. The quenching factors have been assumed as the case A of ref. [3, 4]. The channeling effect has been included. The vertical dotted lines correspond to the energy threshold of the NaI(Tl) detectors considered in DAMA/NaI set-up.

As regards the case of LDM interacting on nuclei, also the Na and I quenching factors [3] and the Na and I channeling response functions given in [29] have been considered. The uncertainties on the Na and I quenching factors have been taken into account as done in ref. [3]. In addition, the presence of the Migdal effect and of the possible SagDEG contributions – we discussed in [28, 13], respectively – has not yet included here for simplicity.

As regards the cross section parameters, the σ_0 terms do not contribute to the annual modulation of the signal. In particular, the measured modulation amplitude easily allows to derive $\sigma_0 \lesssim \sigma_m$. For simplicity, the contributions of the σ_m terms are assumed to be dominant with respect to the contributions of the σ_0 ones.

The results are calculated by taking into account the time and energy behaviours of the *single-hit* experimental data through the standard maximum likelihood method. In particular, they are presented in terms of slices of the three-dimensional allowed volume (m_H, Δ, $\xi\sigma_m$) – where σ_m is alternatively σ_m^e, σ_m^{coh} and σ_m^{inc} – obtained as superposition of the configurations corresponding to likelihood function values *distant* more than 4σ from the null hypothesis (absence of modulation) in each one of the several (but still a very limited number) of the considered model frameworks.

The projection of the whole 4σ allowed volume on the plane (m_H, Δ) gives typical patterns similar as those reported in Fig. 2. Moreover, since the two regions are disconnected, the LDM detection is always dominated by only one of the different target contributions. Therefore, slices of the allowed volume either for electron interacting LDM

or nucleus interacting LDM are presented separately.

In case of electron interacting LDM, the projection of the 4σ allowed volume on the plane (m_H, Δ) for the same dark halo models and parameters described in ref. [3] is reported in Fig. 4 (left). The allowed m_H values and the splitting Δ are in the intervals

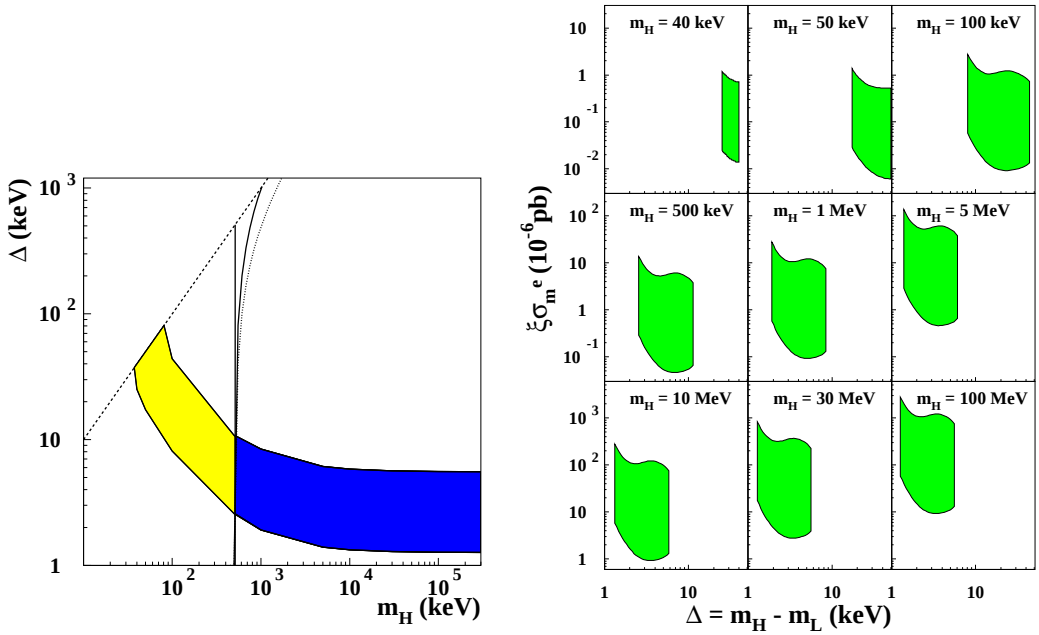

Figure 4: Case of electron interacting LDM. *Left:* Projection of the 4σ allowed 3-dimensional volume on the plane (m_H, Δ) for the same dark halo models and parameters described in ref. [3]. The dashed line ($m_H = \Delta$) marks the case where ν_L is a massless particle. The decay through the detection channel, $\nu_H \to \nu_L e^+ e^-$, is energetically not allowed for the selected configurations. The configurations with $m_H \gtrsim m_e$ (dark area) are interesting for the possible annihilation processes: $\nu_H \bar{\nu}_H \to e^+ e^-$, $\nu_H \bar{\nu}_L \to e^+ e^-$, $\nu_L \bar{\nu}_H \to e^+ e^-$, and $\nu_L \bar{\nu}_L \to e^+ e^-$ in the galactic center. The three nearly vertical curves are the thresholds of these latter processes as mentioned in the caption of Fig. 2. *Right:* examples of some slices of the 4σ allowed 3-dimensional volume for various m_H depicted in the ($\xi\sigma_m^e$ vs Δ) plane.

35 keV $\lesssim m_H \lesssim$ O(GeV) and 1 keV $\lesssim \Delta \lesssim$ 80 keV, respectively. It is worth to note that in such a case the decay through the detection channel: $\nu_H \to \nu_L e^+ e^-$, is energetically forbidden for the given Δ range. The configurations with $m_H \gtrsim 511$ keV (dark area in Fig. 4 (left)) are instead of interest for the possible annihilation processes: $\nu_H \bar{\nu}_H \to e^+ e^-$, $\nu_H \bar{\nu}_L \to e^+ e^-$, $\nu_L \bar{\nu}_H \to e^+ e^-$, and $\nu_L \bar{\nu}_L \to e^+ e^-$, in the galactic center.

As examples, some slices of the 3-dimensional allowed volume for various m_H values are depicted in Fig. 4 (right) in the scenario given above.

In case of nucleus interacting LDM, the projections of the 4σ allowed volumes on the plane (m_H, Δ) are reported in Fig. 5 for the two above-mentioned illustrative cases of coherent (*left*) and incoherent (*right*) nuclear scaling laws. They are evaluated for the same

dark halo models and parameters described in ref. [3, 29]. The allowed m_H values and

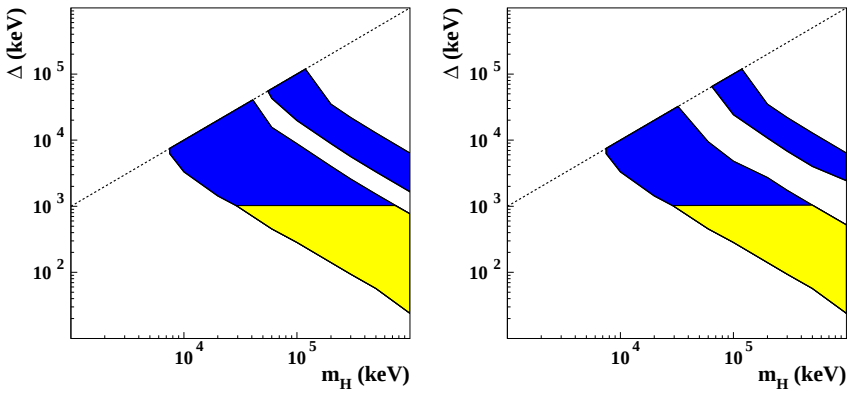

Figure 5: Case of nucleus interacting LDM. Projections of the 4σ allowed 3-dimensional volumes on the plane (m_H, Δ) for the two above-mentioned illustrative cases of coherent (*left*) and incoherent (*right*) nuclear scaling laws. They are evaluated for the same dark halo models and parameters described in ref. [3, 29]. The regions enclose configurations corresponding to likelihood function values *distant* more than 4σ from the null hypothesis (absence of modulation). The dashed lines ($m_H = \Delta$) mark the case where ν_L is a massless particle. The decays through the diagram involved in the detection channel are energetically forbidden.

the splitting Δ are in the intervals 8 MeV $\lesssim m_H \lesssim$ O(GeV)[2] and 25 keV $\lesssim \Delta \lesssim$ 120 MeV, respectively (see Fig. 5).

It is worth to note that for nuclear interacting LDM the 3-dimensional allowed configurations are contained in two disconnected volumes, as seen e.g. in their projections in Fig. 5. The one at larger Δ at m_H fixed is mostly due to interaction on Iodine target, while the other one is mostly due to interaction on Sodium target.

As examples, some slices of the 3-dimensional allowed volumes for various m_H values in the ($\xi\sigma_m$ vs Δ) plane are depicted in Fig. 6 for the two above-mentioned illustrative cases of coherent (*left* panel) and incoherent (*right* panel) nuclear scaling laws.

The allowed phenomenological parameters (masses and cross sections) of LDM can be of interest for various LDM candidates proposed in theories beyond the Standard Model and for the production mechanism of the 511 keV gammas from the galactic bulge.

In conclusion in addition to other candidates, as WIMP/WIMP-like particles and axion-like bosons, already discussed by DAMA collaboration elsewhere [12, 3, 4, 13, 28, 29, 30] there is also possibility for a LDM candidate interacting either with the electrons or with the nuclei to account for the 6.3σ C.L. model independent evidence for the presence of a particle DM component in the galactic halo.

[2]We remind that for m_H values greater than O(GeV) the detection would also be possible through the elastic scattering process [3, 4, 13, 28, 29].

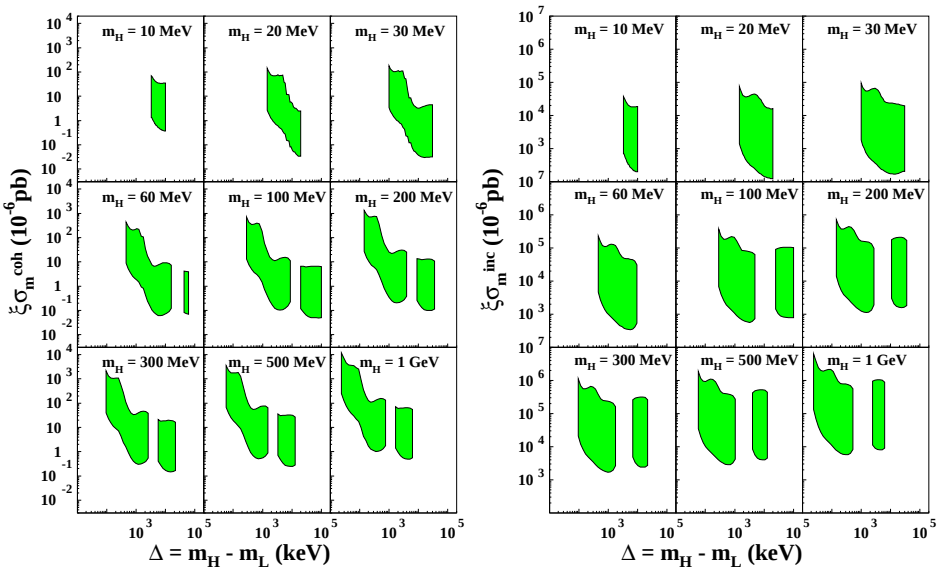

Figure 6: Case of nucleus interacting LDM. Examples of some slices of the 3-dimensional allowed volumes for various m_H values in the ($\xi\sigma_m$ vs Δ) plane for the two above-mentioned illustrative cases of coherent (*left*) and incoherent (*right*) nuclear scaling laws. The 3-dimensional volumes enclose configurations corresponding to likelihood function values *distant* more than 4σ from the null hypothesis (absence of modulation). The same dark halo models and parameters described in ref. [3, 29] have been used.

2 DAMA/LIBRA

In 1996 – while running the DAMA/NaI set-up – DAMA proposed to INFN to develop and to build a one ton set-up to further investigate Dark Matter particles and other rare processes. A second generation R&D project was funded at that time to develop new highly radiopure NaI(Tl) detectors towards the achievement of an intermediate step: the $\simeq$ 250 kg highly radiopure NaI(Tl) DAMA/LIBRA (Large sodium Iodide Bulk for RAre processes) set-up, which is now in data taking.

The DAMA/NaI and the DAMA/LIBRA experiments have the main aim to perform a direct detection of Dark Matter (DM) particles in the galactic halo by exploiting the model independent annual modulation signature. In particular, the DM annual modulation signature exploits the correlation between the Earth velocity in the galactic halo with the number of events induced by DM particles in a suitable low background set-up placed deep underground. In fact, as a consequence of its annual revolution, the Earth should be crossed by a larger flux of DM particles around roughly June 2^{nd} (when its rotational velocity is summed to the one of the solar system with respect to the Galaxy) and by a smaller one around roughly December 2^{nd} (when the two velocities are subtracted). Thus, the contribution of the signal to the counting rate in the k–th energy interval can be written as: $S_k = S_{0,k} + S_{m,k} \cos \omega(t - t_0)$, where: i) $S_{0,k}$ is the constant part of the signal; ii) $S_{m,k}$ is the modulation amplitude; iii) $\omega = \frac{2\pi}{T}$ with period T; iv) t_0 is the phase.

This annual modulation signature is very distinctive since the effect induced by DM particles must simultaneously satisfy all the following requirements: 1) the rate must

contain a component modulated according to a cosine function; 2) with one year period; 3) with a phase roughly around June 2^{nd} in case of usually adopted halo models (slight variations may occur in case of presence of non thermalized DM components in the halo); 4) this modulation must be present only in a well-defined low energy range, where DM particles can induce signals; 5) it must be present only in those events where just a single detector, among all the available ones in the used set-up, actually "fires" (*single-hit* events), since the probability that DM particles experience multiple interactions is negligible; 6) the modulation amplitude in the region of maximal sensitivity has to be $\lesssim 7\%$ in case of usually adopted halo distributions, but it may be significantly larger in case of some particular scenarios such as *e.g.* those of ref.[44]. To mimic such a signature spurious effects or side reactions should be able not only to account for the observed modulation amplitude but also to contemporaneously satisfy all the requirements of the signature; none of these has been found or suggested by anyone over more than a decade.

The corollary question about the nature of the DM particle(s) detected by the annual modulation signature and the related astrophysical, nuclear and particle Physics scenarios requires subsequent model dependent corollary analyses. One should stress that it does not exist any approach to investigate the nature of the candidate in the direct and indirect DM searches which can offer these information independently on assumed astrophysical, nuclear and particle Physics scenarios.

The DAMA/LIBRA set-up, its main features and radiopurity have been discussed in details (see devoted papers in 2008 publication list), while the model independent experimental results obtained by DAMA/LIBRA (exposure of 0.53 ton×yr over 4 annual cycles) and those combined with DAMA/NaI (exposure of 0.29 ton×yr over 7 annual cycles) have been discussed in details (see devoted papers in 2008 publication list) and are shortly reminded in some aspects in the following.

2.1 The model-independent experimental results

DAMA/LIBRA started the first operations in March 2003. The data taking for the investigation of the annual modulation signature has been started on September 9, 2003; this has allowed the decay of medium half-life isotopes. Moreover, it is worth noting that one of the more external detectors has been put out of operation few months after installation because of a PMT break. Since the disinstallation and re-installation of this detector would have required the opening of the set-up, we have delayed this; the related procedure has been performed in September 2008, when an upgrade of the set-up has been realised. Therefore, the exposed mass in the first four annual cycles is 232.8 kg.

A model-independent investigation of the annual modulation signature has been carried out by exploiting the time behaviour of the residual rates of the *single-hit* events in the lowest energy regions. Fig. 7 shows the time behaviour of the model-independent residual rates for *single-hit* events collected by the former DAMA/NaI experiment and by the present DAMA/LIBRA in the (2–4), (2–5) and (2–6) keV energy intervals. The cumulative analysis of the *single-hit* residual rate favours the presence of a modulated cosine-like behaviour with proper features at 8.2 σ C.L.

The same data of Fig. 7 have also been investigated by a Fourier analysis. A clear peak corresponding to a period of 1 year is evident in the lowest (2–6) keV energy interval,

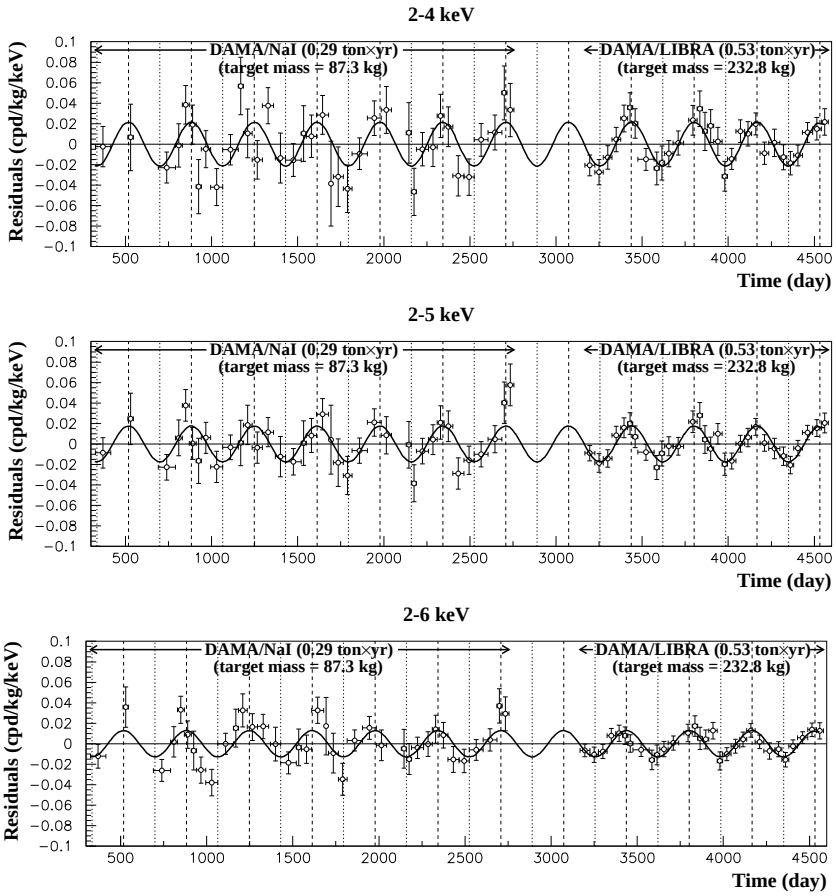

Figure 7: Model-independent residual rate of the *single-hit* scintillation events, measured by DAMA/NaI and DAMA/LIBRA in the (2 – 4), (2 – 5) and (2 – 6) keV energy intervals as a function of the time. The zero of the time scale is January 1^{st} of the first year of data taking of the former DAMA/NaI experiment. The experimental points present the errors as vertical bars and the associated time bin width as horizontal bars. The superimposed curves represent the cosinusoidal functions behaviours $A\cos\omega(t-t_0)$ with a period $T = \frac{2\pi}{\omega} = 1$ yr, with a phase $t_0 = 152.5$ day (June 2^{nd}) and with modulation amplitudes, A, equal to the central values obtained by best fit over the whole data, that is: (0.0215 ± 0.0026) cpd/kg/keV, (0.0176 ± 0.0020) cpd/kg/keV and (0.0129 ± 0.0016) cpd/kg/keV for the (2 – 4) keV, for the (2 – 5) keV and for the (2 – 6) keV energy intervals, respectively. When the period and the phase parameters are released in the fit, values well compatible with those expected for DM particle induced effect are obtained. The dashed vertical lines correspond to the maximum of the signal (June 2^{nd}), while the dotted vertical lines correspond to the minimum. The total exposure is 0.82 ton × yr.

while in the (6 – 14) keV energy interval only aliasing peaks are instead present. Thus, a clear modulation is present in the lowest energy interval, while it is absent just above. In fact, the best fitted modulation amplitude in the (6 – 14) keV energy region is well compatible with zero: (0.0004 ± 0.0010) cpd/kg/keV.

To verify absence of annual modulation in other energy regions and, thus, to also verify the absence of any significant background modulation, the whole energy distribution has been investigated. In particular, we have investigated the rate integrated above 90 keV, R_{90}, as a function of the time. The result excludes any significant background variation. Moreover, fitting the time behaviour of R_{90} with phase and period as for DM particles, a modulation amplitude compatible with zero is found in each running period: $-(0.05 \pm 0.19)$ cpd/kg, $-(0.12 \pm 0.19)$ cpd/kg, $-(0.13 \pm 0.18)$ cpd/kg, and (0.15 ± 0.17) cpd/kg for DAMA/LIBRA-1 to -4 annual cycles, respectively. This excludes the presence of a background modulation in the whole energy spectrum at a level much lower than the effect found in the lowest energy region for the *single-hit* events; in fact, otherwise – considering the R_{90} mean values – a modulation amplitude of order of tens cpd/kg, that $\simeq 100\sigma$ far away from the measured value, would be present.

A further relevant investigation has been done by applying the same hardware and software procedures, used to acquire and to analyse the *single-hit* residual rate, to the *multiple-hits* one. In fact, since the probability that a DM particle interacts in more than one detector is negligible, a DM signal can be present just in the *single-hit* residual rate. Thus, this allows the test of the background behaviour in the same energy interval of the observed positive effect. We remind that similar investigations have already been performed for the last two annual cycles of the DAMA/NaI experiment. Thus, in Fig. 8 the residual rates of the *single-hit* events measured over the four DAMA/LIBRA annual

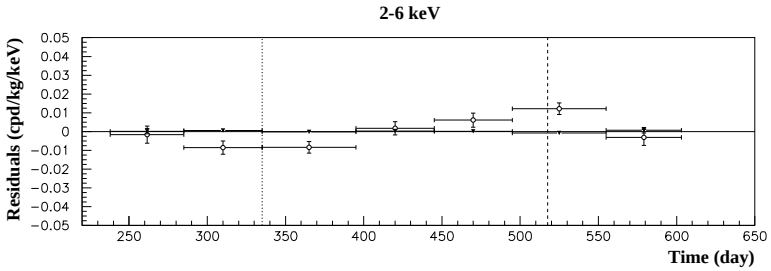

Figure 8: Experimental residual rates over the four DAMA/LIBRA annual cycles for *single-hit* events (open circles) – class of events to which DM events belong – and for *multiple-hits* events (filled triangles) – class of events to which DM events do not belong – in the (2–6) keV energy intervals. They have been obtained by considering for each class of events the data as collected in a single annual cycle and by using in both cases the same identical hardware and the same identical software procedures. The initial time of the scale is taken on August 7^{th}. The experimental points present the errors as vertical bars and the associated time bin width as horizontal bars.

cycles are reported, as collected in a single annual cycle, together with the residual rates of the *multiple-hits* events, in the $(2-6)$ keV energy interval. As already observed, a clear modulation is present in the *single-hit* events, while the fitted modulation amplitudes for the *multiple-hits* residual rate are well compatible with zero: $-(0.0004 \pm 0.0008)$ cpd/kg/keV, $-(0.0005 \pm 0.0007)$ cpd/kg/keV, and $-(0.0004 \pm 0.0006)$ cpd/kg/keV in the energy regions $(2-4)$, $(2-5)$ and $(2-6)$ keV, respectively. Thus, again evidence of annual modulation with proper features as required by the DM annual modulation signature is

present in the *single-hit* residuals (events class to which the DM particle induced events belong), while it is absent in the *multiple-hits* residual rate (event class to which only background events belong). Since the same identical hardware and the same identical software procedures have been used to analyse the two classes of events, the obtained result offers an additional strong support for the presence of a DM particle component in the galactic halo further excluding any side effect either from hardware or from software procedures or from background.

The annual modulation present at low energy can also be shown by depicting the differential modulation amplitudes, $S_{m,k}$ values, as a function of the energy, obtained by maximum likelihood method considering T =1 yr and t_0 = 152.5 day (see Fig. 9). Positive signal is present in the (2–6) keV energy interval, while $S_{m,k}$ values are compatible

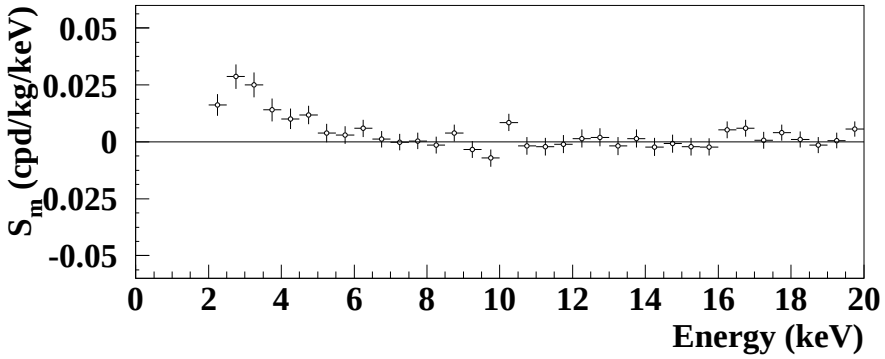

Figure 9: Energy distribution of the $S_{m,k}$ variable for the total exposure (0.82 ton×yr, DAMA/NaI & DAMA/LIBRA). A clear modulation is present in the lowest energy region, while $S_{m,k}$ values compatible with zero are present just above. In fact, the $S_{m,k}$ values in the (6–20) keV energy interval have random fluctuations around zero with χ^2 equal to 24.4 for 28 degrees of freedom.

with zero just above. It has also been verified that the measured modulation amplitudes are statistically well distributed in all the crystals, in all the annual cycles and in the energy bins. In a subsequent analysis, the assumption of the phase t_0 = 152.5 day in the maximum likelihood procedure has been released, alternatively writing the signal as: $S_k = S_{0,k} + S_{m,k} \cos\omega(t - t_0) + Z_{m,k} \sin\omega(t - t_0) = S_{0,k} + Y_{m,k} \cos\omega(t - t^*)$. Fig. 10 (left) shows the 2σ contours in the plane (S_m, Z_m) for the (2–6) keV and (6–14) keV energy intervals and Fig. 10 (right) shows, instead, those in the plane (Y_m, t^*). These results confirm those achieved above by analysing the residuals. In particular, a modulation amplitude is present in the lower energy intervals and the period and the phase agree with those expected for DM induced signals.

In conclusion, also the data of the first four annual cycles of DAMA/LIBRA as previously those of DAMA/NaI fulfil all the requirements of the DM annual modulation signature. As previously done for DAMA/NaI, careful investigations on absence of any significant systematics or side reaction effect have been performed. No modulation has been found in any possible source of systematics or side reactions for DAMA/LIBRA as well; thus, cautious upper limits (90% C.L.) on the possible contributions to the DAMA/LIBRA measured modulation amplitude have been estimated. In addition, it

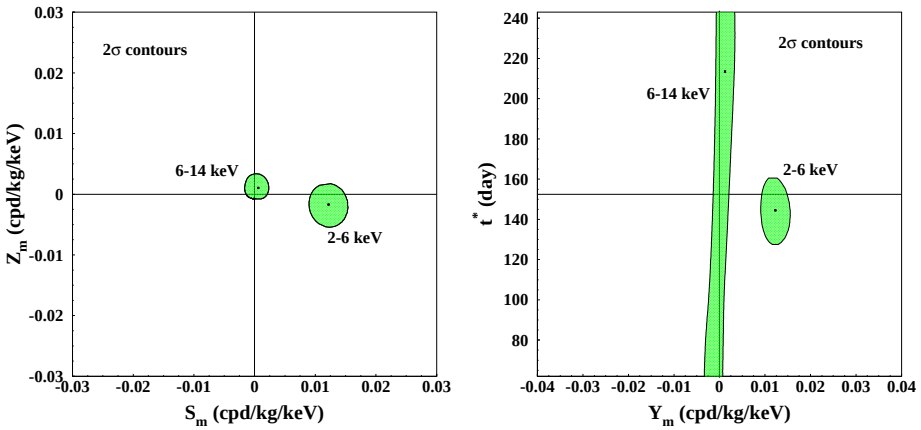

Figure 10: 2σ contours in the plane (S_m, Z_m) (*left*) and in the plane (Y_m, t^*) (*right*) for the (2–6) keV and (6–14) keV energy intervals. The contours have been obtained by the maximum likelihood method, considering the seven annual cycles of DAMA/NaI and the four annual cycles of DAMA/LIBRA all together. The best fit values for the (2–6) keV energy interval are (1σ errors): $S_m = (0.0122 \pm 0.0016)$ cpd/kg/keV; $Z_m = -(0.0019 \pm 0.0017)$ cpd/kg/keV; $Y_m = (0.0123 \pm 0.0016)$ cpd/kg/keV; $t^* = (144.0 \pm 7.5)$ day; while for the (6–14) keV energy interval are: $S_m = (0.0005 \pm 0.0010)$ cpd/kg/keV; $Z_m = (0.0011 \pm 0.0012)$ cpd/kg/keV; $Y_m = (0.0012 \pm 0.0011)$ cpd/kg/keV and t^* obviously not determined.

is worth stressing that neither systematics nor side reaction effect – able to contemporaneously satisfy all the requirements of the signature and to account for the measured modulation amplitude – have been found or suggested by anyone over more than a decade [3]. For detailed quantitative discussions on all the related topics and for results see 2008 publication list and refs. therein.

2.2 Comparison in the field

No other experiment exists, whose result can be directly compared in a model-independent way with those by DAMA/NaI and DAMA/LIBRA. In particular, let us also point out that results obtained with different target materials and/or different approaches cannot intrinsically be directly compared among them even when considering the same kind of candidate and of coupling, although apparently all the presentations generally refer to cross section on nucleon.

In particular, as discussed in the previous LNGS report 2007, claims for contradictions made by experiments insensitive to the DM annual modulation signature, using differ-

[3] We take this occasion to also point out to the attention of the reader that e.g. the DM annual modulation indeed is not a "seasonal" variation and it is not a "winter-summer" effect, as sometimes naively mentioned. In fact, the DM annual modulation is not related to the relative Sun position, but it is related to the Earth velocity in the galactic frame. Thus, in particular, the phase of the DM annual modulation (roughly 2^{nd} June) is well different than those of physical quantities (such as temperature of atmosphere, pressure, other meteorological parameters, cosmic rays flux, ...) instead correlated with seasons.

ent target materials and approaches, exploiting marginal exposures, having well different sensitivities to various DM candidate and interactions, etc. have by the fact no impact even in the single arbitrary scenario they consider without accounting for experimental and theoretical uncertainties, for the many different possibilities and using often crude approximation in the calculation, etc. Moreover, as pointed out (see in the 2008 publication list and in the bibliography), some critical points exist on relevant experimental aspects (energy threshold, energy scale, multiple selection procedures, stabilities, etc.). A relevant argument is also the methodological robustness [52].

It is worth noting that, whenever an experiment using the same identical target material and methodological approach would be available in future, as usual in whatever field of Physics a serious comparison would require – in every case – e.g. a deep investigation of the radiopurity of all the part of the different set-ups, of their specific performances in all the aspects, of the detailed procedures used by each one, of the used exposures, etc.

Finally, as regards the indirect detection searches, let us stress that also no direct model-independent comparison can be performed between the results obtained in direct and indirect activities, since it does not exist a biunivocal correspondence between the observables in the two kinds of experiments. Anyhow, if possible excesses in the positron to electron flux ratio and in the γ rays flux with respect to some simulations of the hypothesized contribution, which is expected from standard sources, might be interpreted in terms of Dark Matter (but e.g. available more complete handling of some aspects of the simulations [53] and the pulsars contribution [54] should be included), this would also be not in conflict with the effect observed by DAMA experiments.

2.3 Conclusions, performed and foreseen upgradings

The model independent results achieved by the second generation DAMA/LIBRA set-up confirms the former DAMA/NaI result; in particular, considering the DAMA/NaI and the DAMA/LIBRA data (total exposure 0.82 ton$\times$yr), the presence of Dark Matter particles in the galactic halo is supported at 8.2 σ C.L.. Deep quantitative analyses exclude any effect either from systematics or from side processes able to account for the observed modulation amplitude and to contemporaneously satisfy all the requirements of the signature.

Corollary investigations on the nature of the DM candidate particle and on related astrophysical, nuclear and particle Physics scenarios are instead model-dependent and – considering the large uncertainties which exist on the astrophysical, nuclear and particle physics assumptions and on the theoretical and experimental parameters needed in the calculations – have no general meaning (as it is also the case of exclusion plots and of the DM particle parameters evaluated in indirect detection experiments).

During September 2008 the first upgrading of the DAMA/LIBRA set-up has been realized and the shield has been opened in HP Nitrogen atmosphere. This has allowed the increase of the exposed mass since one detector has been recovered. Moreover, a new optimization of some PMTs and HVs has been done. Finally, a total replacement of the used transient digitizers with new ones, having better performances, has been realized and a new DAQ with optical fibers has been installed and put in operation. The data

taking has been restarted on October 2008.

In particular, the model independent results achieved by the DAMA/LIBRA set-up has pointed out the relevance to lower the software energy threshold used by the experiment (from the present 2 keV possibly to 1 keV). Thus, the replacement of all the PMTs with other ones with higher quantum efficiency has been approved by INFN-CNS2; this will also improve – as evident – other significant experimental aspects. Efforts are in progress for 2009.

In fact, a larger exposure collected by DAMA/LIBRA (or possibly by DAMA/1ton; see later) and the possible lowering of the 2 keV energy threshold in the data analysis will improve the corollary information on the nature of the DM candidate particle(s) and on the various related astrophysical, nuclear and particle Physics scenarios. Moreover, it will also allow the investigation – with very high sensitivity – of other DM features, of second order effects and of several rare processes other than DM.

3 R&D-III towards DAMA/1ton

A third generation R&D effort towards a possible NaI(Tl) ton set-up has been funded by I.N.F.N.. This new low background NaI(Tl) set-up can act as a "general purpose" experiment (as the previous ones) also allowing to investigate not only other approaches for Dark Matter, but also many other interesting topics in underground Physics having many competitive aspects (see in the LNGS annual report 2007). During 2008 the main design of the mechanical assembling of the detectors, of the shield automated motions and of the calibration system has been defined in the framework of a POR-Abruzzo fellowship, considering a possible location deep underground.

Some other activities have been continued in the light of overcoming the present problems regarding the supplying of high quality NaI and, mainly, TlI powders. Possible purification test, whose achievements however strongly depend on the initial radiopurity of the powders, has been considered at some extent.

4 DAMA/LXe

We pointed out many years ago (see e.g. ref. [55]) the possible interest in using the liquid Xenon as target-detector material for particle dark matter investigations. Since the end of 80's (former Xelidon experiment of the INFN) we have realized several liquid Xenon (LXe) prototype detectors and, then, we have preliminarily put in measurement the set-up used in the data taking of ref. [56, 57] at LNGS. This set-up (having a Cu inner vessel filled by $\simeq$ 6.5 kg - i.e. $\simeq$ 2 l - of liquid Xenon) was firstly upgraded at fall 1995 [58, 59, 60, 61, 62]. At that time it used Kr-free Xenon enriched in ^{129}Xe at 99.5%. Then, in 2000 the set-up was deeply modified reaching the configuration of ref. [63] in order to handle also Kr-free Xenon enriched in ^{136}Xe at 68.8%. The main features of the set-up, details on the data acquisition, on the cryogenic and vacuum systems and on the running parameters control can be found in refs. [61, 62, 63, 64, 65]. Investigations on several rare processes have been carried out with time passing in the various configurations (as well as measurements at low energies both with neutron source and with neutron beams by using

a reference detector) [56, 57, 58, 59, 60, 61, 62, 63, 66, 64, 67, 68, 69, 70] In particular, first and/or competing results have been obtained on some approaches for Dark Matter investigations, on double beta decay modes in ^{136}Xe and ^{134}Xe, on possible charge non-conserving processes, on nucleon, di-nucleon and tri-nucleon decay into invisible channels both in ^{129}Xe and in ^{136}Xe.

On the contrary of the NaI(Tl) case, plans for enlarging the exposed mass have never been considered because of the technical reasons (specific of liquid noble gas detectors and, in particular, of liquid xenon detectors), we pointed out several times in the past (see e.g. [71]) and confirmed by the features of recent detectors (see in 2008 publication list); moreover, the extremely expensive cost of needed Kr-free (and possibly enriched Xenon) is an additional constraint.

After the forbiddeness of using cryogenic liquids in the underground laboratories, the set-up took data just few months until December 2004; then, it has been put in standby waiting for the restarting of the LNGS cooling water plant and of the local water refrigeration system. We profited from this period to perform several upgrades of the apparatus. Finally, thanks to a new chiller system and to the restoring of the use of water plans deep underground, the DAMA/LXe set-up restarted the data taking in December 2007. During 2008 DAMA/LXe was filled with Xenon enriched in ^{136}Xe and it has continuously taken data focusing in this period the high energy region.

5 DAMA/R&D

The DAMA/R&D installation is a low-background set-up used for measurements on low background prototype scintillators and PMTs realized in various R&D efforts with industries. Moreover, it is regularly used to perform small scale experiments also in collaboration with INR Kiev. This set-up has been upgraded several times. The small scale experiments mainly investigate double beta decay modes in various isotopes; both the active and the passive source techniques have been exploited as well as – sometimes – the coincidence technique.

In 2008 the activity of DAMA/R&D was mainly focused on:

1. Investigation on double beta decay modes in ^{64}Zn with the help of a low background $ZnWO_4$ crystal scintillator.

2. New measurements with a larger $ZnWO_4$ crystal of 0.7 kg mass to improve the sensitivity of the experiment to $\varepsilon\beta^+$ decay of ^{64}Zn up to the level of 10^{21} y.

3. New measurements with a $ZnWO_4$ crystal with much better light output to more carefully explore the low energy part of the $ZnWO_4$ energy spectrum, where the $2\nu 2K$ process in ^{64}Zn is expected. Other future improvements are under studies.

4. Search for 2β decay modes in ^{108}Cd and ^{114}Cd by using the data collected in a low-background experiment with a $CdWO_4$ crystal scintillator.

5. Preparation of a new experiment on double beta decay modes of ^{106}Cd by further purifying and depleting from the ^{113}Cd the $\simeq$ 150 g of enriched Cadmium, made available by the INR group.

6. Design of new measurements with low background $CdWO_4$ crystals with Cd enriched in ^{116}Cd as preliminary feasibility study for future measurements able to reach a sensitivity for the $2\beta0\nu$ decay of ^{116}Cd at level at least of 10^{24} yr.

7. Preliminary works for next measurements with new prototypes.

Some of the obtained results are summarized in the following.

5.1 Search for 2β decay in Zinc and Tungsten with the help of low-background $ZnWO_4$ crystal scintillators

Searches for $2\beta^+$ decays, processes with emission of two positrons (or $\varepsilon\beta^+$, electron capture with positron emission; or 2ε, capture of two electrons from atomic shells), are important because they could help to distinguish the mechanism of neutrinoless 2β decay (i.e., if it is due either to the non-zero neutrino mass or to the right-handed admixtures in weak interactions) [72].

The ^{64}Zn isotope is one of the few exceptions among $2\beta^+$ decaying nuclei with a big natural isotopic abundance (48.268%). The mass difference between ^{64}Zn and ^{64}Ni nuclei is 1095.7(0.7) keV and, therefore, both double electron capture (2ε), and electron capture with emission of positron ($\varepsilon\beta^+$) are energetically allowed.

Half-life limits on 2β processes in the decay ^{64}Zn to ^{64}Ni (at 90% C.L.) have been published (see 2008 publication list) and have already been described in the 2007 LNGS report.

In addition to ^{64}Zn, $ZnWO_4$ scintillators contain a few other potentially 2β active isotopes: ^{70}Zn, ^{180}W and ^{186}W. Here new measurements performed with the help of large volume ($0.1 - 0.7$ kg) low background $ZnWO_4$ crystal scintillators are summarized. In this case double beta processes in ^{64}Zn, ^{70}Zn, ^{180}W, and ^{186}W have been searched for.

Two clear, slightly pink colored $ZnWO_4$ crystals produced from single crystals grown by the Czochralski method were used in our experiment. Two batches of zinc oxide from different producers were used to prepare $ZnWO_4$ compounds for the crystal growth. The crystals used for measurements are listed in Table 1. The third scintillator (ZWO-2a) was cut from the large 0.7 kg crystal (ZWO-2).

Table 1: $ZnWO_4$ crystal scintillators used in the present experiments.

Crystal scintillator	Size (mm)	Mass (g)
ZWO-1	$20 \times 19 \times 40$	117
ZWO-2	$\oslash 44 \times 55$	699
ZWO-2a	$\oslash 44 \times 14$	168

The $ZnWO_4$ crystals were alternatively fixed inside a cavity of $\oslash 47 \times 59$ mm in the central part of a polystyrene light-guide 66 mm in diameter and 312 mm in length. The

cavity was filled up with high-pure silicon oil. The light-guide was optically connected on opposite sides by optical couplant to two low radioactive photomultipliers (PMT); the light-guide was wrapped by PTFE reflection tape.

The detector has been installed deep underground in the low background DAMA/R&D set-up. It was surrounded by Cu bricks and sealed in a low radioactive air-tight Cu box continuously flushed with high purity nitrogen gas (stored deeply underground for a long time) to avoid presence of residual environmental Radon. In order to reduce the external background, the Cu box has been surrounded by a passive shield made of 10 cm of high purity Cu, 15 cm of low radioactive lead, 1.5 mm of cadmium and 4/10 cm polyethylene/paraffin. The whole shield has been closed inside a Plexiglas box, also continuously flushed by high purity nitrogen gas.

An event-by-event data acquisition system records the amplitude and the arrival time of the events. Moreover, the sum of the signals from the PMTs was also recorded by a 1 GS/s 8 bit DC270 Transient Digitizer by Acqiris over a time window of 100 μs. To allow a good compromise to handle the data files and taking into account the slow scintillation decay of $ZnWO_4$, 20 MS/s sampling frequency was used during the data taking.

The energy scale and resolution of the $ZnWO_4$ detectors have been measured with ^{22}Na, ^{133}Ba, ^{137}Cs, ^{228}Th and ^{241}Am γ sources. Table 2 summarizes some experimental information.

Table 2: Description of low-background measurements with $ZnWO_4$ crystal scintillators. Time of measurements (t), energy interval of data taking (ΔE), energy resolutions at 662 keV γ line of ^{137}Cs (FWHM), and background counting rates in different energy intervals are specified.

Run	Crystal scintillator	t (h)	ΔE (MeV)	FWHM (%)	Rate (counts/day/keV/kg) in energy interval (MeV)			
					0.2–0.4	0.8–1.0	2.0–2.9	3.0–4.0
1	ZWO-1	1902	0.01–1	11.5	1.93(3)	0.27(1)		
2	ZWO-1	2906	0.05–4	12.6	1.71(2)	0.25(1)	0.0072(7)	0.0003(1)
3	ZWO-2	2130	0.05–4	14.6	1.07(1)	0.149(3)	0.0072(4)	0.00031(7)
4	ZWO-2a	3292	0.01–1	11.0	1.52(2)	0.211(7)		

Knowledge of the radioactive contamination of the $ZnWO_4$ crystals is necessary to describe the background in the energy intervals of the 2β processes in Zn and W. The time-amplitude analysis, the pulse-shape discrimination, and the Monte Carlo simulation were applied in addition to the ICP-MS measurements to reconstruct the measured background spectra of the $ZnWO_4$ detectors, and to estimate their radioactive contamination.

We have found $ZnWO_4$ crystal scintillators extremely radiopure detectors with typical contamination at the level of μBq/kg (^{228}Th and ^{226}Ra), $\leq$ 0.06 mBq/kg (^{210}Po), total activity (U/Th) 0.2–0.4 mBq/kg, $\leq$ 0.4 mBq/kg (^{40}K), $\leq$ 0.05 mBq/kg (^{137}Cs), $\leq$ 0.4 mBq/kg (^{90}Sr–^{90}Y), $\leq$ 0.01 mBq/kg (^{147}Sm), and $\leq$ 3 mBq/kg (^{87}Rb).

There are no peculiarities in the measured energy spectra of the $ZnWO_4$ detectors,

which can be interpreted as double beta decay of Zinc or Tungsten isotopes. Therefore only lower half-life limits have been set.

The response functions of the $ZnWO_4$ detectors for the 2β processes searched for and possible background components in each Run with different detectors were simulated with the help of the GEANT4 code. The initial kinematics of the particles emitted in the decays was generated with the DECAY0 event generator. Details are given in the paper (see 2008 publication list). The energy distributions expected for the $2\nu\varepsilon\beta^+$ and $0\nu\varepsilon\beta^+$ decay of ^{64}Zn, excluded at 90% C.L., are shown in Fig. 11.

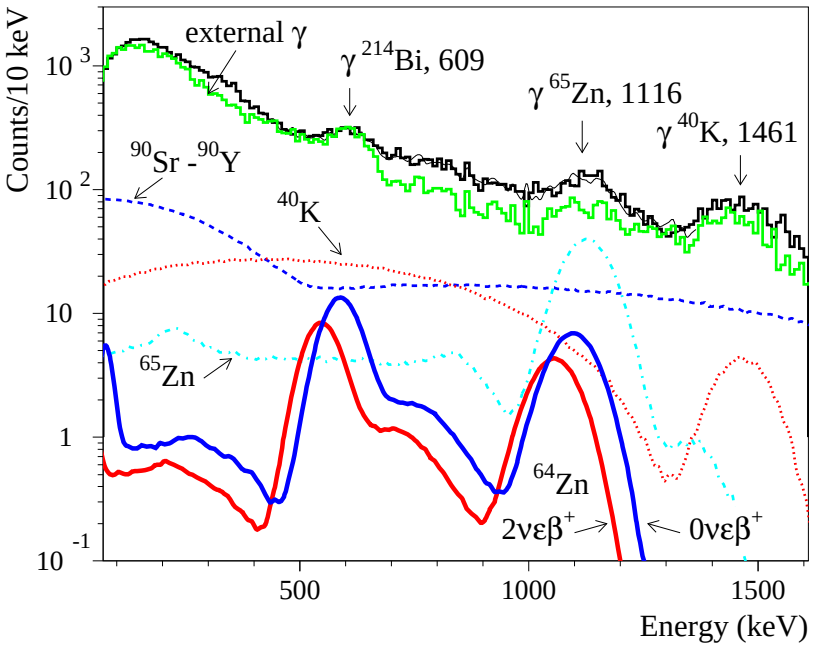

Figure 11: (Color online) The measured energy spectrum of $ZnWO_4$ scintillation crystals (Run 2 + Run 3) together with the response functions for $\varepsilon\beta^+$ process in ^{64}Zn excluded at 90% C.L. Most important components of the background are shown. The energies of γ lines are in keV.

All the limits obtained in the present work for the double beta processes, as well as the results of the most sensitive previous experiments, are presented in Table 3.

In particular, the possible positive indication on the $(2\nu + 0\nu)\varepsilon\beta^+$ decay of ^{64}Zn with $T_{1/2} = (1.1 \pm 0.9) \times 10^{19}$ yr suggested in [77] is not supported. To date only three $2\beta^+$ candidate nuclei (^{40}Ca, ^{78}Kr, and ^{106}Cd) were studied at the similar level of sensitivity ($T_{1/2} \sim 10^{21}$ yr); however, it is worth noting that the theoretical predictions are still higher. The half-life limits on the 2β processes in ^{70}Zn, ^{180}W, and two neutrino mode of 2β decay in ^{186}W established in our work on the level of $10^{18} - 10^{20}$ yr are one order of magnitude higher than those of previous experiments.

New measurements with a new $ZnWO_4$ crystal of better quality are in progress.

Table 3: Half-life limits on 2β processes in Zn and W isotopes.

Transition	Decay channel	Level of daughter nucleus	$T_{1/2}$ limit (yr)	
			Present work 90%(68%) C.L.	Previous results 90%(68%) C.L.
^{64}Zn→^{64}Ni	$0\nu2\varepsilon$	g.s.	$\geq 1.1(2.8) \times 10^{20}$	$\geq 0.7(1.0) \times 10^{18}$ [73]
				$\geq 3.4(5.5) \times 10^{18}$ [74]
	$0\nu\varepsilon\beta^+$	g.s.	$\geq 4.3(5.7) \times 10^{20}$	$\geq 2.8 \times 10^{16}$ [75]
				$\geq 2.4(3.6) \times 10^{18}$ [73]
				$\geq 1.3 \times 10^{20}$ [76]
				$\geq 2.2(6.1) \times 10^{20}$ [74]
	$2\nu\varepsilon\beta^+$	g.s.	$\geq 0.70(2.1) \times 10^{21}$	$= (1.1 \pm 0.9) \times 10^{19}$ [77]
				$\geq 4.3(8.9) \times 10^{18}$ [73]
				$\geq 1.3 \times 10^{20}$ [76]
				$\geq 2.1(7.4) \times 10^{20}$ [74]
^{70}Zn→^{70}Ge	$0\nu2\beta^-$	g.s.	$\geq 1.8(3.0) \times 10^{19}$	$\geq 0.7(1.4) \times 10^{18}$ [73]
	$2\nu2\beta^-$	g.s.	$\geq 2.3(4.0) \times 10^{17}$	$\geq 1.3(2.1) \times 10^{16}$ [73]
	$0\nu2\beta^-$M1	g.s.	$\geq 1.0(1.4) \times 10^{18}$	
^{180}W→^{180}Hf	$0\nu2\varepsilon$	g.s.	$\geq 0.86(1.2) \times 10^{18}$	$\geq 0.9(1.3) \times 10^{17}$ [78]
	$2\nu2K$	g.s.	$\geq 6.6(9.4) \times 10^{17}$	$\geq 0.7(0.8) \times 10^{17}$ [78]
^{186}W→^{186}Os	$0\nu2\beta^-$	g.s.	$\geq 2.1(4.2) \times 10^{20}$	$\geq 1.1(2.1) \times 10^{21}$ [78]
	$0\nu2\beta^-$	2^+ (137.2 keV)	$\geq 2.1(4.2) \times 10^{20}$	$\geq 1.1(2.0) \times 10^{21}$ [78]
	$0\nu2\beta^-$M1	g.s.	$\geq 5.8(8.6) \times 10^{19}$	$\geq 1.2(1.4) \times 10^{20}$ [78]
	$2\nu2\beta^-$	g.s.	$\geq 2.3(2.8) \times 10^{19}$	$\geq 3.7(5.3) \times 10^{18}$ [78]
	$2\nu2\beta^-$	2^+ (137.2 keV)	$\geq 1.8(3.6) \times 10^{20}$	$\geq 1.0(1.3) \times 10^{19}$ [78]

5.2 Investigation of 2β decay of ^{108}Cd and ^{114}Cd

A low background $CdWO_4$ crystal scintillator (40 mm in diameter by 43 mm in length; mass of 433.61 g), already exploited about 10 years ago in the experiment of ref. [79], was used in the present measurements to investigate the 2β decay of ^{108}Cd and ^{114}Cd. This crystal was stored in the Solotvina Underground Laboratory for 10 years at a depth of 1000 m w.e.; in August 2005, the crystal was surface transported in a lead container (with walls ≈12 cm thick) and immediately placed underground in the Gran Sasso National Laboratories to avoid cosmogenic activation. The crystal was washed by ultra-pure nitric acid, and vacuum packed to prevent contact with radon from air.

The $CdWO_4$ crystal was fixed inside a cavity ⌀47 × 59 mm in the central part of a polystyrene light-guide, 66 mm in diameter and 312 mm in length; the cavity was filled with high-purity silicon oil. The light-guide was optically connected on opposite sides to two low radioactive 3" diameter PMTs; the light guide was wrapped by the PTFE reflection tape. The detector was installed deep underground in the low background DAMA/R&D set-up. An event-by-event data acquisition system records amplitude and arrival time of events. Moreover, the sum of the signals from the PMTs was also recorded

by Transient Digitizer over a time window of 100 μs.

The $CdWO_4$ crystals contain several potentially 2β–decaying isotopes of Cd and W. We have considered the 2β decay of ^{108}Cd (natural abundance: 0.89(3)%, and energy release in the 2β decay (Q): 272(6) keV) and ^{114}Cd (natural abundance: 28.73(42)%, and Q = 540(3) keV).

The measurements were carried out in the energy range $\simeq$ 0.03–0.7MeV over 2758 h. The energy dependence of the detector energy resolution was measured with ^{22}Na, ^{133}Ba, ^{137}Cs, ^{228}Th and ^{241}Am sources.

The energy spectrum accumulated in the low-background DAMA/R&D set-up with the $CdWO_4$ detector is presented in Fig. 12. The counting rate in the spectrum below

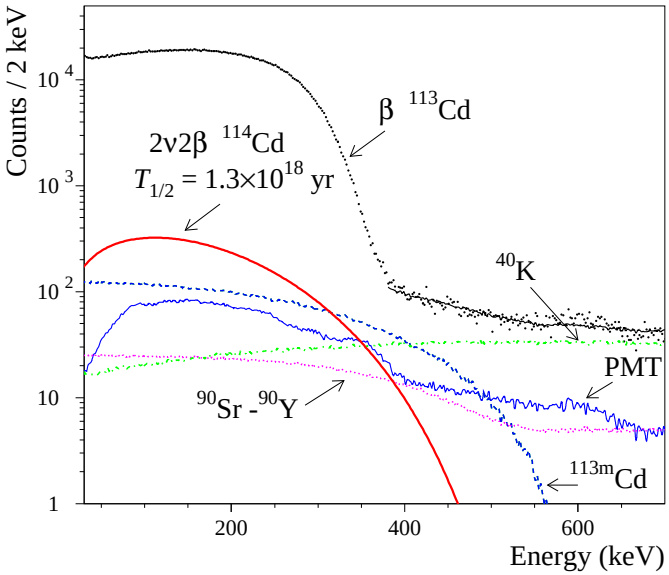

Figure 12: (Color online) Energy spectrum of the $CdWO_4$ scintillator measured over 2758 h in the low background set-up together with the model of the background (shown by solid line at $E > 380$ keV) and its main components: β spectra of ^{40}K, ^{90}Sr–^{90}Y, ^{113m}Cd, and contribution from the external γ quanta from PMTs. An expected energy distribution of $2\nu2\beta$ decay of ^{114}Cd with $T_{1/2}^{2\nu2\beta} = 1.3 \times 10^{18}$ yr (excluded at 90% of C.L.) is also shown.

the energy of $\approx$380 keV is mainly provided by the β decay of ^{113}Cd. Contributions to the background above the energy 380 keV from a possible internal contamination of the $CdWO_4$ scintillator (^{40}K, ^{60}Co, ^{90}Sr-^{90}Y, ^{113m}Cd, ^{137}Cs, active nuclides from U/Th families), and from external γ -rays were simulated with the help of the GEANT4 package; the initial kinematics of the particles emitted in the decay of nuclei was given by an event generator DECAY0. The fit of the background spectrum by this model in the energy interval 380 – 700 keV and the main components of the background are shown in Fig.12. There are no clear peculiarities in the spectrum which could be ascribed to the internal trace contamination by radioactive nuclides. The time-amplitude analysis, the pulse-shape discrimination between $\beta(\gamma)$ and α particles, the simulation of the measured energy spectrum, and the data of the mass-spectrometry measurements by ICP-MS were used to estimate the radioactive contamination of the $CdWO_4$ detector.

For the 2ν double electron capture in ^{108}Cd from the K shell, the total energy released in the detector is equal to $2E_K = 48.8$ keV (where $E_K = 24.4$ keV is the binding energy of the electrons on the K shell of palladium atoms). The detection of such a little energy deposit requires a rather low–energy threshold. The sufficiently low–energy threshold of 28 keV was reached in the present experiment owing to the high quality of the scintillator, to a satisfactory light collection, and to the rejection of the PMT noise by efficient pulse shape discrimination.

Following the procedures described in detail in the devoted paper (see 2008 publication list) it was obtained:

$$T_{1/2}^{2\nu 2K}(^{108}\mathrm{Cd}) \geq 1.1(1.9) \times 10^{18} \text{ yr at } 90\%(68\%) \text{ C.L.}$$

As regards the neutrinoless double electron capture in ^{108}Cd, all the available energy (transferred to X-rays/Auger electrons, gamma quanta or conversion electrons) will give rise to a peak at $Q_{\beta\beta} = 272$ keV value. The response function was simulated with the help of the GEANT4 package and the event generator DECAY0. We assume that all the available energy was transferred to one γ quantum with the energy $Q_{\beta\beta} - 2E_K = 223$ keV, which is the most pessimistic hypothesis from the point of view of the registration efficiency, which in this case has minimal possible value ($\eta = 0.85$). The fit of the measured spectrum in the energy interval 100–320 keV by the sum of the function representing the β spectrum of ^{113}Cd and of the expected $0\nu 2\varepsilon$ peak gives the following limit:

$$T_{1/2}^{0\nu 2\varepsilon}(^{108}\mathrm{Cd}) \geq 1.0(2.7) \times 10^{18} \text{ yr at } 90\%(68\%) \text{ C.L.}$$

It is worth noting that the sensitivity of the experiment to 2β processes in ^{108}Cd can be significantly improved by using $CdWO_4$ crystal scintillators enriched in ^{108}Cd and depleted in ^{113}Cd.

The energy spectrum accumulated in the low background set-up during 2758 h was used to set a limit on the $0\nu 2\beta$ decay of ^{114}Cd. A Gaussian peak at the energy 540 keV with FWHM $= 61$ keV is expected for the $0\nu 2\beta$ decay of ^{114}Cd, and there is no indication in the data for such a peak.

Following the procedures described in detail in the devoted paper (see 2008 publication list) it was obtained:

$$T_{1/2}^{0\nu 2\beta}(^{114}\mathrm{Cd}) \geq 1.1(2.5) \times 10^{21} \text{ yr at } 90\%(68\%) \text{ C.L.}$$

and

$$T_{1/2}^{2\nu 2\beta}(^{114}\mathrm{Cd}) \geq 1.3(2.1) \times 10^{18} \text{ yr at } 90\%(68\%) \text{ C.L.}$$

It should be stressed that a sensitivity to $T_{1/2}^{0\nu 2\beta}$ at the level of 10^{21} yr was previously achieved only for fifteen 2β decaying nuclei from the full list of 69 isotopes [80]. Despite ^{114}Cd has comparatively a low $Q_{\beta\beta}$ value (and, therefore, from this point of view it is not much competitive in the sense of sensitivity to neutrino mass), this nucleus has rather high isotopic abundance: $\delta = 29\%$. This can allow to discuss future large scale experiment without very expensive enriched isotopes. Moreover, the disadvantage of a low $Q_{\beta\beta}$ can

even be an advantage owing to suppression of 2ν mode. Therefore, the energy region of $0\nu2\beta$ signal will be free of the background produced by the $2\nu2\beta$ events, which in general can reach this region due to poor energy resolution of a detector [81]. The suppression of the 2ν mode would be especially important in the search for the $0\nu2\beta$ decay with Majoron ($0\nu2\beta M$) emission, whose distribution is continuous, since in this case the $0\nu2\beta M$ events will not be distinguished from the $2\nu2\beta$ background even with the help of the high energy resolution detector.

5.3 Investigation of double β decay of ^{106}Cd

Measurements with several low background $CdWO_4$ crystals with Cd enriched in ^{106}Cd are planned. The realization of some $CdWO_4$ crystals, enriched in ^{106}Cd at $\simeq 70\%$ and masses of order of kg, is ongoing; they will be used in incoming years to investigate several double beta decay channels of ^{106}Cd with the active source method. The ^{106}Cd isotope is one of the best candidates for the double β^+ decay because of: 1) its natural isotopic abundance and of the possibility to achieve samples enriched up to 100% with the present technology; 2) its rather large $Q_{\beta\beta}$ value (2771 keV) and of the possibility to study the various $2\beta^+$, $\varepsilon\beta^+$ e 2ε decay modes; 3) the favourable theoretical estimates of the half-lives. The final measurements, in particular, will use a low background $CdWO_4$ detector with Cd enriched in ^{106}Cd at 70% and two low background NaI(Tl) which can work in coincidence with it when investigating some decay channels. Already in one-two years of data taking a sensitivity of order of at least 10^{22} yr will be reached.

6 Measurements with DAMA/Ge and LNGS Ge facility

Various R&D developments to improve low background set-ups and scintillators as well as new developments for higher radiopure PMTs are regularly carried out. The related measurements on samples are usually performed by means of the DAMA low background Ge detector, specially realized with a low Z window. It is operative deep underground in the low background facility of the LNGS since many years. Some selected materials are in addition measured with high sensitivity ICP-MS and mass spectrometers.

In particular, main activities during year 2008 were:

- Measurements on samples have regularly been carried out.
- The measurement (named ARMONIA) with a Molybdenum sample (mass $\simeq$ 1 kg enriched in ^{100}Mo at 99.5%) installed in the 4π low-background HP Ge detectors facility has been completed. The aim is to investigate the $2\beta2\nu$ decay of ^{100}Mo to the first excited 0^+_1 level of ^{100}Ru). The full data analysis is in progress.
- New measurements with LiF(W) have been performed aiming mainly to investigate ^{7}Li solar axion; other efforts for future measurements are considered.

- Measurements with about 500 g Ru are in progress, aiming to investigate the 2β processes of ^{96}Ru and ^{104}Ru). It is a preliminary step toward a more sensitive measurement.

- The properties of a lithium molybdate (Li_2MoO_4) single crystal – a potential detector in searches for rare nuclear events – were studied. The results will be described in the LNGS report 2009;

- New measurements on various subjects for incoming years are in preparation.

In the following just some of the results achieved in 2008 are summarized.

6.1 Feasibility studies and preliminary results on ^{7}Li solar axions

The Sun can be an intense source of solar axions, whose energy distribution should be made of a continuum component, due to the particle production through Primakoff effect, and by mono-energetic lines due to the de-excitation of the excited states of the nuclei present in the Sun through magnetic nuclear transitions. In fact, the axions can be emitted instead of gammas in some de-excitation processes with a probability depending on their mass.

M1 transitions from the first excited level of ^{7}Li (E_{exc} = 477.6 keV) in solar core could be source of quasi-monochromatic axions [82]. This ^{7}Li* level is populated in *pp* chain of nuclear reactions in Sun when ^{7}Be nucleus, produced through the ^{3}He + $\alpha \rightarrow$ ^{7}Be + γ reaction, decays to ^{7}Li occupying with 10.5% probability the 477.6 keV level. Coming to Earth, these axions can be resonantly captured by ^{7}Li nuclei. In the subsequent deexcitation process, γ's of 477.6 keV will be emitted (electron conversion coefficient is very low: 7.3×10^{-7} [83]), and, therefore, the possible presence of such axions can be singled out by the presence of the characteristic peak in the energy distribution of a suitable detector placed close to or containing the ^{7}Li sample. The total number of resonant axion absorption processes in a ^{7}Li sample, containing N_7 number of ^{7}Li nuclei, has been calculated [82, 84] by taking into account the current Solar Standard Model as:

$$R = N_7 \times t \times 1.74 \times 10^{-45} \times \left(\frac{m_a}{1\ \mathrm{eV}}\right)^4; \qquad (2)$$

here t is the time of measurements (in seconds). In case no evidence is found for the peak searched for, an upper limit on m_a can be set straightforward.

The first experimental work, searching for the ^{7}Li solar axions, gave the limit: $m_a < 32$ keV [82]. Later it was improved to the value of 16 keV [84]. The limits from ^{7}Li are higher than those obtained considering ^{83}Kr ($m_a < 5.5$ keV [85]) and ^{57}Fe ($m_a < 216$ eV [86]). Nevertheless, they are important since if the hadronic axion mass is higher than excitation energy of ^{83}Kr ($E_{exc} = 9.4$ keV) or ^{57}Fe ($E_{exc} = 14.4$ keV), axions just will not be produced in the ^{83}Kr* and ^{57}Fe* transitions. In addition, the ^{7}Li limits are related with the *pp* chain, the main source of the solar energy, while the ^{57}Fe and ^{83}Kr bounds are subjected to some uncertainties in determination of the iron and krypton abundances in the solar core.

With the aim to preliminarily investigate the ^{7}Li solar axions, measurements on some LiF samples have been carried out by using two low background HP Ge detectors deep underground: GSOR (408 cm^3) and GEBER (244 cm^3). Three LiF samples were used in the measurements: i) two LiF powders of different production of 243 g and 47 g, measured in GSOR detector during 722 h and 914 h respectively); ii) a LiF(W) crystal of 224 g, measured with the GEBER detector during 633 h.

As regard the first samples measurements, comparison of the measured LiF spectrum with the GSOR background shows that the samples are heavily polluted by isotopes from ^{232}Th and ^{238}U chains. As example, Fig. 13 (top) shows the energy distributions measured with and without (background) the 243 g LiF sample for the whole energy range, while Fig. 13 (bottom) shows for the same sample the energy range around the 477.6 keV peak searched for.

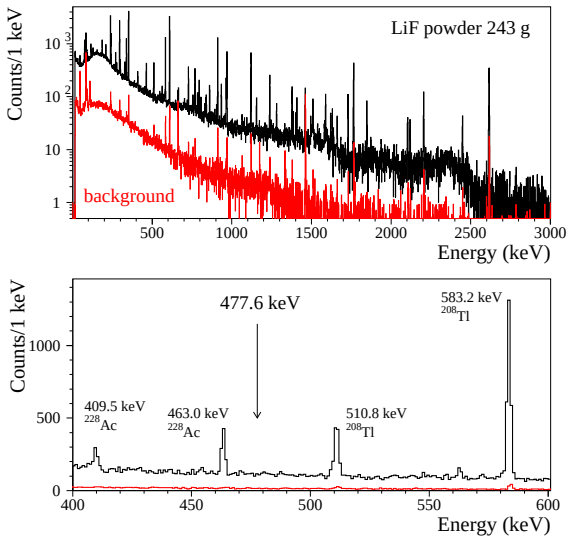

Figure 13: Top: energy distributions measured with the 243 g LiF sample in LNGS HP Ge GSOR detector during 722 h in comparison with the background measured during 1571 h (normalized here to 722 h). Bottom: energy distribution around 477.6 keV.

All peaks in the LiF samples were identified. They belong to usual contaminants: nuclides from U/Th chains, ^{40}K, ^{60}Co, ^{137}Cs. The 47 g sample shows 2–3 times lower U/Th contamination than the first one and only limits on ^{40}K, ^{60}Co, ^{137}Cs and ^{207}Bi were obtained.

The LiF(W) crystal was produced by the Czochralski method in the Institute for Scintillation Materials (Kharkiv, Ukraine) and doped by W at level of 0.04% to improve its scintillation properties. It is very pure and the energy distribution measured with the sample practically coincides with the background. Only limits for radioactive pollutions were derived. Summary of samples and crystal activities are given in the devoted paper (see in 2008 publication list).

In the spectrum collected with the LiF powder sample of 243 g during 722 h peak at energy of 478 keV is absent (see Fig. 13 (bottom)), and only limit on its area with some

confidence level can be set. The more cautious limit on the axion mass is:

$$m_a < 13.9 \text{ keV at } 90\% \text{ C.L..}$$

Data collected with the other LiF sample and with the LiF(W) crystal were processed in a similar way. However, the obtained m_a limits were slightly worse: $m_a < 15.3 - 15.5$ keV.

The obtained value of 13.9 keV is better than the best previous limit of 16.0 keV obtained for the ^{7}Li solar axion mass in the experiment of ref. [84]. While this improvement is modest, nevertheless it is important because it closes the existing window of possible axion masses between the previous limit of 16.0 keV and the 14.4 keV energy of the next potential source of quasi-monochromatic solar axions from ^{57}Fe.

In order to estimate the experimental sensitivity reachable in a future experiment the possible background sources – able to populate the excited level of ^{7}Li with $E_{exc} = 477.6$ keV – have been considered. For details see 2008 publication list. The conclusion of these estimations is that the only background processes potentially important – but just in case of absence of a suitable neutron shield – are: i) possible pollution of the LiF sample by ^{10}B (because of reaction $n + {}^{10}\text{B} \rightarrow {}^7\text{Li}^* + \alpha$); ii) excitation of the 478 keV level of ^{7}Li by α and ^{3}H particles from reaction $n + {}^6\text{Li} \rightarrow {}^3\text{H} + \alpha$.

As regards future measurements, considering that the measured background rate in the energy interval of 475 – 480 keV in the Ge detectors (0.285 counts/h for the GEBER 244 cm^3 detector and 0.105 counts/h for the GSOR 408 cm^3 detector) and the expected efficiencies, a sensitivity to ^{7}Li solar axion mass of $\simeq$8 keV can be obtained with the GSOR detector (which has lower background and higher efficiency) by collecting data during six months with a bigger and pure LiF(W) crystal. It is worth noting that also LiI(Eu) scintillation crystals could be used to search for the ^{7}Li solar axions and to build a large scale experiment; in particular, measurements to investigate radiopurity of LiI(Eu) scintillators are in progress.

6.2 ARMONIA

The measurements, named ARMONIA, with a Molybdenum sample (mass $\simeq$ 1 kg enriched in ^{100}Mo at 99.5%) installed in the 4π low-background HP Ge detectors facility has been completed in 2008. The aim was to investigate the $2\beta2\nu$ decay of ^{100}Mo to the first excited 0_1^+ level of ^{100}Ru by investigating the spectrum of coincidence between two HP Ge detectors when the energy window of one of the detectors is set to the expected energy of the gamma quanta emitted in the $2\beta2\nu$ decay to ^{100}Ru* (540 or 591 keV; width of window 2 keV is in accordance with the energy resolution of the HP Ge at these energies). After some very preliminary analysis on partial statistics [87]; new results, based on a statistics of about 17000 h, have been released (see the paper in the 2008 publication list) the final complete data analysis is in progress.

7 Conclusions

In conclusion, the main activities during year 2008 can be summarized as in the following:

I. Further corollary investigations on the 6.3 σ C.L. model independent evidence for the presence of a particle Dark Matter component in the galactic halo, obtained by DAMA/NaI over seven annual cycles. These works have also a general interest in their theoretical and phenomenological parts.

II. The new DAMA/LIBRA set-up is regularly in data taking. The analysis of an exposure of 0.53 tons$\times$year has been completed and published in all the aspects as regards the model independent annual modulation signature. It confirms the results achieved by the former experiment, and the cumulative analysis of both of them gives a 8.2σ C.L. evidence for the presence of a particle Dark Matter component in the galactic on the basis of the model independent DM annual modulation signature.

III. A first upgrade of DAMA/LIBRA has been performed in fall 2008 to substitute – operating in HP Nitrogen atmosphere – PMT; moreover, new Transient Digitizers and new DAQ with optical read-out have been installed.

IV. A new development for new low background PMTs with high quantum efficiency has been started.

V. The RD-III towards the possible DAMA/1ton is carried out on various aspects.

VI. The DAMA/LXe set-up has regularly collected data.

VII. The DAMA/R&D set-up has been used to perform various kinds of measurements; several data analyses have been completed and other ones are in progress. Various other relatively small scale experiments are in preparation.

VIII. The DAMA/Ge is regularly in operation and, various small scale experiments have been performed, are in progress and in preparation.

2008 Awards:

- Dr. F. Cappella has been awarded by the Italian Physical Society (SIF) for its presentation: "From DAMA/NaI to DAMA/LIBRA" given at the 2007 SIF Conference.
- Dr. F. Nozzoli has won the 2008 Orso Mario Corbino award for young researchers given by the Italian Physical Society.

8 List of Publications during 2008

1. F. Cappella, "From DAMA/NaI to DAMA/LIBRA and beyond", Il Nuovo Cim. B122 (2007) 707 (pubblicato on-line nel 2008).
2. R. Bernabei, "Physics and Astrophysics with low background scintillators", Eur. Phys. J. Special Topics 163 (2008) 207-226.

3. R. Bernabei, P. Belli, F. Montecchia, F. Nozzoli, F. Cappella, A. Incicchitti, D. Prosperi, R. Cerulli, C. J. Dai, H. L. He, H. H. Kuang, J. M. Ma, X. H. Ma, X. D. Sheng, Z. P. Ye, R.G. Wang, Y.J. Zhang, "Possible implications of the channeling effect in NaI(Tl) crystals", Eur. Phys. J. C. 53 (2008) 205.

4. P. Belli, R. Bernabei, F. Cappella, R. Cerulli, C.J. Dai, F.A. Danevich, B.V. Grinyov, A. Incicchitti, V.V. Kobychev, L.L. Nagornaya, S.S. Nagorny, F. Nozzoli, D.V. Poda, D. Prosperi, V.I. Tretyak, S.S. Yurchenko, "Search for 2β processes in^{64}Zn with the help of $ZnWO_4$ crystal scintillator", Phys. Lett. B 658 (2008) 193.

5. R. Bernabei, P. Belli, F. Montecchia, F. Nozzoli, F. Cappella, A. Incicchitti, D. Prosperi, R. Cerulli, C.J. Dai, H.L. He, H.H. Kuang, J.M. Ma, X.H. Ma, X.D. Sheng, Z.P. Ye, R.G. Wang, Y.J. Zhang, "Investigating electron interacting dark matter", Phys. Rev. D 77 (2008) 023506.

6. P. Belli, R. Bernabei, R. Cerulli, F.A. Danevich, A. d'Angelo, V.I. Goriletsky, B.V. Grinyov, A. Incicchitti, V.V. Kobychev, M. Laubenstein, V.M. Mokina, S.S. Nagorny, F. Nisi, D. Prosperi, O.G. Shkulkova, V.I. Tretyak, "^{7}Li solar axions: preliminary results and feasibility studies", Nucl. Phys. A 806 (2008) 388.

7. R. Bernabei, P. Belli, F. Cappella, R. Cerulli, C. J. Dai, H. L. He, A. Incicchitti, H. H. Kuang, J. M. Ma, X. H. Ma, F. Montecchia, F. Nozzoli, D. Prosperi, X. D. Sheng, Z. P. Ye, R.G. Wang, Y.J. Zhang, "Investigation on light Dark Matter", Mod. Phys. Lett. A23 (2008) 2125.

8. R. Bernabei, P. Belli, F. Cappella, R. Cerulli, F.A. Danevich, S. d'Angelo, A. Incicchitti, V.V. Kobychev, S.S. Nagorny, F. Nozzoli, V.M. Mokina, D.V. Poda, D. Prosperi, V.I. Tretyak, "Search for double beta decay processes in ^{108}Cd and ^{114}Cd with the help of low background $CdWO_4$ crystal scintillator", Eur. Phys. J. A 36 (2008) 167.

9. R. Bernabei, P. Belli, A. Bussolotti, F. Cappella, R. Cerulli, C.J. Dai, A. d'Angelo, H.L. He, A. Incicchitti, H.H. Kuang, J.M. Ma, A. Mattei, F. Montecchia, F. Nozzoli, D. Prosperi, X.D. Sheng, Z.P. Ye, "The DAMA/LIBRA apparatus", Nucl. Instr. & Meth. A 592 (2008) 297-315.

10. R. Bernabei, P. Belli, F. Cappella, R. Cerulli, C.J. Dai, A. d'Angelo, H.L. He, A. Incicchitti, H.H. Kuang, J.M. Ma, F. Montecchia, F. Nozzoli, D. Prosperi, X.D. Sheng, Z.P. Ye, "First results from DAMA/LIBRA and combined results with DAMA/NaI", Eur. Phys. J. C 56 (2008) 333-355.

11. P. Belli, R. Bernabei, R. S. Boiko, V.B. Brudanin, R. Cerulli, F.A. Danevich, S. d'Angelo, A.E. Dossovitskiy, B.V. Grinyov, A. Incicchitti, V.V. Kobychev, G.P. Kovtun, A.L. Mikhlin, V.M.Mokina, L.L. Nagornaya, S.S. Nagorny, F. Nisi, R.B. Podvujanyuk, D. Prosperi, D. A. Solopikhin, V.I. Tretyak, I.A. Tupitsyna, A.P. Shcherban, V.D. Virich, "Development of enriched Cadmium tungstate Crystal scintillators to search for double beta decay processes in ^{106}Cd", ROM2F/2008/17, to appear on the Proc. of the Int. conf. NPAE 2008, Kiev, Ukraine.

12. R. Bernabei, P. Belli, F. Montecchia, F. Nozzoli, F. Cappella, A. d'Angelo, A. Incicchitti, D. Prosperi, R. Cerulli, C.J. Dai, H.L. He, H.H. Kuang, J.M. Ma, X.D. Sheng, Z.P. Ye, "First results from DAMA/LIBRA", in the Proceed. of IV NO-VE conference (2008) 271.

13. R. Bernabei, P. Belli, F. Cappella, R. Cerulli, C.J. Dai, A. d'Angelo, H.L. He, A. Incicchitti, H.H. Kuang, J.M. Ma, F. Montecchia, F. Nozzoli, D. Prosperi, X.D. Sheng, Z.P. Ye, "Direct detection of dark matter particles", Il Nuovo Cimento B123 (2008) 928.

14. R. Bernabei, P. Belli, F. Montecchia, F. Nozzoli, F. Cappella, A. d'Angelo, A. Incicchitti, D. Prosperi, R. Cerulli, C.J. Dai, H.L. He, H.H. Kuang, J.M. Ma, X.D. Sheng, Z.P. Ye, "First results from DAMA/LIBRA", to appear in the Proceed. of the XXth Rencontres de Blois 2008, Chateau de Blois (France), May 2008.

15. R. Bernabei, P. Belli, F. Cappella, R. Cerulli, C.J. Dai, A. d'Angelo, H.L. He, A. Incicchitti, H.H. Kuang, J.M. Ma, F. Montecchia, F. Nozzoli, D. Prosperi, X.D. Sheng, Z.P. Ye, "First results from DAMA/LIBRA and combined results with DAMA/NaI", to appear in the Proceed. of the Int. Workshop Vulcano 2008, May 2008.

16. P. Belli, R. Bernabei, F. Cappella, R. Cerulli, F.A. Danevich, B.V. Grinyov, A. Incicchitti, V.V. Kobychev, V.M.Mokina, L.L. Nagornaya, S.S. Nagorny, S. Nisi, F. Nozzoli, D.V. Poda, D. Prosperi, V.I. Tretyak, S.S. Yurchenko, "Preliminary results of search for 2β processes in zinc and tungsten with the help of zinc tungstate crystal scintillator", to appear on the Proc. of the Int. conf. NPAE 2008, Kiev, Ukraine.

17. P. Belli, R. Bernabei, R. S. Boiko, F. Cappella, R. Cerulli, F.A. Danevich, S. d'Angelo, A. Incicchitti, V.V. Kobychev, B.N. Kropivyansky, M. Laubenstein, P.G. Nagornyi, S.S. Nagorny, S. Nisi, F. Nozzoli, D.V. Poda, D. Prosperi, O.G. Shkulkova, V.I. Tretyak, I.M. Vyshnevskyi, S.S. Yurchenko, "Preliminary results on the search for ^{100}Mo 2β decay to the first excited 0_1^+ level of ^{100}Ru", to appear on the Proc. of the Int. conf. NPAE 2008, Kiev, Ukraine.

18. F. Cappella on behalf of DAMA Collaboration, "Search for $\beta\beta$ decay modes at LNGS by DAMA experiment", to appear on the Proc. of the Varenna School 2008 (poster section), Varenna, Italy.

19. R. Bernabei, P. Belli, F. Montecchia, F. Nozzoli, F. Cappella, A. d'Angelo, A. Incicchitti, D. Prosperi, R. Cerulli, C.J. Dai, H.L. He, H.H. Kuang, J.M. Ma, X.D. Sheng, Z.P. Ye, "First results from DAMA/LIBRA", to appear on the Proc. of the Int. conf. NPAE 2008, Kiev, Ukraine.

20. P. Belli, R. Bernabei, F. Cappella, R. Cerulli, C.J. Dai, F.A. Danevich, B.V. Grinyov, A. Incicchitti, V.V. Kobychev, V.M. Mokina, L.L. Nagornaya, S.S. Nagorny, S. Nisi, F. Nozzoli, D.V. Poda, D. Prosperi, V.N. Shlegel, V.I. Tretyak, Y.V. Vasiliev, S.S. Yurchenko, "Radiopurity of $ZnWO_4$ crystal scintillators", to appear on the Proc. of the ISMART-2008 conf., Kharkov, Ukraine.

21. R. Bernabei, P. Belli, F. Cappella, R. Cerulli, C.J. Dai, A. d'Angelo, H.L. He, A. Incicchitti, H.H. Kuang, J.M. Ma, F. Montecchia, F. Nozzoli, D. Prosperi, X.D. Sheng, Z.P. Ye, "First results from DAMA/LIBRA", to appear on the Proceed. of the 4th Patras Workshop on Axions, WIMPs and WISPs, Desy 2008.

22. R. Bernabei, P. Belli, A. Incicchitti and D. Prosperi, "Liquid Noble gases for Dark Matter searches: a synoptic survey", arXiv:0806.0011.

23. R. Bernabei and A. Incicchitti, "Ultra-low level detection of Dark Matter and rare processes", in the volume *Karlsruher Nuklidkarte: Commemoration of the 50th Anniversary*, edited by G. Pfenning, C. Normand, R. Dreher, J. Magill, T. Fanghanel - Publishing Editor: G. Weber, 2008.

24. R. Bernabei, "Segnali dall'Universo oscuro", Le Stelle, vol. 65 (2008) 40.

25. R. Bernabei, P. Belli, F. Cappella, R. Cerulli, C.J. Dai, A. d'Angelo, H.L. He, A. Incicchitti, H.H. Kuang, J.M. Ma, F. Montecchia, F. Nozzoli, D. Prosperi, X.D. Sheng, Z.P. Ye, "First results from DAMA/LIBRA", to appear on the Proceed. of DSU 2008.

26. R. Bernabei, P. Belli, F. Montecchia, F. Nozzoli, F. Cappella, A. d'Angelo, A. Incicchitti, D. Prosperi, R. Cerulli, C.J. Dai, H.L. He, H.H. Kuang, J.M. Ma, X.D. Sheng, Z.P. Ye, "First results from DAMA/LIBRA", to appear on the Proceed. of IDM08.

27. P. Belli, R. Bernabei, A. d'Angelo, A. Incicchitti, D. Prosperi, R. Cerulli, M. Laubenstein, S. Nisi, F.A. Danevich, V.V. Kobychev, V.M.Mokina, S.S. Nagorny, O.G. Shkulkova, V.I. Tretyak, V.I. Goriletsky, B.V. Grinyov, "^{7}Li solar axions: preliminary results and feasibility studies", to appear on the Proc. of the IDM08.

28. P. Belli, R. Bernabei, F. Cappella, R. Cerulli, F.A. Danevich, B.V. Grinyov, A. Incicchitti, V.V. Kobychev, V.M.Mokina, L.L. Nagornaya, S.S. Nagorny, S. Nisi, F. Nozzoli, D.V. Poda, D. Prosperi, V.I. Tretyak, S.S. Yurchenko, "Search for 2β decay of Zinc and Tungsten with the help of low background $ZnWO_4$ crystal scintillators", arXiv:0811.2348v1 (2008), submitted for publication.

29. P. Belli, R. Bernabei, R.S. Boiko, F. Cappella, R. Cerulli, F.A. Danevich, S. d'Angelo, A. Incicchitti, V.V. Kobychev, B.N. Kropivyansky, M. Laubenstein, P.G. Nagornyi, S.S. Nagorny, S. Nisi, F. Nozzoli, D.V. Poda, D. Prosperi, O.G. Polischuk, V.I. Tretyak, I.M. Vyshnevskyi, S.S. Yurchenko, "Updated results of the ARMONIA experiment: 2β decay of ^{100}Mo to excited levels of ^{100}Ru", KINR-annual report 2008.

References

[1] R. Bernabei et al., Il Nuovo Cim. A 112 (1999) 545.

[2] R. Bernabei et al., Eur. Phys. J. C18 (2000) 283.

[3] R. Bernabei el al., La Rivista del Nuovo Cimento 26 n.1 (2003) 1-73.
[4] R. Bernabei et al., Int. J. Mod. Phys. D 13 (2004) 2127.
[5] R. Bernabei et al., Phys. Lett. B 424 (1998) 195.
[6] R. Bernabei et al., Phys. Lett. B 450 (1999) 448.
[7] P. Belli et al., Phys. Rev. D 61 (2000) 023512.
[8] R. Bernabei et al., Eur. Phys. J. C 18 (2000) 283.
[9] R. Bernabei et al., Phys. Lett. B 509 (2001) 197.
[10] R. Bernabei et al., Eur. Phys. J. C 23 (2002) 61.
[11] P. Belli et al., Phys. Rev. D 66 (2002) 043503.
[12] R. Bernabei et al., Int. J. Mod. Phys. A 21 (2006) 1445.
[13] R. Bernabei et al., Eur. Phys. J. C. 47 (2006) 263.
[14] R. Bernabei et al., Int. J. Mod. Phys. A 22 (2007) 3155-3168.
[15] K.A. Drukier et al., Phys. Rev. D 33 (1986) 3495.
[16] K. Freese et al., Phys. Rev. D 37 (1988) 3388.
[17] R. Bernabei et al., Phys. Lett. B389 (1996) 757.
[18] R. Bernabei et al., Phys. Lett. B408 (1997) 439.
[19] P. Belli et al., Phys. Lett. B460 (1999) 236.
[20] R. Bernabei et al., Phys. Rev. Lett. 83 (1999) 4918.
[21] P. Belli et al., Phys. Rev. C60 (1999) 065501.
[22] R. Bernabei et al., Il Nuovo Cimento A112 (1999) 1541.
[23] R. Bernabei et al., Phys. Lett. B515 (2001) 6.
[24] F. Cappella et al., Eur. Phys. J.-direct C14 (2002) 1.
[25] R. Bernabei et al., Eur. Phys. J. A 23 (2005) 7.
[26] R. Bernabei et al., Eur. Phys. J. A 24 (2005) 51.
[27] A. Bottino et al., Phys. Rev. D69 (2004) 037302, Phys. Rev. D68 (2003) 043506.
[28] R. Bernabei el al., Int. J. Mod. Phys. A 22 (2007) 3155-3168.
[29] R. Bernabei et al., Eur. Phys. J. C 53 (2008) 205.
[30] R. Bernabei el al., Phys. Rev. D 77 (2008) 023506.
[31] A. Bottino et al., Phys. Rev. D 67 (2003) 063519.
[32] A. Bottino et al., Phys. Rev. D 68 (2003) 043506.
[33] A. Bottino et al., Phys. Rev. D 69 (2004) 037302.
[34] A. Bottino et al., Phys. Lett. B 402 (1997) 113.
[35] A. Bottino et al., Phys. Lett. B 423 (1998) 109.
[36] A. Bottino et al., Phys. Rev. D 59 (1999) 095004.
[37] A. Bottino et al., Phys. Rev. D 59 (1999) 095003.
[38] A. Bottino et al., Astrop. Phys. 10 (1999) 203.
[39] A. Bottino et al., Astrop. Phys. 13 (2000) 215.
[40] A. Bottino et al., Phys. Rev. D 62 (2000) 056006.

[41] A. Bottino et al., Phys. Rev. D 63 (2001) 125003.
[42] A. Bottino et al., Nucl. Phys. B 608 (2001) 461.
[43] K. Belotsky, D. Fargion, M. Khlopov and R.V. Konoplich, hep-ph/0411093.
[44] D. Smith and N. Weiner, Phys. Rev. D 64 (2001) 043502.
[45] D. Tucker-Smith and N. Weiner, Phys. Rev. D 72 (2005) 063509.
[46] R. Foot, Phys. Rev. D 69 (2004) 036001.
[47] S. Mitra, Phys. Rev. D 71 (2005) 121302.
[48] E.M. Drobyshevski et al., Astron. & Astroph. Trans. 26:4 (2007) 289.
[49] E.M. Drobyshevski, arXiv:0706.3095.
[50] C. Arina and N. Fornengo, arXiv:0709.4477.
[51] A. Bottino et al., arXiv:0710.0553.
[52] R. Hudson, Found. Phys. 39 (2009) 174-193.
[53] F. Donato et al., arXiv:0810.5292; T. Delahaye et al., arXiv:0809.5268.
[54] S. Profumo, arXiv:0812.4457.
[55] P. Belli et al., Il Nuovo Cim. 103A (1990) 767.
[56] P. Belli et al., Il Nuovo Cim. C 19 (1996) 537.
[57] P. Belli et al., Astrop. Phys. 5 (1996) 217.
[58] P. Belli et al., Phys. Lett. B 387 (1996) 222 and Phys. Lett. B 389 (1996) 783 (erratum).
[59] R. Bernabei et al., New J. Phys. 2 (2000) 15.1.
[60] R. Bernabei et al., Eur. Phys. J.-direct C11 (2001) 1.
[61] R. Bernabei et al., Phys. Lett. B 436 (1998) 379.
[62] R. Bernabei et al., in the volume "Beyond the Desert 2003", Springer (2003) 365.
[63] R. Bernabei et al., Nucl. Instr. & Meth. A482 (2002) 728.
[64] R. Bernabei et al., Phys. Lett. B 546 (2002) 23.
[65] F. Cappella, PhD Thesis, Università di Roma "Tor Vergata", 2005.
[66] R. Bernabei et al., Phys. Lett. B 527 (2002) 182.
[67] P. Belli et al., Phys. Rev. D 61 (2000) 117301.
[68] P. Belli et al., Phys. Lett. B 465 (1999) 315.
[69] R. Bernabei et al., Phys. Lett. B 493 (2000) 12.
[70] R. Bernabei et al., Eur. Phys. J. A 27 s01 (2006) 35.
[71] R. Bernabei et al., in the volume "Cosmology and particle Physics", AIP ed. (2001) 189.
[72] M. Hirsch et al., Z. Phys. A 347 (1994) 151.
[73] F.A. Danevich et al., Nucl. Instr. Meth. A 544 (2005) 553.
[74] P. Belli et al., Phys. Lett. B 658 (2008) 193.
[75] H. Kiel, D. Munstermann, K. Zuber, Nucl. Phys. A 723 (2003) 499.
[76] H.J. Kim et al., Nucl. Phys. A 793 (2007) 171.

[77] I. Bikit et al., Appl. Radiat. Isot. 46 (1995) 455.

[78] F.A. Danevich et al., Phys. Rev. C 68 (2003) 035501.

[79] F.A. Danevich et al., Phys. Atom. Nucl. 59 (1996) 1.

[80] V.I. Tretyak, Yu.G. Zdesenko, At. Data Nucl. Data Tables 61 (1995) 43; 80 (2002) 83.

[81] Yu.G. Zdesenko, F.A. Danevich, V.I. Tretyak, J. Phys. G 30 (2004) 971.

[82] M. Krcmar et al., Phys. Rev. D 64 (2001) 115016.

[83] D.R. Tilley et al., Nucl. Phys. A 708 (2002) 3.

[84] A.V. Derbin et al., JETP Lett. 81 (2005) 365.

[85] K. Jakovcic et al., Rad. Phys. Chem. 71 (2004) 793.

[86] T. Namba, Phys. Lett. B 645 (2007) 398.

[87] P. Belli et al., in the volume *"Current problems in Nuclear Physics and Atomic energy"*, ed. INR-Kiev (2006) 479.

The ICARUS T600 Experiment at Gran Sasso Laboratory

Ankowski[1], M. Antonello[2], P. Aprili[3], F. Arneodo[3], B. Baibussinov[4], M. Baldo Ceolin[4], G. Battistoni[5], P. Benetti[6], A. Borio[6], E. Calligarich[6], M. Cambiaghi[6], F. Carbonara[7], F. Cavanna[2], S. Centro[4], A. Cesana[5], K. Cieslik[4], A. G. Cocco[7], A. Dabrowska[8], R. Dolfini[6], C. Farnese[4], A. Fava[4], A. Ferrari[5], G. Fiorillo[7], S. Galli[2], D. Gibin[4], A. Gigli Berzolari[6], A. Giuliano[9], K. Graczyk[1], S. Gninenko[10], A. Guglielmi[4], C. Juszczak[1], J. Holeczek[11], D. Kielczewska[12], M. Kirsanov[10], J. Kisiel[11], T. Kozlowski[13], N. Krasnikov[10], M. Lantz[5], G. Mannocchi[9], M. Markiewicz[8], V. Matveev[10], F. Mauri[+], A. Menegolli[6], G. Meng[4], C. Montanari[6], S. Muraro[5], J. Nowak[1], O. Palamara[3], L. Periale[9], G. PianoMortari[2], A. Piazzoli[6], P. Picchi[9], F. Pietropaolo[4], W. Polchlopek[14], M. Posiadala[12], M. Prata[6], P. Przewlocki[13], A. Rappoldi[6], G. L. Raselli[6], E. Rondio[13], M. Rossella[6], C. Rubbia[3], P. Sala[5], L. Satta[9], D. Scannicchio[6], E. Segreto[3], F. Sergiampietri[15], J. Sobczyk[1], D. Stefan[8], J, Stepaniak[13], R. Sulej[16], M. Szarska[8], M. Terrani[5], G. Trinchero[9], F. Varanini[4], S. Ventura[4], C. Vignoli[6], T. Wachala[8], A. Zalewska[8], K. Zaremba[1].

[1] Wroclaw University of Technology, Wroclaw - Poland
[2] Dipartimento di Fisica e INFN, Università di L'Aquila, Italy
[3] Laboratori Nazionali del Gran Sasso dell'INFN, Italy
[4] Dipartimento di Fisica e INFN, Università di Padova, Italy
[5] Dipartimento di Fisica e INFN, Università di Milano, Italy
[6] Dipartimento di Fisica Nucleare, Teorica e INFN, Università di Pavia, Italy
[7] Dipartimento di Scienza Fisiche, INFN e Università Federico II, Napoli - Italy
[8] H. Niewodniczanski Institute of Nuclear Physics, Krakow - Poland
[9] Laboratori Nazionali di Frascati (INFN), Italy
[10] INR RAS, prospekt 60-letiya Oktyabrya 7a, Moscow, Russia
[11] University of Silesia, 12 Bankowa st., Katowice, Poland
[12] Warsaw Univeristy, Krakowskie Przedmiescie 26/28, Warszawa - Poland
[13] A. Soltan Institute for Nuclear Studies, Poland
[14] AGH University of Science and Technology, Krakow, Poland
[15] Dipartimento di Fisica, Università di Pisa, Italy
[16] Univeristy of Technology, Pl. Politechniki 1, Poland
[+] Deceased

1 Foreword

Since the last report LNGS Annual Report Scientific the ICARUS-T600 detector assembly has proceeded smoothly, through the different issues as analytically listed in the following. However the Collaboration had to face a major problem concerning the commissioning of the liquefier designed, built, and installed by Stirling. This latter started the commissioning on 20^{th} of September and a period of five weeks was allocated for the operation. Various phases were completed, as it will be explained in paragraph 5, but a serious design fault was discovered after about 20 days of activity. The problem concerns the transfer of liquid nitrogen to reservoirs on the top of the detector. As declared by Stirling the layout needs major changes due to the unsuitable design. The new proposed solution needs to be approved by LNGS and it will imply at least four months delay of the commissioning phase of the liquefier. In the mean time the Legal Affair Service of INFN is considering suitable legal actions keeping in mind the interest of the Icarus collaboration, LNGS, and INFN for a prompt start of the Icarus operation.
Coming back to the ongoing activities four main issue can be envisaged:

A. The ICARUS cryogenic plant;

B. The ICARUS read out;

C. The Laboratories infrastructure and safety facilities;

D. The liquefier plant.

The last two items are under the authority of the Laboratory.

2 The ICARUS cryogenic plant.

a. The Air Liquide cryogenic plant has been completed. The vacuum pumping for the insulation panel started in summer 2008.

b. The pumps to evacuate the ICARUS cryostats (for the cleaning phase) are installed and their control cabinet settled in the Control Room.

c. The cryostat airtight tests are ready to be performed. In a first time the cryostats will be put in overpressure; later, the Helium leaks detection will conclude the test.

d. The unloading station has been completed and also already used to unload the liquid Nitrogen needed to start the Stirling test (see later).

e. The ICARUS Control System has been cabled and almost tested. The trial has to be completed during the final commissioning of the plant.

f. An automatic restart procedure for ICARUS process (not previously foreseen) will be implemented early 2009.

g. The interfacing between the Control Systems of ICARUS and that one of Laboratory is almost completed. More tests will be performed at the commissioning level.

h. A large range of spare parts have been provided before the start-up.

i. The tender for the cryogenic liquids is concluded. The first LN_2 delivery has been performed for Stirling test.

3 The ICARUS read out.

a. Installation of the readout electronics racks on the T600 top has been completed, together with the cabling of clock & trigger distribution.

b. Each rack has been commissioned with test-pulse data taking (showing a ∼10 % of broken/ malfunctioning boards which at present have been reserved for less critical corner racks). Ordering of a suitable number of spare DAQ boards has been authorized by INFN.

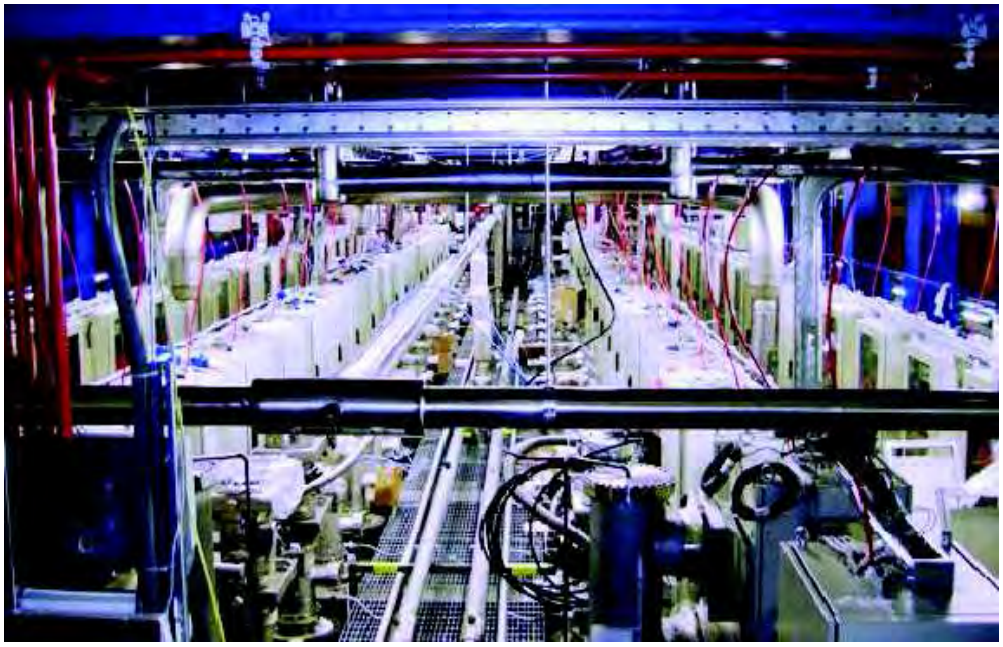

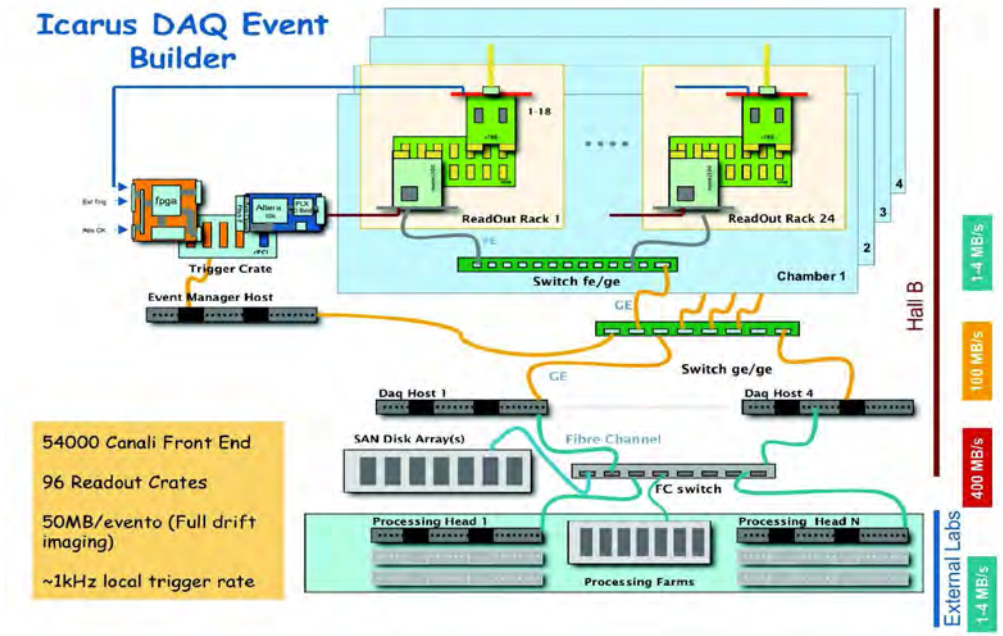

c. The event builder architecture deployment went along, including DAQ computers, storage (∼20 TB), networking (UTP cabling, switches and fibres to control room & to external labs). The setup has been tested this summer with up to 12 racks at a time, final DAQ system commissioning will start as soon as mains power distribution will allow turning on of all racks at the same time.

4 The Laboratory infrastructures.

a. The UPS (the emergency power supply to feed the control system, the valves and the 50 kW heater) has to be fed by the motor generator present underground. The electrical connection is ongoing. In a more general view, a different layout of UPS, to reach a higher level of reliability, has to be implemented by the Labs.

b. The general power supply for ICARUS plant has been delivered Monday 20/10/2008.

c. The new "double" ventilation system for the underground Labs has been successfully tested at the beginning of October. It was requested for the ICARUS operation.

d. The ICARUS exhaust ventilation system has been completed.

e. The secondary water-cooling circuit in Hall B has been upgraded, to obtain the needed cooling power for Stirling system (10 liquefier, 45 kW each), to keep the thermal step within 3°C.

f. The safety facilities has been completed and partially tested. The wall to confine ICARUS site in Hall B will be early assembled.

5 The liquefier plant.

The liquefier plant (Stirling) has been completed and the commissioning started September 20^{th}. One of the two cryogenic tanks (30 m^3) has been filled with LN_2, using the unloading station, under the management of the ICARUS Control System.

i. All 10 units have been switched-on. They operate and produce the liquid nitrogen at the required rate.

ii. A minor "restarting problem" will be settled in a few days.

iii. The major problem concerns the capability of the system to transfer (automatically) the liquid nitrogen from the ground level to the stocking cryostats at the top of the plant (10 m high difference). The layout realized does not manage the gas development in the transit pipes that prevents the pumps operation. The layout has to be

changed. Stirling is proposing a solution that takes 3.5 months to be implemented.

6 The flanges.

Late in December 2008 it was discovered that some of the signal flanges mounted on the cryostats were leaking in a sensible way. Already in 2001 in Pavia the problem was observed. For this reason all the flanges were reworked in CERN to add a layer of Araldite 2011 with the consultancy of TS/MME department. The old flanges were tested after the re-working and the problem seemed solved. The assumption is that aging and mechanical solicitations could cause the deterioration of the performance. It is widely accepted that the architecture of the original signal flanges has major flaws and because of this concern the collaboration already after the 2001 test in Pavia developed a new flange that showed absolute reliability. Unfortunately only some 30 new flanges were available late 2008 (96 is the total number of signal flanges in T600). Anyway this number is sufficient to substitute the defective flanges so that T600 can be evacuated. The collaboration plans in 2009 to build enough flanges of new type in order to be able to substitute all the old flanges, that could cause future problems.

7 Conclusions

Impressive progress in the T600 installation has been achieved in 2008. The bare detector and the data acquisition are essentially ready now.
The T600 plant in the underground laboratory with all required infrastructures has been

more complicated and slower than expected, but it is also nearing its completion.
Some of the T600 start-up procedures, logistics and authorizations have still to be completed.
The actual time-schedule of the T600 operation now is mainly depending on the next progress in the LNGS infrastructures, industrial supplies, contracts, delivery of LAr, logistics and authorizations.
The filling of the nearly 700 ton of liquid Argon is now scheduled to start by the second half of 2009 and it should last 2-3 weeks.
The detector is expected to operate both with cosmic neutrinos and accelerator beam. The scheduled 2008 beam run may be too late, but important cosmic data will be recorded before the end of 2009.

8 List of Publications 2008/2009

1. B. Baibussinov et al. [ICARUS Collaboration] "A new, very massive modular Liquid Argon Imaging Chamber to detect low energy off-axis neutrinos from the CNGS beam (Project MODULAr)" ASTROPARTICLE PHYSICS 29 (2008) 174-187

2. D. Angeli et al. [ICARUS Collaboration] "Towards a new Liquid Argon Imaging Chamber for The MODULAr project" JOURNAL OF INSTRUMENTATION 4 P02003 (2009) 1-30

3. D. Gibin et al. "CNGS neutrino beam: the MODULAr project" Proceedings of the Neutrino Oscillation Workshop (NOW08), Conca Spechiulla(Ba), Italy, Phys. B Proc. Suppl., Volume 188 (March 2009) 355.

4. D. Autiero et al. "The CNGS neutrino beam: status" Proceedings of the Neutrino Oscillation Workshop (NOW08), Conca Spechiulla(Ba), Italy, Phys. B Proc. Suppl., Volume 188 (March 2009) 188.

5. D. Autiero et al. "CNGS neutrino beam for long base-line experiments: present status and Perspectives" Proceedings of the Tenth International Workshop on Tau Lepton Physics, Novosibirsk Russia, Nucl. Phys. B Proc. Suppl., Volume 189 (April 2009) 263.

References

[1] C. Rubbia, The Liquid-Argon Time Projection Chamber: A New Concept For Neutrino Detector, CERN-EP/77-08, (1977).

[2] P. Benetti et al. [ICARUS Collaboration], A 3 Ton Liquid Argon Time Projection Chamber, Nucl. Instrum. Meth. A 332, (1993) 395.

[3] P. Cennini et al. [ICARUS Collaboration], Performance Of A 3 Ton Liquid Argon Time Projection Chamber, Nucl. Instrum. Meth. A 345, (1994) 230.

[4] F. Arneodo et al. [ICARUS Collaboration], First Observation Of 140-Cm Drift Ionizing Tracks In The Icarus Liquid-Argon Tpc, Nucl. Instrum. Meth. A 449, (2000) 36.

[5] P. Cennini et al. [ICARUS Collaboration], Detection Of Scintillation Light In Coincidence With Ionizing Tracks In A Liquid Argon Time Projection Chamber, Nucl. Instrum. Meth. A 432, (1999) 240.

[6] P. Benetti et al. [ICARUS Collaboration], Argon Purication In The Liquid Phase, Nucl. Instrum. Meth. A 333, (1993) 567.

[7] ICARUS Collaboration, A First 600 Ton ICARUS Detector Instal led At The Gran Sasso Laboratory, Addendum to Proposal by the ICARUS Collaboration, LNGS-95/10, (1995).

[8] F. Arneodo et al. [ICARUS Collaboration], Observation Of Long Ionizing Tracks With The ICARUS T600 First Half-Module, Nucl. Inst. Meth., A 508, (2003) 287.

[9] S. Amerio et al. [ICARUS Collaboration], Design, construction and tests of the ICARUS T600 detector, Nucl. Inst. Meth., A 527 (2004) 329.

[10] F.Arneodo et al., [ICARUS Collaboration], The ICARUS Experiment: a Second Generation Proton Decay and Neutrino Observatory at The Gran Sasso Laboratory, LNGS-P28, 2001, LNGS-EXP13/89 add. 1/01.

LUNA. Laboratory for Underground Nuclear Astrophysics

D. Bemmerer[a], C. Broggini[b], A. Caciolli[c], P. Corvisiero[d], H. Costantini[d], Z. Elekes[e], A. Formicola[f], Zs. Fülöp[e], G. Gervino[g], A. Guglielmetti[h], C. Gustavino[f], Gy. Gyürky[e], G. Imbriani[i], M. Junker[f], R. Kunz[g], A. Lemut[d], B. Limata[j], M. Marta[a], C. Mazzocchi[i], R. Menegazzo[b], P. Prati[d], V. Roca[j], C. Rolfs[g], C. Rossi Alvarez[b], E. Somorjai[e], O. Straniero[k], F. Strieder[g], F. Terrasi[l], H.P. Trautvetter[g]

[a]Forschungszentrum Dresden-Rossendorf, Dresden, Germany
[b]INFN, Padova, Italy
[c]Università di Padova and INFN, Padova, Italy
[d]Università di Genova and INFN, Genova, Italy
[e]Institute of Nuclear Research (ATOMKI), Debrecen, Hungary
[f]INFN, Laboratori Nazionali del Gran Sasso (LNGS), Assergi (AQ), Italy
[g]Institut für Experimentalphysik III, Ruhr-Universität Bochum, Bochum, Germany
[h]Università di Torino and INFN, Torino, Italy
[i]Università di Milano and INFN, Milano, Italy
[j]Università di Napoli "Federico II", and INFN, Napoli, Italy
[k]Osservatorio Astronomico di Collurania, Teramo, and INFN Napoli, Italy
[l]Seconda Universitá di Napoli, Caserta and INFN, Napoli, Italy

Abstract

The principal goal of the LUNA Collaboration is the measurement of fusion cross sections relevant for stellar nuclear synthesis. In the course of the year 2008 measurements on the reactions ^{25}Mg(p,γ)^{26}Al and ^{15}N(p,γ)^{16}O have been performed.

1 Introduction

Accurate knowledge of thermonuclear reaction rates is important [1, 2] in understanding the generation of energy, the luminosity of neutrinos, and the synthesis of elements in stars. Due to the Coulomb barrier (height E_c) of the entrance channel, the reaction cross section $\sigma(E)$ drops nearly exponentially with decreasing energy E. Thus it becomes increasingly difficult to measure $\sigma(E)$ and to deduce the astrophysical $S(E)$ factor defined by the equation [2]

$$\sigma(E) = \frac{S(E)}{E}\, exp(-2\,\pi\,\eta), \tag{1}$$

with the Sommerfeld parameter given by $2\,\pi\,\eta = 31.29\,Z_1\,Z_2(\mu/E)^{1/2}$. The quantities Z_1 and Z_2 are the nuclear charges of the interacting particles in the entrance channel, μ is the reduced mass (in units of amu), and E is the center-of-mass energy (in units of keV). The thermal energy region in stars is determined by the Gamow energy window $E_0 \pm \delta E_0$ (the Gamow peak) for a given stellar temperature and lies far below the height of the Coulomb barrier, approximately at $E_0/E_c = 0.01$. Consequentely the observed $\sigma(E)$ data at higher energies often have to be extrapolated to thermal energies. The extrapolations are generally done using the R-matrix formalism and require high quality data over a wide energy range reaching as close as possible to the Gamow peak. But still such an extrapolation into the unknown can lead to considerable uncertainties and data measured inside the Gamow peak are preferred.

The low-energy studies of thermonuclear reactions in a laboratory at the earth's surface are hampered predominantly by the effects of cosmic rays in the detectors. Passive shielding around the detectors provides a reduction of gammas and neutrons from the environment, but it produces at the same time an increase of gammas and neutrons due to the cosmic-ray interactions in the shield itself. A 4π active shielding can only partially reduce the problem of cosmic-ray background. An excellent solution is to install an accelerator facility in a laboratory deep underground [3]. This approach has been persued by the LUNA–collaboration installing a 400 kV accelerator [4] in the underground laboratories of LNGS.

2 The ^{25}Mg(p, γ)^{26}Al reaction

Observations from satellites [5, 6] have discovered a γ-ray line at 1809 keV, which arises from the β-decay of ^{26}Al to ^{26}Mg ($T_{1/2} = 7 \times 10^5$ yr). The intensity of the line corresponds to about 6 solar masses of ^{26}Al in our galaxy. Moreover, the presence of ^{26}Al in the interstellar medium has been determined from the observation of ^{26}Mg isotopic enrichment (extinct ^{26}Al) in carbonaceous meteorites [7]. While the observations from COMPTEL and INTEGRAL provided evidence that ^{26}Al nucleosynthesis is still active on a large scale, the Mg isotopic variations show that ^{26}Mg must have been produced within the last 4.6 billion years (time of the condensation of solar-system material). Any astrophysical scenario for ^{26}Al nucleosynthesis must be concordant with both observations.

The nuclides ^{26}Al are produced mainly via the ^{25}Mg(p,γ)^{26}Al capture reaction. The most important site for the activation of this reaction is the hydrogen-burning shell (HBS), which may be active in off main sequence stars of any mass. In particular, the Mg-Al cycle is at work in the hottest region of the HBS, close to the point of the maximum nuclear energy release. In addition, ^{25}Mg(p,γ)^{26}Al may be also active within the carbon-burning regions in massive stars. In the HBS, the ^{25}Mg(p,γ)^{26}Al reaction starts when the temperature exceeds about 30×10^6 K and between $40 < T/10^6K < 60$ (corresponding to a Gamow energy of about $E_0 = 100$ keV) almost all the original ^{25}Mg is converted into ^{26}Al. At higher temperatures, the destruction of ^{26}Al by ^{26}Al(p,γ)^{27}Si and the refurbishment

of ^{25}Mg by the sequence ^{24}Mg(p,γ)^{25}Al(β^+)^{25}Mg begins to play a relevant role. Once the HBS advances in mass, the ^{26}Al is accumulated within the H-depleted core. A convective dredge up coupled to a huge stellar wind or an explosive ejection of the freshly synthesized material are needed in order to make the ^{26}Al ashes an astronomical observable. However, these processes must occur before the extinction of ^{26}Al through its radioactive decay.

The existence of an active HBS is a common feature in stellar evolution and different classes of stars can have these characteristics: low mass AGB, massive AGB, Novae, Core Collapse Supernovae and Wolf-Rayet stars. Stellar nucleosynthesis studies predict that 30 to 50% of ^{26}Al is produced in the HBS of massive stars (core collapse supernovae or WR-stars). The source of the remaining contribution is unknown and a more precise knowledge of the relevant reaction rates certainly will help in reducing the range of free parameters.

The reaction ^{25}Mg(p,γ)^{26}Al (Q = 6.306 MeV) is dominated by narrow resonances. These resonances have been experimentally verified down to a resonance energy of E_R = 190 keV. From the known level structure of ^{26}Al one expects low-lying resonances at E_R = 93, 109, and 130 keV, among which the 93 keV resonance appeared most important. Indeed, the 93 keV resonance was discovered at LUNA II (figure 1) using the 4π BGO crystal and a ^{25}Mg solid target. For the 130 keV resonance a new upper limit will be available. These new information allow for improved astrophysical calculations of the origin of the 1809 keV line as well as of the chemical evolution of galaxies.

The precision and reliability of absolute values for the resonance strength require unusual efforts in the determination of all quantities entering the determination of these values. In particular the target stoichiometry is a critical parameter. Small, unknown admixtures of oxygen in the chemically enriched ^{25}Mg target, resulting from the evaporation procedure have already a large effect on the determination of the resonance strength. The observed yield, γ-ray spectroscopy for a particular narrow resonance (thick-target yield) depends linearly on the inverse of the effective stopping power [2]. This important quantity includes the active nuclei, i.e. ^{25}Mg, but also inactive nuclei in the target, for example isotopic impurities or other contaminants such as oxygen. Moreover, it is well known in experimental nuclear astrophysics that a solid state target under heavy proton bombardment changes its stoichiometry in the course of the measurement and a frequent control of the target quality is absolutely necessary. This difficulty can be partly solved for the low energy resonance if the strengths of these resonances are determined relative to a precise known resonance at higher energies, where one might study the stoichiometry by a different method. The case of the ^{25}Mg(p,γ)^{26}Al reaction allows for such a normalization by a measurement of the strong E_R = 304 keV resonance with a natural Mg target. Such a target is evaporated from metallic natural Mg pulver with the well known isotopic composition of Mg. In contrast enriched ^{25}Mg targets need to be produced from enriched ^{25}MgO pulver. In order to reduce the uncertainty of the resonance strength of the 304 keV resonance a new determination of this parameter using such natural Mg targets was performed at LNGS. The resonance strength was measured with the standard high efficiency 4π BGO setup - used also for the low energy studies - as well as with a high resolution HPGe detector. The latter was mounted in far geometry from the target to avoid any corrections from possible γ-ray summing effects in the detector. The results of the two methods agreed within their statistical error and will be published

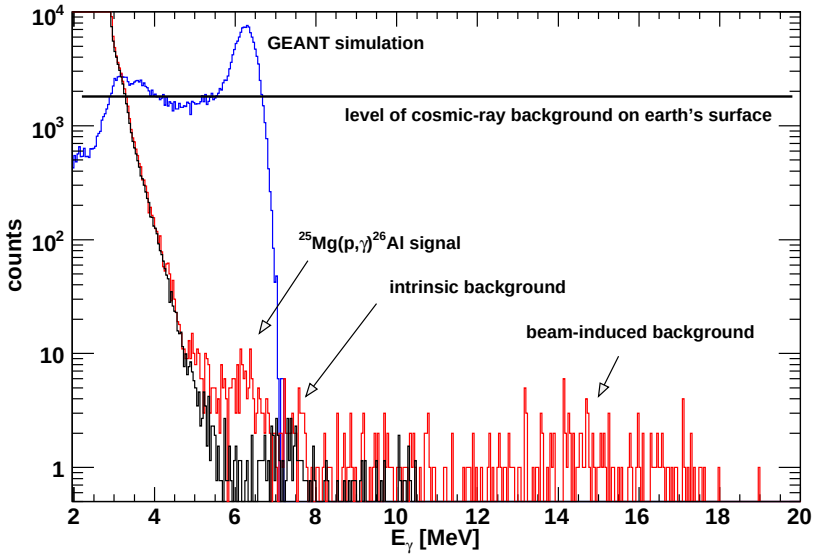

Figure 1: Gamma-ray spectrum of the ^{25}Mg(p,γ)^{26}Al resonance at E = 93 keV obtained with the BGO detector at LNGS and associated background. A high statistics GEANT4 simulation is shown to demonstrate the correct γ-ray energy of the peak.

soon [8]. Furthermore, in the course of this experiment the resonance strengths of the the E_R = 224 keV resonance in ^{24}Mg(p,γ)^{25}Al (see also below) and the E_R = 338 keV resonance in ^{26}Mg(p,γ)^{27}Al were determined independently.

Moreover, the reaction ^{25}Mg(p,γ)^{26}Al is a good example to demonstrate the influence of beam-induced background, which can be much larger than the signal of interest. Thus, in the absence of cosmic-ray background even tiny contaminations of light elements in the ion beam or in the target are observable in a γ-ray spectrum obtained at ultra-low energies. Furthermore, the proton capture on these elements often have high Q-values as in the case of the reaction ^{7}Li(p,γ)^{8}Be (Q = 17.255 MeV), ^{11}B(p,γ)^{12}C (Q = 15.957 MeV), and ^{18}O(p, γ)^{19}F (Q = 7.995 MeV). The capture reactions on ^{11}B and ^{18}O have strong resonances at E_R = 149 and 143.5 keV, respectively, which almost exclude this energy region for precise cross section measurements. The reaction ^{7}Li(p, γ)^{8}Be proceeds through a direct capture process with a fairly high cross section and, indeed, the γ-ray signal of this reaction can be observed in the spectrum of the ^{25}Mg(p,γ)^{26}Al measurement at E_p = 100 keV above the region of interest (Figure 1).

Systematic uncertainties often hamper a precise measurement since these uncertainties are difficult to identify and quantify. To discover systematic errors one has to use different approaches. Recently, the AMS approach (AMS for Accelerator Mass Spectrometry) has been used as such an alternative approach [9]. The ^{26}Al nuclei represents in principal an ideal case for such a study since ^{26}Al is radioactive with a reasonable long half life and the corresponding stable isobar ^{26}Mg does not form negative ions.

A new chemical procedure to extract the ^{26}Al out of the Mg bulk has been developed and tested in the LNGS chemistry laboratory. The new liquid–liquid extraction technique

largely reduces the risk of material loss during the AMS sample preparation. The AMS procedure itsself is now a standard techniques and well established.

However, the quality and stability of the target as outlined above remains a challenge also in this approach. The normalization to a stronger resonance at higher energy of the same reaction, cannot be applied in an AMS experiment since this normalization would lead to the production of a much larger number of reaction products, sometimes several orders of magnitude: such a sample cannot longer be used for AMS. Nevertheless, the underground laboratory might often offer a solution. It is almost impossible to produce isotopically pure targets. For most of the elements these isotopic impurities will be in the order of several percent and a normalization to a known resonance of a reaction on one of the isotopes might be feasible if the quantity of the impurity is known and the detection setup is sensitive enough. In the case of the ^{25}Mg(p,γ)^{26}Al reaction an enriched ^{25}Mg target contained about 1.5% ^{24}Mg and a low energy ^{25}Mg(p,γ)^{26}Al AMS measurement can be normalized to the E_R = 224 keV resonance in ^{24}Mg(p,γ)^{25}Al. Thus, the new determination of the resonance strength of this E_R = 224 keV resonance in ^{24}Mg(p,γ)^{25}Al in the γ-ray spectroscopy experiment of this project also improves the prescision of the AMS result.

3 ^{15}N(p,γ)^{16}O

For stars with masses larger than the Sun, the CNO cycle is the most important process for energy production during the Hydrogen burning phase. The ^{15}N(p,γ)^{16}O reaction (Q-value Q = 12.127 MeV) links the CN cycle to the CNO bi-cycle and all further CNO cycles [10]. The ratio between the reaction rate of the ^{15}N(p,γ)^{16}O and the ^{15}N(p,α γ)^{12}C reactions determines directly the nucleosynthesis of the oxygen isotopes ^{16}O, ^{17}O and ^{18}O as well as the neutrino production coming from the β-decay of ^{17}F. ^{17}F neutrinos are expected to contribute to the low energy solar neutrino flux in Borexino [11].

At astrophysically relevant energies E $\leq$ 1 MeV, the ^{15}N(p,γ)^{16}O excitation function is influenced by two resonances at E_p=335 and 1028 keV (E_x = 12440 and 13090 keV with respective widths of Γ_p = 91 and 130 keV), both decaying predominantly into the ground state of ^{16}O.

The non-resonant cross section has been studied in previous experiments using NaI(Tl) [12] and Ge(Li) [13] detectors, reporting discordant cross section data for E_p = 150 – 2500 keV [13].

Recently, the asymptotic normalization coeffcients (ANCs) for direct capture to ground and several excited states in ^{16}O have been measured [14]. It was found that the low-energy non-resonant yield is dominated by ground state capture, but the new ANC leads to a much lower direct capture cross section than previously. The new ANC values have then been used in an R-matrix fit [14] including also the cross section data from refs. [12, 13], suggesting a factor two lower astrophysical S-factor than previously believed [12, 13, 15]. Another recent R-matrix analysis concentrating on ground state capture was based again on the direct data from [12, 13], and it also indicates a much lower S-factor [16].

In view of the conflicting data [12, 13] and the recent extrapolations [14, 16], new ex-

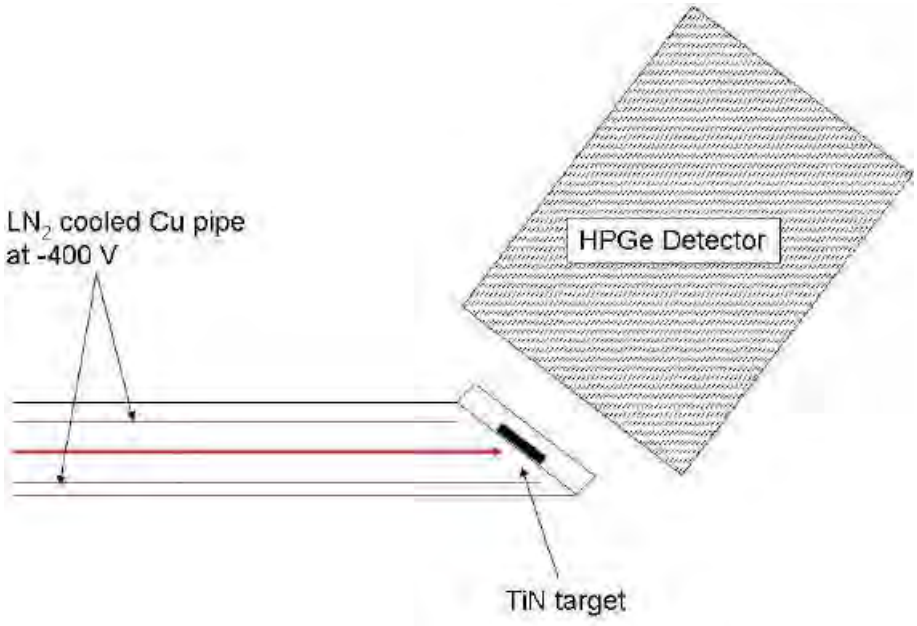

Figure 2: Setup used for investigating the ^{15}N(p,γ)^{16}O with solid state targets and a HPGe detector. The beam direction is indicated by the arrow.

perimental data is clearly called for. The LUNA collaboration aims to experimentally determine the ^{15}N(p,γ)^{16}O cross section directly at energies corresponding to hydrogen burning in novae and AGB stars. The relevant temperatures in novae are T_6 = 200 - 400 (T_6 denoting the central temperature of a star in units of 10^6K), corresponding to Gamow energies of E_0 = 150-240 keV.

3.1 Measurement of the ^{15}N(p,γ)^{16}O reaction over a wide energy range with HPGe Detectors

When extrapoling nuclear data to low energies data sets covering a large energy range are highly demanded. To provided such data in 2007 LUNA has started a collaboration with the Nuclear Structure Laboratory of the Notre Dame University [17]

At the beginning of 2008 the experimental setup used at the Notre Dame University the reaction has been measured in the energy range E_p = 290—1900 keV has been installed at the LUNA 400 kV accelerator at LNGS. Briefly, the setup consisted in a TiN 99% ^{15}N enriched deposited target positioned at close geometry to a HPGe detector (Figure 2). The targets had a thickness of 10–40 keV at 400 keV proton energy beam and were extremely stable lasting several days of beam bombardment. Typical currents were of the order of 100 μA. Regular checks on the target stability have been performed at LUNA exploiting the broad 330 keV resonance in ^{15}N(p,γ)^{16}O and the narrow 278 keV resonance in ^{14}N(p,γ)^{15}O. After the conclusion of the experimental phase at LUNA all targets have been transferred back to Notre Dame to determine their target profile employing the narrow 335 keV resonance in ^{15}N(p,$\alpha\gamma$)^{16}O used as a reference also during the experiments

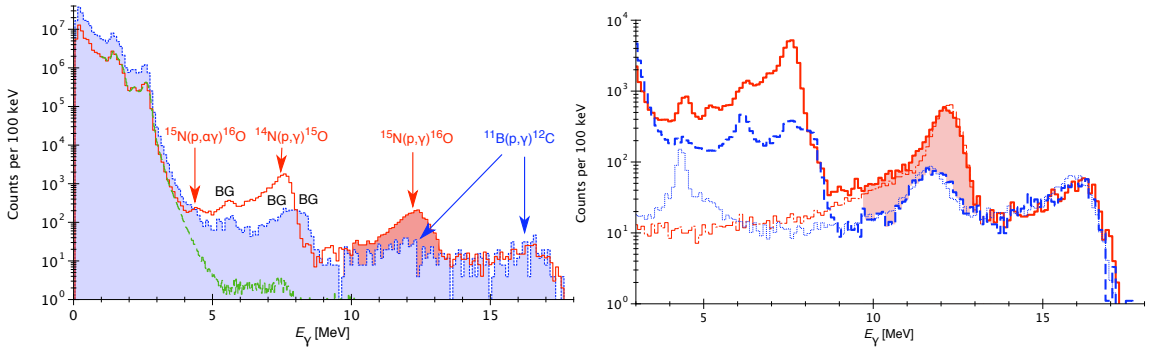

Figure 3: *Left panel:* γ-ray spectrum, $E_p = 150$ keV. Solid (dotted) line: Nitrogen gas in the target (helium gas, rescaled to match the nitrogen spectrum in the 14.4 – 18.0 MeV region). Dashed line, laboratory background. *Right panel:* γ-ray spectrum, $E_p = 220$ keV. Red solid (dot-dashed) line: Experimental, nitrogen gas (simulated, ^{15}N(p,γ)^{16}O). Blue dashed (dotted) line: Experimental, helium gas, rescaled as in the left panel (simulated, ^{11}B(p,γ)^{12}C).

in Notre Dame.

The data obtained at LUNA reach from $E_p = 150$ to 400 keV and data set of the two measurements will cover a very large energy region and in particular the two most important interference regions, allowing a much better extrapolation to astrophysical energies.

In January 2008 the target and detection setup has been installed LNGS.This way the the data set has been extended down to proton energy of 130 keV.
The evaluation of these data will be concluded in 2009.

3.2 Re-visitation of the data experiment obtained with the LUNA gas target – BGO setup

The data acquired in the period from 2003-2004 experiments in the context of the experiments on the ^{14}N(p,γ)^{15}O [18, 19] have been reanalyzed with a focus on the ^{15}N(p,γ)^{16}O reaction. The spectra were taken using a BGO summing detector and a windowless gas target cell [18, 19] filled with 1 mbar of nitrogen gas of natural composition. They clearly show the signature of the ^{15}N(p,γ)^{16}O reaction (Figure 3).

The ^{15}N(p,γ)^{16}O cross section has been determined at twelve center-of-mass interaction energies E between 90 and 230 keV shown in Figure 4 [20]. The statistical uncertainty is typically well below 10%.

The present S-factor data are about a factor two lower than the previous data by ref. [13], but still consistent at 2Σ level given the previous high uncertainties. In the limited overlapping energy region, the present data seem to agree with ref. [12]. The data from the present work extend to energies lower than ever measured before and are signicantly lower than the low-energy extrapolation adopted in the NACRE [15] compilation.

The present data are on average 20% lower than, but given the previous uncertainty still consistent with, the recent R-matrix fit based on an ANC measurement [14]. They

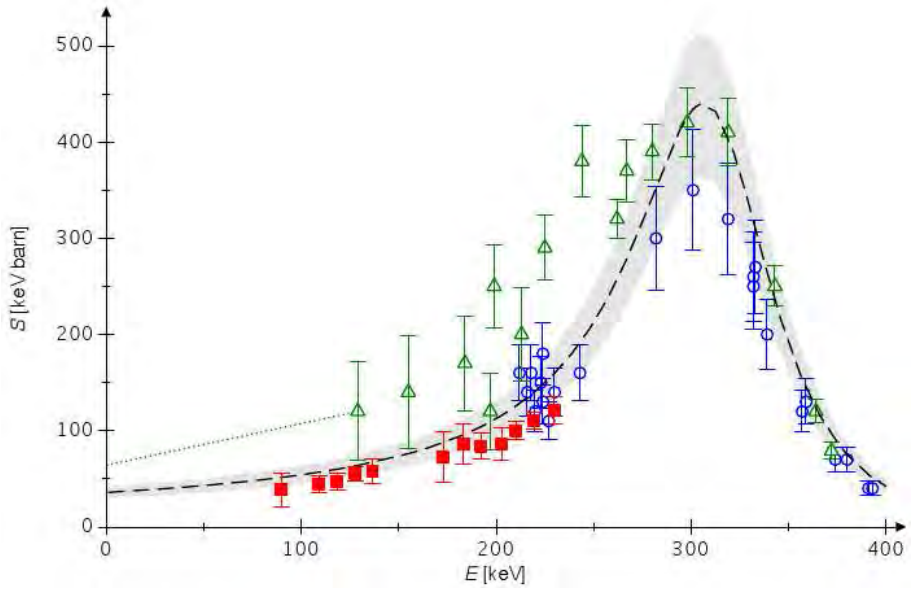

Figure 4: ^{15}N(p,γ)^{16}O astrophysical S–factor. Experimental data from ref. [12] (blue circles, limited to E 210 keV), ref. [13] (green triangles) and the present work [20]. Error bars reflect statistical and systematic uncertainties summed in quadrature. Dotted line, previous low-energy extrapolation by the NACRE compilation [15]. Dashed line, previous R- fit, and shaded area, its quoted 17% uncertainty [14].

are also lower than the fits shown in ref. [16]. These R-matrix fits [14, 16] had relied on direct experimental data from Refs. [12, 13] for the dominating resonant contribution, and it seems prudent to call for a new R-matrix fit, which is beyond the scope of the present work.

Previous one-zone nucleosynthesis calculations of novae [21] have shown that a factor two lower ^{15}N(p,γ)^{16}O rate results in up to 22% reduction in the final ^{16}O yield, depending on the nova temperature. Further implications of the changed ^{15}N(p,γ)^{16}O rate are yet to be studied.

3.3 Measurement of ^{15}N(p,γ)^{16}O at LUNA with and solid state target and BGO detector

Based on the experience gained in the experimental phases described in sec. 3.2 and 3.1 the LUNA collaboration has started an additional experiment on ^{15}N(p,γ)^{16}O. In this approach solid state targets produced at FZ Karlsruhe and similar to those used for the measurements described in sec.3.1 have been mounted inside the LUNA BGO detector (Figure 5) where they have been bombarded by the beam provided by the LUNA 400 kV accelerator. The aim of the experiment is to cover the energy region from E$_R$=370 to 50 keV. These energies correspond to the Gamow peak for ^{15}N(p,γ)^{16}O in Novae and AGB stars. As a consequence after the conclusion of these measurements no extrapolation will be needed any more for these astrophysical environments.

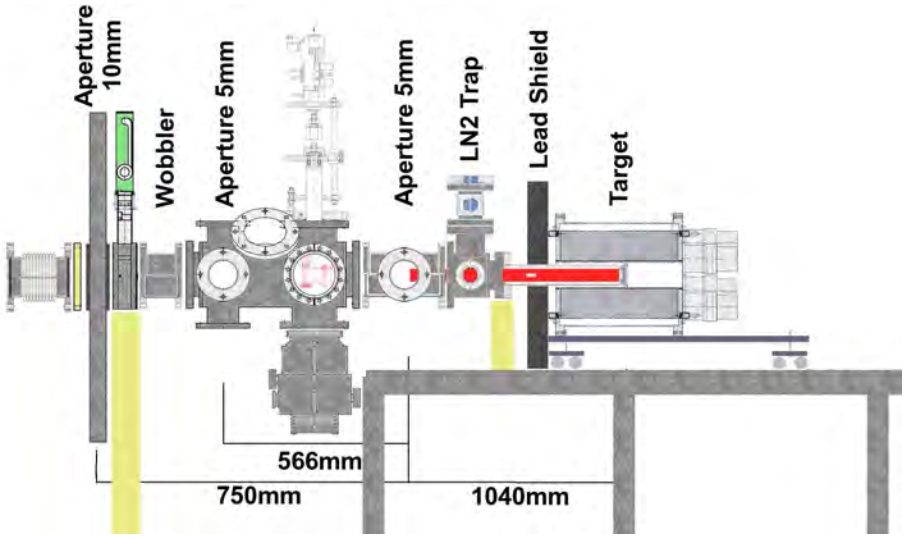

Figure 5: Setup used for investigating the ^{15}N(p,γ)^{16}O with solid state targets and a BGO detector.

In 2008 data down to E_{lab}=82 keV have been taken. A series of systematic tests have been carried out to control the stability of the targets during irradiation including SNMS (Secondary Neutral Mass Spectrometry) at ATOMKI in Debrecen (Hungary) and Nuclear Reaction Analysis at the Nuclear Structure Laboratory of the Notre Dame University (USA) and at the FZ Dresden (Germany). The data taking and analysis will continue in the course of the year 2009.

Acknowledgments

The LUNA collaboration acknowledges the continuous support by the mechanical and the electronic workshop of LNGS. We are grateful to the staff of the LNGS chemistry service.

References

[1] W.A.Fowler, Rev.Mod.Phys. 56, 149 (1984)

[2] C.Rolfs and W.S.Rodney, Cauldrons in the Cosmos (University of Chicago Press, 1988)

[3] G. Fiorentini et al., Z.Phys. A350, 289 (1995)

[4] A. Formicola et al., NIM A 507, 609 (2003)

[5] J. Knödlseder, D. Dixon, K. Bennett et al., A&A 345, 813 (1999).

[6] C. Winkler, T.C. Courvoisier, G. Di Cocco et al., A&A, 411 L1 (2003).

[7] G.J. Wasserburg, in Protostars and planet II, edited by D.C. Black and M.S. Matthews (University of Arizona Press, Tucson, 1985), p.703.

[8] The LUNA collaboration, Phys. Rev. C (in preparation, 2009).

[9] A. Arazi et al., Phys. Rev. C 74 (2006) 025802.

[10] C. Iliadis, Nuclear Physics of Stars (Wiley-VCH) (2007)

[11] L. Stonehill, J. Formaggio and R. Robertson, Phys. Rev. C 69, 015801(2004)

[12] D.F. Hebbard, Nucl. Phys. A 15, 289 (1960)

[13] C. Rolfs and W. Rodney, Nucl. Phys. A 235,450 (1974)

[14] A.M. Mukhamedzhanov et al., Phys. Rev. C 78 015804 (2008)

[15] C. Angulo et al., Nucl. Phys. A 656, 3 (1999)

[16] F.C. Barker,Phys. Rev. C 78 044612 (2008)

[17] LUNA Collaboration, Contrib. to LNGS Annual Report 2007, available at www.lngs.infn.it

[18] A. Lemut et al., Phys. Lett. B 634, 483 (2006)

[19] D. Bemmerer et al., Nucl. Phys. A 779, 297 (2006)

[20] D. Bemmerer et al., http://arXiv.org/abs/0902.0783v1, accepted by J.Phys.G,

[21] C. Iliadis , A. Champagne, J. Jos, S. Starrfield and P. Tupper, Astrophys. J. Suppl. Ser. 142 105 – 137 (2002)

Publications

1. "The ^{3}He(α,γ)^{7}Be S-factor at solar energies: the prompt γ experiment at LUNA", H. Costantini, D. Bemmerer, F. Confortola, A. Formicola, Gy. Gyürky, P. Bezzon, R. Bonetti, C. Broggini, P. Corvisiero, Z. Elekes, Zs. Fülöp, G. Gervino, A. Guglielmetti, C. Gustavino, G. Imbriani, M. Junker, M. Laubenstein, A. Lemut, B. Limata, V. Lozza, M. Marta, R. Menegazzo, P. Prati, V. Roca, C. Rolfs, C. Rossi Alvarez, E. Somorjai, O. Straniero, F. Strieder, F. Terrasi. H.P. Trautvetter, Nuclear Physics, Section A 814 (2008), pp. 144-158

2. "Precision study of ground state capture in the ^{14}N(p,γ)^{15}O reaction", M. Marta, A. Formicola, Gy. Gyürky, D. Bemmerer, C. Broggini, A. Caciolli, P. Corvisiero, H. Costantini, Z. Elekes, Zs. Fülöp, G. Gervino, A. Guglielmetti, C. Gustavino, G. Imbriani,M. Junker, R. Kunz, A. Lemut, B. Limata, C. Mazzocchi, R. Menegazzo, P. Prati, V. Roca, C. Rolfs, M. Romano, C. Rossi Alvarez, E. Somorjai, O. Straniero, F. Strieder, F. Terrasi, H.P. Trautvetter, A. Vomiero, Physical Review C 78(2008), 022802(R)

3. "Nuclear Astrophysics at LUNA: Status And Perspectives", P. Prati, D. Bemmerer, R. Bonetti, C. Broggini, P. Corvisiero, F. Confortola, E. Conti, H. Costantini, Z. Elekes, A. Formicola, Zs. Fülöp, G. Gervino, A. Guglielmetti, Gy. Gyürky, C. Gustavino, G. Imbriani, M. Junker, A. Lemut, B. Limata, M. Marta, C. Mazzocchi, R. Menegazzo, V. Roca, C. Rolfs, C. Rossi Alvarez, E. Somorjai, O. Straniero, F. Strieder, F. Terrasi, and H. P. Trautvetter, AIP Conf. Proc. 1012 (2008), 305-312

4. "Comparison of the LUNA ^{3}He(α,γ)^{7}Be activation results with earlier measurements and model calculations", Gy. Gyürky, D. Bemmerer, F. Confortola, H. Costantini, A. Formicola, R. Bonetti, C. Broggini, P. Corvisiero, Z. Elekes, Zs. Fülöp, G. Gervino, A. Guglielmetti, C. Gustavino, G. Imbriani, M. Junker, M. Laubenstein, A. Lemut, B. Limata, V. Lozza, M. Marta, R. Menegazzo, P. Prati, V. Roca, C. Rolfs, C. Rossi Alvarez, E. Somorjai, O. Straniero, F. Strieder, F. Terrasi and H. P. Trautvetter, J. of Phys. G 35 (2008) 014002

5. "Measurement of ^{25}Mg(p,γ)^{26}Al resonance strengths via gamma spectrometry", A. Formicola, A. Best, G. Imbriani, M. Junker, D. Bemmerer, R. Bonetti, C. Broggini, A. Caciolli, F. Confortola, P. Corvisiero, H. Costantini, Z. Elekes, Zs. Fülöp, G. Gervino, A. Guglielmetti, Gy. Gyürky, C. Gustavino, A. Lemut, B. Limata, M. Marta, C. Mazzocchi, R. Menegazzo, P. Prati, V. Roca, C. Rolfs, C. Rossi Alvarez, E. Somorjai, O. Straniero, F. Strieder, F. Terrasi and H. P. Trautvetter, J. of Phys. G 35 (2008) 014013

6. "Ground state capture in ^{14}N(p,γ)^{15}O studied above the 259 keV resonance at LUNA", H. P. Trautvetter, D. Bemmerer, R. Bonetti, C. Broggini, A. Caciolli, F. Confortola, P. Corvisiero, H. Costantini, Z. Elekes, A. Formicola, Zs. Fülöp, G. Gervino, A. Guglielmetti, Gy. Gyürky, C. Gustavino, G. Imbriani, M. Junker, A. Lemut, B. Limata, M. Marta, C. Mazzocchi, R. Menegazzo, P. Prati, V. Roca, C. Rolfs, C. Rossi Alvarez, E. Somorjai, O. Straniero, F. Strieder, F. Terrasi, S. Vezzu and A. Vomiero (LUNA Collaboration), J. Phys. G 35 (2008) 014019

List of Conferences

1. C.Broggini, "Luna and the Sun", Physics of massive neutrinos, talk at "Physics of Massive Neutrinos", Milos, 20-22 May 2008

2. C.Broggini, "Underground nuclear astrophysics and the Sun", invited talk at "XXVIII Physics in collision conference", Perugia, 25-28 Giugno 2008

3. C.Broggini, "Luna and the neutrinos from the Sun", talk at "Neutrino oscillation workshop", Conca Specchiulla, 6-13 September 2008

4. D. Bemmerer, "Laboratory for Underground Nuclear Astrophysics (LUNA)", Poster presentation, "IEEE Nuclear Science Symposium", Dresden, 19-26 October 2008

5. A. Caciolli, "Status of the $^{15}N(p,\gamma)^{16}O$ reaction study", oral contribution at "XCIV Congresso Nazionale della Societa' Italiana di Fisica", Genova, 22 - 27 settembre 2008

6. A. Caciolli, "LUNA: The $^{15}N(p,\gamma)^{16}O$ reaction and the ^{17}F neutrinos from the sun Neutrinos", Oral contribution at "Particle in Nuclear and in Astrophysics", 5th Annual Meeting of ENTApP N6/WP, ETC* Trento, 16-21 November 2008

7. A. Caciolli, "Ultra-sensitive in-beam γ-ray spectroscopy for nuclear astrophysics at LUNA", Invited talk at the FZD Dresden (Germania)

8. H. Costantini, "Nuclear Astrophysics at the Gran Sasso Underground Laboratory", October 2008 Invited talk at "Nuclear Physics Underground workshop in the occasion of the DNP08", Oakland, CA, USA October 2008

9. A. Formicola, "Status of S(0) factors", invited talk at "The physics of the sun and the solar neutrinos: An update", LNGS, Assergi 16–17 October 2008

10. A.Lemut, "Underground Nuclear Astrophysics", Invited talk at "XXXI Symposium on Nuclear Physics", January 7th-10th 2008, Hotel Hacienda Cocoyoc, Cocoyoc, Mexico

11. M. Marta, "Precision study of the $^{14}N(p,\gamma)^{15}O$ reaction at LUNA", oral presentation at "German Physics Society Spring Meeting (DPG Frühjahrstagung)", 10.–14.03.2008, Darmstadt, Germany

12. M. Marta, "Precision study of ground state capture in the $^{14}N(p,\gamma)^{15}O$ reaction", Poster presentation at "10th International Symposium on Nuclei in the Cosmos", 27.07.-01.08.2008, Mackinac Island, Michigan, USA

13. F. Strieder, "Measurement of the low energy resonances of the reaction $^{25}Mg(p,\gamma)^{26}Al$", oral presentation at "German Physics Society Spring Meeting (DPG Frühjahrstagung)", 10.–14.03.2008, Darmstadt, Germany

LVD. Large Volume Detector

The LVD Collaboration

N.Yu.Agafonova[9], M.Aglietta[14], E.D.Alyea[7], P.Antonioli[1], G.Badino[14], G.Bari[1], M.Basile[1], V.S.Berezinsky[9], M.Bertaina[14], R.Bertoni[14], A. Bonardi[14], G.Bruni[1], G.Bruno[5], G.Cara Romeo[1], A.Chiavassa[14], J.A.Chinellato[3], L.Cifarelli[1], F.Cindolo[1], A.Contin[1], V.L.Dadykin[9], E.A. Dobrynina[9], L.G.Dos Santos[3], R.I.Enikeev[9], W.Fulgione[14], P.Galeotti[14], M.Garbini[1,15], P.L.Ghia[5,14], G.Giuliani[5,14], P.Giusti[1], F.Gomez[14], F.Grianti[4], G.Iacobucci[1], E.Kemp[3], E.V.Korolkova[9], V.B.Korchaguin[9], V.V.Kuznetsov[9], M.Luvisetto[1], A.A.Machado[5], A.S.Malguin[9], H.Menghetti[1], N.Mengotti Silva[3], C.Morello[14], R.Nania[1], G.Navarra[14], K.Okei[10], L.Periale[14], R.Persiani[1], A.Pesci[1], P.Picchi[14], I.A.Pless[8], A.Porta[14], A.Romero[14], V.G.Ryasny[9], O.G.Ryazhskaya[9], O.Saavedra[14], K.Saitoh[13], G.Sartorelli[1], M.Selvi[1], N.Taborgna[5], N.Takahashi[12], V.P.Talochkin[9], G.C.Trinchero[14], S.Tsuji[11], A.Turtelli[3], P.Vallania[14], S.Vernetto[14], C.Vigorito[14], L.Votano[4], T.Wada[10], R.Weinstein[6], M.Widgoff[2], V.F.Yakushev[9], G.T.Zatsepin[9], A.Zichichi[1,*]

[1] *University of Bologna and INFN-Bologna, Italy*
[2] *Brown University, Providence, USA*
[3] *University of Campinas, Campinas, Brazil*
[4] *INFN-LNF, Frascati, Italy*
[5] *INFN-LNGS, Assergi, Italy*
[6] *University of Houston, Houston, USA*
[7] *Indiana University, Bloomington, USA*
[8] *Massachusetts Institute of Technology, Cambridge, USA*
[9] *Institute for Nuclear Research, Russian Academy of Sciences, Moscow, Russia*
[10] *Okayama University, Okayama, Japan*
[11] *Kawasaki Medical School, Kurashiki, Japan*
[12] *Hirosaki University, Hirosaki, Japan*
[13] *Ashikaga Institute of Technology, Ashikaga, Japan*
[14] *IFSI-INAF, Torino; University of Torino and INFN-Torino, Italy*
[15] *Museo Storico della Fisica, Centro Studi e Ricerche "E. Fermi", Rome, Italy*

[*] *Spokesperson of the LVD experiment*

Abstract

The Large Volume Detector (LVD) in the INFN Gran Sasso National Laboratory, Italy, is a ν observatory mainly designed to study low energy neutrinos from the gravitational collapse of galactic objects.

The experiment has been monitoring the Galaxy since June 1992, under increasing larger configurations: in January 2001 it has reached its final active mass $M = 1$ kt. LVD is one of the largest liquid scintillator apparatus for the detection of stellar collapses and, besides SuperKamiokande and Amanda, it is a member of the SNEWS network, that has become fully operational since July 1st, 2005.

During 2008 there was a long run of the CNGS project: LVD was fully operative; we report about the detected CNGS events.

1 The LVD experiment

1.1 Scientific ground

The Large Volume Detector (LVD), located in the hall A of the INFN Gran Sasso National Laboratory, Italy, is a multipurpose detector consisting of 1000 tons of liquid scintillator arranged in a compact and modular geometry (a front view is shown in fig.1). The major purpose of the LVD experiment is the search for neutrinos from Gravitational Stellar Collapses (GSC) in our Galaxy [1].

Indeed, in spite of the lack of a "standard" model of the gravitational collapse of a massive star, the correlated neutrino emission appears to be well established. At the end of its burning phase a massive star ($M > 8M_{\odot}$) explodes into a supernova, originating a neutron star which cools emitting its binding energy $E_B \sim 3{\cdot}10^{53}$ erg mostly in neutrinos. The largest part of this energy, almost equipartitioned among neutrino and antineutrino species, is emitted in the cooling phase: $E_{\bar{\nu}_e} \sim E_{\nu_e} \sim E_{\nu_x} \sim E_B/6$ (where ν_x denotes generically $\nu_\mu, \bar{\nu}_\mu, \nu_\tau, \bar{\nu}_\tau$ flavors). The energy spectra are approximatively a Fermi-Dirac distribution, with different mean temperatures, since ν_e, $\bar{\nu}_e$ and ν_x have different couplings with the stellar matter: $T_{\nu_e} < T_{\bar{\nu}_e} < T_{\nu_x}$.

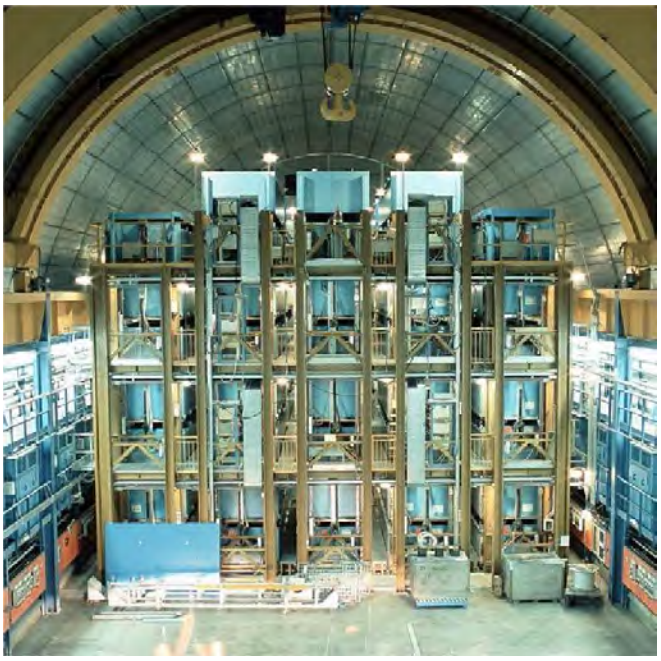

Figure 1: *Front view of the LVD detector in the hall A of the Gran Sasso National Laboratory, INFN.*

LVD is able to detect $\bar{\nu}_e$ interactions with protons in the scintillator, which give the main signal of supernova neutrinos, with a very good signature. Moreover, it can detect ν_e

through the elastic scattering reactions with electrons, $(\nu_e + \bar{\nu}_e)$ through charged current interactions with the carbon nuclei of the scintillator, and it is also sensitive to neutrinos of all flavors detectable through neutral currents reactions with the carbon nuclei. The iron support structure of the detector can also act as a target for electron neutrinos and antineutrinos. The products of the interaction can exit iron and be detected in the liquid scintillator. The amount of neutrino-iron interaction can be as high as about 20% of the total number of interactions. The signal observable in LVD, in different reactions and due to different kinds of neutrinos, besides providing astrophysical informations on the nature of the collapse, is sensitive to intrinsic ν properties, as oscillation of massive neutrinos and can give an important contribution to define some of the neutrino oscillation properties still missing.

1.2 The detector

The LVD experiment has been in operation since 1992, under different increasing configurations. During 2001 the final upgrade took place: LVD became fully operational, with an active scintillator mass $M = 1000$ t.
LVD consists of an array of 840 scintillator counters, 1.5 m^3 each, viewed on the top by three photomultipliers (visible in fig. 2). Up to 2004, before a re-calibration of the full detector, the counters were divided in two subsets: the external ones (43%), operated at energy threshold $\mathcal{E}_h \simeq 7$ MeV, and inner ones (57%), better shielded from rock radioactivity and operated at $\mathcal{E}_h \simeq 4$ MeV. After the re-calibration (which, started in 2004, ended during 2005) all the counters are operated at a common threshold, $\mathcal{E}_h \simeq 4$ MeV.

Figure 2: *Top view of the LVD detector in the hall A of the Gran Sasso National Laboratory, INFN.*

To tag the delayed γ pulse due to n-capture, all counters are equipped with an additional discrimination channel, set at a lower threshold, $\mathcal{E}_l \simeq 1$ MeV.
Other relevant features of the detector are:
(i) good event localization and muon tagging;
(ii) accurate absolute and relative timing: $\Delta t_{abs} = 1\,\mu s$, $\Delta t_{rel} = 12.5\,ns$;
(iii) energy resolution: $\sigma_E/E = 0.07 + 0.23 \cdot (E/\mathrm{MeV})^{-0.5}$;
(iv) very high duty cycle, i.e. $> 99.5\%$ in the last eight years;
(v) fast event recognition.

1.3 Supernova neutrino interactions in LVD

The observable neutrino reactions in the LVD scintillator are:

(1) $\bar{\nu}_e p, e^+ n$, (physical threshold $E_{\bar{\nu}_e} > 1.8\ MeV$) observed through a prompt signal from e^+ above threshold $\mathcal{E}_h$ (detectable energy $E_d \simeq E_{\bar{\nu}_e} - 1.8$ MeV $+2m_e c^2$), followed by the signal from the $np, d\gamma$ capture ($E_\gamma = 2.2$ MeV), above $\mathcal{E}_l$ and with a mean delay $\Delta t \simeq 185\ \mu$s.

(2) ν_e ^{12}C,^{12}N e^-, (physical threshold $E_{\nu_e} > 17.3\ MeV$) observed through two signals: the prompt one due to the e^- above $\mathcal{E}_h$ ($E_d \simeq E_{\nu_e} - 17.3$ MeV) followed by the signal, above $\mathcal{E}_h$, from the β^+ decay of ^{12}N (mean life $\tau = 15.9$ ms).

(3) $\bar{\nu}_e$ ^{12}C,^{12}B e$^+$, (physical threshold $E_{\bar{\nu}_e} > 14.4\ MeV$) observed through two signals: the prompt one due to the e^+ ($E_d \simeq E_{\bar{\nu}_e} - 14.4\,\text{MeV} + 2m_e c^2$) followed by the signal from the β^- decay of ^{12} B (mean life $\tau = 29.4$ ms). As for reaction *(2)*, the second signal is detected above the threshold $\mathcal{E}_h$.

(4) $\overset{(-)}{\nu}_\ell$ ^{12}C, $\overset{(-)}{\nu}_\ell$ ^{12}C* ($\ell = e, \mu, \tau$), (physical threshold $E_\nu > 15.1\ MeV$), whose signature is the monochromatic photon from carbon de-excitation ($E_\gamma = 15.1$ MeV), above $\mathcal{E}_h$.

(5) $\overset{(-)}{\nu}_\ell$ e^-, $\overset{(-)}{\nu}_\ell$ e^-, which yields a single signal, above $\mathcal{E}_h$, due to the recoil electron.

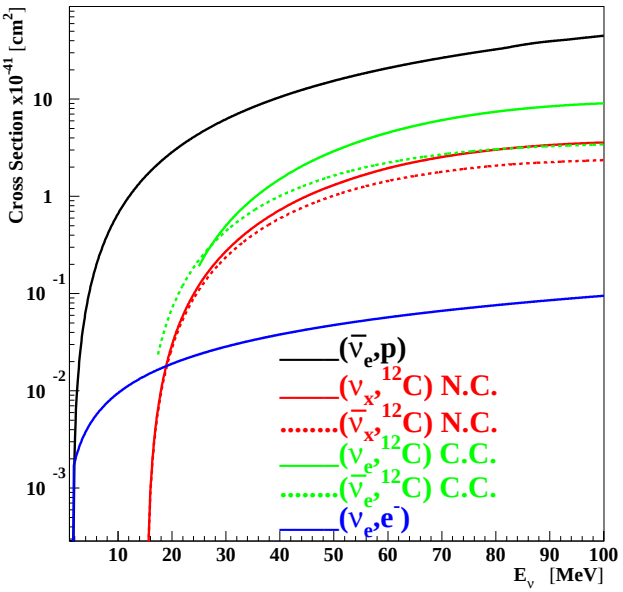

Figure 3: *Cross section behavior for the different neutrino reactions observable in the LVD scintillator.*

The LVD detector is supported by an iron structure made basically by two components: the tank (mean thickness: 0.4 *cm*), containing the scintillator, and the "portatank" (mean thickness: 1.5 *cm*) hosting a cluster of 8 tanks. The higher energy part of the ν flux can thus be detected also with the $\nu(\bar{\nu})$Fe interaction, resulting in an electron (positron) that may exit the iron and release energy in the scintillator. The reactions of interest are the following:

(6) ν_e ^{56}Fe,^{56}Co e^-. The mass difference between the nuclei is $\Delta_{m_n} = m_n^{\text{Co}} - m_n^{\text{Fe}} = 4.055$ MeV, the first Co allowed state being at 3.589 MeV. Other higher energy allowed states are present in ^{56}Co: considering $E_{e^-}^{\text{kin}} = E_{\nu_e} - \Delta_{m_n} - E_{\text{level}} - m_e$ MeV, where E_{level} is the energy difference between the excitation level and the ground state level, this can take values: $3.589, 4.589, 7.589, 10.589\ MeV$. The efficiency for electron and gammas (also produced in the interaction) to reach the scintillator with energy higher than $\mathcal{E}_h$ is greater than 20% for $E_\nu > 30$ MeV and grows up to 70% for $E_\nu > 100$ MeV. On average, the detectable electron energy is $E_d \simeq 0.45 \times E_\nu$.

(7) $\bar{\nu}_e$ ^{56}Fe,^{56}Mn e^+, the energy threshold and the efficiency are very similar to those of reaction *(6)*.

The number of all the possible targets present in the LVD detector is listed in table 1.

Table 1: Number of targets in the LVD detector.

Target Type	Contained in	Mass	Number of targets
Free protons	Liquid Scintillator	1000 t	9.34 10^{31}
Electrons	LS	1000 t	3.47 10^{32}
C Nuclei	LS	1000 t	4.23 10^{31}
Fe Nuclei	Support Structure	900 t	9.71 10^{30}

1.4 Effects of neutrino oscillations in the SN signal

There are many experimental works suggesting neutrino conversion among flavors in the recent few years, through the study of atmospheric, solar, reactor and accelerator neutrinos. The interpretation of all these phenomena in terms of neutrino oscillations is rather robust, because it is able to include all the experimental data (except the LSND signal). In the standard three flavor scenario, six parameters must be determined by oscillation experiments: 3 mixing angles ($\theta_{\rm sol}$, θ_{13}, $\theta_{\rm atm}$), 2 squared mass differences ($\Delta m^2_{\rm sol}$ and $\Delta m^2_{\rm atm}$) and 1 CP-violation phase δ. A recent analysis of all the available experimental data constrains the "atmospheric" and "solar" parameters to be in the following 99% $C.L.$ ranges:
$\Delta m^2_{\rm sol}$ $(7.2 \div 8.9)\, 10^{-5}$ eV^2
$|\Delta m^2_{\rm atm}|$ $(1.7 \div 3.3)\, 10^{-3}$ eV^2
$\theta_{\rm sol}$ $30^\circ < \theta_{\rm sol} < 38^\circ$
$\theta_{\rm atm}$ $36^\circ < \theta_{\rm atm} < 54^\circ$
However the other parameters are not completely determined: the θ_{13} mixing angle is only upper limited, mainly by the Chooz experiment data ($\sin^2\theta_{13} < 3.\ 10^{-2}$ at the 99% $C.L.$), the sign of $\Delta m^2_{\rm atm}$ (that fixes the so–called mass hierarchy) is completely unknown, as well as the CP–violation phase δ.
Because of the wide range of matter density in the stellar envelope, a supernova explosion represents a unique scenario for further study of the neutrino oscillation mixing matrix. Indeed neutrinos can cross two resonance density layers and therefore the resulting possible mixing scenarios are different from the solar ones. The emerging neutrino spectra are sensitive to the sign of $\Delta m^2_{\rm atm}$ and to the value of θ_{13}.

We have studied how neutrino oscillations affect the signal detected by LVD and also evaluate the impact on the signal of the astrophysical parameters of the supernova explosion mechanism, such as the total energy emitted in neutrinos, the star distance, the neutrino–sphere temperatures and the partition of the energy among the neutrino flavors. Preliminary results have been presented previously in [3] [4] [5] and are now published in [6].

For a normal mass hierarchy (NH) scheme, ν (not $\bar{\nu}$) cross two resonance layers: one at higher density (H), which corresponds to $\Delta m^2_{\rm atm}, U^2_{e3}$, and the other at lower density (L), corresponding to $\Delta m^2_{\rm sol}, U^2_{e2}$. For inverted mass hierarchy (IH), transitions at the higher density layer occur in the $\bar{\nu}$ sector. Given the energy range of SN ν (up to ~ 100 MeV) and considering a star density profile $\rho \propto 1/r^3$, the adiabaticity condition is always satisfied

at the L resonance for any LMA solution, while at the H resonance, this depends on the value of U^2_{e3}. When $U^2_{e3} \geq 5 \cdot 10^{-4}$ the conversion is completely adiabatic, meaning that the flip probability between two adjacent mass eigenstates is null ($P_h = 0$). In the adiabatic case and NH, the $\bar{\nu}_e$ produced in the SN core arrive at Earth as ν_1, and they have a high ($U^2_{e1} \simeq cos^2\theta_{12} \simeq 0.7$) probability to be detected as $\bar{\nu}_e$. On the other hand, the original $\bar{\nu}_x$ arrive at Earth as ν_2 and ν_3 and are detected as $\bar{\nu}_e$ with probability $U^2_{e2} \simeq sin^2\theta_{12}$.

The oscillations scheme can be summarized as:
$F_e = P_h U^2_{e2} F^0_e + (1 - P_h U^2_{e2}) F^0_x$ and
$F_{\bar{e}} = U^2_{e1} F^0_{\bar{e}} + U^2_{e2} F^0_{\bar{x}}$ for normal hierarchy;
$F_e = U^2_{e2} F^0_e + U^2_{e1} F^0_x$ and
$F_{\bar{e}} = P_h U^2_{e1} F^0_{\bar{e}} + (1 - P_h U^2_{e1}) F^0_{\bar{x}}$ for inverted hierarchy,
where F^0_{any} are the original neutrino fluxes in the star and F_{any} are the observed ν fluxes. One can notice that, in the antineutrino channel, the non adiabatic ($P_h = 1$), IH case, is equivalent to the NH case (which does not depend on adiabaticity).

With respect to the astrophysical parameters, we assumed a galactic supernova explosion at a typical distance of $D = 10$ kpc, parametrized with a pure Fermi–Dirac energy spectrum ($\eta = 0$) with a total energy $E_b = 3 \cdot 10^{53}$ erg and perfect energy equipartition $f_{\nu_e} = f_{\bar{\nu}_e} = f_{\nu_x} = 1/6$; we fixed $T_{\nu_x}/T_{\bar{\nu}_e} = 1.5$, $T_{\nu_e}/T_{\bar{\nu}_e} = 0.8$ and $T_{\bar{\nu}_e} = 5$ MeV.

For the chosen supernova parameters, it results that the expected number of events and their energy spectrum depend on the unknown oscillation parameters: the mass hierarchy and the value of θ_{13}.

In conclusion, for our choice of the astrophysical parameters, the expected signal of neutrinos in the LVD detector from a supernova core collapse greatly benefits of the neutrino oscillation mechanism, practically in all the possible detection channels, especially if the transition is adiabatic and the hierarchy inverted (since in LVD the most relevand signal is given by $\bar{\nu}_e$).

The expected number of events in the various LVD detection channels and in the different oscillation scenarios are shown in table 2.

Table 2: Expected results in the various LVD detection channels and in the mean energy of the detected $\bar{\nu}_e$ p events.

	No Oscillation	Non Adiabatic	Adiabatic NH	Adiabatic IH
$\bar{\nu}_e$ p	346.	391.		494.
$\langle E_{\bar{\nu}_e} \rangle$ in $\bar{\nu}_e$ p	25. MeV	30. MeV		37. MeV
CC with ^{12}C	8.	22.	29.	27.
CC with ^{56}Fe	22.	72.	95.	92.
NC with ^{12}C	27			

However, being aware of the fact that the astrophysical parameters of the supernova mechanism are up to now not well defined, we performed the same calculations using different values of them. The resulting differences are in fact important; they are mainly due to the poor theoretical knowledge of the physics of the gravitational collapse. This will be hopefully improved after the occurence and detection of the next galactic supernova, to which the LVD experiment can give a significant contribution.

2 LVD and its experimental activity in 2008

2.1 Supernova physics

2.1.1 Monitoring the Galaxy

LVD has been continuously monitoring the Galaxy since 1992 in the search for neutrino bursts from GSC [1].

Its active mass has been progressively increased from about 330 t in 1992 to 1000 t in 2001, always guaranteeing a sensitivity to gravitational stellar collapses up to distances $d = 20$ kpc from the Earth, even in the case of the lowest ν-sphere temperature.

In fig. 4 we show the duty cycle of the experiment and the average active mass, during the last 8 years. Considering just the last year (2008) the average duty cycle was 99.86% and the average active mass in the same period 972 t.

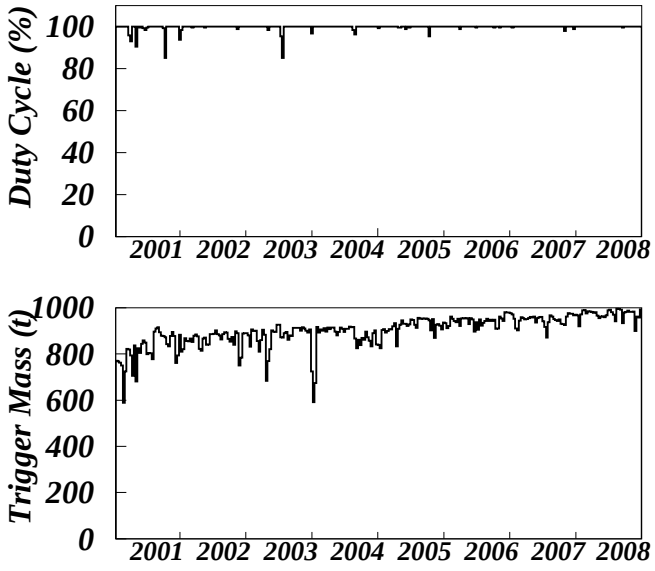

Figure 4: LVD duty cycle and trigger mass during the last eight years of data acquisition.

All events are processed on the base of their time sequence, searching for cluster not compatible with a poissonian fluctuation of the background. No significant signal has been registered by LVD during 16 years of data acquisition. Since the LVD sensitivity is higher than expected from GSC models (even if the source is at a distance of 20 kpc and for soft neutrino energy spectra) we can conclude that no gravitational stellar collapse has occurred in the Galaxy in the whole period of observation: the resulting upper limit to the rate of GSC, updated to 2008, at 90% C.L. is 0.15 events/yr (see [16] for comparison).

2.1.2 On-line recognition of supernova neutrino bursts and SNEWS

Since the first, and unique, observation of ν's from gravitational stellar collapse was guided by the optical observation and since the optical observation of a stellar collapse in our Galaxy is not probable, the detector capabilities of identifying a ν burst in the absence

[1] The results of this search have been periodically updated and published in the ICRC and Neutrino Conference Proceedings, since 1993 until 2008. [7, 8, 9, 10, 11, 12, 13, 14, 15]

of an "external trigger" must be carefully demonstrated. In the presence of an electromagnetic counterpart, on the other hand, the prompt identification of the neutrino signal could alert the worldwide network of observatories allowing study of all aspects of the rare event from its onset.
The SNEWS (SuperNova Early Warning System) [17, 18] project is an international collaboration including several experiments sensitive to a core-collapse supernova neutrino signal in the Galaxy and neighbour. Its goal is to provide the astronomical community with a prompt and confident alert of the occurrence of a Galactic supernova event, generated by the coincidence of two or more active detectors. In July 2005, after a few years of tuning, the charter members of SNEWS (i.e., LVD, Super-K and SNO[2]) together with the newly joined Amanda/IceCube, started the effective operation of the network, which means that the alert is really sent to the list subscribers, in the case of an at least two-fold coincidence (see *http://snews.bnl.gov* to get your own SN alert !).
The LVD performance from the point of view of the on-line identification of a neutrino burst have been discussed in [19]. The core of the algorithm for the on-line selection of candidate neutrino bursts is the search for a cluster of signals within a fixed-duration time window, Δt. The candidate burst is simply characterized by its multiplicity m, i.e., the number of pulses detected in Δt, and by Δt itself. All the other characteristics of the cluster, e.g., detailed time structure, energy spectra, ν flavor content and topological distribution of signals inside the detector are left to a subsequent independent analysis. Based on this principle, the LVD data are continuously analyzed by an on-line "supernova monitor". In detail, each data period, T, is scanned through a "sliding window" with duration Δt = 20 s, that is, it is divided into N = $2 \cdot \frac{T}{\Delta t} - 1$ intervals, each one starting in the middle of the previous one, so that the unbiased time window is 10 s. The frequency of clusters of duration 20 s and multiplicity $\geq$ m, due to background, is:

$$F_{im}(m, f_{\rm bk}, 20\ s) = 8640 \cdot \sum_{\rm k \geq m}^{\infty} P(k; 20 \cdot \frac{f_{\rm bk}}{s^{-1}})\ event \cdot day^{-1} \qquad (1)$$

where $f_{\rm bk}$ is the background counting rate of the detector for $E_{\rm vis} \geq E_{\rm cut}$, $P(k; f_{\rm bk}\Delta t)$ is the Poisson probability to have clusters of multiplicity k if $f_{\rm bk}\Delta t$ is the average background multiplicity, and 8640 is the number of trials per day [3]. In LVD the search for burst candidates is performed for both energy cuts: 7 and 10 MeV. The chosen F_{im}, below which the detected cluster will be an on-line candidate supernova event, is 1 per 100 year working stand-alone while it is relaxed to 1 per month working in coincidence with other detectors, as in the SNEWS project.

The selection method defines a candidate as any cluster of $m \geq m_{\rm min}$ signals within a window of Δt = 20 s. For a known background rate, $m_{\rm min}$ corresponds to a chosen $F_{\rm im}$ which is set as a threshold. This multiplicity represents the minimum number of neutrino interactions required to produce a supernova "alarm", and contains two terms, one due to

[2]Actually the SNO experiment is stopped and decommissioned

[3]Once a candidate cluster (m, 20s) has been identified, the algorithm will search for the most probable starting point of the signal within the time window. For all possible sub-clusters with multiplicity $2 \leq k \leq m$ and duration $0 \leq \Delta t \leq 20s$ the corresponding Poisson probability $P_{k \geq m}$ is calculated and the absolute minimum identified. The time of the first event of the least probable sub-cluster is assumed as the start time of the signal.

the background, $f_{\rm bk}\Delta t$, and the other due to the neutrino signal. In particular, for LVD, considering only inverse beta decay (IBD) reactions, which are the dominant ones at least in the "standard" supernova model, and simply approximating the detector response to $E_{\rm vis} = E_{\bar{\nu}_{\rm e}} - 0.8$ MeV, one can write:

$$m_{\rm min} = f_{\rm bk}\Delta t + M_{\rm act}\ N_{\rm p}\ \epsilon(E_{\rm cut}) \int_0^{10s} dt \int_{E_{\rm cut}+0.8MeV}^{100MeV} \Phi(E_{\bar{\nu}_{\rm e}}, t) \cdot \sigma(E_{\bar{\nu}_{\rm e}}) dE_{\bar{\nu}_{\rm e}} \qquad (2)$$

where: $M_{\rm act}$ is the active mass, $N_{\rm p} = 9.34\ 10^{28}$ is the number of free protons in a scintillator ton, $\epsilon(E_{\rm cut})$ is the trigger efficiency approximated as constant ($\epsilon = 0.9$ for $E_{\rm cut} = 7$ MeV and $\epsilon = 0.95$ for $E_{\rm cut} = 10$ MeV), $\sigma(E_{\bar{\nu}_{\rm e}})$ is the IBD cross section and $\Phi(E_{\bar{\nu}_{\rm e}}, t)$ the differential $\bar{\nu}_{\rm e}$ intensity at the detector. The upper limit in the time integral (10 s) corresponds to the maximum unbiased cluster duration.
Hence the integral on the right side of (2) is the detector burst sensitivity, S, in terms of minimum neutrino flux times cross section integrated over Δt and ΔE, and is expressed as number of neutrino interactions per target:

$$S_{E_{\rm cut}} = (m_{min} - f_{\rm bk}\Delta t)/(M_{\rm act} \cdot N_{\rm p} \cdot \epsilon) \qquad (3)$$

The values of S are shown in table 3, for the two LVD thresholds of the imitation frequency, i.e., $F_{\rm im} = 1$ per 100 years and $F_{\rm im} = 1$ per month and two values of $E_{\rm cut}$. As it can be seen, an important improvement can be obtained by increasing the energy cut from 7 to 10 MeV: the minimum cluster multiplicity, for example at $F_{\rm im} = 1$ per 100 years, goes from 22 to 10, allowing an improvement of almost a factor of two in the sensitivity $S_{\rm E_{cut}}$.

Table 3: On-line burst sensitivity for different selection algorithms, for two energy thresholds $\rm E_{cut}$ and for two values of imitation frequency; m_{min} represents the minimum cluster multiplicity (in parenthesis the minimum number of requested "signed" H signals for the IBD-B algorithm).

			$F_{im} = 1$ month^{-1}		$F_{im} = 1 \cdot 10^{-2}$ year^{-1}	
$\rm E_{cut}$=7 MeV	algorithm	$\rm M_{act}$	m_{min}	$S_{\rm E_{cut}}$	m_{min}	$S_{\rm E_{cut}}$
	on-line	1000	18	$1.6 \cdot 10^{-31}$	22	$2.1 \cdot 10^{-31}$
	IBD-A	1000	7	$1.5 \cdot 10^{-31}$	10	$2.2 \cdot 10^{-31}$
	IBD-B	1000	15(5)	$1.3 \cdot 10^{-31}$	19(7)	$1.7 \cdot 10^{-31}$
$\rm E_{cut}$=10 MeV						
	on-line	1000	8	$8.3 \cdot 10^{-32}$	10	$1.1 \cdot 10^{-31}$

It must be noted that in the on-line algorithm described so far we have neglected the capability of LVD to detect both products of the IBD reaction (see section 2.1). We can consider the signature of the reaction to build different burst selection algorithms. For example, we can require that all the high threshold (H) signals in the cluster are "signed", i.e., accompanied by a delayed low threshold (L) one (algorithm IBD-A). The sensitivity of the algorithm IBD-A is shown in Table 3: even if the minimum multiplicity is lower, and the background rate is reduced, because of the n-capture efficiency ($\epsilon_{\rm n} = 0.5$) the IBD-A method has comparable effectiveness or even less then the on-line one.
We can also build several different algorithms, intermediate between the on-line and the IBD-A ones, requiring that only a fraction of the H signals in the cluster are accompanied by L ones (IBD-B)[4]. However, even if the IBD-B method efficiency results higher (as can be seen in the table, where an example is given), it does not exceed the on-line one enough to justify the loss of simplicity of the on-line algorithm and its independence from the model of supernova neutrino emission. Moreover, the on-line algorithm is sensitive to all possible neutrino interactions in LVD, both in the liquid scintillator and in the iron structure (that can represent up to 15% of the total number of interactions).

2.2 CNGS beam monitor

The Cern Neutrinos to Gran Sasso (CNGS) project is a high energy, wide band ν_μ beam set up at Cern and sent towards the INFN Gran Sasso National Laboratory (LNGS). Its main goal is the observation of the ν_τ appearance, through neutrino flavour oscillation, by the Opera experiment.

As shown in [20], due to its large area and active mass, LVD can act as a very useful beam monitor, detecting the interaction of neutrinos inside the detector and the muons generated by the ν interaction in the rock upstream the detector. The monitor capabilities have been confirmed during the first CNGS run in August 2006 [21] and fall 2007 [22]. Here we report about the events detected by LVD during the CNGS run in 2008.

2.2.1 The CNGS beam

The information about the CNGS beam characteristics are taken by the LHCLOG_CNGS_OPERA database (hereafter DB) [23]. Two main quantities are relevant for each proton extraction:

- the UTC time of the spill (in ns),
- the number of extracted protons on target (p.o.t.)

The CNGS beam started its operation on 18^{th} June, 2008 (first spill at 14:56:13.470 UTC) and finished on 3^{rd} November (last spill at 07:21:12.340 UTC). In the following we will refer to this run as Run2008. The total number of protons delivered against the graphite target is 1.78 10^{19}. The beam intensity per each spill is shown in figure 5.

[4]We reject all the clusters which have a number of "signed" H signals $\leq k$, such that: $\sum_{r=0}^{r=k} P(r,m,p) \leq P_0$, where $P(r,m,p)$ is the binomial probability to have r signed pulses in a cluster of multiplicity m. We choose $P_0 = 0.1$ as an example, the case $P_0 = 0$ corresponding to the on-line algorithm.

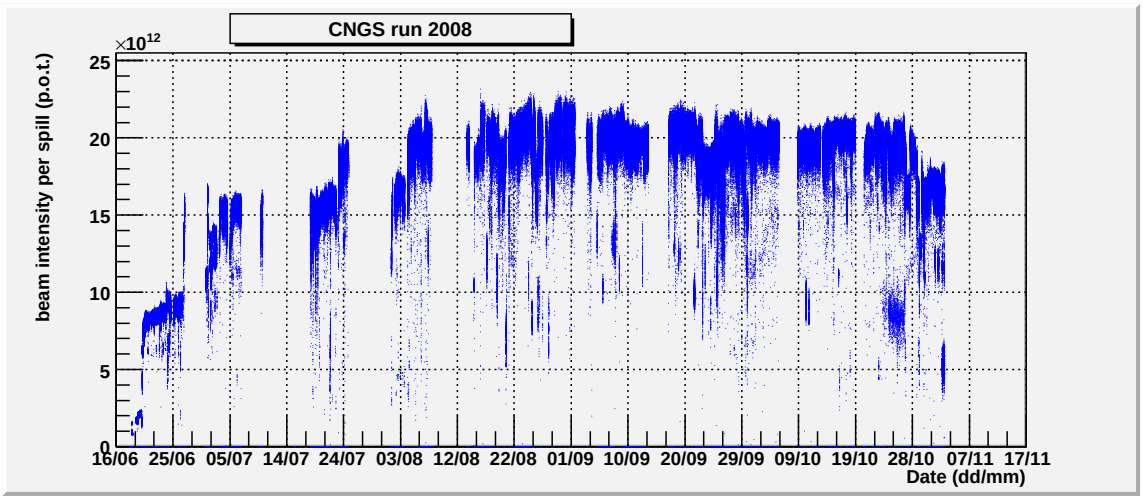

Figure 5: Beam intensity (in protons on target) per each spill.

2.2.2 MC simulation of the expected events

The CNGS events in LVD can be subdivided into two main categories:

- ν_μ charged current (CC) interactions in the rock upstream the LNGS; they produce a muon that can reach LVD and be detected,
- ν_μ CC and neutral current (NC) interactions in the material (liquid scintillator and iron of the support structure) of LVD.

We developed a full Montecarlo simulation that includes the generation of the neutrino interaction products, the propagation of the muon in the Gran Sasso rock and the response of the LVD detector. The details of the simulation were described in [20]; however, with respect to that paper, some modifications were done with up–to–date informations. In particular we now use the CNGS flux calculated in 2005 by the Fluka group [24] and the neutrino cross section NUX-FLUKA [25]. There are also some modifications in the detector: there are actually 7 active levels of scintillation counters instead of the 8 previously considered, and the energy threshold for the definition of a CNGS event is now 100 MeV instead of 200 MeV.

The resulting number of expected events, at the nominal intensity 4.5 10^{19} p.o.t./y is 33400/y, equivalent to 7.422 10^{-16} events per p.o.t. (considering 200 effective days per year it corresponds to $\sim$ 165 CNGS events per day): 78% are muons from the rock, 17% are CC interactions in the detector and 5% are NC.

During Run2008 the total number of p.o.t. was 1.78 10^{19}, thus 13211 events are expected in LVD.

2.2.3 CNGS detected events

The LVD events are filtered using a very loose selection cut: we require to have at least one scintillation counter with an energy release larger that 100 MeV. The resulting rate is

quite stable, with an average value of about 0.13 Hz, and it's mainly due to cosmic muon events.

Among this sample the first selection criteria is based on the coincidence of the LVD event time with the beam spill time written in the DB. Two main corrections have been done: the neutrino time of flight from Cern to the LNGS (2.440 ms) and the propagation of the GPS time signal from the outside laboratories to slave clocks in the underground hall (42116, 42064 and 42041 ns respectively for tower 1, 2 and 3), measured in July, 2006 together with the other experiments at LNGS [26].

After applying all these corrections, we search for the CNGS events in the interval $[-15, +25]$ μs around the start time of the beam spill. In this way 13348 events are selected; their distribution in the time window is shown in figure 6.

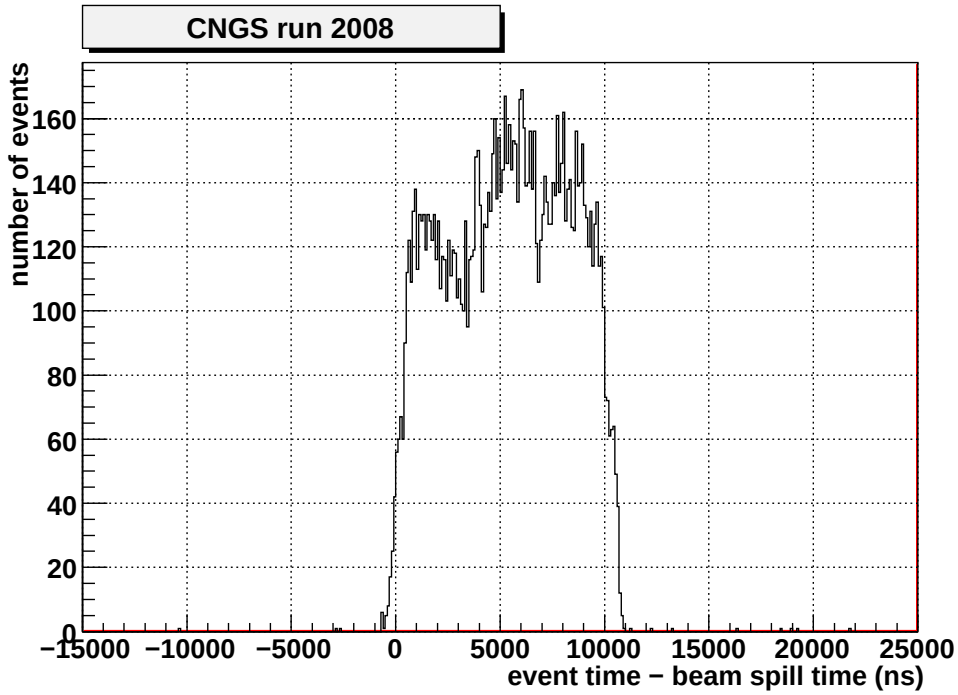

Figure 6: Distribution of the detection time of the CNGS events, with respect to the initial time of the beam spill.

In figure 7 we show the comparison between the expected and detected event rate per each day of data acquisition; the agreement is very good.

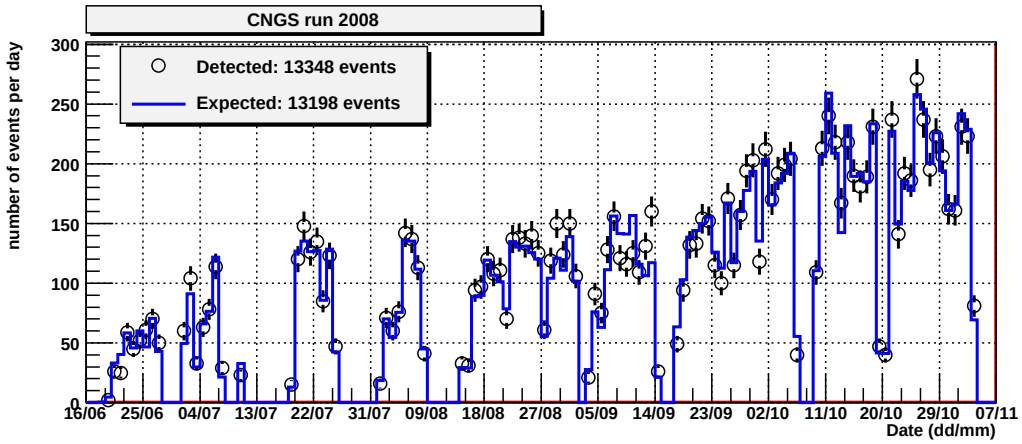

Figure 7: Number of events per day: observed (black circles) and expected (blue line).

Two examples of typical CNGS events in LVD are shown in figure 8 (muon from the rock) and 9 (neutrino interaction inside the detector).

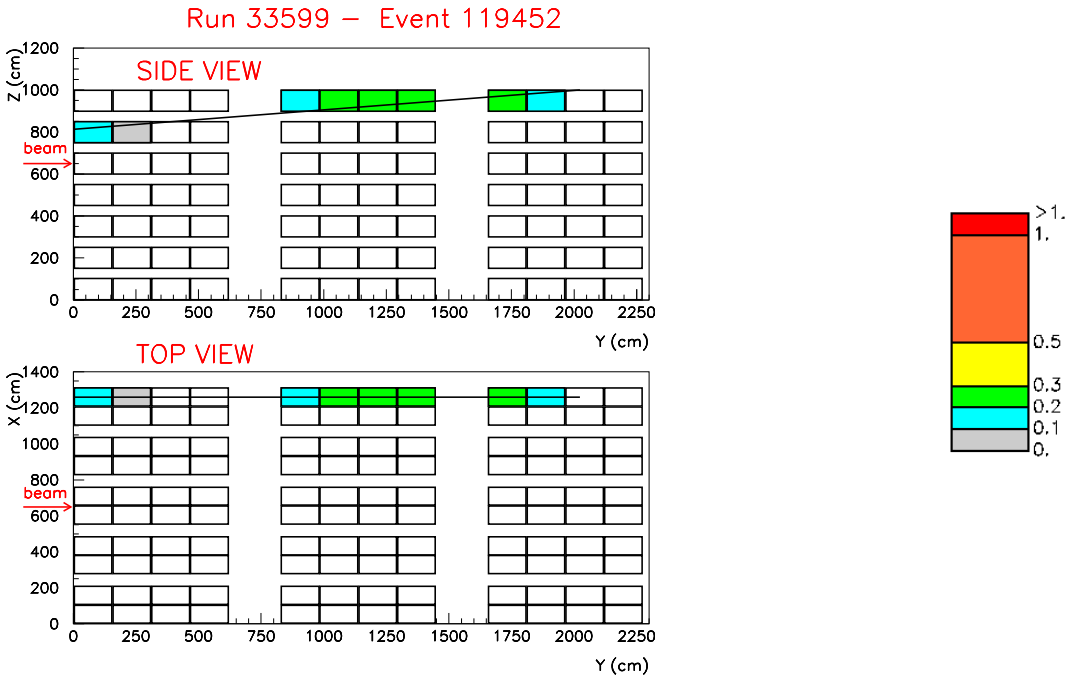

Figure 8: Display of a CNGS events: typical charged current interaction in the rock upstream LVD, producing a muons that go through the detector. The colours represent the amount of energy released in the scintillation counters; the legenda is expressed in GeV. The black straight line is the result of a linear fit to the hit counters.

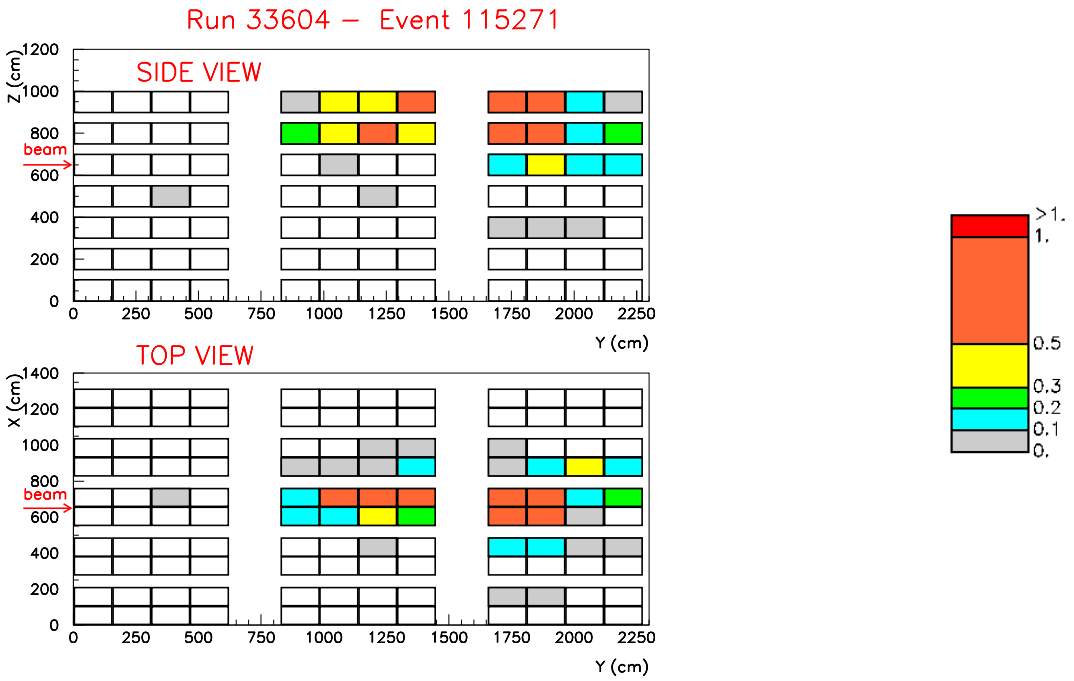

Figure 9: Display of a CNGS events: neutrino interaction inside the LVD detector. The colours represent the amount of energy released in the scintillation counters; the legenda is expressed in GeV.

Background

The background is estimated considering the rate of events among which the CNGS events are searched for, with an average value of 0.13 Hz. The time window where we search for the events around the beam spill time is 40 μs wide, and the number of useful spills in the DB is 1009490. Thus the number of events due to the background, during Run2008, is

$$N_{bkg} = 0.13\ Hz \times 40\ \mu s \times 1009490 = 5$$

, practically negligible.

2.2.4 Summary

We presented the results of the events detected in 2008 by the LVD detector in coincidence with the CNGS beam. The CNGS run was started in June 2008, with an overall number of 1.78 10^{19} protons delivered on the target. The LVD detector was fully operative during the whole run, with an average active mass of 970 t.

LVD can detect the CNGS neutrinos through the observation of penetrating muons originated by ν_μ CC interactions in the rock upstream the LNGS and through internal CC and NC neutrino interactions.

The expected number of events, as predicted by our Montecarlo simulation, is 13211. We searched for the CNGS events by looking at the time coincidence with the beam spill

time; the number of detected events is 13348.

We estimate that the number of events due to the background is about 5 in the whole run time.

3 List of publications in 2008

- *On-line recognition of supernova neutrino bursts in the LVD detector*
  Astroparticle Physics 28 (2008) 516-522.
  e-Print Archive: 0710.0259 [astro-ph]

- *Sarch for neutrino bursts from stellar collapses into neutron stars or black holes with the LVD experiment at Gran Sasso*
  To appear in the proceedings of NEUTRINO 2008, Christchurch, New Zealand, 25-31 June, 2008.

- *The LVD Core Facility: A Study of LVD as muon veto and active shielding for dark matter experiments.*
  To appear in the proceedings of IDM 2008: 7th International Workshop on the Identification of Dark Matter 2008, Stockholm, Sweden, 18-22 Aug 2008.
  e-Print: arXiv:0811.2884 [hep-ex]

- *Performances and stability of a 2.4 ton Gd organic liquid scintillator target for anti-nu(e) detection.*
  By the MetaLS collaboration and LVD Collaboration (I.R. Barabanov et al.). Mar 2008. 3pp.
  e-Print: arXiv:0803.1577 [physics.ins-det]

References

[1] LVD Collaboration, Il Nuovo Cimento **A105** (1992) 1793

[2] A. Strumia, F. Vissani, `astro-ph/0302055`.

[3] LVD Collaboration, Nucl. Phys. B Proc. Sup. 110, (2002) 410-413, astro-ph/0112312

[4] A. Zichichi, *The most powerful scintillator supernova neutrino detector*, talk presented at the symposium *LVD: the First Ten Years*, LNGS, 28-29 October, 2002).

[5] LVD Collaboration, 28th ICRC Conf. Proc., HE 2.3, 1297, 2003

[6] N. Yu. Agafonova *et al.*, *Study of the effect of neutrino oscillations on the supernova neutrino signal in the LVD detector*, Astropart. Phys. **27**, 254-270 (2007) [arXiv: hep-ph/0609305].

[7] LVD Collaboration, 23th ICRC Conf. Proc., HE 5.1.1, Vol.4, 468, 1993

[8] LVD Collaboration, 24th ICRC Conf. Proc., HE 5.3.6, Vol.1, 1035, 1995

[9] LVD Collaboration, 25th ICRC Conf. Proc., HE 4.1.12, 1997

[10] LVD Collaboration, 26th ICRC Conf. Proc., HE 4.2.08, Vol.2, 223, 1999

[11] LVD Collaboration, 27th ICRC Conf. Proc., HE 230, 1093, 2001

[12] LVD Collaboration, 28th ICRC Conf. Proc., HE 2.3, 1333, 2003

[13] LVD Collaboration, 29th ICRC Conf. Proc., OG 2.5, 59, 2005

[14] LVD Collaboration, 30th ICRC Conf. Proc., HE 2.3, 2007

[15] LVD Collaboration, NEUTRINO 2008 Conf. Proc. in press

[16] M.Ikeda *et al.*, The Astrophysical Journal, 669:519-524, 2007

[17] http://hep.bu.edu/∼snnet/

[18] P. Antonioli et al., New J. Phys., 6 (2004) 114

[19] N. Yu. Agafonova *et al.*, *On-line recognition of supernova neutrino bursts in the LVD detector*, Astropart. Phys. **28**, 516-522 (2008) [arXiv:0710.0259].

[20] M. Aglietta et al., *CNGS beam monitor with the LVD detector*, Nuclear Instruments and Methods in Physics Research **A 516**, 96 (2004).

[21] N. Yu. Agafonova et al., *First CNGS events detected by LVD*, Eur. Phys. J. **C 52**, 849-855 (2007) [arXiv:0710.1536 hep-ex].

[22] N. Yu. Agafonova et al., *The Large Volume Detector*, in the 2007 LNGS Annual Report, p. 114 (2007).

[23] C. Roderick, LHC LOGGING - CNGS-OPERA gateway database user guide, https://edms.cern.ch/file/750206/1/LHCLOG_CNGS_OPERA_GW_DB_GUIDE.pdf.

[24] A. Ferrari et al., *An updated Monte Carlo calculation of the CNGS neutrino beam*, CERN-AB-Note-2006-038, EDMS No. 745389.
Fluxes available in http://www.mi.infn.it/∼psala/Icarus/cngs.html

[25] G. Battistoni et al., *The FLUKA nuclear cascade model applied to neutrino interactions*, Proceedings of NUINT'02, December 2002, University of California, Irvine, USA.
Available online at http://nuint.ps.uci.edu/proceedings/sala.pdf

[26] D. Autiero et al., *Measurement of the fibre delays for the GPS signal underground distribution*, internal note, (2006).

OPERA

N. Agafonova[1], A. Anokhina[2], S. Aoki[3], A. Ariga[4], T. Ariga[4], L. Arrabito[5], D. Autiero[5], A. Badertscher[6], A. Bagulya[7], F. Bersani Greggio[17], A. Bertolin[9], M. Besnier[10], D. Bick[11], V. Boyarkin[1], C. Bozza[12], T. Brugière[5], R. Brugnera[13,9], G. Brunetti[14,15], S. Buontempo[16], E. Carrara[13,9], A. Cazes[5], L. Chaussard[5], M. Chernyavsky[7], V. Chiarella[17], N. Chon-Sen[18], A. Chukanov[16], M. Cozzi[14], G. D'Amato[12], F. Dal Corso[9], N. D'Ambrosio[19], G. De Lellis[20,16], Y. Déclais[5], M. De Serio[21], F. Di Capua[16], D. Di Ferdinando[15], A. Di Giovanni[22], N. Di Marco[22], C. Di Troia[17], S. Dmitrievski[23], A. Dominjon[5], M. Dracos[18], D. Duchesneau[10], S. Dusini[9], J. Ebert[11], O. Egorov[24], R. Enikeev[1], A. Ereditato[4], L. S. Esposito[19], J. Favier[10], G. Felici[17], T. Ferber[11], R. Fini[21], D. Frekers[25], T. Fukuda[8], C. Fukushima[26], V. I. Galkin[2], V. A. Galkin[27], A. Garfagnini[13,9], G. Giacomelli[14,15], M. Giorgini[14,15], C. Goellnitz[11], T. Goeltzenlichter[18], J. Goldberg[28], D. Golubkov[24], Y. Gornoushkin[23], G. Grella[12], F. Grianti[17], M. Guler[29], C. Gustavino[19], C. Hagner[11], T. Hara[3], M. Hierholzer[30], K. Hoshino[8], M. Ieva[21], K. Jakovcic[31], B. Janutta[11], C. Jollet[18], F. Juget[4], M. Kazuyama[8], S. H. Kim[35], M. Kimura[26], B. Klicek[31], J. Knuesel[4], K. Kodama[32], D. Kolev[33], M. Komatsu[8], U. Kose[29], A. Krasnoperov[23], I. Kreslo[4], Z. Krumstein[23], V.V. Kutsenov[1], V.A. Kuznetsov[1], I. Laktineh[5], C. Lazzaro[6], J. Lenkeit[11], A. Ljubicic[31], A. Longhin[13], G. Lutter[4], A. Malgin[1], K. Manai[5], G. Mandrioli[15], A. Marotta[16], J. Marteau[5], V. Matveev[1], N. Mauri[14,15], F. Meisel[4], A. Meregaglia[18], M. Messina[4], P. Migliozzi[16], P. Monacelli[22], K. Morishima[8], U. Moser[4], M. T. Muciaccia[34,21], N. Naganawa[8], M. Nakamura[8], T. Nakano[8], V. Nikitina[2], K. Niwa[8], Y. Nonoyama[8], A. Nozdrin[23], S. Ogawa[26], A. Olchevski[23], G. Orlova[7], V. Osedlo[2], D. Ossetski[27], M. Paniccia[17], A. Paoloni[17], B. D Park[8], I. G. Park[35], A. Pastore[34,21], L. Patrizii[15], E. Pennacchio[5], H. Pessard[10], V. Pilipenko[25], C. Pistillo[4], N. Polukhina[7], M. Pozzato[14,15], K. Pretzl[4], P. Publichenko[2], F. Pupilli[22], R. Rescigno[12], D. Rizhikov[27], T. Roganova[2], G. Romano[12], G. Rosa[36], I. Rostovtseva[24], A. Rubbia[6], A. Russo[20,16], V. Ryasny[1], O. Ryazhskaya[1], A. Sadovski[23], O. Sato[8], Y. Sato[37], V. Saveliev[27], A. Schembri[36], W. Schmidt Parzefall[11], H. Schroeder[30], H. U. Schütz[4], J. Schuler[18], L. Scotto Lavina[16], H. Shibuya[26], S. Simone[34,21], M. Sioli[14.15], C. Sirignano[12], G. Sirri[15], J. S. Song[35], M. Spinetti[17], L. Stanco[13], N. Starkov[7], M. Stipcevic[31], T. Strauss[6], P. Strolin[20,16], V. Sugonyaev[13], S. Takahashi[8], V. Tereschenko[23], F. Terranova[17], I. Tezuka[37], V. Tioukov[16], P. Tolun[29], V. Tsarev[7], R. Tsenov[33], S. Tufanli[29], N. Ushida[32], V. Verguilov[33], P. Vilain[38], M. Vladimirov[7], L. Votano[17], J. L. Vuilleumier[4], G. Wilquet[38], B. Wonsak[11] V. Yakushev[1], C. S. Yoon[35], Y. Zaitsev[24], A. Zghiche[10], and R. Zimmermann[11].

1. INR-Institute for Nuclear Research of the Russian Academy of Sciences, RUS-117312 Moscow, Russia
2. SINP MSU-Skobeltsyn Institute of Nuclear Physics of Moscow State University, RUS-119992 Moscow, Russia
3. Kobe University, J-657-8501 Kobe, Japan
4. Centre for Research and Education in Fundamental Physics, Laboratory for High Energy Physics (LHEP), University of Bern, CH-3012 Bern, Switzerland
5. IPNL, Université Claude Bernard Lyon 1, CNRS/IN2P3, F-69622 Villeurbanne, France
6. ETH Zurich, Institute for Particle Physics, CH-8093 Zurich, Switzerland
7. LPI-Lebedev Physical Institute of the Russian Academy of Sciences, RUS-117924 Moscow, Russia
8. Nagoya University, J-464-8602 Nagoya, Japan
9. INFN Sezione di Padova, I-35131 Padova, Italy
10. LAPP, Université de Savoie, CNRS/IN2P3, F-74941 Annecy-le-Vieux, France
11. Hamburg University, D-22761 Hamburg, Germany
12. Dipartimento di Fisica dell'Università di Salerno and INFN, I-84084 Fisciano, Salerno, Italy
13. Dipartimento di Fisica dell'Università di Padova, I-35131 Padova, Italy
14. Dipartimento di Fisica dell'Università di Bologna, I-40127 Bologna, Italy
15. INFN Sezione di Bologna, I-40127 Bologna, Italy
16. INFN Sezione di Napoli, 80125 Napoli, Italy
17. INFN - Laboratori Nazionali di Frascati dell'INFN, I-00044 Frascati (Roma), Italy
18. IPHC, Université de Strasbourg, CNRS/IN2P3, F-67037 Strasbourg, France
19. INFN - Laboratori Nazionali del Gran Sasso, I-67010 Assergi (L'Aquila), Italy
20. Dipartimento di Fisica dell'Università Federico II di Napoli, 80125 Napoli, Italy
21. INFN Sezione di Bari, I-70126 Bari, Italy
22. Dipartimento di Fisica dell'Università dell'Aquila and INFN, I-67100 L'Aquila, Italy
23. JINR-Joint Institute for Nuclear Research, RUS-141980 Dubna, Russia
24. ITEP-Institute for Theoretical and Experimental Physics, RUS-117259 Moscow, Russia
25. University of Münster, D-48149 Münster, Germany
26. Toho University, J-274-8510 Funabashi, Japan
27. Obninsk State University, Institute of Nuclear Power Engineering, RUS-249020 Obninsk, Russia
28. Department of Physics, Technion, IL-32000 Haifa, Israel
29. METU-Middle East Technical University, TR-06531 Ankara, Turkey
30. Fachbereich Physik der Universität Rostock, D-18051 Rostock, Germany
31. IRB-Rudjer Boskovic Institute, HR-10002 Zagreb, Croatia
32. Aichi University of Education, J-448-8542 Kariya (Aichi-Ken), Japan
33. Faculty of Physics, Sofia University "St. Kliment Ohridski", BG-1000 Sofia, Bulgaria
34. Dipartimento di Fisica dell'Università di Bari, I-70126 Bari, Italy
35. Gyeongsang National University, 900 Gazwa-dong, Jinju 660-300, Korea
36. Dipartimento di Fisica dell'Università di Roma "La Sapienza" and INFN, I-00185 Roma, Italy
37. Utsunomiya University, J-321-8505 Tochigi-Ken, Utsunomiya, Japan
38. IIHE, Université Libre de Bruxelles, B-1050 Brussels, Belgium

Abstract

The OPERA neutrino detector at the underground Gran Sasso Laboratory (LNGS) was designed to perform the first detection of neutrino oscillations in appearance mode through the study of $\nu_\mu \to \nu_\tau$ oscillations. The apparatus consists of a lead/emulsion-film target complemented by electronic detectors. It is placed in the high-energy long-baseline CERN to LNGS beam (CNGS) 730 km away from the neutrino source. Runs with CNGS neutrinos were successfully conducted in 2007 and 2008 for a total luminosity of 1.864×10^{19} p.o.t. (*proton on target*), and an initial sample of neutrino events has been collected and reconstructed. After a brief description of the beam and of the experimental apparatus we report on the first data and related analysis results.

1 Introduction

The solution of the long-standing solar and atmospheric neutrino puzzles has come from the hypothesis of neutrino oscillations. This implies that neutrinos have non vanishing and non-degenerate mass eigenstates, and that their flavor eigenstates involved in weak interaction processes are a superposition of the mass eigenstates.

Several experiments carried on in the last decades with solar and reactor neutrinos, as well as with atmospheric and accelerator neutrinos, contributed to build-up our present understanding of neutrino mixing. Atmospheric neutrino oscillations have been studied mainly by the Kamiokande, MACRO, Super-Kamiokande and SOUDAN2 experiments. Long baseline experiments with accelerator neutrinos (K2K and MINOS) confirmed the oscillation scenario first pointed out by the Super-Kamiokande experiment supporting the $\nu_\mu \to \nu_\tau$ oscillation channel for atmospheric neutrinos, while the CHOOZ and Palo Verde reactor experiments excluded the $\nu_\mu \to \nu_e$ channel as the dominant one.

However, the direct appearance of a different neutrino flavor is still an important open issue. This is the main goal of the OPERA experiment [1, 2] that uses the long baseline (L=730 km) CNGS neutrino beam from CERN to LNGS. The challenge of the experiment is to measure the appearance of ν_τ from ν_μ oscillations in an almost pure muon-neutrino beam. This requires the detection of the short-lived τ lepton ($c\tau = 87.11$ μm) produced in the charged-current interaction of a ν_τ. This sets two conflicting requirements: a large target mass needed to have sufficient statistics and an extremely high accuracy detector technique to observe the short-lived τ lepton.

The τ is identified by the detection of its characteristic decay topologies either in one prong (electron, muon or hadron) or in three prongs. The τ track is measured with a large-mass active target made of 1 mm thick lead plates (target mass and absorber material) inter-spaced with thin nuclear emulsion films (high-accuracy tracking devices). This detector is historically called Emulsion Cloud Chamber (ECC). Among past applications it was successfully used in the DONUT experiment for the first direct observation of the ν_τ.

The OPERA detector [2] is made of two identical Super Modules (SM) each consisting of a target section of about 625 tons made of lead/emulsion-film ECC modules (hereafter called "bricks"), of a scintillator tracker detector (TT) needed to trigger the read-out and pre-localize neutrino interactions within the target, and of a muon spectrometer (Figure 1). A single SM has longitudinal dimensions of about 10 m. The detector is equipped with an automatic machine (the Brick Manipulator System, BMS) that allows the on-line removal of bricks from the detector. Ancillary facilities exist for the handling, the development and the scanning of the emulsion films. The film scanning is performed with two independent types of scanning microscopes: the European Scanning Sytem (ESS) in Europe and the S-UTS in Japan.

A target brick consists of 56 lead plates of 1 mm thickness interleaved with 57 emulsion films [3]. The plate material is a lead alloy with a small calcium content to improve its mechanical properties [4]. The transverse dimensions of a brick are 12.8×10.2 cm^2 and the thickness along the beam direction is 7.9 cm (about 10 radiation lengths). The construction of more than 150,000 bricks for the neutrino target has been accomplished by an automatic machine, the Brick Assembly Machine (BAM) operating underground in

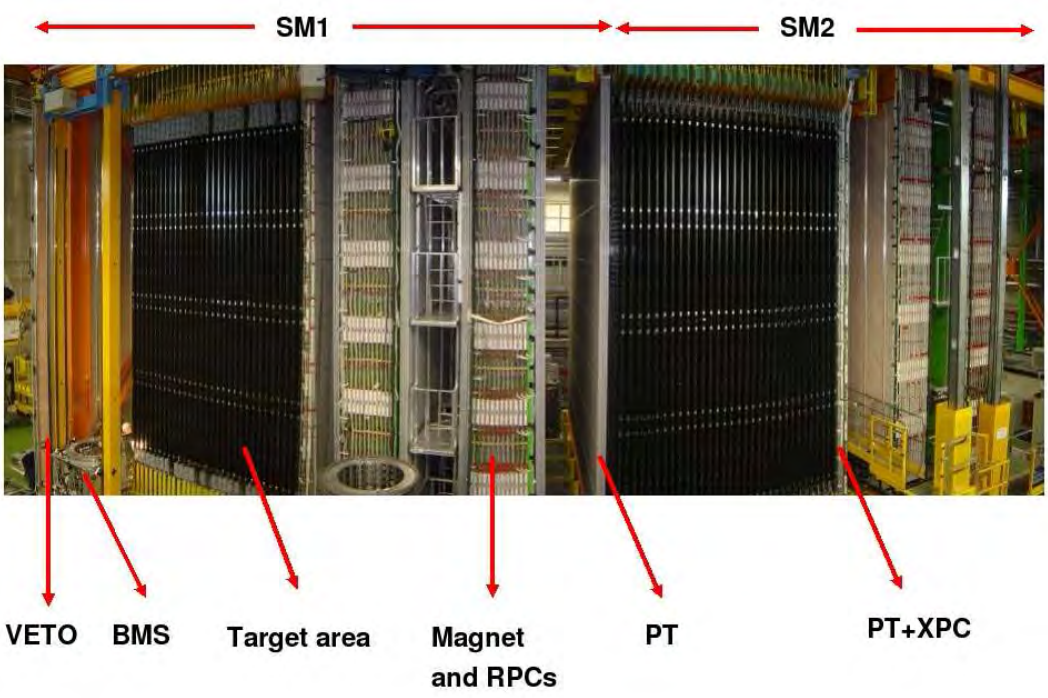

Figure 1: Fish-eye view of the OPERA detector. The upper horizontal lines indicate the position of the two identical supermodules (SM1 and SM2). The "target area" is made of walls filled with ECC bricks interleaved with planes of plastic scintillators (TT). Arrows also show the position of the VETO planes, the drift tubes (PT), the RPC with diagonal strips (XPC), the magnets and the RPC installed between the magnet iron slabs. The Brick Manipulator System (BMS) is also visible. See [2] for more details.

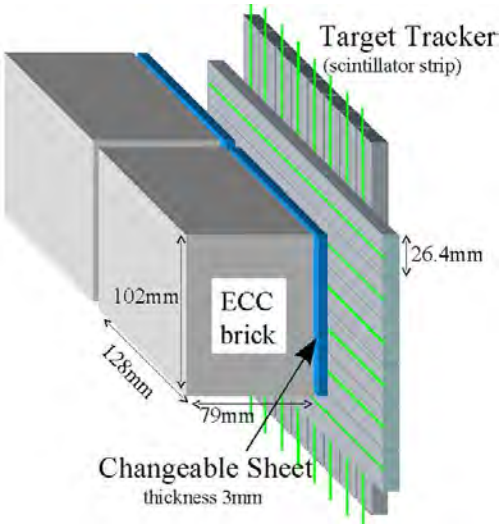

Figure 2: Schematic view of two bricks with their Changeable Sheet and target tracker planes.

order to minimize the number of background tracks from cosmic-rays and environmental radiation. The BAM was delivered at LNGS in July 2006 and made operational in September 2006. The commissioning was completed in February 2007. The production lasted from March 2007 to June 2008 with an average rate of 650 assembled bricks/day. In this period, the brick production at the BAM was based on two shifts/day of 8 hours each, 5 working days a week. Each shift involved 7 operators plus 1 site manager. At the end of mass production the BAM had assembled 146621 bricks (June 2008). A few thousand more have been produced at the beginning of 2009 after the delivery of the remaining lead, delayed by an accident which occurred at lead producing factory (JL Goslar, Germany) in June 2008. The bricks have been inserted in the detector target by BMS and housed in a light support structure placed between consecutive TT walls. The BMS support structure has been designed with the requirement of minimizing the material along the neutrino beam direction in order to reduce to the 0.1% level the number of interactions in regions not instrumented with emulsion films or scintillators.

In order to reduce the emulsion scanning load the use of Changeable Sheets (CS) [5] successfully applied in the CHORUS experiment was extended to OPERA. Tightly packed doublets of emulsion films are attached to the downstream face of each brick and can be removed without opening the brick. Charged particles from a neutrino interaction in the brick cross the CS and produce a trigger in the TT scintillators. Following this trigger the brick is extracted and the CS developed and analyzed in the scanning facilities at LNGS and in Nagoya. The information of the CS is used for a precise prediction of the position of the tracks in the most downstream films of the brick, hence guiding the so-called *scan-back* vertex finding procedure.

The brick, CS and TT layout [5] is schematically shown in Figure 2.

A charged-current event, as reconstructed in the emulsion films, is shown in the bottom

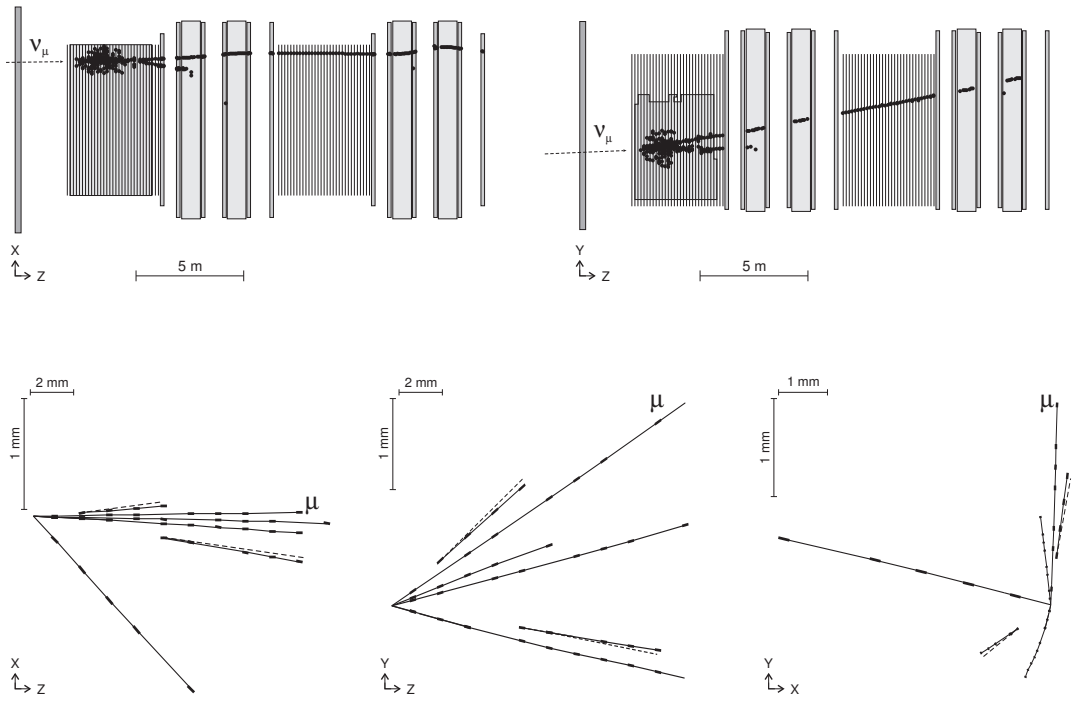

Figure 3: Top panel: on line display of an event seen by the OPERA electronic detectors (side and top views): a ν_μ interacts in one of the first bricks of the first supermodule (SM) yielding hadrons and a muon which is seen in both SMs and whose momentum is measured by the magnets of the two SMs. Bottom panel: the vertex of the same event observed in the emulsion films (side, top and front views). Note the two $\gamma \to e^+e^-$ vertices: the opening angle between them is about 300 mrad. By measuring the energy of the γ's one obtains a reconstructed invariant mass of 110 ± 30 MeV consistent with the π^0 mass.

panel of Figure 3. In this case the detected event dimensions are of the order of a few millimeters, to be compared with the > 10 m scale of the whole event reconstructed with the electronic detectors (top panel of Figure 3).

First data were collected by the OPERA detector in 2006 with the electronic detectors alone and then in 2007 and 2008 for the first time with target bricks installed.

2 Real time detection of CNGS Beam

The CNGS neutrino beam was designed and optimized for the study of $\nu_\mu \to \nu_\tau$ oscillations in appearance mode, by maximizing the number of charged current (CC) ν_τ interactions at the LNGS site. For a detailed description of the CNGS beam we refer to [2].

After the beam commissioning run in 2006, the CNGS run started on September 2007 at rather low intensity. The first event inside the OPERA target was observed on October 3^{rd}. Unfortunately, due to a fault of the CNGS facility, the physics run lasted only a few

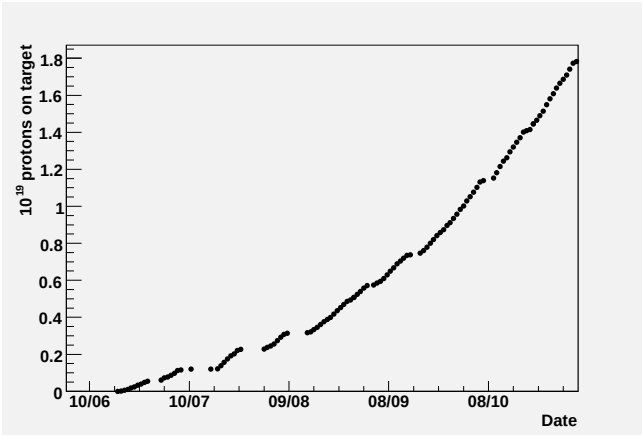

Figure 4: Integrated protons on target intensity as a function of time for the 2008 CNGS run (June-November). The holes correspond to CNGS stop periods.

days. During this run 0.082×10^{19} p.o.t were accumulated with a mean value of 1.8×10^{13} protons per extraction: this represented 3.6 effective nominal days of run. With such an integrated intensity about 32 neutrino interactions in the bricks and about 3 events in the scintillators of the target tracker were expected. This has to be compared with the 38 on time events collected as originating in the target region (bricks plus target tracker).

A longer run took place in 2008 when 1.782×10^{19} protons were delivered on the CNGS target. OPERA collected about 10100 events on time with the arrival of the beam at the Gran Sasso and among them 1700 interactions in the bricks. The other events originate outside the target region (spectrometer, OPERA supporting structures, rock surrounding the cavern, hall structures). The run was characterized by a poor initial efficiency of the CERN complex (with an average of about 40%) continuously improving till the end of the run. Finally an average efficiency of about 60% was achieved. In particular, after the stop of the LHC activities due to an accident, the SPS worked in a semi-dedicated mode for the CNGS from October to November allowing to gather the same number of protons as from June to August.

The 2008 CNGS integrated proton on target intensity as a function of time is shown in Figure 4.

During the 2007 and 2008 CNGS runs, all electronic detectors were operational. The trigger rate was 15 Hz and the live time of the Data Acquisition system exceeded 99%. The total number of events collected by applying a minimum bias filter is larger than 10 millions. The selection of the beam related events is based upon a time stamp, thanks to the time synchronization accuracy between the CERN beam GPS tagging and the OPERA timing system which is about 100 ns.

The interactions in the material surrounding the OPERA target were analyzed and used for the monitoring of the CNGS beam and of the OPERA detector.

The classification algorithm was implemented to provide very high efficiency in the selection of neutrino interactions inside the OPERA target both for CC and NC events, to the expense of a slightly low purity in the rejection of neutrino interactions in the

external material.

In the 2008 run 1663 events were classified as interactions in the target (expected 1723) with a contamination from outside events of 7%.

The beam direction estimated by the averaged angle is found to be tilted vertically by $(3.5 \pm 0.2)^\circ$ in agreement with the value of 3.3° expected from geodesy.

3 Event Identification: from ECC Extraction to Kinematical Reconstruction

In the following the breakdowns of the different steps which are carried out to analyze the neutrino interaction events are described: from the identification of the "fired" brick up to the detailed kinematical analysis of the vertex in the emulsion films.

Once a trigger in the electronic detectors is selected to be compatible with an interaction inside the brick, the following procedure, named "Brick Handling", is applied:

1. the whole electronic detector data are processed by the reconstruction program and the most probable brick, inside which the neutrino interaction may have occurred, is selected;

2. the brick is removed from the detector by the BMS and exposed to X-rays for film-to-film alignment. There are two independent X-ray exposures: the first one ensures a common reference system to the CS films doublet and the brick (frontal exposure); the second produces thick lateral marks on the brick edges used for internal alignment and film numbering;

3. after first X-ray exposures the CS doublet is detached from the brick and developed underground while the brick is stored underground in a box with 5 cm thick iron shielding to reduce the radioactivity background.

4. if the CS scanning is successful in locating tracks compatible with those reconstructed in the electronic detectors, the brick is brought to the surface laboratory and exposed to cosmic-rays for about 24 hours inside a pit. The pit has been built to select high-energy particles in order to provide straight tracks in the bricks for a refined (sub-micrometric) film-to-film alignment;

5. the brick emulsion films are then developed in the OPERA developing laboratory at LNGS (Figure 5) and dispatched to the various scanning laboratories. Half of the removed bricks are sent to Japan for emulsion measurement, the other half is measured in the European laboratories. The CS of the European bricks are all measured at the LNGS Scanning Station (Figure 5) for event confirmation and localization.

The overall efficiency for the selection of bricks with neutrino interactions inwards depends of the convolution of several effects and measurements. We address here the issues on the two most important ones, the Changeable Sheet measurement and the Brick

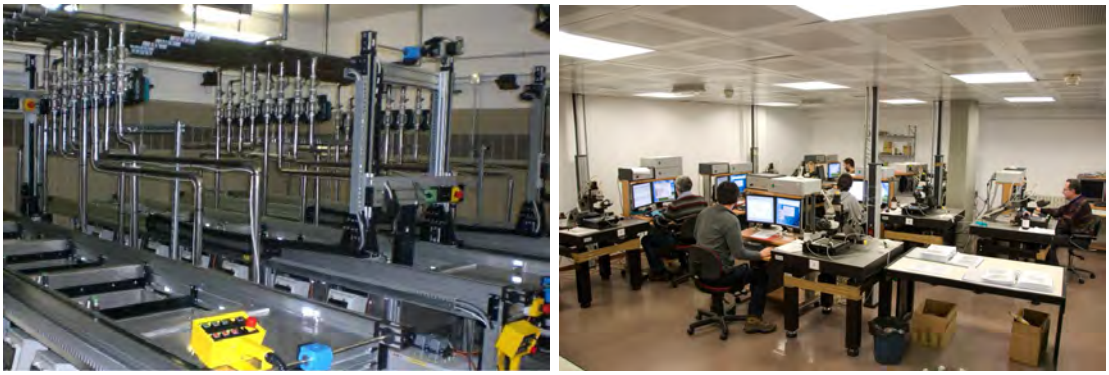

Figure 5: Left: Two chains of the film development facility at the LNGS external laboratory. Right: The European CS Scanning Station at LNGS.

Finding. For the time being preliminary results have been obtained from the analysis of the first samples of events in 2007 and 2008 runs.

The ability in selecting the "fired" brick is the convolution of several effects and measurements. Here we discuss the two most important ones, the Brick Finding procedure and the Changeable Sheet measurement, for which preliminary results have been obtained from the analysis of partial samples of already scanned events.

The tracking efficiency of single emulsion films can be measured by exposure to high-energy pion beams [6]. However, the measurement of the CS doublet efficiency in situ, in the OPERA detector, is by far more challenging, given the coarse resolution in the extrapolation of tracks from the electronic detectors to the CS.

At the present, we are studying the CS tracking efficiency by two independent approaches: (a) all tracks produced in already located neutrino vertices are followed downstream and searched for in the corresponding CS doublet; (b) muon tracks reconstructed by the electronic detectors and found in the CS are normalized to the total number of CC events where at least one track (not necessarily the muon) is found in the CS. The two methods yield a preliminary efficiency for finding a track in both films of the CS doublet which is compatible with the conservative expectation of $\sim 90\%$ on a single film.

The brick finding algorithm exploits the tracking capabilities of the OPERA electronic detectors and, by combining this information with the output of a Neural Network for the selection of the most probable wall where the interaction occurred, provides a list of bricks with the associated probability that the interaction occurred therein. A preliminary estimate of the brick finding efficiency, limited to the extraction of the most probable brick, is compatible with the Monte Carlo estimate of $\sim 70\%$ computed for a standard mixture of CC and NC events. A higher efficiency can be obtained by extracting also bricks ranked with lower probabilities.

All tracks measured in the CS are sought for in the most downstream films of the brick and followed back until they are not found in three consecutive films. The stop is considered as the signature of a primary or secondary vertex. The vertex is then confirmed by scanning a volume with a transverse size of 1 cm^2 for 11 films in total, upstream and downstream of the stopping point. Preliminary results on the vertex location efficiency

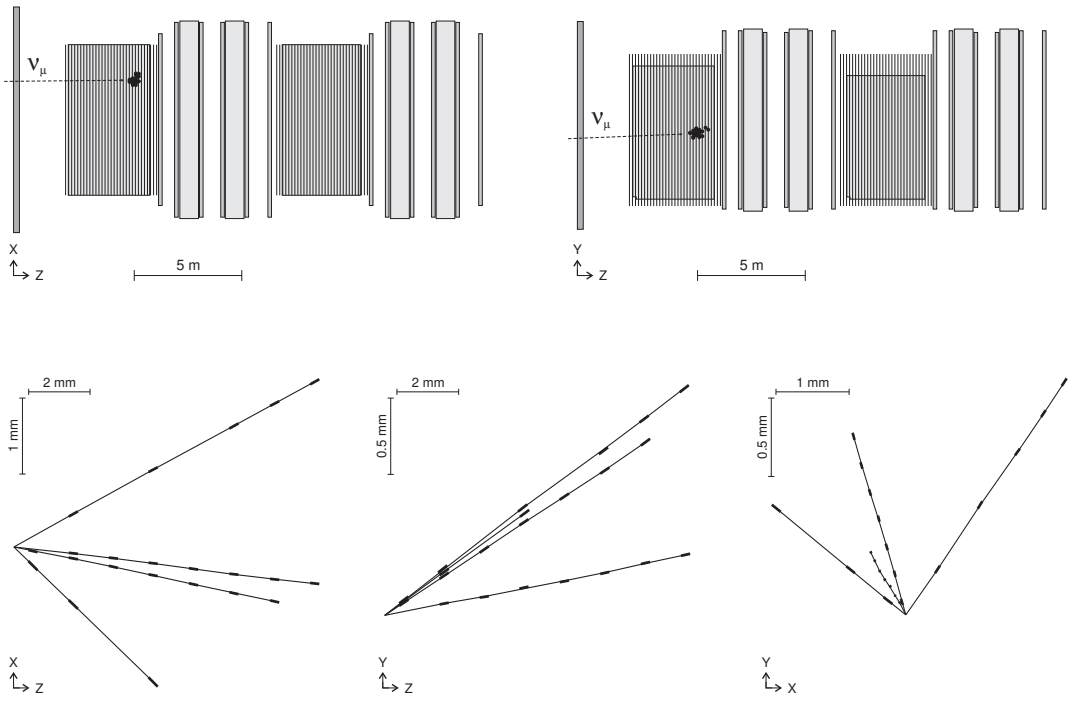

Figure 6: Online display of one NC event seen by the OPERA electronic detectors. The emulsion reconstruction is shown in the bottom panels: top view (bottom left), side view (bottom center), front view (bottom right).

as measured with the data are in agreement with the Monte Carlo expectations of $\sim 90\%$ and $\sim 80\%$ for CC and NC events, respectively.

Typical NC and CC events are shown in Figures 6 and 7, respectively.

In the subsample of located neutrino interactions charm decay topologies were searched for. Two such events were found. By using the neutrino-induced charm-production cross-section measured by the CHORUS experiment, about 3 charged-charm decays are expected to be observed in the analyzed sample.

4 Conclusions

The 2007 and 2008 CNGS successful runs constitute an important milestone for the OPERA experiment at LNGS. First neutrino interaction events with lead/emulsion bricks have been collected and these events allowed to check the complete analysis chain starting from the trigger to the neutrino vertex location in the emulsions and then to the topological and kinematical characterization of the event.

The major achievements can be summarized as follows:

- all electronic detectors performed excellently allowing the precise localization of the brick hit by the neutrino;

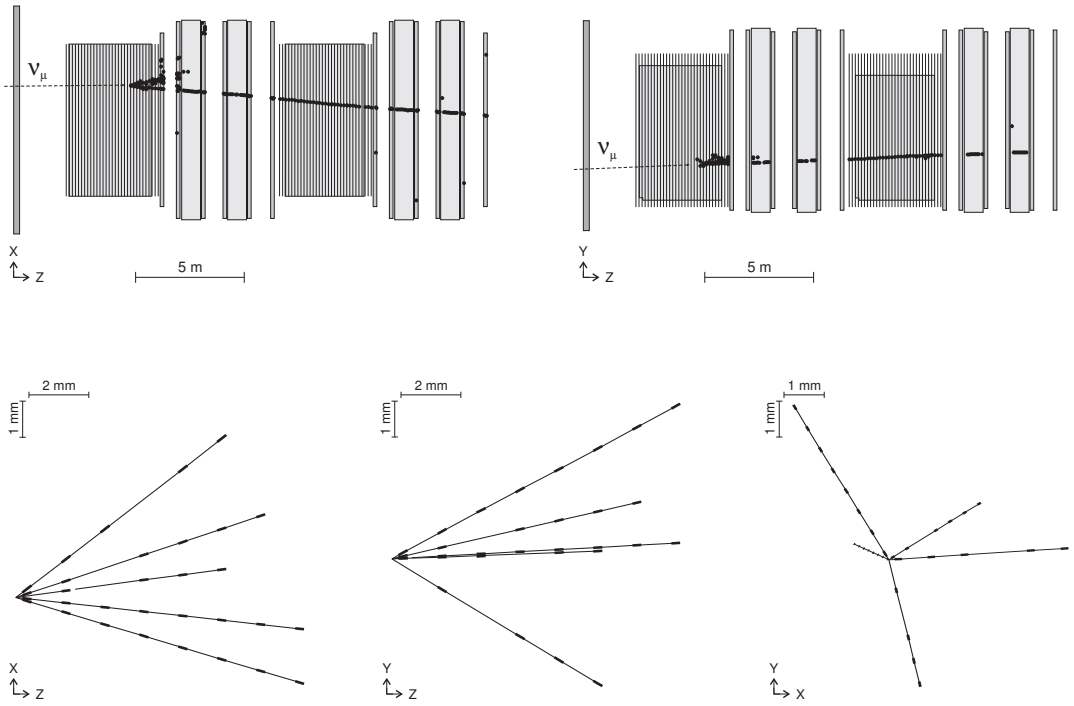

Figure 7: Online display of one CC event seen by the OPERA electronic detectors. The emulsion reconstruction is shown in the bottom panels: top view (bottom left), side view (bottom center), front view (bottom right).

- the electronic detector event reconstruction was tuned to the brick finding procedure, operated for the first time with real neutrino events. Identification of the brick where the interaction occurred has been done by using real data providing satisfactory results;
- all experimental activities that go from brick removal upon identification to the X and cosmic-ray exposures, brick disassembly and emulsion development, have been successfully accomplished. So far a rate of more than 100 brick per week can be routinely handled;
- the interface emulsion (CS) scanning was performed with the expected efficiencies. In particular, the track finding efficiency in a CS doublet was measured in OPERA and is in agreement with test beam results;
- the vertex location was successfully attempted for both CC and NC, although a quantitative estimate of the efficiency is still under evaluation;
- the topological and kinematical analyses of the vertices were successfully exploited and led to an unambiguous interpretation of neutrino interactions. In particular, in the reported analyzed event sample, two events with charm-like topologies were found. This is consistent with the neutrino-induced charm-production cross-section. The kinematical analysis of the two events showed that the background originated by sources other than charm-production is expected to be smaller than 10^{-3} events.

References and list of publications

[1] R. Acquafredda *et al.* [OPERA Collaboration], "First events from the CNGS neutrino beam detected in the OPERA experiment," New J. Phys. **8** (2006) 303 [arXiv:hep-ex/0611023].

[2] R. Acquafredda *et al.* [OPERA Collaboration] "The OPERA experiment in the CERN to Gran Sasso neutrino beam", to be submitted to JINST.

[3] T. Nakamura *et al.*, "The Opera Film: New Nuclear Emulsion For Large-Scale, High-Precision Experiments," Nucl. Instrum. Meth. A **556** (2006) 80.

[4] A. Anokhina *et al.* [OPERA Collaboration], "Study of the effects induced by lead on the emulsion films of the OPERA experiment," JINST **3** P07002 (2008).

[5] A. Anokhina *et al.* [OPERA Collaboration], "Emulsion sheet doublets as interface trackers for the OPERA experiment," JINST **3** (2008) P07005

[6] L. Arrabito *et al.*, "Track reconstruction in the emulsion-lead target of the OPERA experiment using the ESS microscope," JINST **2** (2007) P05004

[7] K. Kodama *et al.*, "Momentum measurement of secondary particle by multiple Coulomb scattering with emulsion cloud chamber in DONuT experiment," Nucl. Instrum. Meth. A **574** (2007) 192.

THEORY GROUP

The research is organized in the six working groups: FA51, GS51, CT51, PD51, PI12, PI21, that are generically denoted as IS (from "Iniziative Specifiche"). It concerns as main areas: astroparticle physics (mainly FA51), phenomenology of Planck scale physics (GS51), supernova neutrinos (CT51), cosmology, large scale structures and dark matter (PD51, a new IS), computer simulations of gauge theories (PI12), particle physics phenomenology (mainly PI21). There is a tradition of collaboration between the LNGS theory group and several experimental groups. In this report, we describe the activities of the theory group in 2008.

Members of the group: R. Aloisio, Z. Berezhiani, V. Berezinsky, D. Boncioli, P. Blasi, M.L. Costantini, G. Di Carlo, A. Gazizov, A.F. Grillo, E. Luzio, A. Maiezza, F. Nesti, G. Pagliaroli, P. Panci, L. Pilo, N. Rossi, F. Tortorici, F.L. Villante, F. Vissani.

Updated information and further info at: `http://theory.lngs.infn.it/index.html` .

Astroparticle Physics (FA51)

The Astroparticle group of LNGS in 2008 included R. Aloisio, V. Berezinsky, A. Gazizov, F. Vissani and visitors V. Dokuchaev (Institute for Nuclear Research, Moscow), Yu. Eroshenko (Institute for Nuclear Research, Moscow), B. Hnatyk (Lviv University, Ukraine), S. Grigorieva (Institute for Nuclear Research, Moscow). The group worked in close collaboration with P. Blasi (Arcetri Observatory, Firenze), A. Vilenkin (Tufts University, USA), M. Kachelriess (NUST, Trondheim, Norway), S. Ostapchenko (Karslrue, Germany) and others.

Scientific work

The main field of the work is astroparticle physics, including ultra high energy cosmic rays, and high energy neutrino and cosmology. From the works of 2008 one may be mentioned: V. Berezinsky, M. Kachelriess, M.Aa. Solberg, Phys. Rev. D **78** (2008) 123535. This work changes noticeably the status of superheavy dark matter (SHDM). The SHDM is characterized by most natural production due to gravitational interaction at the epoch soon after inflation. The problem for this model was particle candidate. In all cases the suggested particle candidate belongs to the hidden sector of theory, that made the model somewhat exotic. In the present work the lightest supersymmetric particle is considered as superheavy. It is demonstrated that superheavy supersymmetry remains perturbative despite the huge hierarchical problem, and superheavy neutralino, the lightest supersymmetric particle, gives most reasonable particle candidate for SHDM.

Conferences, seminars and other activities

R. Aloisio works as the scientific secretary of the LNGS scientific committee and as the organizer of LNGS seminar.

V. Berezinsky works as a member of Int. Advisory board of JEM-EUSO.

R. Alosio presented invited talks at Italian Physical Society meeting in Bologna 26 - 28 March, 2008, and at Texas Symposium on Relativistic Astrophysics in Vancover (Canada) on 7 - 14 December 2008.

V. Berezinsky presented invited talks at 4th Int. Workshop on "Neutrino Oscillations" (Venice, April 15 - 18, 2008), 12th Workshop on Cosmology and Dark Matter (Kyoto, June 3 -7, 2008), JEM-EUSO Workshop June 13 -15 (Tokyo), 3d Int. Workshop ARENA, Rome, June 25 - 27, 2008, Workshop NOW08, September 6 - 13, 2008 (Otranto), RESCEU Symposium on Astroparticle Physics and Cosmology, November 11 - 14, 2008 (Tokyo), EUSO Workshop Dec. 5 - 7 (Torino).

F. Vissani, together with F. Ferroni, acted as Director of the 170th Varenna School "Measurements of Neutrino Masses" (Jun.08). He lectured on theoretical aspects of neutrino masses for students of Milano U. (May.08 and Sep.08) and on neutrinos from supernova remnants in LNS, Catania (Sep.08).

Publications in journals, proceedings and preprints

[1] R. Aloisio, F. Tortorici
Super Heavy Dark Matter and UHECR Anisotropy at Low Energy.
Astropart. Phys. **29** (2008) 307.

[2] R. Aloisio, V. Berezinsky, P. Blasi, S. Ostapchenko
Signatures of the transition from Galactic to extragalactic cosmic rays.
Phys. Rev. D **77** (2008) 025007. e-Print: arXiv:0706.2834

[3] V. Berezinsky, V. Dokuchaev, Yu. Eroshenko
Remnants of dark matter clumps.
Phys. Rev. D **77** (2008) 083519.

[4] V. Berezinsky, M. Kachelriess, M. Aa. Solberg
Supersymmetric superheavy dark matter.
Phys. Rev. D **78** (2008) 123535.

[5] V. Berezinsky
Astroparticle Physics: Puzzles and Discoveries.
Journal of Physics: Conference Series, **120** (2008) 1.

[6] F.L. Villante, F. Vissani.
How precisely neutrino emission from supernova remnants can be constrained by gamma ray observations?
Phys. Rev. D **78** (2008) 103007.

[7] F. Vissani, F.L. Villante.
Cosmic rays and neutrinos from supernova remnants (or: the time when H.E.S.S. met Ginzburg and Syrovatskii).
Nucl.Instrum.Meth.A **588** (2008) 123.

[8] V. Berezinsky
UHE neutrino astronomy and neutrino oscillations.
Proc. 4th Neutrino Oscillations Workshop, ed. Milla Baldo Ceolin, 137, (2008).
e-print arXiv:0901.1428

[9] R. Aloisio, V. Berezinsky, A. Gazizov
Superluminal problem in diffusion of relativistic particles and its phenomenological solution.
e-print arXiv:0805.1867

[10] R. Aloisio, V. Berezinsky, A. Gazizov
Secondary protons from ultra high energy cosmic ray nuclei: is the Greisen-Zatsepin-Kuzmin cutoff unavoidable?
e-print 0803.2494.

[11] V. Berezinsky,
Propagation and origin of ultra-high energy cosmic rays.
Advances in Space Research, 41 (2008) 2071.

[12] R. Aloisio, V. Berezinsky, S. Grigorieva
Analytic calculations of the spectra of ultra-high energy cosmic ray nuclei. I. The case of CMB radiation.
e-Print: arXiv:0802.4452 [astro-ph]

[13] V. Berezinsky
Ultra High Energy Cosmic Ray Protons: Signatures and Observations.
e-print:0901.0254

[14] A. Maiezza. Tesi di Laurea at L'Aquila U., relatori P. Monacelli, F. Vissani.
Fenomeni di violazione di numero leptonico nei modelli left-right.
http://www.infn.it/thesis/thesis_dettaglio.php?tid=2430

[15] D. Boncioli. Tesi di Laurea at L'Aquila U., relatori R. Aloisio, A.F. Grillo.
Propagazione di raggi cosmici di energie ultra alte provenienti da sorgenti extra-galattiche. Simulazioni con sorgenti da cataloghi, studio delle anisotropie risultanti e confronto con i dati di Auger.
http://www.infn.it/thesis/thesis_dettaglio.php?tid=2512

Phenomenology of Planck Scale (GS51)

Members: A. Grillo, E. Luzio, R. Aloisio. Visitors: F. Girelli, S. Liberati, L. Maccione, F. Mendez, L. Sindoni. Collaboration with G. Amelino-Camelia (University of Rome, "La Sapienza").

Scientific work

The group has started a program to study in detail phenomenological effects of Doubly Special Relativity (DSR). In particular, we studied the time delay of Very High Energy gamma signals in the framework of the so called "Rainbow Gravity" theories, inspired by DSR. This work has been done in collaboration with F. Mendez (Universidad de Santiago de Chile). We have recently started, in collaboration with the GS51 groups of Roma and SISSA (Trieste) and the l'Aquila-Gran Sasso Auger Group, a discussion of possible effects of Lorentz Invariance Violations in the developement of Cosmic Ray Showers in the atmosphere. The general idea is to verify whether these efffects can modify and/or complement the strong constraints on the parameter space for Lorentz Violations that follow from Cosmic Ray experiments like Auger.

Conferences, seminars and other activities

A. Grillo has been invited to the workshop "Noncommutative deformations of special relativity" in Edinburgh, 7-11 July 2008, and to the Perimetr Institute (Waterloo, Canada). In both cases he gave seminars on the relevance of the results coming from the Pierre Auger Observatory on the possibility of constraining the parameter space for Lorentz Invariance Violations. A. Grillo is also a member of the Pierre Auger Collaboration.

Publications in journals, proceedings and preprints

[1] A. F. Grillo, E. Luzio, F. Mendez.
Time delay of light signals in an energy-dependent spacetime metric.
Phys. Rev. D **77** (2008) 104033.

Supernova Neutrinos (CT51)

Members: M.L. Costantini, G. Pagliaroli, F. Vissani. They worked in collaboration with F.L. Villante (Aquila U.); A. Ianni of Borexino; A. Drago (Ferrara U.); W. Fulgione (Turin U.) and other members of the LVD team; E. Coccia and other members of VIRGO team.

Scientific work

The main reason of this activity is to explore the potential of supernova neutrino observations. Our first task has been to use the data of SN1987A to test the standard scenario for neutrino emission (also termed neutrino assisted, delayed, or Bethe and Wilson scenario). The main results are documented in [1]; references [2, 3, 4] are preparatory works. In particular, ref. [1] provides a 2-3 sigma evidence for an initial phase of increased antineutrino luminosity (presumably connected with the explosion) as the one expected in the standard scenario. Based on the accumulated experience, we wrote a code to describe a generator of events; we studied the effect of neutrino masses on the signal; we investigated the connection of neutrino signal and gravitational waves (works in preparation). Also, we outlined in [5] a plan of research on non-standard scenarios for neutrino emission.

Conferences, seminars and other activities

G.P. gave talks on "Core collapse SNe: Neutrinos as a Trigger for GW search" GWADW 2008, Isola d'Elba, 12-18 May 2008; on "SN Core-Collapse & Neutrinos" at 13th Summer Institute at Gran Sasso National Laboratory, Astroparticle Physics in the Age of LHC, September 22 - October 8, 2008, LNGS, Assergi, Italy; and "SN neutrinos as an external trigger for GW search" at the ET-ILIAS_GWA joint meeting, EGO-VIRGO site, 24-26 Nov. 2008. She presented a poster on "Neutrino mass bound from SN1987A" at the International School of Physics "Enrico Fermi", Varenna, June 17-27 2008.

F.V. gave invited talks on SN1987A neutrinos at NOVE2008 (Apr.08) at the XCIV meeting of SIF (Oct.08) and at Comm.II of INFN (Oct.08). He provided introductory lectures on Neutrino Astronomy for the students of the Technical University of Munich in visit to LNGS (Jul.2008) and also at the LNS, Catania (Sep.2008).

Publications in journals, proceedings and preprints

[1] G. Pagliaroli, F. Vissani, M.L. Costantini, A. Ianni.
Improved analysis of SN1987A antineutrino events.
e-Print: arXiv:0810.0466 [astro-ph].

[2] F. Vissani, G. Pagliaroli.
Features of Kamiokande-II, IMB and Baksan observations and their interpretation in a two-component model for the signal.
e-Print: arXiv:0810.0456 [astro-ph].

[3] F. Vissani, G. Pagliaroli.
How much can we learn from SN1987A events? Or: an analysis with a two-component model for the antineutrino signal.
Proceedings of Neutrino oscillations in Venice (NOVE 2008), pp. 215-231, edited M. Baldo-Ceolin.

[4] G. Pagliaroli, M.L. Costantini, F. Vissani.
Analysis of neutrino signals from SN1987A.

Proceedings of IFAE 2007, pp. 225-230, edited by G. Carlino, G. D'Ambrosio, L. Merola, P. Paolucci e G. Ricciardi; e-Print: arXiv:0804.4598 [astro-ph].

[5] A. Drago, G. Pagliara, G. Pagliaroli, F.L. Villante, F. Vissani.
Formation of quark phases in compact stars and SN explosion.
AIP Conf.Proc.1056 (2008) 256.

Computer Simulations of Gauge Theories (PI12)

Member: G. Di Carlo. We have a longstanding collaboration based on the INFN-MEC agreement with the University of Zaragoza (Spain) and in particular with V. Azcoiti, E. Follana and A. Vaquero.

Scientific work

The two general goals of this activity are the study of 1) non perturbative aspects of lattice gauge theories 2) qcd at finite temperature and density and topological structures.

Our activity during 2008 mainly regarded the study of models presenting the so-called sign problem. We are trying to extend the old monomer-dymer algorithm ideas (up to now applied only in the infinite strong coupling limit, beta=0) to simulate the system for larger beta. Work in this direction is in progress; a possible applications outside lattice QCD is the Hubbard model far from the half-filling. Apart from this, we have reconsidered an old problem on realization of discrete symmetries in lattice QCD, using an approach that some of us introduced few years ago; the results are reported in a paper appeared in JHEP. In this line we have also analysed the structure of the Aoki Vacua in Lattice QCD with Wilson fermions; a paper on the subject has been accepted for publication in Phys. Rev. D in early 2009.

Publications in journals, proceedings and preprints

[1] V. Azcoiti, G. Di Carlo, A. Vaquero.
Parity realization in Vector-like theories from Fermion Bilinears.
JHEP **04** (2008) 035

[2] V. Azcoiti, G. Di Carlo, A. Vaquero.
QCD with two flavors of Wilson fermions: The QCD vacuum, the Aoki vacuum, and other vacua.
Phys. Rev. D **79** (2009) 014509

Particle Physics Phenomenology (PI21)

Members: Z. Berezhiani, F. Nesti, P. Panci, L. Pilo, N. Rossi, F. Villante.
Visitors: D. Comelli (INFN Ferrara), O. Kancheli (ITEP Moscow), A.S. Sakharov (CERN & MEPHI, Moscow), A.P. Serebrov (PNPI St.-Petersburg).

Scientific work

One research line was dedicated to the origin of dark matter, namely to the cosmological fine tuning problem questioning to why the observable and dark matter fractions in the universe are so close, just about a factor 5. This proportion could occur in a natural way if dark matter originates from a hidden gauge sector having as complex microphysics as the sector of ordinary particles, (e.g., the mirror sector), and the baryon (i.e., particle-antipartcile) asymmetry in both sectors emerge by one mechanism, related to the B-L and CP violating, out-of-equilibrium processes between the ordinary and hidden sector particles [1].

Another line of the research was focused on the massive phase of gravity following from the Lorentz symmetry breaking, realized by coupling the metric of the general relativity to additional spin-two fields (so called bigravity or multi-gravity). We have studied the infrared modification of the Newton law: namely, we found and analyzed the exact sphericallly symmetric solutions *á la* Schwarzschild in the system of two metrics [2]. Astrophysical implications of bigravity theories for the galactic rotational curves were discussed in [5]. Another approach related to the spontaneous Lorentz-breaking by the dynamical tensor condensate and the Goldstone origin of gravity was discussed in [10].

Conferences, seminars and other activities

Int. Workshop *"Hot Topics in Modern Cosmology"* SW2, Cargese, France, May 2008 (talks of Z. Berezhiani, F. Nesti, L. Pilo, F. Villante); Int. Conf. *"Slow Neutrons in Particle Physics"*, Grenoble, France, May 2008 (invited talk of Z. Berezhiani); Int. Conf. *"Quantum Gravity/Geometry"*, QG2, Nottingham, UK, June 2008 (invited talk of F. Nesti); Int. Workshop *on the origin of C, P, T violations*, CPT@ICTP, Trieste, Italy, July 2008 (invited talks of Z. Berezhiani and F. Nesti); Int. *Neutrino Oscillation Workshop* NOW 2008, Otranto, Italy, Sept. 2008 (invited talk of F. Villante); 13th Gran Sasso Institute *"Astroparticle Physics at the Age of LHC"*, LNGS, Assergi, Italy, Oct. 2008 (lectures of Z. Berezhiani, F. Nesti and F. Villante); Int. Conf. TSU'90, Tbilisi, Georgia, Oct. 2008 (invited talk of Z. Berezhiani); Int. Workshop PHYSUN *"The Physics of the Sun and the Solar Neutrinos: an update"*, LNGS, Assergi, Italy, Oct. 2008 (talk of F. Villante); Int. Psi/G Workshop on *"Consistent Modifications of Gravity"*, Paris, France, Nov. 2008 (invited talk of F. Nesti).

Z. Berezhiani gave invited seminars at the Univ. Autonoma, Barcelona, Spain, and at the Inst. of Physics, Tbilisi, Georgia; F. Nesti gave invited seminar at the Univ. Lausanne, Switzerland, L. Pilo gave invited seminars at the Univ. Padua and at the Oxford University, UK.

Publications in journals, proceedings and preprints

[1] Z. Berezhiani.
Unified picture of ordinary and dark matter genesis.
Eur. Phys. J. ST **163** (2008) 271.

[2] Z. Berezhiani, D. Comelli, F. Nesti, L. Pilo.
Exact Spherically Symmetric Solutions in Massive Gravity.
JHEP **0807** (2008) 130.

[3] M. Raidal et al. (F. Nesti co-author),
Flavour physics of leptons and dipole moments.
Eur. Phys. J. C **57** (2008) 13.

[4] F. Nesti, R. Percacci.
Graviweak Unification.
J. Phys. **A41** (2008) 075405.

[5] N. Rossi.
Dark halo or bigravity?
Eur. Phys. J. ST **163** (2008) 291.

[6] F.L. Villante, F. Vissani.
How precisely neutrino emission from supernova remnants can be constrained by gamma ray observations?
Phys. Rev. D **78** (2008) 103007.

[7] F. Vissani, F.L. Villante.
Cosmic rays and neutrinos from supernova remnants (or: the time when H.E.S.S. met Ginzburg and Syrovatskii).
Nucl. Instrum. Meth. A **588** (2008) 123.

[8] S. Raby et al. (Z. Berezhiani co-author),
DUSEL Theory White Paper.
e-Print: arXiv:0810.4551 [hep-ph]

[9] Z. Berezhiani, A. Lepidi.
Cosmological bounds on the 'millicharges' of mirror particles.
e-Print: arXiv:0810.1317 [hep-ph]

[10] Z. Berezhiani, O.V. Kancheli.
Spontaneous Breaking of Lorentz-Invariance and Gravitons as Goldstone Particles.
e-Print: arXiv:0808.3181 [hep-th]

[11] Z. Berezhiani.
More about neutron - mirror neutron oscillation.
e-Print: arXiv:0804.2088 [hep-ph]

The WArP Programme

The WArP Collaboration

R.Acciarri[a], M.Antonello[b], B. Baibussinov[c], M.Baldo-Ceolin[d], P.Benetti[e], F.Calaprice[f], E.Calligarich[g], M.Cambiaghi[e], N.Canci[a], F.Carbonara[h], F.Cavanna[a], S. Centro[d], A.G.Cocco[i], F.Di Pompeo[a], G.Fiorillo[h], C.Galbiati[f], V. Gallo[h], L.Grandi[b], G. Meng[c], C.Montanari[g], O.Palamara[b], L.Pandola[b], F. Pietropaolo[c], G.L.Raselli[g], M.Roncadelli[g], M.Rossella[g], C.Rubbia[1b], E.Segreto[b], A.M.Szelc[j], F.Tortorici[b], S. Ventura[c], C.Vignoli[g]

[a] *Università dell'Aquila e INFN, L'Aquila, Italy*
[b] *INFN - Laboratori Nazionali del Gran Sasso, Assergi, Italy*
[c] *INFN - Sezione di Padova, Padova, Italy*
[d] *Universitá di Padova e INFN, Padova, Italy*
[e] *Universitá di Pavia e INFN, Pavia, Italy*
[f] *Princeton University - Princeton, New Jersey, USA*
[g] *INFN - Sezione di Pavia, Pavia, Italy*
[h] *Universitá di Napoli e INFN, Napoli, Italy*
[i] *INFN - Sezione di Napoli, Napoli, Italy*
[j] *IFJ PAN, Krakow, Poland*

[1]Spokesman of the WArP Collaboration

1 Introduction

The status of the WArP activities during 2008 is reported.
Main activity obviously was the construction of the WArP 100 litres detector, which has been completed by December 2008. In this context several key issues have been solved in particular for what concerns the characterization and the optimization of the wavelength shifting/reflective layer and the characterization of the photomultipliers response.
An update of our estimates of the backgrounds for the 100 litres detector is also briefly reported.
Runs with the WArP 2.3 litres prototype were also carried on both with standard and with depleted argon. Lack of performance in the light yield limited our capability to extract conclusive results (which are reported in the following) and induced a strong activity to understand the cause of the low light yield. This activity is currently concentrated on the analysis of the effects of water outgassing. The remarkably large effect of the residual water absorption, of the order of a few $10^5 cm^{-1}$ is shown in Figure 1. Even the

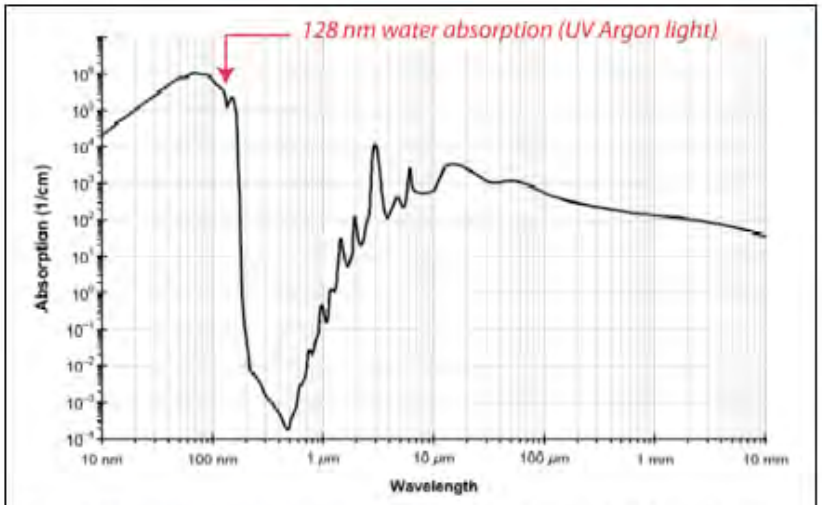

Figure 1: Water absorption in cm-1 at normalized density as a fuction of the light wawelength. We remark the huge absorption around the 128 nm line due to Argon scintiilation, of the order of a few times 105 cm-1.

smallest contaminations for instance over the walls of the TPB wave shifter may introduce substantial losses of the light yield due to LAr. The elimination of water contamination is currently under active investigation.
The activity for the extraction and purification of massive quantities of low activity argon coming from underground wells is also going on in US.

2 2. Status of WArP-100 construction

2.1 Detector assembly

Assembly of the WArP 100 litres detector started in July 2007, when the installation area in Hall B became available: positioning of the external shields floor (Pb and Polyethilene slabs), assembly of the sustaining anti-seismic structure and positioning of the main cryostat were achieved by the end of 2007 (Fig. 2). At the same time, all the 342 PMTs of the WArP-100 detector, after delivery by ETL were tested for functionality at liquid argon temperature at INFN-Napoli test facility. Construction of the de-humidified clean

Figure 2: Picture of the installation area in Hall B. The de-humidified clean room, the detector support structure (green) and the liquid argon storage tank are visible.

room for the detector assembly in Hall-B followed, between September 2007 and March 2008 (Fig .3-left). In parallel other two facilities for pre-assembly operations [(1) mechanical components pre-assembly, (2) vacuum evaporation of wavelength shifter on reflective layers] were readied in the LNGS Assembly Hall, above ground. Pre-assembly operations started in February 2008 with the installation of the ultra-low radioactivity, divider sockets on the PMTs and was carried on between March and May 2008 with the installation of reflective foil and photomultiplier holders onto the copper supports forming the detector structure (inner 100 lt volume and external active veto). In June 2008 the main phase of the pre-assembly procedure, i.e. the deposition of a wavelength shifter film on the reflective foils (about 240 pieces), was started using a dedicated vacuum evaporation system (Fig. 3-right), and successfully completed at the end of September 2008. In the meantime, between March and April 2008, the polyethylene internal shield was assembled

Figure 3: (a) Wavelength shifter Vacuum Deposition system, developed in INFN-Pavia, and installed in LNGS Assembly Hall for the evaporation procedure. **(b)** reflective foil and photomultiplier holders onto the copper supports in the pre-assembly stock-house.

underground inside the main cryostat. The top flange of the cryostat was then positioned inside the clean room and appended to it the detector assembly (copper components with PMT holders and the mirror foil with wavelength shifter coating) was finally initiated. The WArP-100 active volume (the inner part of the detector) was assembled between May and July 2008. Functionality of the inner detector set of photomultipliers (37 units) was later verified in dark conditions at the end of September 2008. Assembly of the outer part of the detector (active veto) started in July 2008 and completed by mid November 2008, including the cabling of the about 300 PMTs (Fig. 4). Positioning of the full detector inside the main cryostat, by moving back in place the top flange of the cryostat, has been performed on December 19th. Detector commissioning was started immediately after with vacuum pumping operation. During this phase (at least two months), the external components of the cryogenic and purification systems will be installed (liquid and gas phase recirculation/purification circuits, filling lines,), as well as the installation of the passive shield walls (Poly-Ethilene and Lead shields). Detector cooling and filling phase are expected to take place by spring 2009.

2.2 Filters Activation/Regeneration

WArP 100 lt detector is provided with a liquid/gas Argon recirculation/purification system for mainly oxygen and water removal; the purification system is based on custom stainless steel cartridges filled with Zeolite (1/3 by volume content) and Trigon (2/3). Zeolite acts as a mechanical molecular sieve trapping essentially moisture and CO_2 in the Argon flow. Trigon is a molecular reagent formed by alumina bulk (80-90%) with metallic oxides (in particular CuO 10-14%): purifier beads retain oxygen by chemical reaction with the metal to form the metal oxide. Before (after) use both Zeolite and Trigon have to be activated (regenerated). To provide activation/regeneration a dedicate set-up has been built up (see Fig. 6): Basic procedure for activation/regeneration is as follows.

- A dedicate oven has been designed and assembled at LNGS (Warp Facility Hall di Montaggio), Fig 7. It is used to preheat the adsorber to around 300 C. Then a mixture of 5% hydrogen and 95% argon by volume content is opened and gas

is allowed to flow through a gas preheater, the heated cartridge, and then finally vented to the atmosphere.

- Zeolite is activated/regenerated only by hot mixture flushing; on the contrary hydrogen reacts exothermically with the metal oxides in the Trigon filter to produce water vapor and results in a further increase in adsorbent temperature. Beads in the adsorber can start to break down above 350 C; temperature, gas mixture flow and outgoing moisture are carefully monitored during the process.

- Regeneration takes approximately one hour, after which the filter is flushed with Argon gas and allowed to cool down. Adsorber is then ready for using.

Four standard WArP cartridges are being activated for their use within the WArP Gas Argon recirculation system (3 units) and Liquid Argon recirculation system (1 unit).

2.3 External Lead Shield: final assembly

The WArP-100 detector set-up is surrounded by an external passive shield for neutrons (70 cm wall of polythene) and for gammas (10 cm wall of Lead). All materials for the external shield have delivered at LNGS during 2007. The Lead shield is made by lead bricks contained into stainless steel boxes forming an octagonal wall around the cryostat. The stainless steel boxes have been delivered in July 2008. The positioning of the lateral wall is started (Oct. 2008, see Fig. 8). The mounting procedure foresees the positioning of the stainless steel boxes inside the WArP sustaining anti-seismic mechanical structure and the filling of the boxes with the lead bricks (on going). Finally, the box front and top sides are welded and the boxes anchored to the sustaining structure. Completion of the procedure is foreseen by mid January 2009.

3 Simulation of neutron background in WArP 100 lt

The neutron-induced background expected in WArP 100 lt has been evaluated by means of dedicated Monte Carlo simulations based on Geant4. Nuclear recoils from neutron interactions (and also inelastic interactions, if the γ-ray escapes) on ^{40}Ar give the very same signature of the dark matter signal. Neutron background hence represents the ultimate limit to the experimental sensitivity.
Besides the use of passive neutron shielding, two additional tools can be used to identify and reject nuclear recoils due to neutron interactions in the internal detector:

- anti-coincidence with the 8-ton active veto;

- localization capability of the inner detector to reject events giving more than one (spatially-resolved) energy deposition.

The efficiency of the rejection tools depends on the energy threshold of the veto and on the spatial resolution of the inner detector. At the moment, the energy threshold of

the active veto is expected to be of 30 keV; WIMP events in the inner detector are looked for within an energy window from 20 to 100 keV. The liquid argon in the veto around the inner detector is at least 60 cm in all directions; the active veto is surrounded by 35 cm of non-instrumented liquid argon. A realistic model of the WArP 100 lt set-up has been coded in the Geant4 simulation.

The internal detector and the active veto are surrounded by a passive neutron shielding made of polyethylene, divided in two parts: a 60-cm thick layer surrounds the cryostat, while an additional 10-cm layer is placed inside the cryostat (in the liquid Argon) and absorbs neutrons produced in the stainless-steel dewar. Since external neutrons are effectively absorbed by the passive shielding, the main contribution (%) to the neutron background comes from neutrons produced in the materials themselves by radioactivity and from cosmic ray interactions in the detector materials or in the surrounding rock. Neutrons due to radioactivity are emitted via spontaneous fission and/or (α, n) interactions from natural α emitters, the most relevant sources for WArP being stainless steel (dewar, cathode, passive shielding, flanges, support structures) and photo-multipliers. The copper structure in the active veto gives a negligible neutron flux because of the considerably better radio-purity than stainless-steel and photo-multipliers. The production rate and the energy spectrum of neutrons emitted in the WArP materials by spontaneous fission and (α,n) reactions have been estimated by means of the Sources 4A code, taking into account the measured contaminations in ^{238}U and ^{232}Th (or the corresponding upper limits). Neutron production rate in the stainless-steel used for the cryostat and for the internal parts is 3.38 neutrons/(day ton). Similarly, the neutron production rate from the photo-multipliers is estimated to be of 14 neutrons/(year unit).

Neutrons produced in the individual detector parts (according to the spectrum and the rate calculated with Sources 4A) have been tracked in the WArP set-up using Geant4 in order to evaluate the efficiency of the active veto and the background anticipated for dark matter searches. Neutron flux and spectrum for the external neutrons (produced in the Gran Sasso rock) have been taken from *H. Wulandari et al., Astrop. Phys. 22 (2004), 313*. High energy muons have been generated in the rock above the set-up with the proper energy and angular distributions to take into account the possibility of muon-induced showers producing neutrons. Only a fraction 30% of the neutron or muon-induced events in the internal detector can actually mimic WIMP-interactions: in the other cases, the energy is partially or totally released by minimum ionizing particles, e.g. following (n, n' γ) interactions. These latter events can be effectively rejected by pulse shape analysis on S1 (primary scintillation signal in LAr) and they are not considered as a background for WIMP searches. In Table 1 it is summarized the rate of neutron-induced background events in the inner detector (20-100 keV window) which cannot be rejected by veto anti-coincidence (30 keV threshold). The residual background is dominated by photo-multipliers and by μ-induced interactions.

Background presented in Table 1 is estimated in the assumption of 30 keV threshold in the active veto. If the veto threshold is set to 50 (100) keV, the background rate in the inner detector increases up to 5.3 (8.7) events/year. In the extreme case of no active veto (namely, the external liquid argon buffer acts as a passive shielding only), the background

rate increases up to about 130 events/year.
A further improvement can be achieved by pulse shape analysis on S2. In fact one can reject neutron-induced events giving more than one (spatially-resolved) energy deposition in the inner detector. The rejection efficiency can be estimated by Monte Carlo simulation, once the expected spatial resolution of the internal detector is known. In the assumption that two energy depositions can be resolved if their distance is larger than 1 cm along the z-coordinate (drift axis) or larger than 2 cm along the xy plane, only 36% of neutron-induced events survive the cut, namely background is further reduced by a factor of about 2.8 (about 30% of neutron-induced events are genuinely single-site in the inner detector, so they cannot be rejected by multiplicity).
In conclusion, in the assumption of 30 keV threshold in the active veto and spatial resolution in the inner detector of 1(2) cm in the z (xy) direction, respectively, the anticipated neutron-induced background for WArP dark matter searches is 1.2 events/year in the 20-100 keV energy window. Background is increased for higher threshold of the active veto and/or worse spatial resolution of the inner detector.

4 Low activity Argon tests

Presence of ^{39}Ar isotope in natural Argon is commonly considered as a major source of background in the WIMP search with Argon based technology, especially at large mass scale (tons). The ^{39}Ar is a β-emitter with specific activity in natural Ar of about 1 Bq/kg and β-energy end-point at 565 keV. The discrimination criteria with double-phase Argon detectors exhibit very effective rejection power of γ/βbackground from Ar-recoil signals, however ^{39}Ar β-event can be mis-identified as nuclear recoil due to statistic fluctuations of the signal shapes and of the identification parameters used to discriminate the nature of the ionizing particle.

4.1 ^{39}Ar Depleted Argon extraction in US

With previous sampling campaigns (WArP Princeton) it has been demonstrated (2007) that underground wells contain Argon depleted in ^{39}Ar content with respect to the atmospheric concentration. In the course of 2008 it was addressed the possibility and practicality of extracting large quantities of underground argon from gas streams containing minute concentrations of Argon (a few tens of parts per million) on the industrial scale required for the development of large scale dark matter detectors. A technique suitable for processing large flow rates of natural gas has been developed, capable of concentrating the argon phase by a factor 1001,000 in a single pass. This technique was tested on a CO_2 stream, but it is applicable to a variety of natural gas streams.
It was demonstrated that it is possible to concentrate traces of argon from an underground stream into a crude argon product stream with argon concentrations up to about 10%. The small-scale plant built in Princeton is already capable of producing 0.50.6 kg a day of depleted argon, with a recovery fraction of the argon entering the plant in the range

6080%. Operation of the small-scale plant is cost-effective, and the plant could be used to produce a few hundred kilograms of depleted argon target in the time span of 12 years.

4.2 Depleted Argon tests with the 2.3 liter chamber

During April 2008, the 2.3 lt prototype has been filled with a sample of low activity Argon, i.e. depleted in the ^{39}Ar radioactive isotopic content. The low activity Argon sample used in this test was produced by centrifugation of natural Argon and, according to the producer (Russia), it should be depleted in the ^{39}Ar isotope content at least by a factor 100. The sample has been characterized in Bern (Loosly Group) and the ^{39}Ar content was found to be below the instrumental sensitivity, i.e. less than 1/30 of the ^{39}Ar content in natural Argon.
The 2.3 lt detector, already used in several previous tests, during this test exhibited an unexpectedly low light yield (¡ 1phel/keV). The reasons of this are still under study: the present preferred explanation is found in the H_2O out-gassing from the large amount of plastics (PEEK) inserted in the chamber volume to minimize the dead space around the active 2.3 lt volume (the available low activity Argon was just in the amount needed to fill the active part of the detector). Residual amount of water may easily lead to a strong degradation of the TPB wave-shifting layer covering all the inner surfaces of the sensitive volume and therefore to a reduction of the light yield available for collection at the PMTs. In fact, the low light yield affects the primary scintillation spectrum resolution and reduces the possibility to perform a reliable comparison with Montecarlo predictions to determine, through a fit procedure, the single components of the background spectrum. The measured event rates in the case of the depleted Argon run and in a previous run with the same 2.3 lt chamber filled with standard Argon are compared within the energy range 100-600 keV. The energy spectra obtained in the two test runs are reported in Fig. 9 and the main results are summarized in Tab. 2. The energy calibration for primary signal spectra (scintillation in LAr) has been obtained in both runs by means of a ^{137}Cs source (full absorption peak 662 keV). As reported in Tab. 2, the higher light yield of the standard Argon run (LY 1.6 phel/KeV) allowed to identify the shapes and intensities of single radioactive components, that for simplicity are indicated as 39Ar and residual (85Kr, ^{232}Th, ^{40}K and ^{60}Co), while in the low activity Argon run the single components of the scintillation spectrum could not be separated (and therefore, the reduction factor of the 39Ar content can only roughly be estimated).
The observed total rate in the depleted Argon run is a factor 4 lower than the rate in the standard Ar run. Assuming that the contribution due to the residual (^{85}Kr, ^{232}Th, ^{40}K and ^{60}Co) background is similar (if not identical) in the two runs, the ^{39}Ar content in the depleted Argon sample is inferred to be about 1/40 of the ^{39}Ar content in natural Argon. However, due to the poor energy resolution experienced during the test, this result cannot be considered as conclusive and further tests are needed.
The unexpectedly low Light Yield that characterized the low-activity Ar run with the 2.3 lt detector triggered a careful review and long series of experimental tests of the main aspects of the light collection system implemented with the WArP experimental

technology:

- Light Yield study;
- Variations of the Liquid Argon scintillation properties in presence of contaminants (O_2, N_2, H_2O): test performed with a dedicated experimental set-up (0.7 lt LAr chamber);
- Precise characterization of the optical properties of the WArP optical system (mirror reflector + wavelength shifter): dedicated measurements at ENEA Laboratories;
- Performance of the PMTs: study of the Quantum Efficiency (at CERN) and of the photoelectron collection efficiency (at Princeton and Naples.

These issues are briefly reported here below.

5 Light Yield studies

5.1 Test of the Optical System with a 0.7 lt dedicated LAr detector (LNGS).

An intense test activity has been carried out (April-July 2008) with a small dedicated detector (0.7 lt of liquid argon). The liquid argon volume is housed in a PTFE cylindric cell (radius of 10 cm, height of 10 cm) and is viewed by a single photomultiplier (2 and 3 inch. ETL standard WArP photomultiplier). The internal surface of the cell is entirely covered by a dielectric reflective layer (3M-VM2000, with a reflectivity of 98% around 430 nm), upon which is deposited a film of wavelength shifter (ThetraPhenylButadiene-TPB) converting the 128 nm liquid argon scintillation light into blue light (about 430 nm) detectable by the photomultiplier (PMT).
The most relevant test activity concerned the measurement of the light yield obtainable with the set-up with:

- Different techniques of deposition of the TPB upon the reflective layer;
- Different quantities (surface densities) of TPB deposited on it . Three deposition techniques have been explored:
- Spraying TPB on the VM2000 surface (samples produced at CERN);
- Spraying TPB in a polystyrene matrix on the VM2000 surface (samples produced at CERN);
- Evaporating pure TPB on the VM2000 surface with the Vacuum deposition set-up described above.

For each one of the three solutions a large number of tests has been performed by changing the quantity of TPB deposited on the reflective layer. In all cases an interval of TPB surface densities, ranging from 100 μg/cm^2 to 1000 μg/cm^2, has been explored. In many cases during these tests, light yield values above 2 photo-electrons/keV have been stably obtained with the best value close to 3 photo-electrons/keV (with evaporation technique). The result of this optimization procedure is reported in Tab. 3.

The high value of the Light Yield obtained in particular with the Vacuum deposition method well agrees with expectations based on MonteCarlo simulations. Extrapolating this result (MonteCarlo simulation) to the WArP 100 lt detector, a value of LY 4 phel/keV is expected. On the other hand, the low LY value found with the 2.3 lt prototype during the low-activity Ar test run is unexpected. The choice of the optical system (VM2000 mirror layer coated with evaporated TPB film) seems to be excluded as an explanation of it.

5.2 Test of the PMT voltage setting and of Earth magnetic field with a 0.7 lt dedicated LAr detector (LNGS)

Another set of tests with the 0.7 lt detector concerned the optimization of the voltage drop between the PMT cathode and the first dynode (VK-d1), in order to maximize the photo-electron collection efficiency at this stage. Contextually also the effect of the Earth magnetic field on the electron collection efficiency has been studied.
In order to perform these tests the cell was filled with LAr and the light yield was measured with different values of VK-d1 and with different orientations of the cell (and of the PMT) with respect to the Earth magnetic field.
In Fig.10-left it is shown the light yield for the two PMT orientations that respectively minimize and maximize the Earth magnetic field effect as a function of VK-d1. For VK-d values below 300 V this effect is clearly visible and at 200 V the light yield difference between the two orientations is of about 15%. When a ?-metal shield is placed all around the chamber this effect disappears, as shown in Fig.10-right.
The electron collection efficiency at first dynode is strongly dependent on VK-d1 for VK-d1 below 250 V (see Fig.10-right), while for higher values it results to be almost stable. The nominal voltage drop selected for the WArP PMT operation (100 lt detector) is around 350 V.
Effects of the Earth magnetic field or bad voltage setting, inducing reduced photo-electron collection efficiency at the first PMT dynode are also excluded as possible explanations for the low Light Yield value found with the 2.3 lt prototype during the low-activity Ar test run.

5.3 Performance test of the PMTs: (1) study of the Quantum Efficiency (CERN)

The PMTs produced by ETL for the WArP detector have been developed to maximize the light yield, thanks to a (nominal) high Quantum Efficiency (QE¿ 20%), both at warm and

LAr temperature. All delivered PMTs have been individually tested at the INFN-Naples PMT testing facility (single phel. Response, gain, linearity, optimal setting, etc..). The absolute QE of the PMTs (individually provided in data sheets from ETL measurement) was instead never been tested directly by the collaboration.
Within the program of detailed checks of the WArP light detection system (motivated by the unexpected results from the last 2.3 lt prototype run with low-activity Ar) a measurement campaign of the WArP PMT absolute QE has been launched.
With the help of the CERN Detector Technologies Group (PH-DT-TP) the measurement campaign on a limited sample of 2 and 3 inches WArP PMTs has been carried out in August 2008. The set-up is based on a mono-chromatograph spanning 200-800 nm light range (xenon lamp) with 1 nm resolution (Figure 10-top). The measurement consists in recording the current between the cathode and the 1stdynode as a function of the impinging light wave lenght. The quantum efficiency is deduced by comparison with a calibrated high QE Photodiode (2% absolute calibration certified by NIST).
Extensive measurements have been performed, at room temperature, both on the 2 and 3 inch. PMTs: plateau search, radial scan, 1st dynode collection efficiency. The main results are summarized as follows (Fig.11-bottom):

- QE (@420 nm) $\geq$ 20%;
- Active PMT surface $\geq$ 90%;
- Collection efficiency on first dynode $\geq$ 80% (VK-d @ 450 V).

The agreement with the data sheets is remarkable (still in progress are the measurements with the PMTs coated with TPB). This implies that a low PMT QE is excluded as possible explanation for the low Light Yield value found with the 2.3 lt prototype during the low-activity Ar test run.

5.4 Performance test of the PMTs: (2) study of the Collection Efficiency (Princeton)

The Collection Efficiency (CE) is also an important parameter needed for a full characterization of the PMT performance. This quantity is intrinsically much more difficult to measure than QE. Once both QE and CE are measured/available, the global efficiency of the PMT (typically denoted as Detective Quantum Efficiency, DQE = QE ? CE) can be quoted.
The PMTs in use with WArP (ETL-D750UKFLA) are based on fast pmt design where the trade-off between best timing and highest collection tends towards timing. This implies in particular that the voltage drop between the PMT cathode and the first dynode (VK-d1) should be carefully selected. The VK-d1 value in the range 350- 450 V is recommended by ETL as a good compromise between timing, collection, and low after-pulse (as the after-pulse rate increases with the K-d1 voltage). The corresponding CE range of values (from ETL simulations) is 71-78%. Within the program of detailed checks of the WArP

light detection system, a measurement campaign of the WArP PMT Collection Efficiency CE has been also performed at Princeton.
The experimental set-up is very simple and consists of a small cylinder of plastic scintillator (BC-408: 1/4 inch. thick, 15 mm in diameter) coupled to centre of the PMT window. The PMT window and the scintillator are covered with a thin teflon (diffusive/reflecting) sheet. The photon yield of BC408 is known and the QE of the ETL PMT is also known (measurement reported above).
During the test the scintillator is exposed to 22 keV X-rays from a ^{109}Cd source and the light yield (LY, phel/keV) is measured, after calibration by the mean response to single photoelectrons signals. The ratio LY/QE provides with an indication (in arbitrary units) of the Collection Efficiency of the PMT (from photo-cathode to anode).
The same test has been performed by replacing the ETL-D750UKFLA 3 in. PMT with a reference 1 in. PMT (Hamamatsu R6095) whose CE is assumed to be 100% given the favorable relative dimensions of the PMT and of its dynodes (Box&Grid). By comparing the results (ratio LY/QE) from the two PMTs, the Collection Efficiency of the ETL-D750UKFLA 3 in. has been inferred to be CE = 74 % (and the global efficiency DQE = 14.6 %).
This result is in agreement with expectations based on simulation of the PMT geometry. It is worth noting that the Collection Efficiency imposes a limitation on the global efficiency of the PMT. This limitation however seems not sufficient to explain the low Light Yield value found with the 2.3 lt prototype during the low-activity Ar test run.

5.5 Variation of Liquid Argon scintillation light emission in presence of contaminants

Scintillation light emission in LAr can be affected by presence of contaminants at residual level diluted in commercial Argon, such as O_2, N_2 and H_2O. Dedicated studies on the effects induced by O_2, N_2 have been already reported and published. O_2 is very harmful, producing Light Quenching at rate of 0.54 ppm^{-1} μs^{-1}, however LAr filtering adopted in the WArP experimental layout reduces the Oxygen concentration to a negligible value. N_2 is (normally) not filtered out. The residual Nitrogen content in (best grade) commercial Argon used in standard filling operation is at the level of $\geq$ 0.2 ppm and can be considered only marginally responsible for light yield reduction. Water is also present in commercial Argon. It is routinely filtered out at filling time by means of molecular sieves. However, water outgassing (mainly from plastic/PEEK material) can represent an additional source of pollution. Dedicated studies are being carried out to precisely identify the possible effects of water contamination in LAr. Two processes could potentially be ascribed to the presence of water in Ar:

- Argon VUV (128 nm) Light Absorption by H_2O molecules - deposited onto the TPB layer (highly hygroscopic) and in the liquid (Ar+H_2O) volume viewed by the PMT. This process should reduce the total LY, regardless from the type of emission singlet (fast) or triplet (long) Ar2* decay.

- Light Quenching, due to non-radiative collisional reactions in competition with the de-excitation process leading to VUV light emission: $Ar_2^* + H_2O \rightarrow 2\ Ar + H_2O$ This (rather slow) process should affect mainly the LAr long decay time constant (i.e. leading to the decrease of the triplet state excimer concentration $[Ar_2^*]$). Two experimental tests are being set-up (Oct.-Nov. 2008) aiming at the understanding of the effect due to residual water vapor on VUV scintillation light emitted in LAr:

- Exploiting the ICARUS LAr-TPC cryogenic facility at CERN. For this purpose a new chamber has been build. The present layout consists of a 7 liter single phase LAr active volume, equipped with two 8 inches PMTs facing each other (one ETL9357 and one Hamamatsu R5912-02 MOD). Both PMTs have been measured to have 20% QE @ 420 nm and should exhibits the same QE at LAr temperature. The PMT coverage of this layout is about 20%, the rest of the walls being covered with the usual reflector + TPB. The PMTs surfaces are also deposited with TPB. The chamber is fully assembled and is presently under vacuum pumping. The first test will be performed in gas phase at room temperature, and will be followed by tests in liquid phase.

- Exploiting the 2.3 lt prototype at LNGS with a new internal detector configuration. Also this detector is under vacuum pumping (for about one month) and ready for filling.

In order to reduce the possible sources of water vapor, in both detectors the components have been minimized, avoiding the use of materials known to absorb high quantity of moisture (e.g PEEK).

6 Characterization of the optical properties of the WArP optical system

In order to properly match the Argon scintillation light (emission at 128 nm) with the phototube optical properties (glass transmission cut-off at 330 nm), shifting of wavelength is implemented by an efficient w.l.s. compound (TetraPhenilBoutadiene TPB). Moreover, to maximize the hit probability of the shifted photons on the PMT active area (photocatode) by reflection at the active volume boundaries, a highly reflecting layer is used to cover the internal surfaces of the detector.
The WArP optical system is therefore composed by a dielectric mirror (VM2000) layer, with nominal reflectance of the order of 99% in the visible region, coated by a film of TPB deposited by evaporation. All the internal surfaces of the inner detector and of the active veto (except the PMT windows) are thus covered by mirror+wls sheets, appropriately shaped and assembled.
The PMT glass windows are instead coated by an almost transparent film of TPB in a polystyrene matrix, deposited by spraying a solution of TPB and polistirene diluted in Toluene.

A complete characterization in the visible and Near-UV of the two types of layers (reflecting VM2000+TPB layer and transparent TPB+polistirene film) has been obtained by measuring Transmittance, Reflectance and Photoluminescence properties of samples of the two types. The measurements have been performed in collaboration with ENEA with appropriate instrumentation at the ENEA Frascati and Casaccia Laboratories. Photoluminescence (Fig. 12) and excitation photoluminescence (Fig. 13) measurements have been performed at different wavelength of excitation and readout in the range 250-450 nm. Direct Transmittance and Hemispheric (Transmittance and Reflectance) data have been obtained in the wavelength window 250-600 nm (Fig. 14).

In collaboration with the CERN Coatings, Chemistry and Surfaces group (TS-MME-CCS), other parallel studies have been pursued. In particular the effects of TPB hygroscopicity (Fig. 15) and mechanical stability to thermal cycles. Higroscopicity lowers the light yield but is recoverable through vacuum pumping. Mechanical stability is a critical issue. Evaporation is the most effective deposition method: the optimal thickness ranges between 200 and 300 μg/cm^2.

7 Conclusions

The year 2008 has been characterized by a very intense activity. Two main interconnected streams of activity have been pursued, namely (a) completion of the WarP-100 detector assembly and preparation for commissioning and (b) careful review based on a long series of experimental tests of the main aspects of the light collection system implemented with the WArP experimental technology.
The reasons that motivated the new series of experimental tests are related to the unexpected lack and instability of the light yield experienced with the WarP 2.3 lt prototype during various experimental runs performed within the ^{39}Ar-depleted Argon test program. The main parameters of the optical system (characteristics of the phototubes, wavelength shifting / reflective layer, LAr purity) have been checked in depth and found to be fully consistent with specifications. This current activity, carried on both in CERN and in LNGS, is presently concentrated on the evaluation of the effects of water outgassing.
On the other end, construction of the 100 liters detector is fully completed. Start of detector commissioning was done at the end of 2008.

References

[1] C. Rubbia *et al.*, A programme to search for WIMP particles in Liquid Argon at the LNGS, Letter of intent, Univ. of Pavia, July 1999.

[2] WArP Collaboration, Status Report of the current progress of the WArP Experiment, **LNGS-EXP 32/05** (2005);

[3] WArP Collaboration, First results from a dark matter search with liquid argon at 87 K in the Gran Sasso underground laboratory, Astropart. Phys. **28** (2008), 495.

[4] WArP Collaboration, Measurement of the specific activity of ^{39}Ar in natural argon, Nuclear Instruments and Methods in Physics Research A 574, 83 (2007).

[5] D. Acosta-Kane *et al.* (WArP Collaboration), Discovery of underground argon with low level of radioactive 39Ar and possible applications to WIMP Dark Matter detectors, arXiv:0712.0381v1 [astro-ph] (3 Dec 2007)

[6] WArP Collaboration, Effects of Nitrogen contamination in Liquid Argon, to be submitted to Nucl. Inst. and Meth. A

[7] WArP Collaboration, Oxygen contamination in liquid Argon: combined effects on ionization electron charge and scintillation light, to be submitted to Nucl.Inst. and Meth.A

Figure 4: Pictures of the 100 litres detector taken in October 2008.

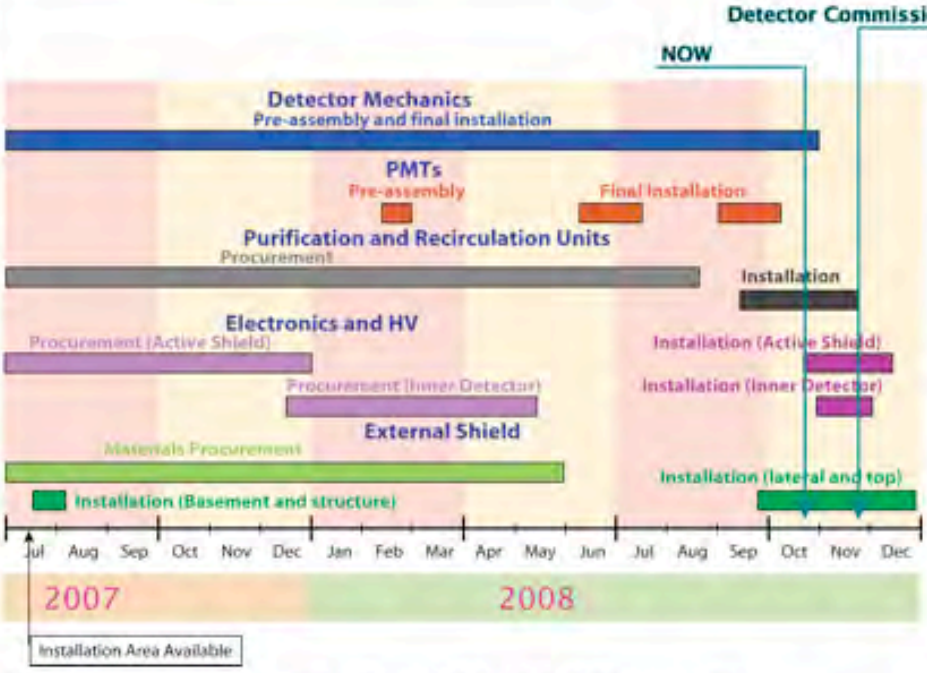

Figure 5: Time Schedule for detector completion and start of commissioning

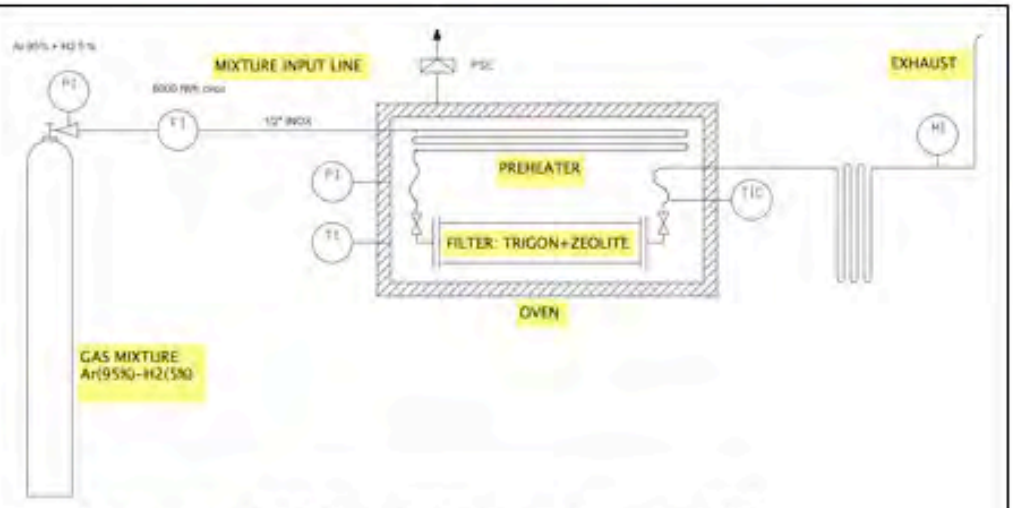

Figure 6: schematic layout of the filter activation/regeneration system at LNGS

Figure 7: Top: the activation oven (LNGS - Hall di Montaggio WarP Area). Middle: a (small) test cartridge (Trigon+Zeolite content) inside the oven for activation process bottom: Picture of the first stage VSA (Vacuum Swing Adsorption) purification unit as installed at the Reliant Dry Ice Plant in Bueyeros, New Mexico. Top center: the control system of the two-stage VSA purification system.

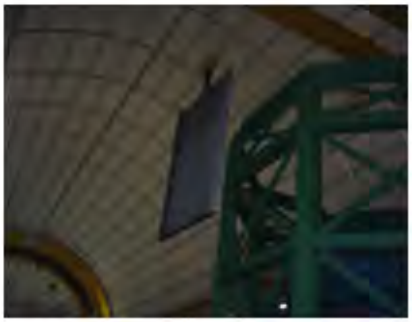

Figure 8: positioning of the first stainless steel box inside the WArP mechanical structure (October 08).

Table 1: Total neutron-induced background in the internal chamber (between 20 and 100 keV), taking into account anti-coincidence with the active veto (30 keV threshold). Rates do not include the further rejection which can be achieved by resolving multiple neutron interactions in the inner detector (see text).

Source	Rate of residual unvetoed events in the inner detector (20-100 keV) veto threshold=30 keV (events/year)
Dewar (12 tons)	0.22
PMTs of active veto	0.70
PMTs of internal detector	1.03
Steel in the chamber (20 kg)	0.05
Steel in the shielding (8 tons)	≤ 0.15
External neutrons	≈ 0.02
Neutrons from cosmic rays	1.1
Total	3.3

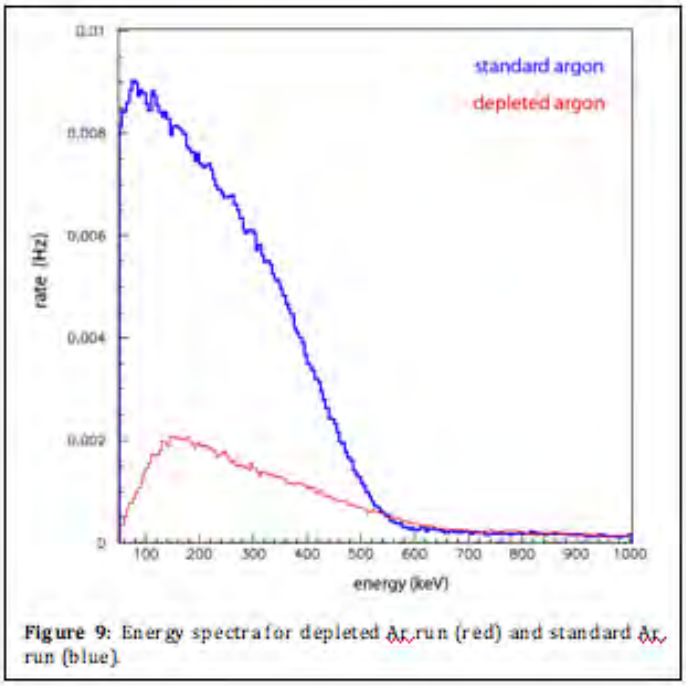

Figure 9: Energy spectra for depleted Ar run (red) and standard Ar run (blue).

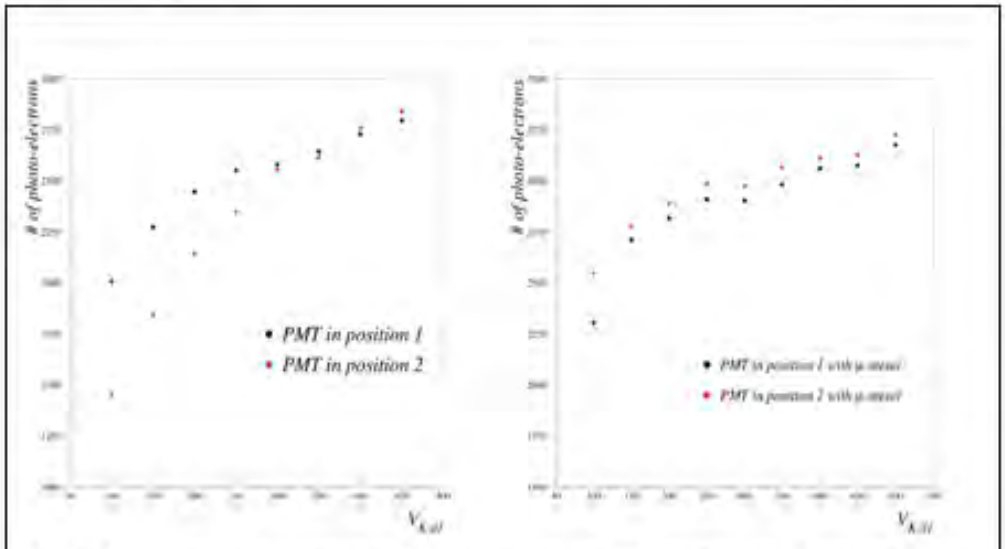

Figure 10 Left: Light Yield measured with the 0.7 μs set-μp (at different values of V_{G-d} (see text) and for the two orientations of the PMT that minimize (black dots) and maximize (red dots) the effect of the Earth magnetic field on the electron collection efficiency on the first dynode of PMT. Right: same as figure 1, left with a μ-metal shield layer placed around the chamber.

Table 2: Rates for the depleted Ar run and for Standard Ar run

Run	Total Rate in 100-600 keV, [Hz]	Estimated ^{39}Ar Rate in 100-600 keV, [Hz]	Estimate residual* background in 100-600 keV, [Hz]
Standard Argon	2.4 ± 0.1	1.9 ± 0.2	0.55 ± 0.06
Depleted Argon	0.6 ± 0.1	//	//

Table 3 *Main results of the light yield test performed with the 0.7 lt set-up.*

Deposition technique	Optimal density (μg/cm²)	Light Yield (phel/KeV)
Spray TPB	600	2.2
Spray TPB+polystyrene		1.5
Evaporation	400-750	2.8

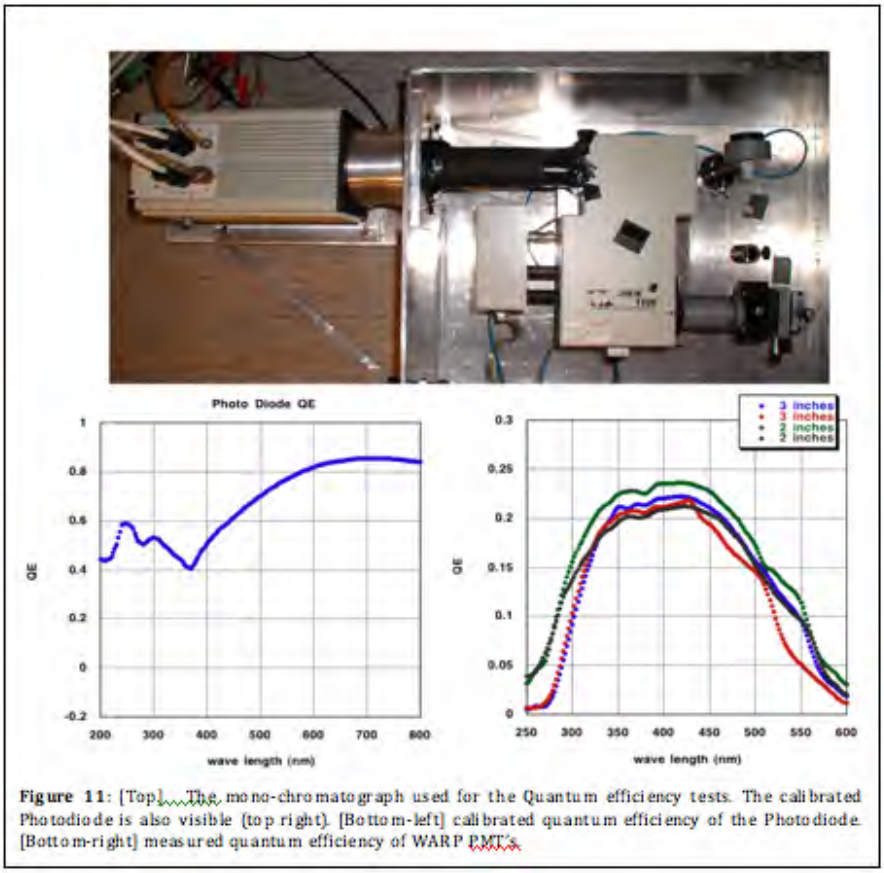

Figure 11: [Top] The mono-chromatograph used for the Quantum efficiency tests. The calibrated Photodiode is also visible (top right). [Bottom-left] calibrated quantum efficiency of the Photodiode. [Bottom-right] measured quantum efficiency of WARP PMT's.

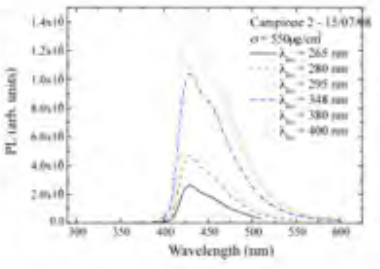

Figure 12: Photoluminescence Excitation spectra TPB over VM2000 obtained with several wavelength of readou9t

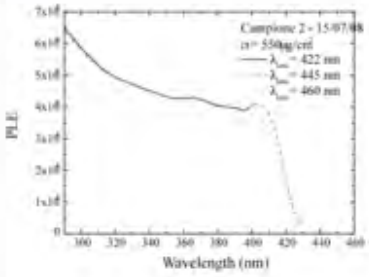

Figure 13 Photoluminescence spectra of TPB over VM2000 obtained with several wavelength of excitation

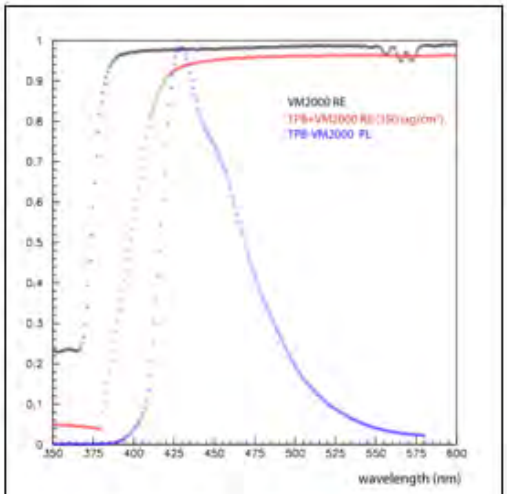

Figure 14: Characterization of the WArP Optical system - Hemispheric reflectance of TPB over VM2000 (and comparison with naked VM2000). The TPB-VM2000 photoluminescence spectrum is also plotted.

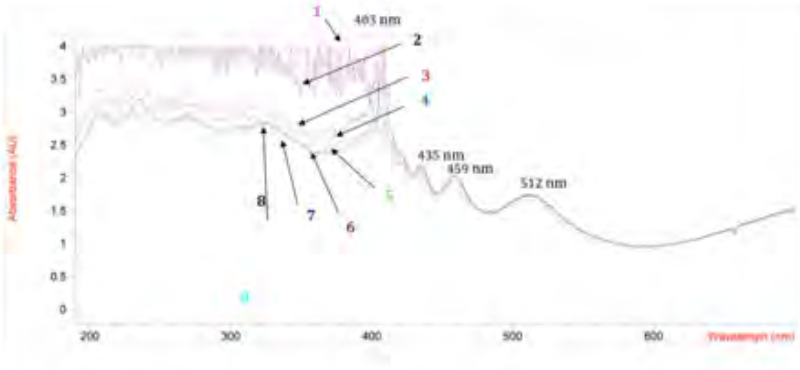

TPB run 3

1	pos 1 (quartz/TPB)
2	pos 2 (TPB/quartz)
3	pos 2 after 30 minutes
4	pos 2 after 50 minutes
5	pos 2 after 100 minutes
6	pos 2 after 165 minutes
7	pos 2 after 225 minutes
8	pos 2 after 285 minutes
0	reference quartz cell

Figure 15: Absorbance of TPB as a function of wavelength. The efficiency decreases with time is due to water absorption. Vacuum pumping (or exposure to flow of dry atmosphere) ensures full recovery.

The XENON100 Dark Matter Experiment

Elena Aprile[a] *, Katsushi Arisaka [g], Francesco Arneodo[c], Ali Askin[b], Laura Baudis[b], Ethan Brown [g], Joao Cardoso[e], David Cline [g], Luis Coelho[e], Serena Fattori[c] [f], Alfredo Ferella[b], Karl-Ludwig Giboni[a], Alexander Kish[b], Jose A. Matias Lopes[e], Yuan Mei[d], Antonio Jesus Melgarejo[a], Kaixuan Ni[a], Uwe Oberlack[d], Emilija Pantic [g], Guillaume Plante[a], Bin Choi[a], Kyungeun Elizabeth Lim[a], Roberto Santorelli[b], Joaquim Santos[e], Marc Schumann[d], Peter Shagin[d], Artin Teymourian [g], Eirini Tziaferi[b], Hanguo Wang [g], Taehyun Yoon[a]

[a] Department of Physics, Columbia University, New York, NY 10027, USA
[b] Physics Department, University of Zurich, Switzerland
[c] INFN, Laboratori Nazionali del Gran Sasso, Assergi, 67100, Italy
[d] Department of Physics and Astronomy, Rice University, Houston, TX 77251, USA
[e] Department of Physics, University of Coimbra, R. Larga, 3004-516, Coimbra, Portugal
[f] Dipartimento di Fisica, Università de L'Aquila, Italy
[g] University of California, Los Angeles

* Spokesperson

Abstract

The XENON100 experiment aims to detect cold dark matter particles via their elastic collisions with xenon nuclei. An ultra-low background, two-phase time projection chamber with a total of 170 kg of xenon (65 kg in the target region and 105 kg in the active shield) has been installed in 2008 at the Gran Sasso Underground Laboratory (interferometer tunnel) and is currently in commissioning phase. We review the design and performance of the detector and its associated systems, present status, preliminary calibration results, background prediction and projected sensitivity.

1 Introduction

Numerous observations (e.g. [1]) point to the existence of a non-luminous, non-baryonic component of our universe known as dark matter in the form of Weakly Interacting Massive Particles, or WIMPs. Direct detection of WIMPs is being pursued by several experiments placed in different underground laboratories around the world. In recent years, experiments based on noble liquids have advanced at a much faster rate than the more established cryogenic experiments. In particular, the XENON10 experiment, with its successful performance in a very fast time, has brought liquid xenon (LXe) detectors to the forefront of the field [2, 3].

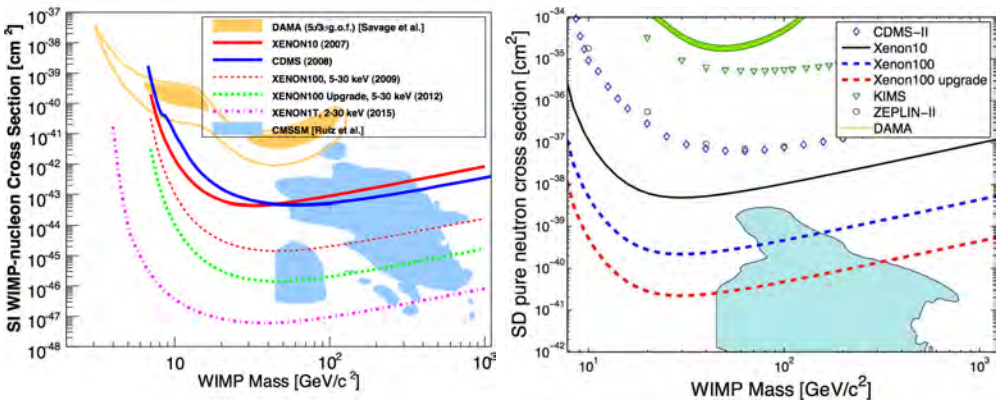

Figure 1: Spin-independent (left) and spin-dependent pure neutron (right) WIMP-nucleon cross sections as a function of WIMP mass, probed by different stages of the XENON program. On the left, the low mass WIMP region allowed by DAMA [4] is from [5], and the current most stringent limits from XENON10 [2] and CDMS [6] are shown as solid curves. Blue shaded regions are from theoretical models [7].

XENON10 was the first prototype developed within the XENON dark matter program to prove the concept of a two-phase xenon time projection chamber (XeTPC) for dark matter search. The key technologies and performance characteristics relevant for the realization of a larger (ton-scale) XENON experiment are being addressed with the current detector, XENON100, and its upgrade. We will complete the commissioning of XENON100 in early 2009 and will accumulate data for a dark matter search throughout the year. With a raw exposure of 6000 kg-days, free of background events, XENON100 will reach $\sigma \sim 2 \times 10^{-45}$ cm^2 at 100 GeV, more than a factor of 20 better than current limits [2, 6], by the end of 2009. An upgraded XENON100 will further improve the sensitivity by another order of magnitude by 2012 (Figure 1).

2 The XENON100 Detector

The XENON100 detector uses the same principle of operation and many design features successfully tested in the XENON10 prototype [8]. It is a position-sensitive XeTPC, with

the sensitive LXe volume viewed by two arrays of photomultiplier tubes (PMTs), to detect simultaneously the primary scintillation signal (S1) and the ionization signal via the proportional scintillation mechanism (S2). The sensitive target can be "fiducialized" to keep only the inner core free of background. In addition, the high ionization density of nuclear recoils in LXe leads to an enhancement in S1 and reduction in S2, compared to electronic interactions. The S2/S1 ratio therefore discriminates WIMP nuclear recoils from γ and β backgrounds with an efficiency of 99.5–99.9%, as demonstrated with XENON10 [2].

A schematic drawing of the XENON100 detector and a photo are shown in Fig.2 (right). The active volume contains 65 kg of LXe and is instrumented with 178 PMTs in two arrays, 98 in the gas and 80 in the liquid. All PMTs are Hamamatsu R8520-06-Al 1" square, optimized for Xe 178 nm light and selected for low radioactivity. The quantum efficiency (QE) of these tubes was also recently improved from $\sim 24\%$ to $\sim 35\%$.

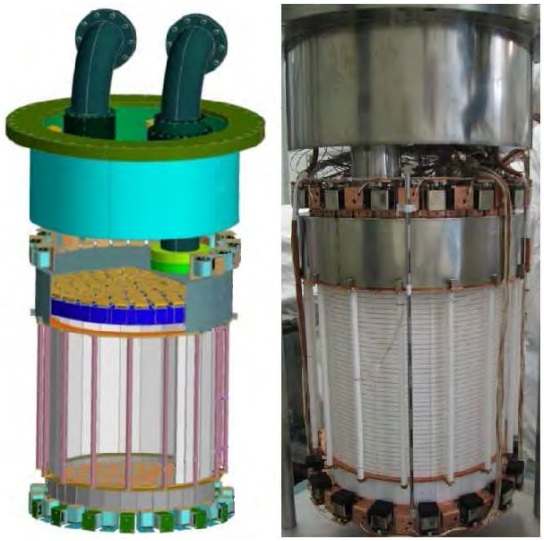

Figure 2: Drawing and a photo of the XENON100 TPC.

The active target is enclosed in a PTFE cylinder of 15 cm radius and 30 cm height. This PTFE cylinder reflects scintillation light with high efficiency [9], and optically separates the LXe target from the surrounding LXe which is necessary to separate the TPC with its electric field from the walls of the vessel. 64 PMTs turn this outer LXe volume into an active LXe veto, with a total mass of 105 kg, including LXe layers above the top and below the bottom PMT arrays. Custom-made, low radioactivity, high voltage feedthroughs are used to bias the cathode and the anode, creating 1 kV/cm drift field across the 30 cm LXe gap, and 13 kV/cm field in the 5 mm gas proportional scintillation region. The LXe level is held stable within the stack of meshes, about 3 mm below the anode. The top PMT array is mounted within the bell, a few centimeters above the meshes.

The TPC structure, supported by the bell, is enclosed in a double walled vessel made of SS 316Ti selected for its low activity, especially in ^{60}Co. All additional instrumentation was removed from the detector vessels as much as possible, and mounted outside the lead/polyethylene shield, in particular all electrical feed-throughs and the cryocooler. This reduced the amount of radioactivity within the shield significantly. The cooling system is based on a 170 W pulse tube refrigerator (PTR), originally developed for the MEG experiment [10]. The PTR is used to liquefy Xe and to maintain the liquid temperature during operation.

3 Xe Gas Handling, Purification and Kr Removal System

The XENON100 detector requires a total of 170 kg of Xe to fill the target and the active veto. The gas is stored in four aluminum cylinders connected by high pressure valves, that can be cooled with LN_2 during recovery from the detector.

To reduce electronegative impurities in commercial Xe well below 1 part per billion (ppb) O_2 equivalent that is required for long electron lifetime and long VUV photons absorption length, we are using the system developed for XENON10, based on continuous Xe gas circulation with purification through a high temperature metal getter (SAES). The $\sim$2 ms electron lifetime demonstrated with XENON10 data [8], corresponds to four meters drift length, much longer than the 30 cm maximum drift in XENON100.

LXe, as a condensed noble gas, is readily purifiable for most radioactive impurities. The one notable exception is ^{85}Kr, present in commercial Xe gas at the ppm level. Beta decays of ^{85}Kr (687 keV end point, 10.76 years of half life) presents a serious background for a dark matter search. The gas used in XENON100 was processed by the Spectra Gases Company to reduce the Kr concentration to $\sim$5 ppb, using their cryogenic distillation plant. This level has been achieved in XENON10 [8] with gas also processed by the same company, and verified by positive identification of the beta-gamma coincidences with 1.46 μs time difference from decays ^{85}Kr(β) $\rightarrow^{85m}$Rb(γ) $\rightarrow^{85}$Rb at a 0.454% branching ratio. During the first background run with XENON100, we identified these "delayed-coincidence" events and inferred a Kr/Xe level of 7 ppb, consistent with the value of Spectra Gases.

Figure 3: Picture of the Kr distillation column in commissioning.

In order to reduce the ^{85}Kr level to <50 ppt, required by the XENON100 sensitivity goal (50 ppt of ^{85}Kr contribute a rate of 10^{-3} evts/kg/keV/day), we have purchased a small-scale cryogenic distillation column made by Taiyo-Nippon Sanso. The column has been commissioned at LNGS and has been used to purify part of the XENON100 gas. It is 3 m tall and is designed to deliver a factor of 1000 reduction in Kr at a purification speed of 0.6 kg/hour.

4 Electronics and Data Acquisition

The XENON100 data acquisition (DAQ) system generates the trigger for the TPC, digitizes the waveforms of the 242 photomultipliers, and stores the data in an efficient way. It provides additional information on the measurement, such as timing information and

DAQ live time. The PMT signals are first amplified by a factor 10 (Phillips 776 amplifiers), and then digitized by CAEN V1724 Flash ADCs with 10 ns sampling period, 14 bit resolution, and 40 MHz bandwidth. We have implemented an algorithm on the on-board FPGA of the ADC channels to digitizes the waveform only within an adjustable time window around a signal exceeding an adjustable threshold. This reduces the event size by 90–95% and allows full acquisition at a speed up to 50 Hz, sufficient for taking calibration data and much larger than the total background rate in the detector (∼1 Hz). The complete XENON100 DAQ system is installed underground and is used for measurements since several months.

5 XENON100 Detector: Initial Results

The S1 and S2 response of the XENON100 TPC is monitored with external gamma sources (^{57}Co, ^{137}Cs, ^{60}Co and ^{228}Th). We are investigating a new calibration source, ^{83m}Kr, which is a decay product of ^{83}Rb, has a short half-life of 1.83 h and decays via a cascade of 32 and 9.4 keV transitions.

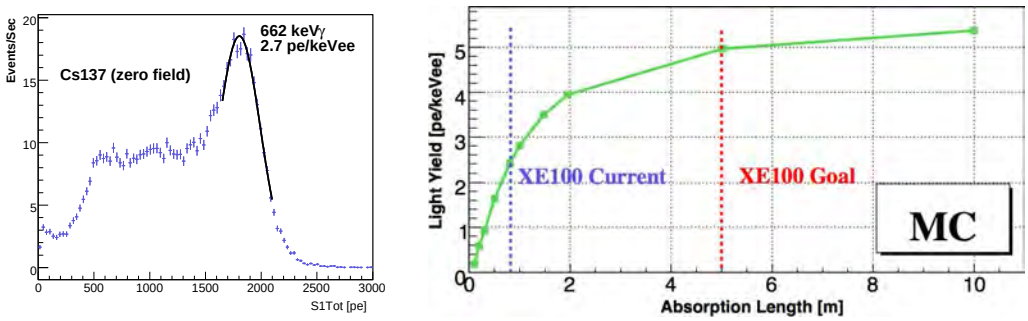

Figure 4: (Left) The measured scintillation light spectrum based on S1 signals from ^{137}Cs. (Right) Current and projected goal of the S1 light yield by increasing the LXe purity in XENON100.

^{83m}Kr will be introduced in the TPC allowing us to carry out S1&S2 calibrations uniformly throughout the volume. The neutron calibration will be performed in the middle of the dark matter search run to verify the TPC's response to nuclear recoils (NRs). Simulation studies show that a one day calibration with a 220 n/s AmBe source will produce more than 1000 NR events/kg in the central 50 kg target in the WIMP search energy window.

Figure 4 shows the current S1 light spectrum of ^{137}Cs 662 keV gamma-rays, measured in XENON100, showing a light yield of 2.7 pe/keVee (zero field), limited by the presence of impurities, mostly H_2O. By comparing with the MC studies of the light collection efficiency, the current light yield implies a 1 m absorption length of UV photons in LXe. With continuous circulation and purification of the Xe through the high temperature getter, we expect to achieve an S1 light yield of at least 5 pe/keVee (zero field) at a 5 m absorption length, which was achieved in XENON10 [8]. Such a light yield gives an average S1 signal of more than 3 pe for 5 keV nuclear recoils, based on a recent

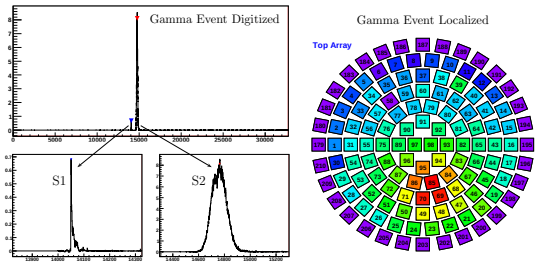

Figure 5: (Left) A typical event waveform from XENON100, showing both S1 and S2 signals. (Right) S2 hit pattern on the top PMT array from the same event, based on reconstructed XY positions.

measurement of the relative scintillation efficiency L_{eff} [11], allowing ∼100% detection efficiency for NRs as low as 5 keV.

Two-phase operation of the TPC has also started. Figure 5 (left) is a waveform from the summed signals, showing clear S1 and S2 signals from a single scatter electron recoil (ER) event. Calibration data from external gamma ray sources (^{137}Cs) are continuously collected to monitor the electron lifetime in the LXe. The top array of the PMTs was designed to optimize the radial position resolution to allow efficient fiducial volume cut for background reduction. Figure 5 (right) shows a typical S2 hit pattern on the top PMT array from the same gamma ray event. From the S2 hit pattern, XY positions can be reconstructed with a radial position resolution of about 2 mm from a few keVee ER events, thanks to the fine granularity of the 1" PMTs.

The first background measurement in XENON100 has been performed with the S1 signal. The measured spectrum, shown in Figure 6, is consistent with Monte Carlo predictions.

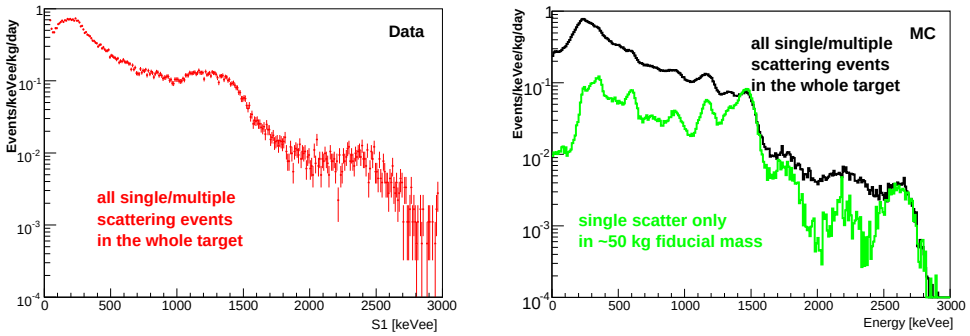

Figure 6: Measured (left) and MC predicted (right) background spectra in XENON100.

6 Plan for an upgraded XENON100 detector

LXe is an excellent medium to shield the fiducial volume from penetrating gamma-rays from radioactivities like U/Th, Co, and K, hence one can rely on the position sensitivity of a TPC to cut the outer volume and achieve a background free inner target. However, LXe is expensive and larger TPC's become increasingly complex: increased drift length requires higher voltage to be brought into the detector and shielded from the photosensors; purification becomes more demanding; event rates in the TPC need to be reduced to accomodate longer drift times, etc. Moreover, self-shielding is less effective for neutrons. It is therefore more cost-effective to achieve a high ratio of *fiducial/total* volume, for a given sensitivity goal, by pushing the radio-purity of new photosensors, such as QUPIDs (Quartz Photon Intensifying Detectors), proposed by K. Arisaka and H. Wang in spring 2007. After a year and half of intensive joint R&D by UCLA and Hamamatsu Photonics Co., it is now a reality.

The upgraded XENON100 detector will replace the current bottom R8520 PMT array with 19 QUPIDs. We will simultaneously remove most of the activity from the stainless steel (SS) cryostat by replacing it with one made with low background oxygen free copper (OFHC). As the activity of the top PMTs will be the dominant background, we double the drift length from current 30 cm to 60 cm, enabling us to achieve the background goal by cutting events from the top. The activity from the top cryostat assembly, made of the lowest activity SS we have identified so far, will add negligible background compared to the top PMTs.

The upgraded XENON100 TPC will not only feature greatly reduced background but will also be a stepping stone for a future ton-scale XeTPC: it will validate the new QUPID technology, and also test HV handling and long drift in LXe, both essential for a XENON1T. At the same time, the current shield needs to be upgraded by adding 20 cm of polyethylene, mounted to the existing steel structure, for additional neutron moderation. Outside of this moderator, we will place a muon veto to tag events caused by high energy neutrons from muon spallation in the shield and other passive materials. The muon veto is made of 60 panels of polished Bicron BC408 plastic scintillator, optically coupled to two Hamamatsu 5946 PMTs, one on each side. The muon veto will cover all sides of the shield except the bottom, with an estimated efficiency at about 98%. A cross-sectional view of the proposed detector mounted inside the upgraded shield is shown in figure 7.

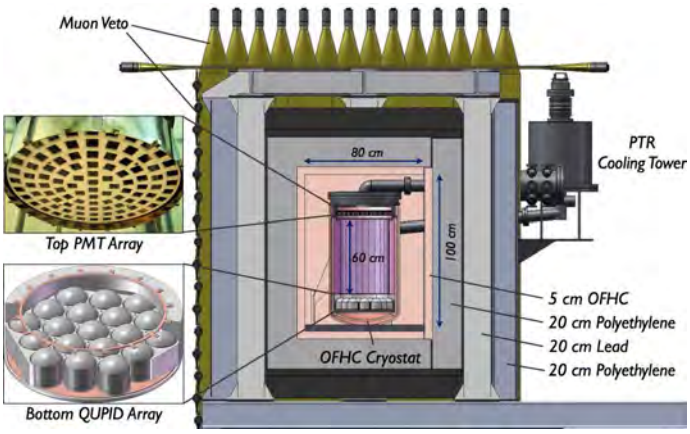

Figure 7: The upgraded XENON100 with QUPIDs on the bottom and OFHC cryostat in the upgraded shield.

7 List of Publications during 2008

- J. Angle, et al. (XENON Collaboration), *First Results from the XENON10 Dark Matter Experiment at the Gran Sasso National Laboratory*, Phys. Rev. Lett. 100, 021303 (2008), also at astro-ph/0706.0039
- J. Angle *et al.*, "Limits on spin-dependent WIMP-nucleon cross-sections from the XENON10 experiment," Phys. Rev. Lett. **101** (2008) 091301 [arXiv:0805.2939 [astro-ph]].
- E. Aprile, L. Baudis, B. Choi, K.L. Giboni, K.E. Lim, A. Manalaysay, M.E. Monzani, G. Plante, R. Santorelli, M. Yamashita *New Measurement of the Relative Scintillation Efficiency of Xenon Nuclear Recoils Below 10 keV* Oct 2008. 8pp. e-Print: arXiv:0810.0274 [astro-ph]
- P. Sorensen et al *The scintillation and ionization yield of liquid xenon for nuclear recoils.* Jul 2008. 8pp. Temporary entry e-Print: arXiv:0807.0459 [astro-ph]
- P. Sorensen *et al.*, "The scintillation and ionization yield of liquid xenon for nuclear arXiv:0807.0459 [astro-ph].
- *Status and Sensitivity Projections for the XENON100 Dark Matter Experiment* E. Aprile and L. Baudis IDM 2008 Proceedings

References

[1] D. N. Spergel *et al.* [WMAP Collaboration], Astrophys. J. Suppl. **170**, 377 (2007).

[2] J. Angle *et al.* [XENON Collaboration], Phys. Rev. Lett. **100**, 021303 (2008).

[3] J. Angle *et al.* [XENON Collaboration], Phys. Rev. Lett. **101**, 091301 (2008).

[4] R. Bernabei *et al.* [DAMA Collaboration], Eur. Phys. J. C **56**, 333 (2008) [arXiv:0804.2741 [astro-ph]].

[5] C. Savage *et al.*, arXiv:0808.3607 [astro-ph].

[6] Z. Ahmed *et al.* [CDMS Collaboration], arXiv:0802.3530 [astro-ph].

[7] L. Roszkowski, R. Ruiz de Austri, and R. Trotta, JHEP **07** (2007) 075, [arXiv:0705.2012 [hep-ph]].

[8] E. Aprile *et al.* [XENON Collaboration], "The XENON10 Dark Matter Search Experiment", in preparation for Phys. Rev. D.

[9] M. Yamashita *et al.*, NIM A **535**, 692 (2004).

[10] T. Haruyama *et al.*, in: *Cryocoolers 13*, Springer, New York, 689 (2005).

[11] E. Aprile *et al.*, arXiv:0810.0274 [astro-ph].

[12] Wilson *et al*, Phys. Lett. B **645**, 153 (2007); M. Carson *et al*, Astrop. Physics **21**, 667 (2004); R. Lemrani *et al*, NIM A**560**, 454 (2006); V. Tomasello *et al*, doi:10.1016/j.physletb.2003.10.071.

[13] D. Mei and A. Hime, Phys. Rev. D **73**, 053004 (2006).

[14] H.-C. Cheng, J.L. Feng and K.T. Matchev, Phys.Rev.Lett. **89** (2002) 211301.

[15] S. Arrenberg, L. Baudis, K. Kong, K.T. Matchev, J. Yoo, Phys. Rev. D78, 056002 (2008)

ERMES
Measurements of environmental radioactivity

Matthias Laubenstein[a], Wolfango Plastino[b,c], Francesco Bella[b], Christian Del Pinto[d], Gaetano De Luca[e]

[a] I.N.F.N.-Laboratori Nazionali del Gran Sasso,
S.S. 17/bis, km 18+910, I-67010 Assergi (AQ) - Italy
[b] Dipartimento di Fisica, Università degli Studi Roma Tre,
Via della Vasca Navale, 84, I-00146 Rome - Italy
[c] I.N.F.N., Sezione Roma Tre,
Via della Vasca Navale, 84, I-00146 Rome - Italy
[d] Protezione Civile Molise,
Centro Funzionale,
I-86020 Campochiaro (CB) - Italy
[e] Dipartimento della Protezione Civile,
Via Vitorchiano, 2,
I-00189 - Roma - Italy

Abstract

In the framework of the ERMES (Environmental Radioactivity Monitoring for Earth Sciences) research project environmental samples from Lazio and Molise were analyzed by means of gamma spectroscopy in the Low Background Laboratory of the Laboratori Nazionali del Gran Sasso (LNGS). A summary of these measurements is presented.

1 Introduction

The ERMES research project includes radioactive analyses of environmental samples like sea water, soils, sediments and volcanic material ([1], [2]). In its framework in 2008 a series of samples has been measured in the Low Background Laboratory (LBL), situated in the underground labs of the LNGS. Sixty-four samples were provided by the Università degli Studi Roma Tre, and 205 samples were delivered by the Civil Protection of Molise in collaboration with, again, the Università degli Studi Roma Tre. The latter set of samples

was measured in order to assess a map showing the natural radioactivity levels in the Regione Molise.

In the LBL are currently installed ten high purity germanium (HPGe) detectors. The laboratory is dedicated principally to material screening measurements for the underground research projects installed in the LNGS. Since those experiments must have very low intrinsic radioactive backgrounds in order to detect the extremely weak signals they are searching for, the intrinsic concentration of natural radioactivity in the materials used for the experimental set-up has to be extremely low. The HPGe detectors and their shielding used for the material screening have been designed and built especially for the purpose to detect very small amounts of radioactivity (in the order of 10^{-10} g/g for uranium and thorium, and 10^{-7} g/g for potassium), and if not detecting it, to put at least very low limits of detection. An extensive description can be found in [3], [4] and [5].

Nevertheless, these specialized detectors can also be used to measure in background-free conditions natural radioactivity, which is occurring usually in concentrations of approximately 10^{-6} g/g in uranium and thorium and 10^{-2} g/g in potassium, which is four to five orders of magnitude higher than the sensitivity of those detectors.

2 Sample preparation and measurement procedure

2.1 Samples of the University of Roma Tre

Sixty-four samples have been measured all coming from the same region, i.e. the Solforata area near Rome (Italy). The samples have been taken in various sites in the area. An in-situ measurement of the natural radioactivity has been performed during the sample taking by means of a hand held NaI detector (ORTEC®). The interpretation of the data obtained is currently ongoing.

2.2 Samples of the Civil Protection Molise

In order to do the very first map of a complete Italian "Regione" concerning natural radioactivity (uranium, potassium and thorium) a large number of samples (205 samples) have been taken throughout the Regione Molise. The samples have been measured and the resulting data is currently under examination.

2.3 The sample preparation

The sample mass was between 400 g and 1000 g for the Solforata area and between 150 g and 500 g for the Molise. The samples have not been treated at all, but have been measured as is. They were filled into a Marinelli beaker and measured on the HPGe detector. In order to increase the throughput for such a large amount of samples the measurement time was determined such, that the smallest peak to be used in the analysis had about 100 counts. Thus the measurement time was on the order of 30 minutes to 2 hours for the Solforata samples, and 30 minutes to 5 hours for the Molise samples.

After the measurement the aliquots of the samples have been dried at 80 ^{o}C for 24 hours, and the results for the specific activities have been corrected to dry weight.

2.4 Measurement and data analysis procedures

2.4.1 Measurement geometry

The samples are placed in a Marinelli beaker around the detector. Thus the innermost Cu insert of the detector shielding had to be taken out. This reduction of the shielding did not deteriorate the performance of the detector in a significant way, as the measurement times were rather short. In fact, the removal of the Cu insert resulted only in a slight increase of the continuous background below 1000 keV, which is due to the bremsstrahlung of ^{210}Pb in the lead shield.

2.4.2 Data analysis

The efficiency determination of each measurement was done via software using the Monte-Carlo technique. The computer code written is using the GEANT 4 software package [6] and was validated comparing its results with measurements performed using certified extended radioactive sources with different geometry and in different distances from the detector endcap. The spectrum analysis is done using a thoroughly tested fitting routine developed at the University of Milano. The peak shape is fit with a Gaussian peak and linear background, having the possibility to perform also the unfolding of up to 10 peaks. In case of low counting rates, where statistics is poor or where actually no net activity can be seen, the analysis is done manually summing simply the number of counts per energy channel the regions of interest (ROI) of peak and background, choosing the appropriate width of the ROI to 2.5 times the full width of half the maximum (FWHM) of the full energy peak, which is determined by calibration with radioactive standards.

The overall uncertainty budget for the gamma spectroscopy measurements is reported in table 1. The given total uncertainty is referring to the analysis of one full energy peak (e.g. ^{40}K). In case the radionuclide analyzed has more than one gamma energy emission the single results of each photo peak can be combined statistically by averaging, which of course decreases the uncertainty for the combined result somewhat (e.g. ^{228}Ra).

Table 1: *Uncertainty budget for the gamma spectrometric measurements (relative uncertainties).*

counting	1.5%
background	1.5%
efficiency	10.0%
total	10.2%

3 Discussion

For each sample series the radioactivity concentration of thorium, uranium, potassium and cesium has been analyzed. The uncertainties stated are the combined standard

uncertainty [9]. The data was compared to the decision thresholds, which were calculated according to [10] using $\alpha = 0.5$, and $b = 2.5$ FWHM.

3.1 The radionuclides

3.1.1 ^{232}Th-series

The nuclides analyzed in this naturally occurring decay chain are the gamma emitting nuclides ^{228}Ac, ^{212}Bi and ^{208}Tl. The results obtained from these nuclides give also the possibility to determine whether secular equilibrium is present in the decay chain (from ^{228}Ra on) or not.

3.1.2 ^{238}U-series

The nuclides assessed in this naturally occurring decay chain are the gamma emitting nuclides ^{234m}Pa, ^{226}Ra, ^{214}Pb and ^{214}Bi. These nuclides give also the possibility to determine whether secular equilibrium is present between ^{238}U and ^{226}Ra, which due to the long half-life of the latter one ($t_{1/2} = 1600$ a [7]) could show some disequilibrium, given the different chemical behavior of the elements uranium and radium, which could for example cause depletion of one nuclide with respect to the other.

3.1.3 ^{235}U-series

The nuclides analyzed in this naturally occurring decay chain are the gamma emitting nuclide ^{235}U. The contribution in the 185.71 keV gamma ray of ^{235}U from the contribution of ^{226}Ra with an emission at 186.2 keV was disentangled subtracting simply the ^{226}Ra content obtained via its daughter products.

3.1.4 Potassium

The concentration of this element is determined by measuring its primordial radioactive isotope ^{40}K. This nuclide emits with 10.67 % probability during its decay also gamma rays with an energy of 1460.83 keV. The natural abundance of ^{40}K is (1.17 ± 0.01) % [8].

3.1.5 ^{137}Cs

The concentration of this radionuclide ($t_{1/2} = 30.17$ a [7]) is determined by its emission of gamma-rays with an energy of 661.67 keV. It is produced solely by human activity (release by nuclear power plants and reprocessing plants, nuclear bomb test fall-out).

3.2 Measurement results

3.2.1 Results of the samples

As the tables containing the measurement results would be too lengthy, the authors invite to check for the data in the publications, which will be available soon. Only naturally occurring radionuclides could be positively identified, a part from occasionally occurring

^{137}Cs. Possible loss of ^{222}Rn-daughters due to diffusion out of the sample containers was excluded at a 2% level. True coincidence summing effects occurring in the ^{238}U- and ^{232}Th-series were estimated to be less than 2%, well below the overall uncertainty of the measurement.

4 Summary

In this report of the ERMES research project a summary of the gamma spectrometry measurements performed in 2008 has been presented. During data analysis no other radionuclide than the ones reported was identified. Of course, this measurement technique can only provide information about gamma emitting radionuclides. A direct determination of uranium, thorium and potassium as a complementary measurement (e.g. by means of ICP-MS) has not yet been performed. As for now only a short descriptive summary was presented. Detailed analysis and interpretation of the data is under way.

Acknowledgements

The authors want to thank prof. Eugenio Coccia for his kind collaboration and Alessia Giampaoli, Alessandra Carlotta Re, Alba Formicola, Massimo Orsini, and Massimiliano De Deo of the LNGS for their extraordinarily useful and precious assistance.

Moreover, the authors greatly acknowledge the collaboration with the Protezione Civile Molise, and especially, with Dr. Giuseppe Antonio Giarrusso.

References

[1] Plastino, W. et al., ERMES, Annual Report 2003 - Laboratori Nazionali del Gran Sasso, LNGS/EXP-01/04 (2004) p. 203.

[2] Laubenstein, M. et al., ERMES, Annual Report 2005 - Laboratori Nazionali del Gran Sasso, LNGS/EXP-03/06 (2006) p. 167.

[3] Arpesella, C., A low background counting facility at Laboratori Nazionali del Gran Sasso, Appl. Rad. Isot., 47 (1996) p. 991.

[4] BOREXINO collaboration, Measurements of extremely low radioactivity levels in BOREXINO, Astropart. Phys. 18 (2002), p. 1

[5] Laubenstein, M. et al., Underground measurements of radioactivity, Appl. Rad. and Isot. 61, 2-3 (2004), p. 167

[6] Geant4 Collaboration, GEANT4: A Simulation Toolkit, Nucl. Instr. Meth. A 506 (2003), 250-303

[7] Chu, S.Y.F., Ekström L.P. and Firestone R.B., WWW Table of Radioactive Isotopes, database version 1999-02-28 from URL http://nucleardata.nuclear.lu.se/nucleardata/toi/

[8] Commission on Atomic Weights and Isotopic Abundances, Report for the International Union of Pure and Applied Chemistry, Isotopic Composition of the Elements 1989, Pure and Applied Chemistry **70** (1998).

[9] ISO/IEC/OIML/BIPM, Guide to the expression of uncertainty in measurement, (1st corrected edition), International Standard Organisation, Geneva, Switzerland (1995).

[10] ISO 11929-3, Determination of the detection limit and decision threshold for ionising radiation measurements Part 3, International Standards Organisation, Geneva, Switzerland, (2000).

GIGS. The Interferometric Station at LNGS

Antonella Amoruso[a,b], Luca Crescentini[a,b,c]

[a] Dip.to di Fisica Univ. di Salerno, Salerno - Italy
[b] INFN - Gruppo collegato di Salerno, Salerno - Italy
[c] Spokeperson

Abstract

1 Introduction

Since several years two geodetic extensometers are working at LNGS. Both instruments are unequal-arm Michelson interferometers, using a 90-m long measurement arm and a <40-cm long reference arm, and sharing the same stabilized HeNe laser source. Nominal sensitivity is about 3×10^{12} and, in the present configuration, recording rate is 600Hz. The two interferometers are monitoring extension along two orthogonal directions, striking N66E (BC interferometer) and N24W (BA interferometer).

Few years ago, we performed ([5], [4]) preliminary studies of the Free Core Nutation (FCN), a rotational eigenmode which appears in addition to the well-known Chandler period ($\approx$ 435 days). This mode is due to the pressure coupling between the liquid core and the solid mantle which acts as a restoring force. The FCN causes a resonance on the Earth response to tidal forcing whose period T_{FCR} (situated in the diurnal tidal band) and quality factor Q depend on the core-mantle boundary (CMB) ellipticity, the Earth's inelasticity, and the viscomagnetic coupling of the CMB. The unusual depth of the Gran Sasso station largely reduces contamination caused by environmental effects in the diurnal band of recorded tides. Preliminary analyses were performed using different packages (ETERNA 3.40, [15]; VAV, [13]; ACS, [3]) neglecting environmental effects. Ocean loading effects (expected small) were computed using the GOTIC2 ([9]) package, Earth models 1066A and Gutenberg-Bullen and global ocean models NAO.99b and CSR4.0. We obtained values of the FCR period consistent with but slightly lower than those published by others, and a more realistic quality factor. The Mediterranean Sea, even if characterized by liquid tides of small amplitude with respect to open oceans, gives the largest contribution to ocean loading at Gran Sasso. Global ocean models cover the Mediterranean Sea poorly and often discard the Adriatic Sea, thus claiming for the use of local tidal models. In 2007 we computed ocean loading effects using SPLOTL ([2]), which includes CSR3.0,

FES95.2, GOT00.2, and TPX06.2 global ocean models. For the Mediterranean sea, we replaced the global models with the local one developed at the Oregon State University. Unfortunately, it included only four tidal components, i. e. two diurnal (O_1 and K_1) and two semidiurnal (M_2 and S_2) ones. More recently, we have obtained an improved Mediterranean model at 1/30 degree resolution from the Oregon State University. Bathymetry source is GEBCO 1min bathymetry. The model assimilates 531 cycles of Topex + Jason and 114 cycles of Topex2 (interlaced between old Topex tracks) and includes eight constituents (M_2, S_2, N_2, K_2, K_1, O_1, P_1, and Q_1).

Although the interferometers measure strain directly, local distortions, such as cavity effects due to tunnel installation, surface topography, and inhomogeneities in elastic constants, can bias strain measurement significantly, even if do not add stochastic noise. Siting effects can also produce coupling among the different strain components, so that measured strain is not equal to the large-scale Earth strain. Strain distortions can be estimated under the assumption that the scale of these effects is much smaller than the scale of the measured stress and strain perturbations. This assumption holds for observations of Earth tides. Cavity effects are expected to be small on both Gran Sasso interferometers, since they measure extension along the axis of two tunnels and the distance between the end-monuments and the tunnel end faces are more then one tunnel diameter. Topographic effects are expected to be small on BA, but as large as 20% to 40% on BC, since BA is approximately parallel to the local trend of the Apennines mountain chain and BC is approximately perpendicular to it. During 2008, we estimated local effects using reference Earth tide strains, taking into account ocean loading effects computed using the new ocean loading modelling.

We have also completed our research on long-period toroidal earth free oscillations from the great SumatraAndaman earthquake. Earths free oscillations can be observed after most large earthquakes and are also detectable in seismic noise records, but the gravest oscillations with periods ¿ 1000 s are observable only after the largest events. Spectra from both seismic and gravimeter data from the Sumatra-Andaman earthquake exhibit the gravest Earth oscillations with unprecedented signal-to-noise levels. Because horizontal seismic records are often noisy and superconducting gravimeter data is sensitive primarily to vertical motion, measurements of horizontal strain offer an important data complement, especially for the detection and characterization of toroidal free oscillations ${}_nT_l$. Modal splitting and coupling effects, however, affect the oscillation envelope of all modes with angular degree $l \geq 1$. For the gravest modes Earths steady rotation inuences coupling and splitting most strongly, so a good estimate of likely coupling effects can be made without detailed knowledge of Earths aspherical structure. Uncertainty in estimatede seismic moment release, particularly between seismic and geodetic measurements, for the 2004 Sumatra-Andaman event could potentially reveal large slow coseismic motions on the fault system. Published estimates of the average fault area and slip of the 2004 Sumatra-Andaman earthquake do not agree about a possible slow slip component, so the observation of the gravest toroidal free oscillations could represent a good opportunity to advance knowledge about the hypothetical slow part of the Sumatra-Andaman source. Data recorded during the great Sumatra-Andaman earthquake of December 26, 2004 observed by the Gran Sasso interferometers show a high S/N. BC-BA is independent of laser frequency uctuations, so S/N is the highest and our results relate to this shear strain

component.

Preliminary studies of possible correlations between strain data and local hydrology (spring discharge in the Gran Sasso area, hydrochemical and isotope data of groundwater collected within LNGS, fracture network in the Gran Sasso massif) have also been performed. These researches continues those in [1], aimed to a better understanding of the Gran Sasso aquifer, and in particular of unsteady recharge processes, water-rock interactions, lithological and fault role on ow and groundwater transit time in the unsaturated and saturated zones.

2 Local effects

Environmental effects have been studied using VAV/2003 (([14]). Local air temperature and pressure proved to give a small effect to tidal strain measurements out of the S1 tidal component.

We have also computed theoretical (solid + ocean loading) strain tides using SPOTL ([2]), Love numbers from IERS2003 (frequency-independent, but different in the diurnal and semi-diurnal bands; [10]), mass-loading Green functions for the Gutenberg-Bullen earth model A ([8]), three different global ocean models (TPXO7.1, [7]; GOT00.2,[12]; CSR4.0,[6], and one local Mediterranean Sea model, at 1/30 deg resolution (four diurnal constituents, Q1, O1, P1, K1; four semi-diurnal constituents, N2,M2, S2, K2, http://www.coas.oregonstate.edu/research/po/research/tide/med.html). If the same local model is used for the Mediterranean Sea, all tested global models give very similar results. Since at Gran Sasso ocean loading tidal strain is smaller than solid Earth one by about an order of magnitude, total tidal strain predicted after merging the Mediterranean Sea model into different global models are practically undistinguishable. We have also checked for differences in the results when using two variants of the Gutenberg-Bullen model A for computing mass-loading Green functions. Total tidal strain at Gran Sasso is practically independent of the Earth model used for computing mass-loading Green functions. The phasor plot in Figure 1 shows ocean loading correction to theoretical solid tides (computed for a spherical non-rotating Earth, SNRE) for the two interferometers. Correction essentially consists in a small rotation of phasors, whose amount and sign depends on the tidal component and the interferometer.

To estimate local effects, we have assumed that discrepancies between tidal predictions and observations out of the FCR spectral region are only due to local distorion (because of heterogeneities, topography, etc.). We estimate local effects using reference Earth tide strains, a xy coordinate system (with the x-axis directed along BC and the y-axis directed along BA) and a matrix representation of the relationship between instrument and remote strains. Local effects on the extension along BA ($\varepsilon_{\mathrm{B}A}$) can be described by the three coupling coefficients $\alpha_{\mathrm{B}A}$, $\beta_{\mathrm{B}A}$, $\gamma_{\mathrm{B}A}$:

$$\varepsilon_{\mathrm{B}A} = \alpha_{\mathrm{B}A}\varepsilon_{\mathrm{x}x} + \beta_{\mathrm{B}A}\varepsilon_{\mathrm{y}y} + \gamma_{\mathrm{B}A}\varepsilon_{\mathrm{x}y}$$

and similarly for the extension along BC ($\varepsilon_{\mathrm{B}C}$). The six unknown coefficients describing local effects have been estimated by comparing predicted and observed amplitudes and phases of the larger tides out of the FCR range, namely Q1, O1, N2, M2, and K2. We

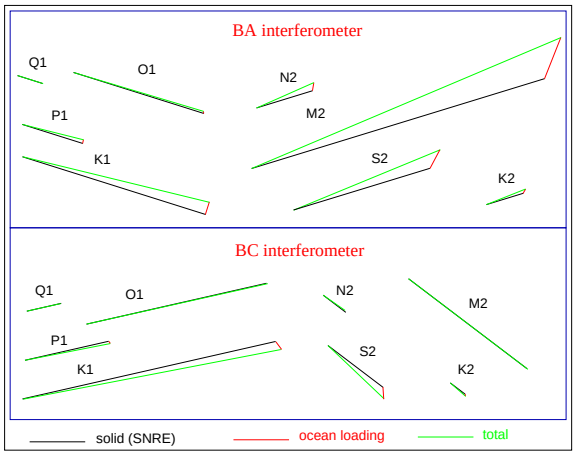

Figure 1: Figure 1. Phasor plot of predicted solid (solid lines), ocean loading (dotted lines), and total (dashed lines) tidal strain. Ocean model: TPXO7.1 and local Mediterranean model; Earth model for mass-loading Green functions: Gutenberg-Bullen model A; Love numbers: IERS 2003.

did not use S2 because of possible residual contamination from air pressure effects. The phasor plot in Figure 2 (in which case we have used the TPXO7.1 ocean model, the local Mediterranean model, the Gutenberg-Bullen model A for mass-loading Green functions, and the IERS 2003 Love numbers) clearly shows that discrepancies are fully recovered by using the coupling matrix (dashed and dotted lines are indistinguishable).

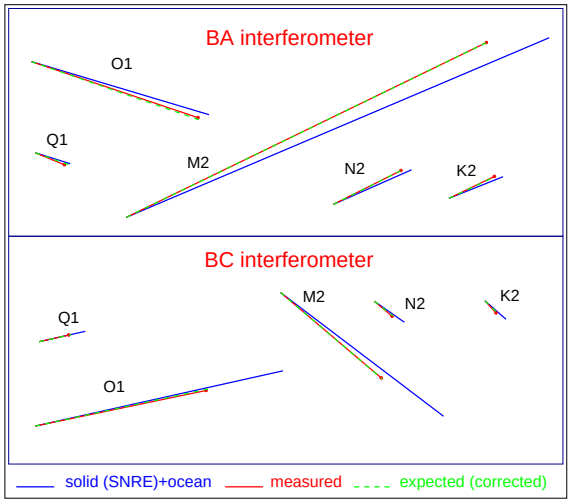

Figure 2. Phasor plot of predicted total (solid lines), observed (dotted lines), and corrected (through the coupling matrix, dashed lines) tidal strain. Ocean model: TPXO7.1 and local Mediterranean model; Earth model for mass-loading Green functions: Gutenberg-Bullen model A; Love numbers: IERS 2003.

Coupling coefficients obtained using different Earth and ocean models, and first-differenced strain time series are very similar (even if not identical) to those shown in Figure 2. Coupling among different strain components is faint but, as expected, strain measured along BC is reduced by about 30% because of topographic effects.

3 Long-period toroidal Earth free oscillations from the great Sumatra-Andaman earthquake

We have completed ([11]) the analysis of strain data related to seismic free oscillations excited by the 2004 December 26 Sumatra-Andaman earthquake. Since the main source of instrumental noise can be mitigated by differencing data from the crossed strainmeter arms, the resulting differential strain data set offered an unprecedented resolution of the seismic toroidal free oscillations with periods $T > 1000$ s, resolving oscillatory motions with amplitudes of 0.1-0.3 nanostrain above natural noise levels of 0.02-0.05 nanostrain. Measured horizontal divergence strain is too noisy to detect the gravest spheroidal modes ${}_0S_2$, ${}_1S_2$, ${}_0S_3$ and ${}_2S_1$, but allows resolution of many prominent spheroidal free oscillations at periods less than 2000 s. The splitting and coupling of free oscillation frequencies and vibrational patterns, associated with Coriolis force and Earths deviations from sphericity, cause many observed seismic free oscillations to depart from a simple exponentially decaying cosinusoid. All free oscillations in the Gran Sasso data set are observed as multiplets, comprised of several singlet free vibrational modes with closely spaced frequencies that can exhibit both constructive and destructive interference as time passes. As a result, several free oscillations do not reach peak amplitude in the Gran Sasso data set for as long as 24 hr after the earthquake onset. Employing an envelope estimator based on multiple-taper spectrum analysis, we have reconstructed the time evolution of selected free oscillations for comparison with synthetic seismograms that include normal-mode coupling effects from Coriolis force, attenuation and ellipticity. Envelopes estimated for the Gran Sasso differential data set for free oscillations with period $T < 1000$ s (frequencies $f > 1$ mHz) are approximated adequately by a composite Centroid-Moment-Tensor (CMT) source with ve subevents and an aggregate $M_w = 9.3$ moment-magnitude. Envelopes for several toroidal free oscillations with $T > 1000$ s are predicted less well. The amplitude of the rarely observed mode ${}_0T_2$ is overpredicted at Gran Sasso by roughly a factor of two, and nearby modes ${}_0T_3$ and ${}_0T_5$ are underpredicted. We have conrmed this amplitude discrepancy by comparing measured and predicted ${}_0T_3$ and ${}_0T_5$ oscillation envelopes at selected exceptionally low-noise seismic stations that recorded ${}_0T_2$ with a signal-to-noise ratio of 2 or more. We have also found that, with the exception of the gravest observed mode ${}_0S_2$, the spheroidal modes on the vertical seismometer components are t fairly well by the composite CMT source model. Although a complex adjustment to the source faulting model has not been ruled out as a factor, the grouping of signicant amplitude anomalies at periods longer than 1000 s suggests a cause whose duration exceeds that of the Sumatra-Andaman rupture (600 s). We have not conclusively identified the causes for the observed amplitude anomalies. We have compared hypotheses related to (1) short-term rupture complexities, (2) post-rupture strain release, (3) coupling to Earths secular modes and (4) tsunami-feedback (primarily) on the coastlines of the Indian Ocean. We

have found strong reasons to doubt the viability of the rst and third hypotheses, as well as simple steps or ramps of post-rupture strain release. Slow strain-release models with oscillatory behaviour would be needed to effect seismic amplitude anomalies restricted to $f < 1$ mHz. The tsunami-feedback mechanism is restricted to $f < 1$ mHz by the nature of tsunami propagation in the open ocean. The tsunami-feedback mechanism seems most plausible; its viability deserves further investigation.

4 Preliminar strain-hydrology analyses

As expected, long-term (seasonal) behaviour of the strain time series is strongly correlated with the water table changes. Preliminar analyses involving springs located at different places in the Gran Sasso area evidence strong differences in between interferometers BA and BC. This peculiarity and the already known difference in the pressure-strain transfer function for BA and BC may be linked to the features of fracture network and Darcy's fluxes. More analyses, including a deep insight on hydrochemical and isotope data and fracture network, are required before drawing any conclusion. This study is carried out in co-operation with R. Adinolfi Falcone, A. Falgiani, M. Petitta, and M. Tallini.

5 Acknowledgments

We thank Fabrizio Tronca and Costantino Fischione for their help with logistics. The Interferometric Station at Gran Sasso is supported in the frame of the Accordo di Programma between Istituto Nazionale di Fisica Nucleare and Istituto Nazionale di Geofisica e Vulcanologia.

References

[1] Adinolfi Falcone R., A. Falgiani, B. Parisse, M. Petitta, M. Spizzico, and M. Tallini, *J. Hydrol.*, **357**, 368-388, 2008.

[2] Agnew D.C. , *SIO Ref. Ser. 96-8, 35 pp.*, Scripps Institution of Oceanography, La Jolla, CA, 1996.

[3] Amoruso A., L. Crescentini, and R. Scarpa, *Geophys. J. Int.*, **140**, 493-499, 2000.

[4] Amoruso A., L. Crescentini, and L. Ruggiero, EGU 2nd General Assembly, Wien, 2005.

[5] Crescentini L., A. Amoruso, and L. Ruggiero, AGU Fall Meeting, S. Francisco, 2004.

[6] Eanes R. J.,*Eos Trans. AGU*, **75(16)**, 108, 1994.

[7] Egbert G. D., and S. Y. Erofeeva, *J. Atmos. Oceanic Technol.*, **19 (2)**, 183-204, 2002.

[8] Farrell W. E.,*Rev. Geophys and Space Phys.*,**10**, 761-797, 1972.

[9] Matsumoto K., T. Sato, T. Takanezawa, and M. Ooe, *J. Geod. Soc. Japan*, **47**, 243-248, 2001.

[10] McCarthy D. D., and G. Petit (eds.),*IERS Technical Note, No. 32*, 2004.

[11] Park J., A. Amoruso, L. Crescentini, and E. Boschi,*Geophys. J. Int.*, **173**, 887-905, 2008.

[12] Ray R. D.,*NASA Technical Memorandum 209478*, 1999.

[13] Venedikov A. P., J. Arnoso, and R. Vieira, *Computers and Geosciences*, **29**, 487-502, 2003.

[14] Venedikov, A. P., J. Arnoso, and R. Vieira, *Computers and Geosciences*, **31**, 667-669, 2005.

[15] Wenzel H.-G., *Bull. Inf. Marees Terrestres*, **124**, 9425-9439, 1996.

TELLUS. A new electromagnetic strainmeter for the monitoring of ground-field deformations.

V. Sgrigna[a], L. Conti[b], D. Zilpimiani[c]

[a] Dipartimento di Fisica e Sezione INFN, Università Roma Tre, Rome, Italy.
[b] Sezione INFN di Perugia e Dipartimento di Fisica, Università Roma Tre, Rome, Italy.
[c] Institute of Geophysics, Georgian Academy of Sciences, Tbilisi, Georgia.

Abstract

During 2008 an original differential electromagnetic strainmeter has been made for wide base-length and high-resolution ground-based continuous measurements of deformation processes. The equipment consists of a couple of central and peripheral units located at a sight distance relatively to each other. Each unit includes an antenna, an electronic package, and the power supply system. The central Unit is linked to a computer through an analog-to-digital converter. The equipment has been designed, built, assembled and calibrated in the ESPERIA Laboratory of the Department of Physics of the Roma Tre University. It can process, transfer and store data to a mass memory unit.

1 The Tellus experiment

The activity carried out during 2008 by the TELLUS team has been the construction of an original new electromagnetic strainmeter (patent pending) for the monitoring of deformation processes. These events have great importance both in engineering and science applications, such as in structural deformation surveys and in geophysical applications, respectively. A schematic representation of the instrument is reported in figure 1. As it can be seen, it is a dual frequency strainmeter. Basically, the instrument is a differential interferometer working in the microwaves frequency range and consists of "elementary" one-dimensional (1-D) modules through which it is possible to measure the change (Δl) of the distance (l) between two assigned points. By using several 1-D modules of such kind one may to determine all the strain tensor components ϵ_{ij}. In fact, in a material with a homogeneous strain field, the measured change of the distance gives directly the strain component

$$\epsilon = \frac{\Delta l}{l} \tag{1}$$

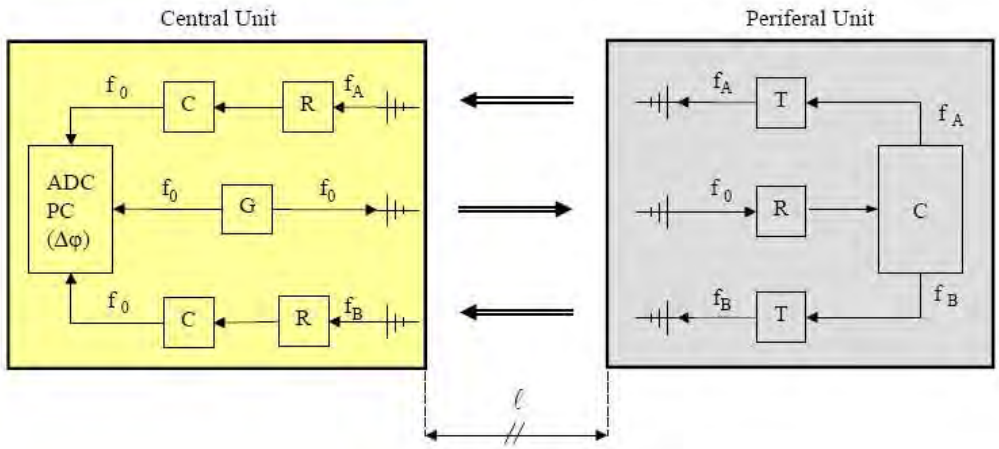

Figure 1: Schematic representation of the dual frequency electromagnetic strainmeter.

in the direction of the measurements. To determine the total strain tensor in a plane (two normal strains and one shearing), a minimum of three 1-D modules (that is a 3-D strainmeter) must be installed in three different directions.

2 Construction details

As shown in figure 1, each elementary module is constituted by a couple of central and peripheral units. These two units, are located at a sight distance l relatively to each other. Each unit includes an antenna, an electronic package, and the power supply system. The central unit is linked to a computer (PC) through an analog-to-digital converter (ADC). The electromagnetic signal of frequency $f_0 = 2$ GHz emitted by generator G is sent by the antenna of the central unit to the peripheral unit where it is divided (by dividers R) and converted (by mixers C) into two signals of frequency $f_A = 1.5$ GHz and $f_B = 2.5$ GHz. Two transmitters (T) send back signals f_A and f_B to the central unit where they are both converted again into waves of equal frequency f_0, so to be compared in phase with the reference wave which also has frequency f_0. The amplitude and frequency stability of signals is fundamental for the high-accuracy phase measurements requested by these kind of applications. The signal frequency stability is fixed by generator and selective filters specifications, while the amplitude stability is given by limiters. The reference signal is obtained by deriving towards the phase-detector the same EM-wave of frequency f_0 emitted by generator G of the central unit before it arrives at the antenna of the transmitters to be sent to the peripheral unit. The differential phase differences between the transmitted and returned signals allows to determine Δl changes without any effect due to possible fluctuations of atmospheric conditions (i.e., of refraction index of the medium).

3 Calibration

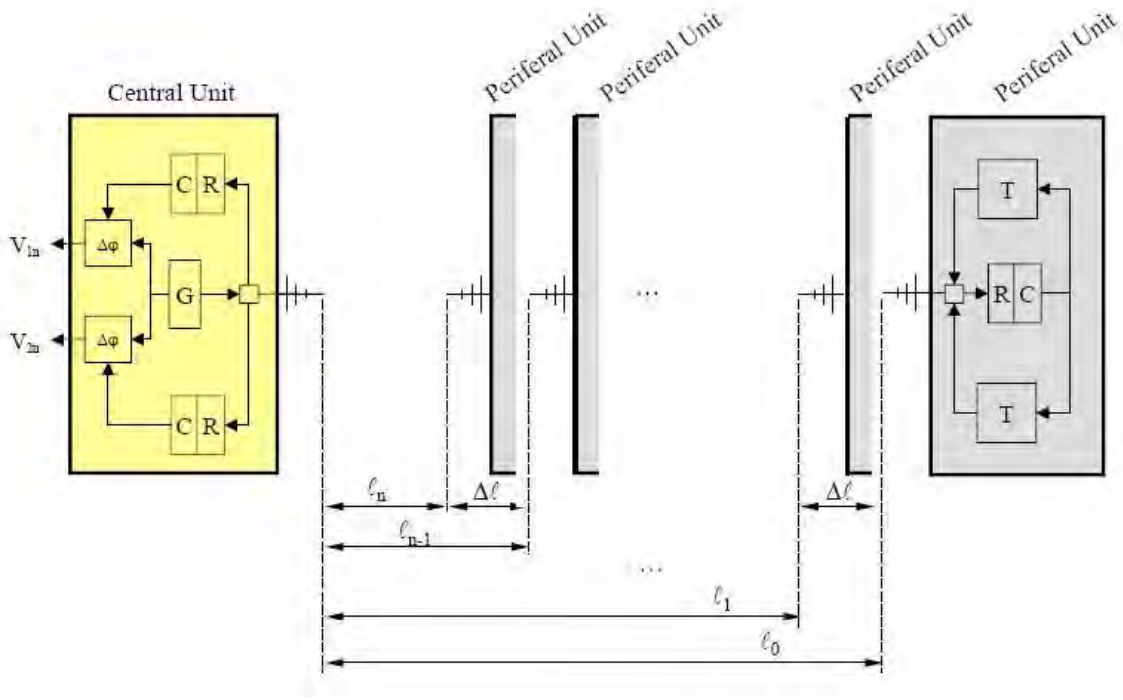

Figure 2: Schematic representation of the calibration procedures.

As shown in figure 2, the instrument has been calibrated in laboratory by changing step-by-step, of a fixed quantity Δl, the distance l between the antennas of the central and peripheral units and detecting the output potential differences V_{1n} and V_{2n} of the two phase detectors ($\Delta\phi$). At the beginning of calibration procedures the antennas of central unit (mounted on a fixing support) and peripheral unit (mounted on a sliding support) were positioned at the two opposite ends of a rectilinear guide at a relative distance l_0 = 600 mm. Then, the sliding support holding the antenna of the peripheral unit was moved along the guide by a numerical control machine. This allowed the antenna to reach 61 successive positions (e.g., 61 measurement data) $l_0, l_1, l_2, \ldots, l_{n-1}, l_n$ spaced by constant intervals Δl = 10mm, with a resolution of 0.01 mm. To construct calibration curves in correspondence to each position l, the output potential differences V_{1n}, V_{2n}, were detected and reported *vs* distance l. Results are shown in figures 3-4. V and l data in each calibration curve are reported with errors (1mV and 0.01mm, respectively). Such procedure has been repeated five times, so that each point of calibration curves reported in figures 3 and 4 is the average value of five repeated measurements. A best fitting carried out on the data exhibits a sinusoidal trend with correlation coefficient r = 0.99. Note that, as expected, the best fitting of calibration points is obtained with harmonic functions and data follow a sinusoidal trend with a change Δl of l_0 (baselength) corresponding to a phase shift $\Delta l = 2\pi$, according to the theory.

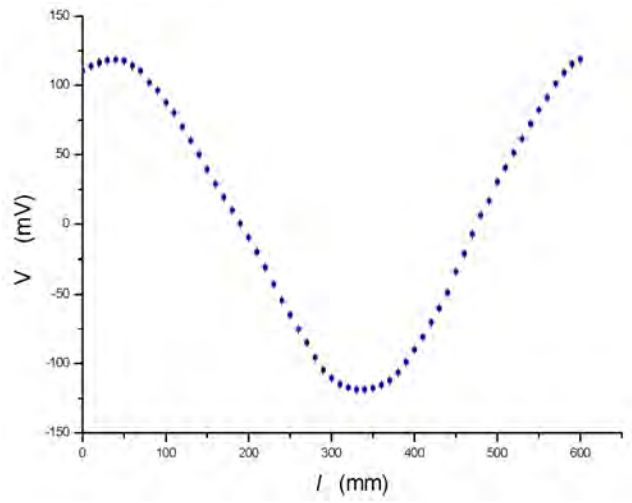

Figure 3: Calibration curve related to the return signal of frequency f_A.

4 Discussion and Conclusions.

A new and original strainmeter has been designed and constructed at the ESPERIA Laboratory of the Physics Department of the Roma Tre University. The methodological and technical solutions adopted for the instrument (mainly, the use of a two-frequency method and the possibility to keep constant in time the phase difference between input and output signals of the peripheral unit, even in presence of an amplification of output signals), demonstrate to be a good solution for simultaneously performing with a sole instrument: continuous measurements (monitoring) of Δl changes

- by detecting phase differences with a resolution of 0.1^o or less between direct and return em signals of frequency of the order of GHz
- in a wide baselength range (from hundreds meters to decades of kilometers)
- at high resolution (of the order of 10^{-1}mm) and dynamic range (about 80 dB)
- independently by possible fluctuations of the refraction index of the medium.

The prototype we have made can perform a strain monitoring with a resolution of about 10^{-9} in the strain interval of about $10^{-9} \div 10^{-6}$. At present no instrument is available with these characteristics for many applications such as geodetic surveys, geotechnical/structural measurements of local deformations, deformation events associated with earthquake and volcanic activities, geological and hydrogeological disarrangement, slope stability, movements of structures with respect to the foundation rocks, monitoring of dams and power plants structures as well as of horizontal and vertical movements of manufactures, etc. Also positive characteristics of the instrument are the use of high frequency ($\sim GHz$) and low-power ($\sim W$) penetrating waves, which also are stable both in amplitude and frequency. Normally, a 1GHz and 1W signal may reach distances of

about 10km or more (for a double distance one should quadruplicate the power). The use of a so low-power signals implies a low-power consumption and that of solar panels and low-capacity batteries involves a large work autonomy of the strainmeter.

List of References including Publications during the year 2008

1. Sgrigna, V., A. Buzzi, L. Conti, P. Picozza, C. Stagni, D. Zilpimiani, 2008. The ESPERIA satellite project for detecting seismic-associated effects in the topside ionosphere. First instrumental tests in space, Earth Planets and Space, 60, 463-475.

2. Sgrigna, V., Buzzi, A., Conti, L., Stagni L., Zilpimiani, D., 2008. TELLUS. Ground deformations and their effects in the near-Earth space, Laboratori Nazionali del Gran sasso, INFN, Annual Report 2007, LNGS/EXP-01/08, May 2008, pp.187-190.

3. Massonnet, D., 1998. Radar Interferometry and its Application to Changes in the Earth's Surface, Review of Geophysics, 36, 441-500.

4. Maseroli, R., 1995. Il Sistema di Riferimento WGS84, Boll.Geodes. Sci. Aff., 54, 1619-1626.

5. Massonnet, D., M., Rossi, C., Carmona, F., Adragna, G.,Peltzer, K., Feigi, and T., Rabaute, 1993. The Displacement Field of the Landers Earthquake Mapped by Radar Interferometry, Nature, 364, 138-142.

6. Lockner, D.A., J.D., Byerlee, V., Kuksenko, A., Ponomorev, and V., Sidorin, 1991. Nature, 350, 39-42.

7. Dubrov, M.N., V.A., Aleshin, and A.P., Iakovlev, 1989. Wideband Laser Strainmeters as a New Instrument for Geophysical Research, Gerland Beitraege zur Geophysik, 98, 292-300.

8. Sgrigna, V., A. Buzzi, L. Conti, P. Picozza, C. Stagni, D. Zilpimiani, 2008. The ESPERIA satellite project for detecting seismic-associated effects in the topside ionosphere. First instrumental tests in space, Earth Planets and Space, 60, 463-475.

9. Sgrigna, V., Buzzi, A., Conti, L., Stagni L., Zilpimiani, D., 2008. TELLUS. Ground deformations and their effects in the near-Earth space, Laboratori Nazionali del Gran sasso, INFN, Annual Report 2007, LNGS/EXP-01/08, May 2008, pp.187-190.

10. Massonnet, D., 1998. Radar Interferometry and its Application to Changes in the Earth's Surface, Review of Geophysics, 36, 441-500.

11. Maseroli, R., 1995. Il Sistema di Riferimento WGS84, Boll.Geodes. Sci. Aff., 54, 1619-1626.

12. Massonnet, D., M., Rossi, C., Carmona, F., Adragna, G.,Peltzer, K., Feigi, and T., Rabaute, 1993. The Displacement Field of the Landers Earthquake Mapped by Radar Interferometry, Nature, 364, 138-142.

13. Lockner, D.A., J.D., Byerlee, V., Kuksenko, A., Ponomorev, and V., Sidorin, 1991. Nature, 350, 39-42.

14. Dubrov, M.N., V.A., Aleshin, and A.P., Iakovlev, 1989. Wideband Laser Strainmeters as a New Instrument for Geophysical Research, Gerland Beitraege zur Geophysik, 98, 292-300.

Patents

1. Sgrigna, V., Conti, L., Zilpimiani, D., 2008. "Variable Feedback Method for signal conditioning and related data acquisition, spectral analysis and digital management system " (patent RM2008A000688).

2. Sgrigna, V., Zilpimiani, D., 2000. "Method for detecting displacements, movements and deformations of ground and manufactures and related device" (patent RM2000A000392).

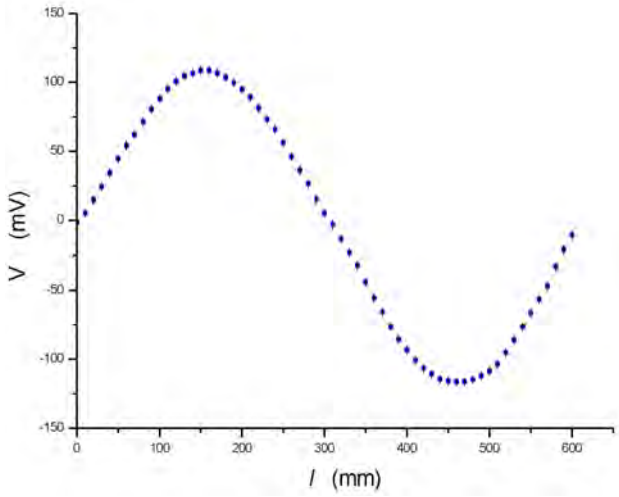

Figure 4: Calibration curve related to the return signal of frequency f_B.

UNDERSEIS - Underground Seismic Array

C. Fischione[b,*], L.A. Formisano[c], D. Galluzzo[a], M. La Rocca[a], R. Scarpa[a,b], F. Tronca[b,*]

[a] Osservatorio Vesuviano, I.N.G.V. - Napoli, Italy
[b] Dipartimento di Matematica e Informatica, Università di Salerno, Italy
[c] Dipartimento di Fisica - Università di Salerno, Italy
[*] Spokesperson

Abstract

This report describes a geophysical instrument installed in the underground physics laboratories of Gran Sasso (LNGS-INFN), located in the seismic zone of central Apennines, Italy. This instrument is aimed to monitor seismic radiation with very high sensitivity; it is a small aperture seismic array composed by 20 three-components short period seismometers (Mark L4C-3D).

1 Introduction

The physics of earthquakes is based on the measurements of radiated seismic waves and ground displacement associated with this phenomena. The inertial pendulum is the oldest and most diffused instrument used to measure the main features of seismic waves. The advantages of this instrument are the simplicity of the theory, the high sensitivity, the robust design and the simple calibration methods, in spite of the quite reduced frequency band and linearity (Wielandt, 1983). Other instruments based on different physical principles, such as strainmeters and gyroscopes, are only partially used by seismologists (Benioff, 1935; Farrell, 1969; Aki and Richards, 1980). Networks of short period seismometers are as far the most diffused system to monitor local and regional seismicity (Lee and Stewart, 1981). Broad-band instruments make up a powerful system to study the details of seismic sources and also to study large earthquakes at global scale (Lee and Wallace, 1995). Strainmeters and tiltmeters (Agnew, 1986) are used to study the lower frequencies radiated from seismic sources and allow to detect slow earthquakes and strain steps (i.e. anelastic deformations around seismic sources). Moreover arrays of seismometers and accelerometers are used to study the Earth structure at global, regional and local scale (Green, 1965; Kedrov and Ovtchinnikov, 1990; Mikkeltveit, 1985), earthquake source

process (Spudich and Oppenheimer, 1986; Goldstein and Archuleta, 1991), nuclear underground explosions (Bolt, 1976; Chouet, 1996) and, more recently, for the analysis of complex signals associated to the volcanic activity (see f.i. Goldstein and Chouet, 1994; Chouet et al., 1997; Almendros et al., 1991). The main advantage of the seismic arrays consists in their ability to detect small signals through multichannel waveform stacking (Capon, 1969). The area is interested by relevant seismicity associated with the mainly distensive tectonics affecting the Apennines since the late Pliocene (D'Agostino et al., 2001; Galadini et al., 2003). The last large historical event is the 1915, $M_S = 6.8$ Fucino earthquake, which caused about 32000 casualties, recently modelled by a normal fault striking along the Apennines (Amoruso et al., 1998). In addition, swarms of low- to moderate-size earthquakes occur quite frequently, the most recent on 1992, 1994 and 1996 (De Luca et al., 2000). This massif is intersecting a main seismogenetic fault where the occurrence of slow earthquakes has been recently detected through two wide-band geodetic laser interferometers (Crescentini et al., 1999; Amoruso et al., 2002). This quite relevant rate of seismicity, joint to the low-noise conditions and site response associated to the underground setting, make the Gran Sasso underground laboratories an ideal site for high-resolution seismic observations (De Luca et al., 1998).

2 The Underground Seismic Array

A seismic array is a set of seismographs distributed over an area of the Earth's surface at spacing narrow enough so that the signal waveform may be correlated between adjacent seismometers (Aki and Richards, 1980).

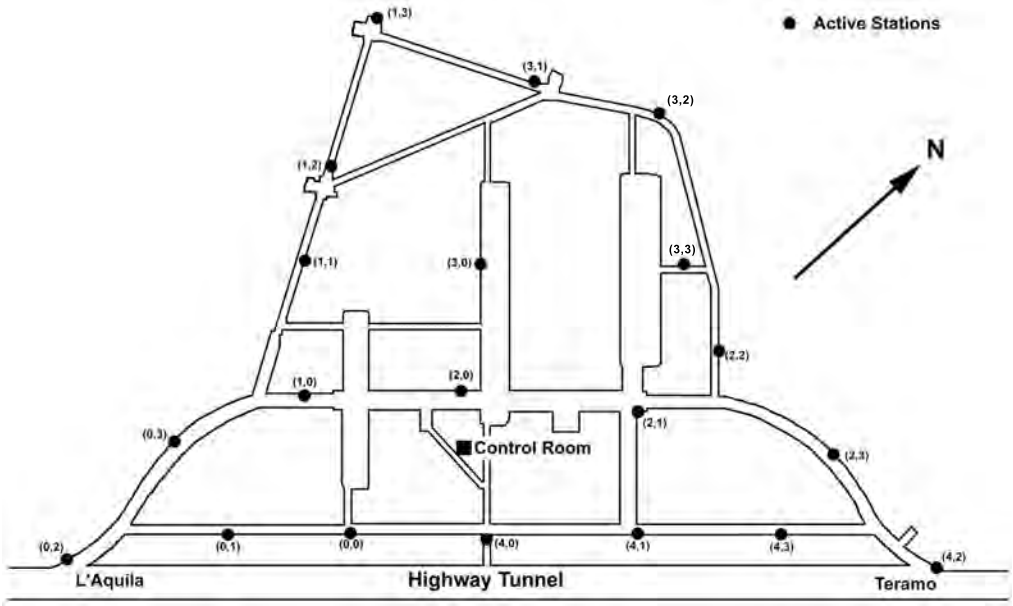

Figure 1: Map of the Underground Seismic Array. The notation (n,m) shows the line number (n) and the station number (m).

The design of the UnderSeis hardware and software components began on the late 90's; over the following years, major upgrades were developed under a technological effort jointly carried out by engineers from the University of Granada (Spain), University of L'Aquila (now the team moved to the University of Salerno), and INGV - Osservatorio Vesuviano. The array become fully operative since May, 2002. In its present configuration, it consists of 19 elements, each equipped with a MARK Product L4C-3D, 1 Hz, 3-component seismometer. The average sensor spacing is on the order of 90 m, and the largest distance among sensors is about 400 m. Seismic signals are digitized locally at each individual seismometer with a dynamic range of 24 bits and sampling frequency of 100 Hz. Data synchronization is achieved via a Master Oscillator which transmit the UTC synchronized pulses from an atomic clock to the different ADC boards. The synchronized data packets are then sent via serial cable connection to a set of five nodal PCs, which are in turn connected via an Ethernet network to a central data server and an on-line processor (Scarpa et al., 2004).

3 The Fontari Array (FonArray) in Campo Imperatore

Since the beginning of june 2007, a new temporary surface array, consisting of 6 stations, was installed in the Fontari Plain,near Campo Imperatore (1950 m above sea level). It was placed with good approximation vertically above the underground array (UnderSeis). Figure 2 (on the right) shows the geometric configuration of FonArray, and the technical details are:

- channels: 18;
- sensors: 6 short period 3D seismometers Lennartz LE 3D Lite (frequency 1 Hz);
- data storage: magneto/optical disk (512 Mb) or memory cards (1 Gb, 2 Gb or 5 Gb);
- time synchronization: GPS;
- power supply: 12 V by solar panels and batteries;
- acquisition: continuous, 125 Hz sampling.

Four stations were installed indoor (garages, old buildings), but two had to be installed outdoor. Figure 2 (on the left) shows the configuration of the station known as FON6. Array acquisition lasted about six months, from june to november 2007. Maintenance operations were carried out weekly: they consisted in data recovering (disks and memory card substitution), GPS time synchronization check, solar panels and batteries charge check, in addition to occasional operations. FonArray data can be used for several data analysis, especially if analysed together with UnderSeis ones. Arguments for next research activities are resumed as follows:

- seismic noise analysis with array techniques, in order to evaluate a surface velocity model;
- comparison between seismic noise recorded at FonArray and seismic noise recorded at UnderSeis;
- earthquakes analysis with various techniques, giving particular attention to events recorded together by FonArray and UnderSeis;
- polarization studies of primary and secondary waves for local and regional earthquakes;
- polarization analysis of seismic noise.

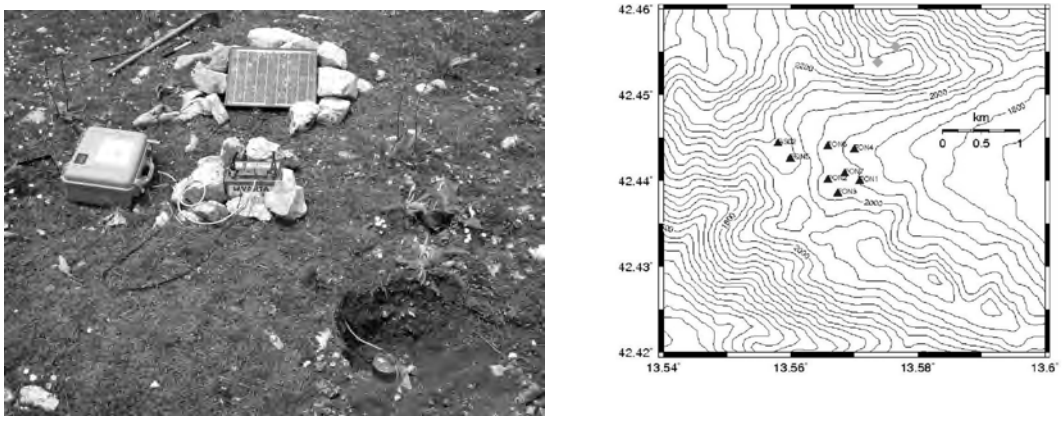

Figure 2: Left: FON6 station, as all the other FonArray ones, consisted in a Lennartz 3D-lite sensor, a solar panels and batteries power supply and a Lennartz MarsLite station with a GPS timing system. Right: FonArray geometric configuration. Stations GS02 and FON5 are also shown in the picture: after a short period of acquisition, they were dismantled.

4 Low frequency tremor along the Apennines

4.1 Low frequency deep tremor

This section reviews the main observations on low frequency tremor made along the Apennines, which constitute the main seismic active zone of Italy. The observations made in recent years indicate that this phenomena are quite rare and apparently uncorrelated with slow earthquake. Until now only one event characterized by low frequency content and duration of several hours has been detected in january 2004, without any correlations

with the occurrence of slow or regular earthquakes. The signal to noise ratio of this event is very low, but the results of array analysis, its spectrum and duration makes it compatible with a low frequency non volcanic tremor. Tremors, likely originated by fluid flows inside magma chambers and conduits, are traditionally observed in volcanic environment (Chouet, 1996). In the last decade a new category of low frequency seismic signals, called deep non volcanic tremor, has been discovered away from volcanoes along subduction zones of Japan (Obara, 2002), and successively along the west coast of North America, from California to British Columbia, Canada (Rogers and Dragert, 2003; Kao et al., 2006; Gomberg et al., 2007). In Japan the deep tremor is often associated with low frequency earthquakes of low magnitude (Shelly et al., 2007). Swarms of these events are related to tectonic activity of subduction zones and in particular to the creeping zones of these faults representing shear slip on the plate interface. In both Japan and Cascadia subduction zones, the major swarms of tremors, lasting from hours to weeks, are associated with slow slip located along the subduction plane, possibly connected to large and catastrophic earthquakes (Ide et al., 2007b). Along the Cascadia these tremors occur every 13-15 months and have been related to the slip of a very large fault capable to generate a Magnitude 9 earthquake (Rogers and Dragert, 2003). This explains the increase of studies aimed to understanding the mechanisms of these events. The deep tremor observations made in Cascadia and Japan are characterized by a small amplitude, not clear onset, absence of impulsive phases and frequency content usually in the band 1-8 Hz (La Rocca et al., 2005; Obara and Hirose, 2006). Most of these features are similar to the volcanic tremor but its occurrence is away from volcanoes and generally its location is at 20-70 km depths. The amplitude of these events is close to a micron/s and this observation does not allow to record this activity at most of the Italian stations. At the UnderSeis array the seismic noise is of the order of 0.1 micron/sec due to its underground location and thus this array provides an unique opportunity to detect the possible occurrence of this phenomenon in Italy.

4.2 Seismic data analysis

The coherence of the seismic wavefield among the array stations (Foster and Guinzy, 1967; Vernon et al., 1991) has been computed for all data recorded since 2003. Local and regional earthquakes appear as high amplitude, short duration peaks in the coherence results. Only one different type of signal, characterized by duration of several hours (from about 19:00 of 13 january until 01:00 of 14 january, 2004), has been evidenced by a coherence higher than the value corresponding to the seismic noise. Figure 3 (left figure) shows the enhancement of the coherence, which rises clearly above the background value of about 0.35 for several hours. This unique episode has been recorded without the occurrence of any relevant local or regional earthquake. It is also noteworthy that any signal has been detected at the interferometric station. At a visual inspection the seismograms show the presence of signals which are common to the most of stations, but characterized by an extremely low signal to noise ratio. Figure 3 (right figure) shows 30 s of signals recorded at 21:48 by the EW components, filtered in the 1-4 Hz band. Spectra have been computed for both the low frequency signal and the seismic noise, taking the average among several windows recorded both before and after the interesting

event (Figure 4, on the left). The spectral ratio indicates a frequency content between 1 Hz and 4 Hz for the signal recorded between 19:00 and 01:00 (Figure 4, on the left).

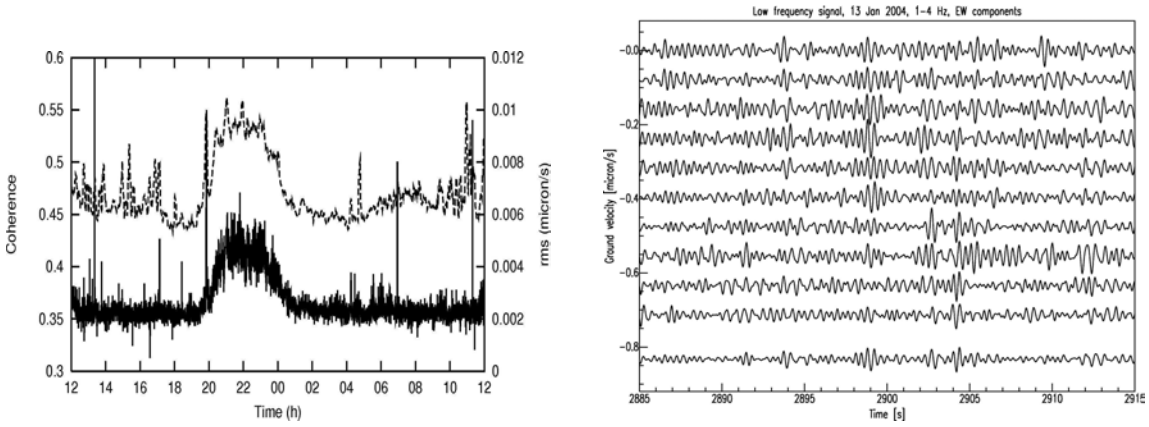

Figure 3: Left: Mean coherence among the three components averaged in the frequency band 1-4 Hz (continuous line), and rms amplitude of the seismic signal in the same frequency band (dashed line). Right: Ten seismograms recorded by the EW components during the low frequency tremor episode. The bottom trace is the signal stacking. The short transients appear more evident in the stacked signal, where the SNR is clearly enhanced.

The rms of the stacked signals filtered in the same frequency band, 1-4 Hz, has been computed for many hours, before, during and after the occurrence of the low frequency event. An example of stacked signal is shown in Figure 3, on the right, at the bottom. The improvement of the SNR is evident in this seismogram, which highlight the short transients common to all stations. Stacked seismograms have been used to compute the rms over a 60 s sliding window, in order to follow the event evolution in time. The result, shown in Figure 3 (left figure), demonstrates that the coherence increase follows very well the amplitude increase of the signal. The most of peaks in the rms signal correspond to local disturbances at some stations. Some common peaks in the rms and coherence signals are produced by small local earthquakes. The high peak around 19:50, clearly visible in both signals, represents a $M = 4$ earthquake occurred in Greece, 735 km from the array. The coherence as a function of frequency has been computed for both the low frequency signal and the seismic noise recorded some hours before and after. The comparison between the two coherences, depicted in Figure 4 (on the right), shows the main differences in the same frequency band, 1-4 Hz. Array analysis has been performed in this frequency band using all available stations, which at that time were 12. Results are characterized by low values of slowness, whose distribution is centered at about 0.2 s/km, while the backazimuth shows a highly scattered pattern with predominance of values in the north sectors (Figure 5, left figure). However, given the small extension of the array at that time and the high apparent velocity, the backazimuth is not very reliable. The absence of impulsive phases in the signal does not permit an appropriate classification of the seismic waves. However, the high apparent velocity and the H/V ratio greater than 1

indicate a predominance of shear waves impinging the array with a small incidence angle. Polarization analysis applied to the stacked seismograms yields results much more stable than the single station analysis, as expected.

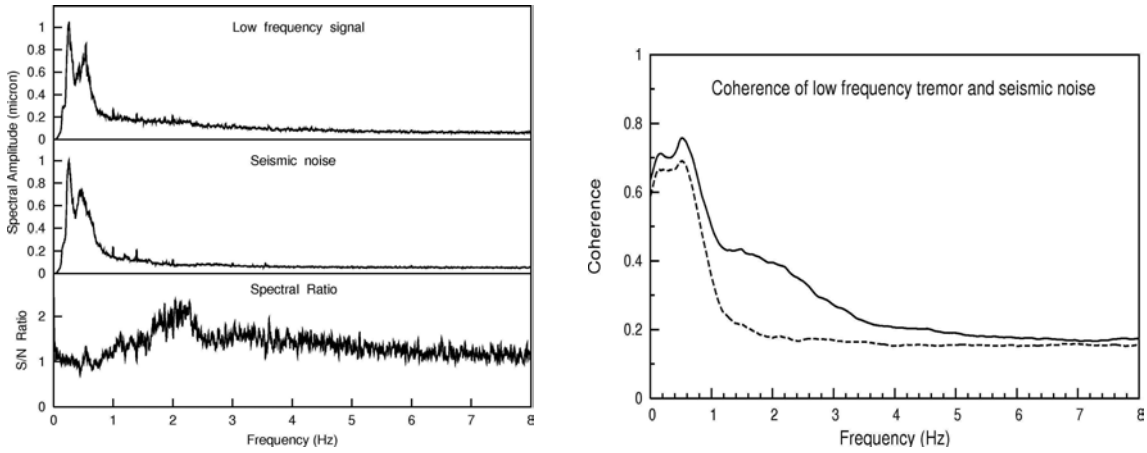

Figure 4: Left: Spectra of the low frequency signal (top), of the seismic noise (middle plot), and spectral ratio between them (bottom). Right: Comparison of the coherence as function of frequency computed for the low frequency signal (continuous line) and for seismic noise (dashed line).

The distribution of polarization azimuth, shown in Figure 5 (on the right), is strongly anisotropic, being the NE-SW direction observed with very high probability while the NW-SE particle motion is completely absent in the wavefield. Unfortunately, this pattern is observed very often at the UnderSeis array, even for the seismic noise, thus suggesting a local site or propagation effect unrelated with the low frequency tremor. The low frequency event recorded on january 13-14 2004 has many features similar to the deep tremor observed in other regions around the world, such as the low amplitude, low frequency contents, duration of hours. However, the very low SNR does not allow a detailed characterization of the seismic wavefield, essential to infer on the nature and origin of this event.

5 Conclusions

An expanding variety of unusual earthquakes has been recently discovered, such as low frequency tremor. They have much longer durations than ordinary earthquakes of comparable seismic moment. Ide et al. (2007a) have shown that these slow events follow a simple, unified scaling relationship that clearly differentiates their behavior from that of regular earthquakes. The anomalous coherent seismic tremor event occurred on january 13, 2004 may be related to the occurrence of a non volcanic tremor episode. However the small amplitude of this signal does not allow to infer more details that can help in understanding its source process. At the end of 2007 the amplifiers gain of the seismic instruments have been increased by two order of magnitude in order to further improve

the capability to detect very small signals. Further experimental work will be of great help to understand if the tremor episodes can be recorded in the peculiar tectonic domain of the Apennines. Our present observations suggests the absence of any correlation between slow earthquakes and the tremor episode in the Apennines.

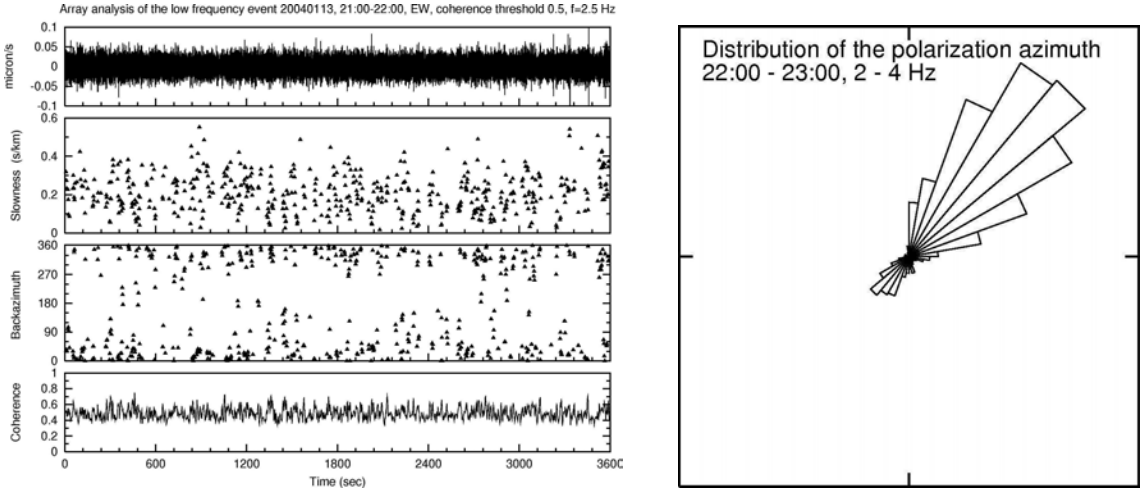

Figure 5: Left: Results of array analysis in the frequency domain applying the Beam Forming method to the EW components. Top plot shows the stacked EW seismogram, then slowness, backazimuth and coherence of the wavefield are shown for one hour of signals, from 21:00 to 22:00. In the second and third plots only results relative to windows characterized by coherence higher than 0.5 have been plotted. Right: Distribution of the polarization azimuth obtained by the analysis of one hour of stacked seismograms.

6 Acknowledgements

The financial support from Consorzio Gran Sasso and Laboratori Nazionali del Gran Sasso made possibile the realization of the seismic array. We acknowledge E. Bellotti and E. Boschi for support and stimulation. The authors thanks G. Saccorotti which helped in improving the quality of the report. This work has been realized in the framework of the program agreement between Istituto Nazionale di Geofisica e Vulcanologia - Osservatorio Vesuviano, Istituto Nazionale di Fisica Nucleare - Laboratori Nazionali del Gran Sasso and Universit degli Studi di Salerno, Dipartimento di Fisica e di Matematica ed Informatica. We aknowledge also the financial support from MIUR-PRIN2005 project $\ll$*Analisi e modellistica dei processi sismici e deformativi nell'Appennino centrale*$\gg$.

7 List of Publications

1. R. Scarpa, A. Amoruso, L. Crescentini, C. Fischione, L.A. Formisano, M. La Rocca, F. Tronca, 2008. *Slow earthquake and low frequency tremor, along the Apennines.*

Annals of Geophysics, Vol. 51, N. 2/3, April/June 2008.

2. F. Tronca, C. Fischione, G. Saccorotti, R. Scarpa, 2008. *Recent seismicity in central Italy as observed by the Gran Sasso underground seismic array.* Submitted to Bull. Seism. Soc. Am.

References

[1] Agnew D. C., 1986. *Strainmeters and tiltmeters*. Rev. Geophys. 24, 579-624.

[2] Aki K. and Richards P., 1980. *Quantitative seismology: Theory and methods*. Freeman, San Francisco, California, 932 pp.

[3] Crescentini L., Amoruso A., Scarpa R., 1999. *Constraints on slow earthquakes dynamics from a swarm in Central Italy*. Science, 286, 2132-2134.

[4] Benioff H., 1935. *A linear strain seismographs*. Bull. Seism. Soc. Am. 25, 283-309.

[5] Bolt B. A., 1976. *Nuclear explosions and earthquakes. The parted veil*. Freeman, San Francisco.

[6] Capon J., 1969. *High resolution frequency-wavenumber spectrum analysis*. Proc. IEEE 57, 1408-1418.

[7] Chouet B., 1996. *New methods and future trends in seismological volcano monitoring*. In "Monitoring and mitigation of volcano hazards", R. Scarpa and R. Tilling (Eds.), Springer-Verlag, New York.

[8] Chouet B., G. Saccorotti, M. Martini, P. Dawson, G. De Luca, G. Milana and R. Scarpa, 1997. *Source and path effects in the wavefields of tremar and explosions at Stromboli Volcano, Italy*. J. Geophys. Res., 102, 15,129-15,150.

[9] Amoruso A., Crescentini L., Morelli A., Scarpa R., 2002. *Slow rupture of an aseismic fault in a seismogenic region of Central Italy*. Geophys. Res. Lett., 29, 2219, doi: 10.1029/2002GL016027.

[10] De Luca G., Del Pezzo E., Di Luccio F., Margheriti L., Milana G. and Scarpa R., 1998. *Site response study in Abruzzo (centraI Italy): underground array versus surface stations*. J. Seismol., 2, 223-226.

[11] Farrell W. E., 1969. *A gyroscopic seismometer: measurements during the Borrego earthquake*. Bull. Seism. Soc. Am. 59, 1239-1245.

[12] Green Jr., Frosh B. A. and Romney C. F., 1965. *Principles of an experimental large aperture seismic array*. Proc. IEEE 53, 1821-1833.

[13] Kedrov O. K. and V. M. Ovtchinnikov, 1990. *An on-line analysis system for three component seismic data: method and preliminary results*. Bull. Seism. Soc. Am. 80, 2053-2071.

[14] Lee W. H. K. and Stewart S. W., 1981. *Principles and applications of microearthquake networks*. Academic Press, New York, 293 pp.

[15] Lee T. and Wallace T. C., 1995. *Modern Global Seismology*. Academic Press, New York, 517 pp.

[16] Mikkeltveit S., 1985. *A new regional array in Norway: design, work and results from analysis of data from a provisional installation, in The Vela Program*. A twenty- Five Review of Basic Research, edited by U. A. Kerr (Defence Advanced Research Project Agency), 546-553.

[17] La Rocca M., McCausland W., Galluzzo D., Malone S., Saccorotti G., Del Pezzo E., 2005. *Array measurement of deep tremor signals in the Cascadia subduction zone*. Geophys. Res. Lett., 32, doi:10.1029/2005GL023974.

[18] Schmidt R. O., 1986. *Multiple emitter location and signal parameter estimation*. IEEE Trans Antennas Propagation 34, 276-280.

[19] Wielandt E., 1983. *Design principles of electronic inertial seismometers*. In H. Kanamori and E. Boschi (Eds.) "Earthquakes: Observation, Theory and Interpretation". Proc. Int. School of Phys. "E. Fermi", North Holland, Amsterdam.

[20] R. Scarpa, R. Muscente, F. Tronca, C. Fischione, P. Rotella, M. Abril, G. Alguacil, W. De Cesare, M. Martini, 2004. *UNDERSEIS - Underground Seismic Array*. Seis. Res. Lett. Vol. 75, number 4, July/August 2004.

[21] G. Saccorotti, B. Di Lieto, F. Tronca , C. Fischione, R. Scarpa, R. Muscente, 2006. *Performances of the UNDERground SEISmic array for the analysis of seismicity in central Italy*. Annals of Geophysics, Vol. 49, number 4/5, August/October 2006.

[22] Ide, S., D. R. Shelly, and G. C. Beroza 2007b. *Mechanism of deep low frequency earthquakes: Further evidence that deep non-volcanic tremor is generated by shear slip on the plate interface*. Geophys. Res. Lett., 34, L03308, doi:10.1029/2006GL028890.

[23] Gomberg J., Rubinstein J.L., Zhigang Peng, Creager K.C., Vidale J.E., Bodin P., 2007. *Widespread Triggering of Nonvolcanic Tremor in California*. Science, doi: 10.1126/science.1149164.

[24] Obara K., H. Hirose 2006. *Non-volcanic deep low-frequency tremors accompanying slow slips in the southwest Japan subduction zone*. Tectonophysics, 417, 33-51, 2006.

[25] Vernon F. L., Fletcher J., Carrol L., Chave A., Sembera E., 1991. *Coherence of Seismic Body Waves From Local Events as Measured by a Small Aperture Array*. Journal of Geophysical Research, 96,139.

[26] Obara K., 2002. *Nonvolcanic deep tremor associated with subduction in Southwest Japan*. Science, 296, 2002; doi: 10.111/science.1070378.

[27] Rogers G., Dragert H., 2003. *Episodic tremor and slip on Cascadia subduction zone: the chatter of silent slip*. Science,300, 1942-1943.

[28] Shelly D. R., G. C. Beroza, S. Ide, 2007. *Non-volcanic tremor and low-frequency earthquake swarms*. Nature, vol. 446, 2007; doi:10.1038/nature05666.

[29] Kao H., S.-J. Shan, H. Dragert, G. Rogers, J. F. Cassidy, K. Wang, T. S. James, and K. Ramachandran, 2006. *Spatial-temporal patterns of seismic tremors in northern Cascadia.*. Geophys. Res., 111, B03309, doi:10.1029/2005JB003727.

[30] Foster M. R., Guinzy N. J., 1967. *The coefficient of coherence: its estimation and use in geophysical data processing*. Geophysics, 22, 602-616.

Ultra High Energy Cosmic Rays with the Pierre Auger Observatory

F.Arneodo[1], D. Boncioli[2], A. F. Grillo[1], M. Iarlori[2], C. Macolino[2],
S. Parlati[1], S. Petrera[2], V.Rizi[2], F. Salamida[2]

1 Laboratori Nazionali del Gran Sasso
2 INFN and Physics Department, L'Aquila University

1 Introduction

The origin of the highest energy cosmic rays is one of the most exciting questions of astroparticle physics. Even though a general concept linking magnetic field and size of possible sources (the so called "Hillas plot" [2]) is the basis of our current understanding, up to now there are no generally accepted source candidates known to be able to produce particles of such extreme energies.

At these energies cosmic rays are expected to exhibit a suppression in the energy spectrum because of their interaction with the microwave background radiation (CMB). This feature, known as the Greisen-Zatsepin-Kuz'min (GZK) effect [3], is at about $\sim 6 \cdot 10^{19}$ eV for protons. It limits the horizon from which these particles can be observed to a distance below about 100 Mpc (depending on the primary mass). The non-observation of the GZK effect in the data of the AGASA experiment [4] has motivated several theoretical and phenomenological models trying to explain the absence of the GZK effect. More recently both HiRes [5] and Auger [6] have shown evidence of a suppression such as expected from the GZK effect with high statistical significance. The recent observation of directional correlations of the most energetic Auger events with the positions of nearby Active Galactic Nuclei [7] complements the observation of the GZK effect very nicely.

Mass composition is another important key to discriminate among different models about the origin of high-energy cosmic rays. Such measurements are difficult due to their strong dependence on hadronic interaction models. Only primary photons can be discriminated safely from protons and nuclei and recent upper limits to their flux largely constrain existing top-down models.

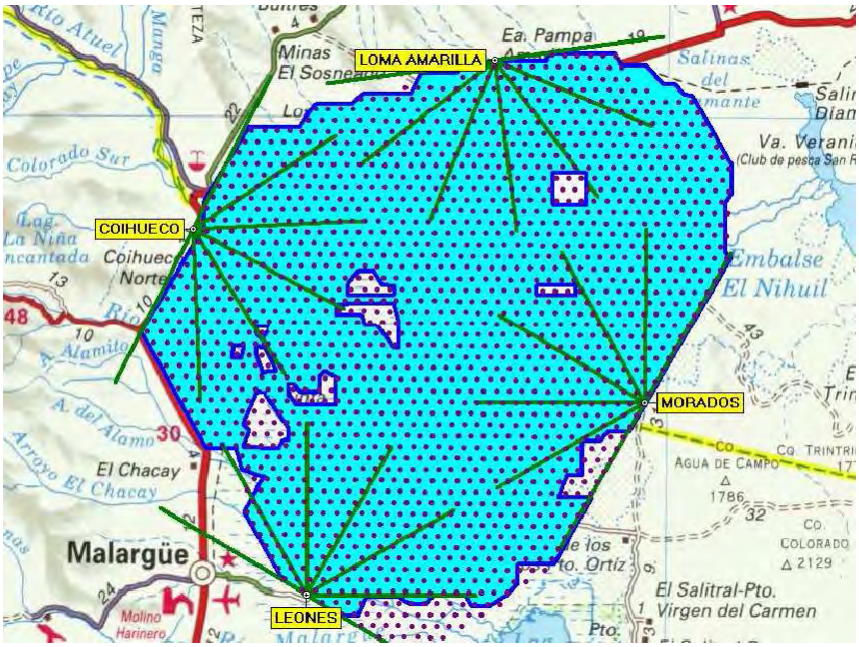

Figure 1: The southern site of the Pierre Auger Observatory. Dots represent the position of the 1600 tanks that cover a 3000 km^2 area. The dark area shows the amount of tanks deployed by June 2008. The Surface Detector is overlooked by four fluorescence telescopes: Los Leones, Los Morados, Loma Amarilla and Coihueco.

2 The Pierre Auger Observatory

The Pierre Auger Observatory is the largest extensive air-shower experiment in the world. In its final configuration it will consist of two sites, one in each terrestrial hemisphere. This will allow to reach a full sky coverage, crucial for anisotropy studies[1]. Each site will be instrumented with an array of surface detectors overlooked by a group of fluorescence telescopes.

The southern site of the Pierre Auger Observatory is located in Malargüe, province of Mendoza, Argentina at 1400 m above sea level. It covers an area of about 3000 km^2 instrumented with 1600 Cherenkov tanks with a 1.5 km spacing. By June 2008 all the detector stations have been deployed. The location and the status of the southern site are shown in Figure 1.

Each station consists of polyethylene tank, 3.6 m diameter and 1.2 m high, enclosing a liner filled with high purity water. The Cherenkov light produced by the shower particles in the water is detected by three 9 in. diameter photomultipliers. Power is provided by batteries connected to two solar panels and time synchronisation relies on a GPS receiver. A specially designed radio system is used to provide communication between the surface detectors and the central computers of the Observatory.

The tanks forming the Auger Surface Detector (SD) are overlooked by 4 fluorescence sites: Los Leones, Los Morados, Loma Amarilla and Coihueco. The construction of the Fluorescence Detectors (FD) is also completed and all the four FD are currently taking

data. Each site is constituted of 6 independent optical units (telescopes). Each unit houses a Schmidt optical system composed of a segmented mirror and a 20 × 22 PMT pixel camera, each pixel viewing 1.5° × 1.5°. The signal from the camera is read by a FADC electronics providing a time resolution of 100 ns.

3 The Energy Spectrum

Most of the energy spectrum data available today at UHE are provided by AGASA, HiRes and Auger (see Fig. 2). The two last experiments recently published spectrum analyses [5, 6] showing evidence of a flux suppression as expected by the GZK effect with significances of about 5 and 6 σ respectively at slightly different energies (5.6 and 4 $\times 10^{19}$ eV). Shifting the energy scale by about +15% for Auger and about -25% for AGASA with respect to HiRes the three spectra agree rather well up to about 5 $\times 10^{19}$ eV. At higher energies the AGASA data do not exhibit any flux suppression and thus are inconsistent with the other data.

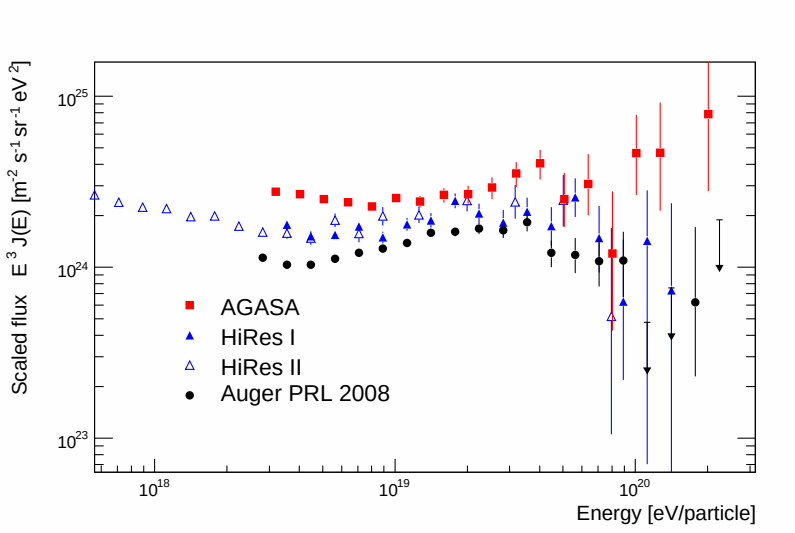

Figure 2: Cosmic ray flux measurements (multiplied by E^3) from AGASA [4], HiRes [5] and Auger [6].

Typical uncertainties of the energy scale are on the order of 20 ÷ 25%. Ground arrays like AGASA rely entirely on EAS simulations with their uncertainties originating from the limited knowledge of hadronic interactions. Fluorescence telescopes, such as operated by HiRes and Auger, observe the longitudinal shower development in the atmosphere. In this way, the atmosphere is employed as a homogenous calorimeter. Nonetheless possible differences in their energy recostruction are still present because of different assumptions (e.g. fluorescence yield, event reconstruction, analysis cuts).

Even though the Auger spectrum in [6] is based on surface data, the energy calibration is quite new. In fact the method used by Auger to measure the energy spectrum exploits

the hybrid nature of the experiment with the aim of using the data itself rather than simulations. For each event the tanks of the SD measure the particle density expressed in units of VEM (Vertical Equivalent Muons) and the times of arrival which are used to determine the axis of the shower. The dependence of the particle density on the distance from the shower axis is fitted by a lateral distribution function (LDF). The LDF fit allows determining the particle density S(1000), expressed in units of VEM, at the distance of 1000 m from the axis. This quantity is a good energy estimator [15] in the sense that it is strongly correlated with the energy of the cosmic ray and almost independent of the mass. The energy estimator S(1000) depends on the zenith angle because of the atmosphere attenuation. The value of S(1000) corresponding to the median zenith angle of 38° (S_{38}) is used as reference and the zenith angle dependence of the energy estimator is determined assuming that the arrival directions are isotropically distributed. This procedure is traditionally called *Constant Intensity Cut*. The absolute calibration of S_{38}

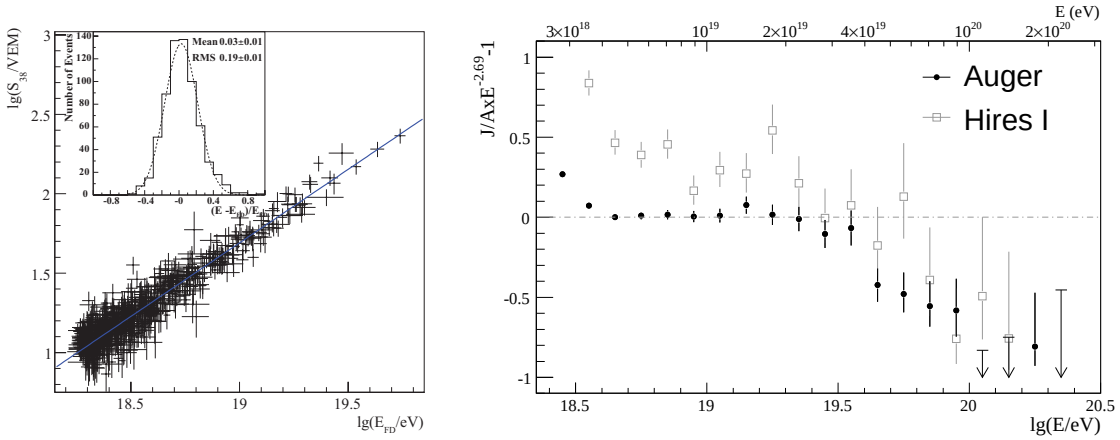

Figure 3: *Left*: Auger calibration of SD data: correlation between surface detector signal and FD energy. The fractional differences between the two energy estimators are inset. *Right*: Fractional difference between Auger and HiRes I data relaltive to a spectrum with index of 2.69.

is derived from the hybrid events using the calorimetric energy measured by the FD which is then corrected for the missing energy using the mean value between proton and iron (uncertainty about 4% at 10^{19} eV). This absolute calibration, which defines the energy scale, is at present affected by a systematic error of about 20%, mainly due to uncertainties on the fluorescence yield and on the calibration of the FD telescopes. The energy calibration, obtained from the subset of hybrid events (see Fig. 3) is then used for the full set of events with higher statistics measured by the SD.

The flux suppression in Auger and HiRes as well as the possible difference in their energy scales is evident when plotting the fractional difference with respect to a power law spectrum. Fig. 3, right panel, shows this fact for a spectral index of 2.69 which is the one fitted by Auger below 4 $\times 10^{19}$ eV.

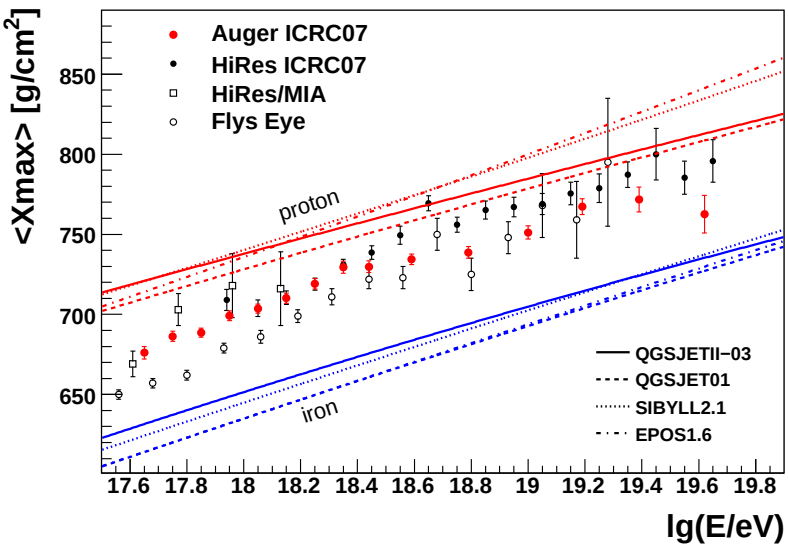

Figure 4: $\langle X_{max} \rangle$ as a function of energy compared with proton and iron predictions using different hadronic interaction models.

4 Primary Composition

Measuring the composition of cosmic rays is crucial to obtain a full understanding of their acceleration processes, propagation and relation with galactic particles. The atmospheric depth X_{max} denotes the longitudinal position of the shower maximum, which is directly accessible with the FD. It grows logarithmically with the energy of the primary particle. The behaviour of X_{max} for different primary particles like photons, protons and heavier nuclei can be conceptually understood in the framework of the Heitler and superposition models [16], which provides good agreement with detailed Monte Carlo simulations. New results based on HiRes-Stereo and Auger hybrid data at the ICRC [17, 18] are reported in Fig. 4. Both data sets agree very well up to $\sim 3 \cdot 10^{18}$ eV but differ slightly at higher energies. The differences between the two experiments are within the differences observed between p- and Fe-predictions for different hadronic interaction models. With these caveat kept in mind, both experiments observe an increasingly lighter composition towards the ankle. At higher energies, the HiRes measurement yields a lighter composition than Auger.

Another important issue concerning the primary composition is the search for photons and neutrinos in EAS. The Auger Observatory has set new photon limits with both the hybrid and SD detection methods [19, 20]. The new limits are compared to previous results and to theoretical predictions in Fig. 5 for the photon fraction. In terms of the photon fraction, the current bound at 10 EeV approaches the percent level while previous bounds were at the 10 percent level. A discovery of a substantial photon flux could have been interpreted as a signature of top-down (TD) models. In turn, the experimental limits now put strong constraints on these models. For instance, certain SHDM (Super Heavy

Dark Matter) or TD models discussed in the literature [21] predict fluxes that exceed the limits by a factor 10.

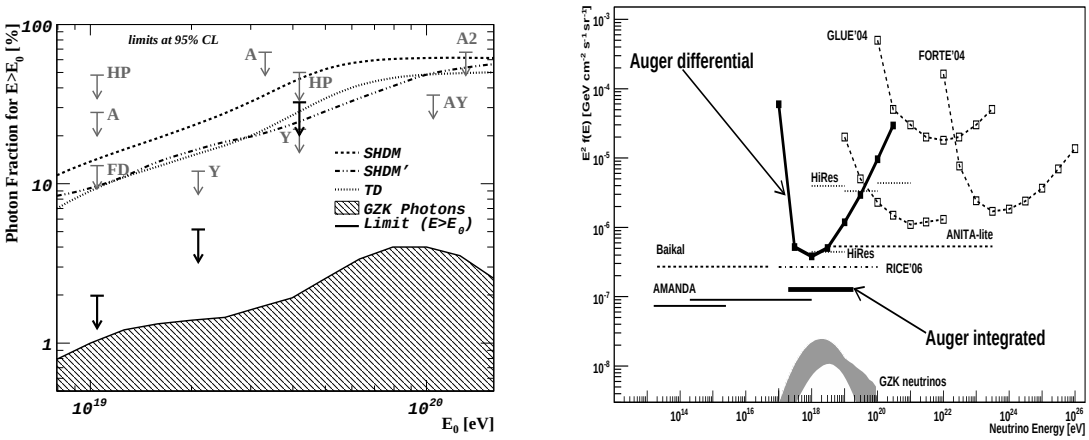

Figure 5: *Left*: The upper limits on the fraction of photons in the integral cosmic ray flux derived from Auger SD (black arrows) along with previous experimental limits (HP: Haverah Park; A1, A2: AGASA; AY: AGASA-Yakutsk; Y: Yakutsk; FD: Auger hybrid limit). Also shown are predictions from top-down models (SHDM, SHDM', TD) and predictions of the GZK photon fraction. For references see [20]. *Right*: Limits at the 90% C.L. for a diffuse flux of ν_τ assuming a 1:1:1 ratio of the 3 neutrino flavors and the expected flux of GZK neutrinos. For references see [22]

Neutrino induced showers can be also identified if they occur deep in the atmosphere under large zenith angles, or by their special topology in the case of Earth-skimming tau neutrinos. Identification criteria have been developed to find EAS that are generated by tau neutrinos emerging from the Earth. Auger has searched for tau neutrinos in the data collected up to August 2007. No candidates have been found and an upper limit on the diffuse tau neutrino flux has been set. In Fig. 5 this result [22] is shown.

5 Arrival Directions

Most of the recent results are from the Auger Collaboration who have started a detailed investigation of the angular directions of the cosmic rays. While no excess has been found from the Galactic Centre in the EeV energy range, evidence for anisotropy has been found in the extreme energy region.

Observation of an excess from the region of the Galactic Centre in the EeV energy region were reported by AGASA [23] and SUGAR [24]. The Auger Observatory is suitable for this study because the Galactic Centre (constellation of Sagittarius) lies well in the field of view of the experiment. The angular resolution of the SD of Auger depends on the number of tanks activated by the shower and it is better than one degree at high-energy. However, with statistics much greater than previous data, the Auger search [25] does not show abnormally over-dense regions around the GC.

A big step towards the discovery of the UHECR sources has been recently made by the Pierre Auger Collaboration [7, 26]. The highest energy events recorded so far were scanned for correlations with relatively nearby AGNs ($z \leq 0.024$ corresponding to $D \leq 100$ Mpc) listed in the Véron-Cetty/Véron catalogue [28]. AGNs where used only up to a maximal redshift z_{max}, which was a free parameter in the correlation scan. Two other free parameters were the minimal energy of the cosmic ray events E_{thr} and the maximum separation between reconstructed cosmic ray direction and the AGN position ψ. The scan was performed over data taken during the first two years of stable operation (01/2004 - 05/2006) and a significant minimum of the chance probability calculated assuming isotropic arrival directions was observed. After the parameters of this *explorative scan* ($z_{max} = 0.018$, $\mathrm{E}_{thr} = 56\ EeV$, $\psi = 3.1°$) were fixed, the consecutive data set (06/2006-08/2007) was used to verify the correlation signal and the hypothesis of an *isotropic source distribution* could be rejected at more then 99% confidence level. A sky map of the 27 events above the energy threshold of $\mathrm{E}_{thr} = 56\ EeV$ together with the selected AGN is shown in Fig. 6. Also shown are the events selected during a follow-up analysis of stereo data from the HiRes Collaboration [27], which do not show a significant correlation.

The interpretation of the observed anisotropy is ongoing and a much larger event statistics will be needed to investigate, for example, whether the AGNs act only as tracers for the underlying true sources and whether the angular separation between AGN and UHECR can be related to magnetic deflections.

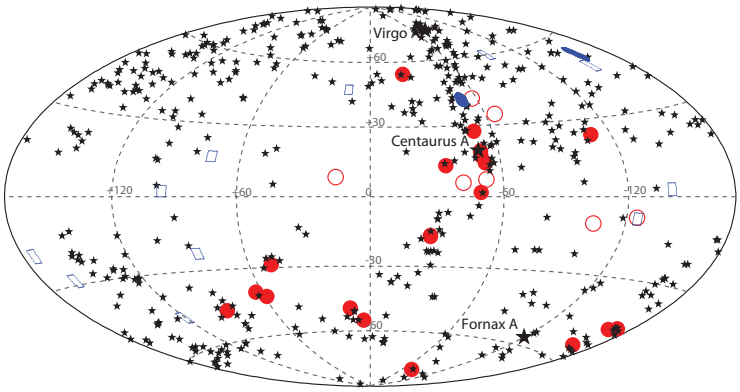

Figure 6: The sky seen with UHECRs with energy above 56 EeV detected with the surface array of Auger (red circles, [7, 26]) and with the HiRes detector in stereo mode (blue squares, [27]) in galactic coordinates. Filled markers denote cosmic rays within 3.1° from AGNs with redishift $z < 0.018$ (black stars, [28]). The relative exposures of the two experiments are not shown for simplicity. Very roughly Auger (HiRes) is blind to a part of the left (right) side of this plot and then their exposures are rather complementary. Detailed exposures can be found in the original papers.

6 L'Aquila and Gran Sasso contributions to the Pierre Auger analysis

6.1 Hybrid Exposure of the Pierre Auger Observatory

The flux of cosmic rays J as a function of energy is defined as:

$$J(E) = \frac{1}{\Delta E}\frac{N^D(E)}{\mathcal{A}(E)T}; \tag{1}$$

where $N^D(E)$ is the number of detected events in the energy bin E, $\mathcal{A}(E)$ is the energy dependent aperture of the detector, T is the uptime of the detector and ΔE is the width of the energy bin E. The product $\mathcal{A}(E)T$ is usually referred to as the exposure, $\mathcal{E}(E)$. The calculation of the hybrid exposure relies on a very detailed simulation of both fluorescence (FD) and surface detector (SD) responses.

The exposure, as a function of primary shower energy, can be written as:

$$\mathcal{E}(E) = \int_T \int_\Omega \int_{A_{gen}} \varepsilon(E)\ \mathrm{d}S\ \cos\theta\ \mathrm{d}\ \Omega\ \mathrm{d}T; \tag{2}$$

where $\varepsilon(E)$ is the detection efficiency including quality cuts, $\mathrm{d}S$ and A_{gen} are respectively the differential and total generation areas, $\mathrm{d}\Omega = \sin\theta \mathrm{d}\theta \mathrm{d}\phi$ and Ω are respectively the differential and total solid angles. ϕ goes from 0 to 2π and θ from 0 to a maximum angle. Several factors (fast growth of surface array and ongoing extension of the fluorescence detector, seasonal and instrumental effects) obviously introduce changes of the detector configuration with time. In this case the hybrid exposure is obtained summing up the contributions coming from the different configurations (i.e times).

In order to reproduce the exact working conditions of the experiment and the entire sequence of the different occurring configurations, a large sample of Monte Carlo data have been produced. The effect of the different data taking configurations has been taken into account and simulated using an accurate calculation of the hybrid detector uptime. Moreover the influence of clouds and atmospheric conditions on the exposure calculation have been taken into account using the information of the atmospheric monitoring[29] of the Pierre Auger Observatory

The simulated data sample consists of longitudinal energy deposit profiles generated using CONEX [30] code. The energy spectrum ranges from 10^{17}eV to 10^{21}eV according to a power-law function with differential spectral index -2 (re-weighted to -3.0 when comparing data to simulation) and zenith angles between 0° and 70°. The simulation has been validated by comparing the distribution of reconstructed observables to experimental ones.

The distribution of particles at ground is not provided by CONEX. However, the time of the station with the highest signal is sufficient information for this analysis. This time is needed in the hybrid reconstruction for determining the incoming direction of the showers, and the impact point at ground.

Once the shower geometry is known, the longitudinal profile can be reconstructed and the energy calculated. The tank trigger simulation is performed using a parameterisation

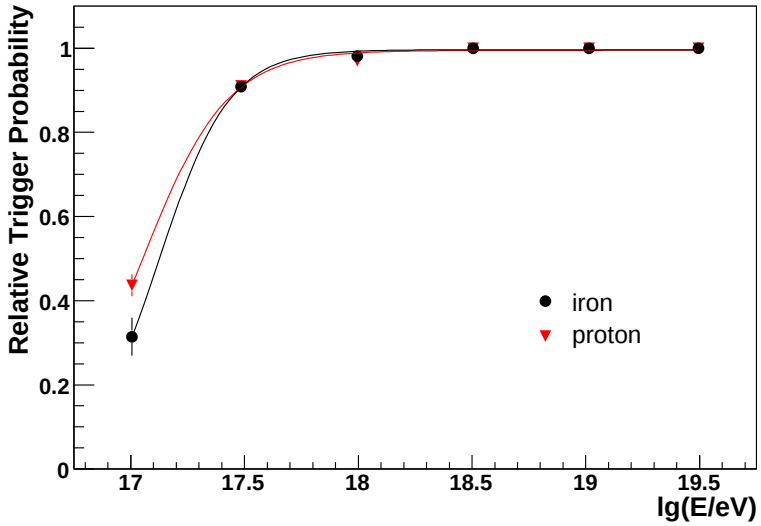

Figure 7: Hybrid trigger efficiency for proton and iron primaries from the full CORSIKA simulation method.

based on "Lateral Trigger Probability" functions (LTPs) [31]. They give the probability for a shower to trigger a tank as a function of primary cosmic ray energy, mass, direction and tank distance to shower axis.

A cross check with a full hybrid simulation was performed using CORSIKA showers [32], in which FD and SD response are simultaneously and fully simulated. As it is shown in Figure 7 the hybrid trigger efficiency (an FD event in coincidence with at least one tank) is flat and equal to 1 at energies greater than 10^{18} eV. In this energy range, the hybrid trigger efficiency also coincides with the one derived on the basis of the LTPs method. Moreover the difference between the two primaries becomes negligible for energies larger than $10^{17.5}$ eV. A detailed description of the hybrid detector simulation program is given in [33].

In Figure 8 the hybrid exposure at the last reconstruction level is shown. Exposure at this level depends very weakly on chemical composition, giving a spectrum basically independent of any assumption on primaries mass.

6.2 Search for clustering of ultra high energy cosmic rays

An approach in the search of the origin of high-energy cosmic rays is the search of clustering signals by the means of the autocorrelation analysis. The autocorrelation analysis does not depend on *a priori* knowledge of the possible sources and, therefore, does not require a specific hypotesis of the source.
The autocorrelation signal of the highest-energy events, with the contribution of the L'Aquila group, is therefore being investigated[35].
The method consits in evaluating the two-point angular correlation function, given by the number of pairs separated by less than an angle α among the N events with energy larger

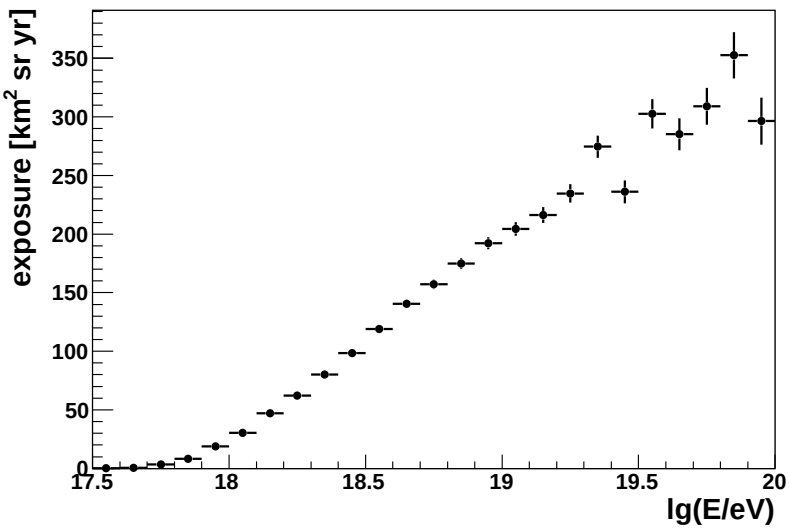

Figure 8: Hybrid Exposure as a function of shower primary energy. It refers to the last reconstruction level once all cuts have been applied.

than a given threshold E:

$$n_p(\alpha) = \sum_{i=2}^{N} \sum_{j=1}^{i-1} \Theta(\alpha - \alpha_{ij})$$

where α_{ij} is the angular separation between events i and j and Θ is the step function. The expected number of pairs is obtained by generating a large number of Monte Carlo simulations with the same number of events with an isotropic distribution modulated by the exposure of the detector, from which the mean number of pairs and the 95% CL band is extracted for each angular scale. The chance probability for any excess of pairs at a fixed angle α and energy threshold is found with the method proposed by Finley and Westerhoff[36], in which a scan over the minimum energy and the angle is performed. For each value of E and a chance probability is estimated by generating a large number of isotropic Monte Carlo simulations of the same number of events, and computing the fraction of simulations having an equal or larger number of pairs than the data for those values of E and . The most relevant clustering signal corresponds to the values of α and E that have the smaller value of the chance probability, P_{min}.
Finally, the probability that such clustering arises by chance from an isotropic distribution is estimated by performing a similar scan on a large number of isotropic data sets simulated by the Monte Carlo technique and finding the fraction of the simulations having a smaller P_{min} than the data. The results of this method applied to Auger data up to August,31(st) 2007 are reported in [34].
Moreover, other techniques have been developed for determining the intrinsic anisotropy of the ultra-high energy cosmic rays, consisting in an improved two point method and a three point method.
Recents works on this subject, in which our group is involved, regard the sensitivity to

uncertainties in energy and angle reconstruction for the three methods and their results when Auger latest data are considered.

References

[1] The Pierre Auger Collaboration, Astropart. Phys. 27 (2007) 244.

[2] A. M. Hillas, Annu. Rev. Astron. Astrophys., **22**, 425 (1984).

[3] K. Greisen, Phys. Rev. Lett. **16**, 748 (1966) and G.T. Zatsepin and V.A. Kuz'min, Sov. Phys. JETP Lett. (Engl. Transl.), **4**, 78 (1966).

[4] M. Takeda et al. [AGASA Collaboration], Astropart. Phys. **19**, 447 (2003).

[5] R.U. Abbasi et al. [HiRes Collaboration], Phys. Rev. Lett. **100**, 101101 (2008).

[6] J. Abraham et al. [Pierre Auger Collaboration], Phys. Rev. Lett. **101**, 061101 (2008).

[7] J. Abraham et al. [Pierre Auger Collaboration], Science **318**, 938 (2007).

[8] M. Nagano and A. A. Watson, Rev. Mod. Phys. **72**, 689 (2000).

[9] N. Chiba et al., Nucl. Instrum. Meth., **A311**, 338 (1992).

[10] T. Abu-Zayyad et al., Nucl. Instrum. Meth. **A450**, 253 (2000).

[11] J. Abraham et al., Nucl. Instrum. Meth. **A523**, 50 (2004).

[12] M. Fukushima et al. [Telescope Array Collaboration], Proc. 30th ICRC, Mérida, p. 955 (2007).

[13] K.-H. Kampert, J. Phys. Conf. Ser., **120**, 062002 (2008).

[14] D. G. Bergman and J. W. Belz, J. Phys. G, **34** R359 (2007).

[15] D. Newton et al., Astropart. Phys. **26**, 414 (2007).

[16] J. Matthews, Astropart. Phys. **22**, 387 (2005)

[17] Y. Fedorova et al. [HiRes Collaboration], Proc. 30th ICRC, Mérida, p.1236 (2007).

[18] M. Unger et al. [Pierre Auger Collaboration], Proc. 30th ICRC, Mérida, p.594 (2007).

[19] J. Abraham et al. [Pierre Auger Collaboration], Astropart. Phys. **27**, 155 (2007)

[20] J. Abraham et al. [Pierre Auger Collaboration], Astropart. Phys. **29**, 243 (2008).

[21] References to theoretical models can be found e.g. in [20].

[22] J. Abraham et al. [Pierre Auger Collaboration], Phys. Rev. Lett. **100**, 211101 (2008).

[23] M. Teshima et al., Proc. 27th ICRC, Hamburg, vol. 1, p. 337 (2001).

[24] J.A. Bellido et al., Astropart. Phys. **15**, 167 (2001).

[25] J. Abraham et al. [Pierre Auger Collaboration], Astropart. Phys. **27**, 244 (2007).

[26] J. Abraham et al. [Pierre Auger Collaboration], Astropart. Phys. **29**, 288 (2008).

[27] R.U. Abbasi et al. [HiRes Collaboration], arXiv eprints: 0804.0382v1 (2008).

[28] M.-P. Véron-Cetty, P. Véron, Astron. Astrophys. **455**, 773 (2006).

[29] S. Y. BenZvi *et al.*, Nucl. Instrum. Meth. A574 (2007) #171

[30] T. Bergmann *et al*, Astropart. Phys. 26 (2007) 420.

[31] E. Parizot for the Pierre Auger Collaboration, Proc. 29th ICRC. Pune (2005) 7, 71-74.

[32] D. Heck *et al*, Report FZKA 6019, (1998).

[33] L.Prado *et al*, Nucl. Instr. Meth. A545 (2005) 632.

[34] Correlation of the highest-energy cosmic rays with the positions of nearby active galactic nuclei. By Pierre Auger Collaboration (J. Abraham/ et al./ ¡http://www.slac.stanford.edu/spires/find/hep/wwwauthors?key=7566816¿)., Astropart.Phys.29:188-204,2008, e-Print: arXiv:0712.2843 [astro-ph]

[35] Search for clustering of ultra high energy cosmic rays from the Pierre Auger Observatory. By M.Ave et al., Auger Tech. Note GAP 2008-015.

[36] C. B. Finley and S. Westerhoff, Astropart. Phys. 21 359 (2004).

LIBS-X

X ray laser induced breakdown spectroscopy

A.Reale[1], G.Tomassetti[+,1], L.Palladino[1], A.Ritucci[1], P.Zuppella[1], P.Tucceri[1], S.Prezioso[1], A.Gaudieri[1], S.Santucci[1], L.Ottaviano[2], F.Bussolotti[2], S.Piperno [2], M.Rinaldi[2], A.Poma[3], L.Reale[3], F.Flora[4], L.Mezi[4], P.Dunne[5], J.Kaiser[6]

[1]*Physics Dept. of University of L'Aquila, LNGS-INFN, Assergi(AQ),I taly*
[2]*Physics Dept. of University of l'Aquila, LNGS-INFN,Italy*
[3]*Dept. of University of l'Aquila, LNGS-INFN,Italy*
[4]*Dept. FIM-FIS-ACC, ENEA-Frascati, Italy*
[5]*School of Physics, Univ College Dublin, Belfield, Dublin 4,Ireland*
[6]*Inst of Phys. Eng., Brno University of Technology, Brno, Czeck Rep.*

1 Introduction

The original intent of LIBS-X experiment was the characterization of a capillary discharge soft X ray laser at 46.9nm (built according a technique initiated by JJ Rocca at Colorado Univ) as a tool for elemental analysis, mainly in biological samples. As reported in the previous report, since 2007 we splitted the original proposal into two main goals: the prosecution of a series of LIBS measurements mainly with a Nd-YAG laser at Brno University and to the use of our laser for interferometric lithography applications. This has been a consequence of the high level the coherence degree of our laser, to its limitations in energy(150microjoule/pulse,0.2Hz), to the appearence of different competencies in the group. Concerning the first topic, the technique consists essentially in detecting the fluorescence lines of trace elements in a sample. Such lines are present in the radiation emitted by the hot plasma obtained by focusing f.i., an excimer or Nd-YAG laser on the sample. The use of our soft X ray laser with a shorter wavelength could be interesting for studying surfaces, thin films and micrometric structures, with high spatial resolution because of the very small diameter focal spot (few micron) we can achieve. The high fluence(of the order of 10-100GW) can generate a plasma such that the critical density is about 10^{23} cm^{-3} and also the laser can ionize the atoms of the target by a single photon interaction. This makes the mechanism of deposition of the energy different from the conventional plasmas. The second topic, the interference lithography, is a technique

very promising for creating nanoscale periodic structures on a photosensitive surface like a photoresist or a LiF crystal, by a careful matching of the dose to the considered photoresist and by the control of the liftoff process. Using our table top laser we are in conditions of obtaining modulation of the interference fringes with very high spatial resolution and depositing metallic strips on silicon that, as Bragg gratings or similar devices,are very important for optophotonics and optoelectronics applications.

1.1 Experimental results in 2008

Concerning the first goal, the detection of contamination in biological samples, in 2007 we created ablation craters on SiO_2/Si and LiF of 6 micron diameter and 1.5 micron depth (see A.Ritucci et al Optics Lett: 31, 1, (2006)), but in 2008 we tried without success to detect the fluorescence from the plasma. The failure arises presumibly because of the insufficient material ablated but, more probably, it is due the very poor collection efficiency of the fluorescence in the alignment of the optical waveguide with its extremity so near to the focal point. In the next months we shall try again by some microlenses. To gain experience in meanwhile on X ray microscopy and elemental analysis we used soft X ray plasma sources, as synchrotron radiation at a storage ring (Fig. 1) and a Nd:YAG laser (Fig. 2), as also reported in the list of publications.

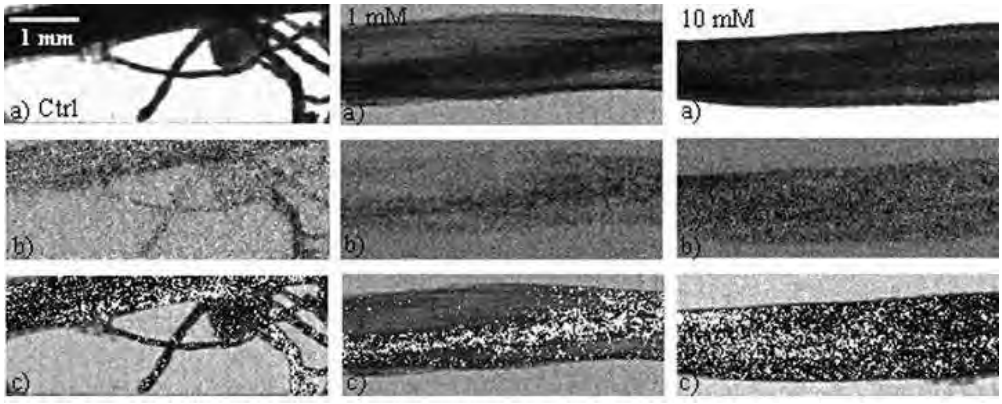

Figure 1: *Results of the sulfur detection in Zea mays root samples. The samples were treated in a solution of PbAc (of a concentration of 0 mM-Ctrl, 1 mM, and 10 mM) for10 days. (a) Planar radiograph taken at the energy 2.4795 keV, (b) results of the dual-energy analysis-the sulfur content within the sample, and (c) distribution of the sulfur (white) within the sample. It is hypothesized the detection of the sulfur in the sulfidril-reach residues of the phyto-chelatin molecules chelating the lead metal present in the roots due to the treatment([9]).*

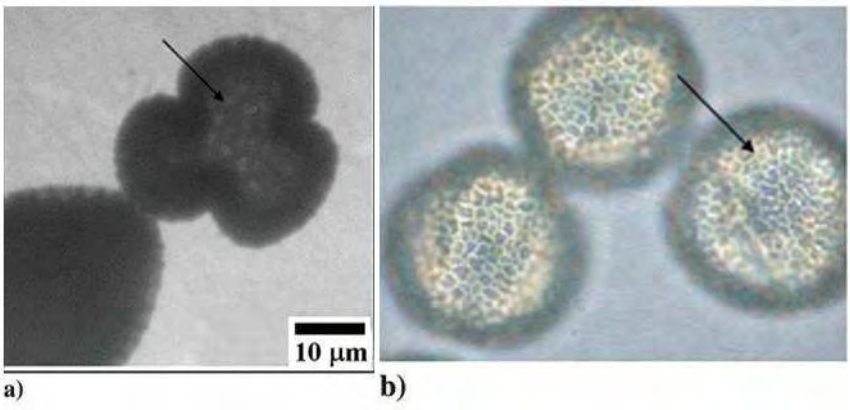

Figure 2: *X-ray microradiography of the pollen grain of Olea europea var. ascolana. The image on LiF is obtained with ten shots and clearly shows the presence of the sporopollenin thickening (black arrow) (a); the corresponding optical microscope image is obtained with the x100 objective and it also shows the sporopollenin wall thickening (black arrow) (b). [Color figure can be viewed in the online issue, which is available at www.interscience.wiley.com.]([8])*

Concerning the second goal, i.e. the characterization of our laser for Interference Lithography(IL), since 2007 we reported on periodic structures by IL on photosensitive polymers with half-pitch less than 50 nm.

In 2008 the potentiality of the technique has been improved with regular patterns down to 22.5 nm on PMMA/Si (Fig 3),together with some applications to nanooptics and nanoelectronics fields.

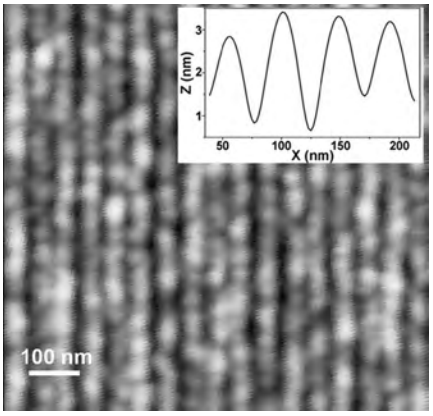

Figure 3: *AFM scan of EUV-IL patterned PMMA/Si(100) with 22.5 nm half-pitch. Upper inset: Average of 256 horizontal height line profile taken on the AFM image([12]).*

To this purpose the first result has been a complete EUV pattering encoding on the photoresist and its transferring into a Si substrate. After optimizing the PMMA thickness, controlling the metal deposition and a liftoff process on the exposed PMMA/SiO2/Si samples, we have fabricated (600nm large) arrays, 200 nm spaced, 12 nm Nickel strips on Si surface (Fig 4).

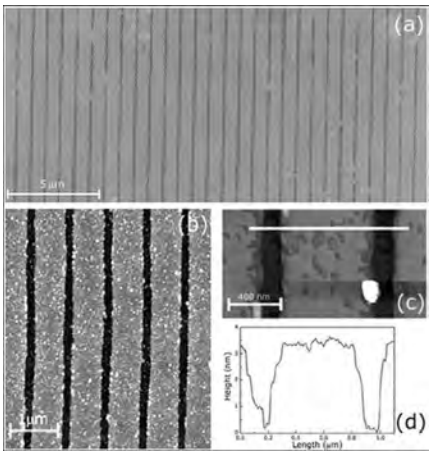

Figure 4: *SEM images of the regular distribution of the metallic strips as obtained after the Ni deposition and lift-off process. (b) AFM topographic images of metallized substrate. Traces of organic lift-off residuals on the metal electrodes are visible as bright speckle-like features. (c) High resolution AFM micrograph of a RIE-treated metallic strips. (d) Height profile across of three Ni electrodes (see panel (c))([6]).*

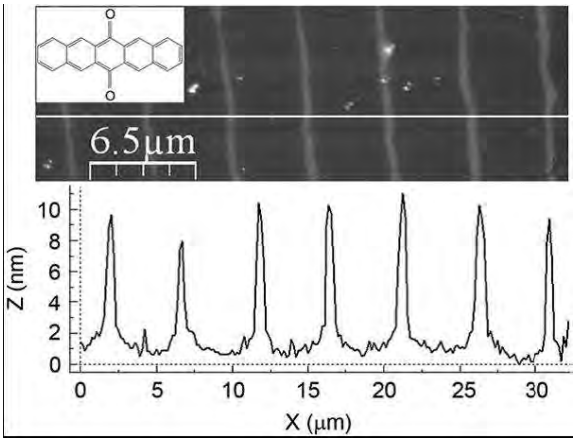

Figure 5: *AFM image and corresponding line profile of a 15 nm patterned PMMA/Si with semi-period (half pitch) of 2.5 μm. The bare silicon substrate is exposed between the PMMA lines. Inset: PQ molecular structure ([7]).*

The second result (Fig 5) was the realization of photoluminescent high resolution pattern of thin organic films in an effort to use them at submicrometric scale. An enhanced light emission was observed in correspondence of PQ(pentacenequinone) films lying on the PMMA lines, 10 times higher than the one observed on the PQ/Si interface([7]).

2 Conclusions

Concerning metal compound contamination in biological samples, in 2007 we are able to produce in insulators 5-6 micron diameter and 1.5 micron depth(25 shots), but even in 2008 we have be not yet been able to detect fluorescence. In the next months we shall try to improve the device by some special microlenses on the waveguide. In meanwhile, to gain experience we used, for elemental analysis, soft X ray plasma sources as a Nd:YAG laser and ELETTRA and DAFNE storage rings synchrotron radiation. Results are reported in the list of publications below. Concerning the second goal, in 2008 the potentiality of our apparatus for Interference Lithography has been increased with the realization of periodic regular patterns with half-pitch less down to 22.5 nm on photosensitive polymers (PMMA/Si), together with some applications to the nanooptics and nanoelectronics fields.

The first application has been a complete EUV pattering encoding on the photoresist and its transferring into a Si substrate: we have fabricated (600nm large) arrays of 200 nm spaced, 12 nm thickness Nickel strips on Si surface. The second result was the realization of photoluminescent high resolution pattern of thin organic films in an effort to use them at submicrometric scale. An enhanced light emission was observed in correspondence of PQ(pentacenequinone) films lying on the PMMA lines, 10 times higher than the one observed on the PQ/Si interface, as reported in [8].

Finally, as an important by product of our main activity, spectra have been collected from a Xe discharge capillary source in the extreme ultraviolet(EUV) region of the spectrum between 10 and 18 nm in the frame of a projection lithography program of the collaboration ([11]).

3 Acknowledgements

The work summarized in this 2008 Annual Report of LNGS has been supported by the Italian Ministero dell'Universit e della Ricerca(FIRB Project), by the National Institute of Nuclear Physics, by the Consorzio di Ricerca Gran Sasso, by the Ministry of Education of Czech Republic, by the University Center of Dublin Seed Fund, by the Cost actionMP061 and the P:O:R:-In-CO projects of Regione Abruzzo,Italy.
This Report is dedicated to the memory of our group leader and friend Prof. Giuseppe Tomassetti.

4 Partecipation to national or international workshops and conferences

- L.Reale - Poster at the School on synchrotron X ray and IR methods focusing on environmental sciences-January 21-23, Karlsruhe, Germany
- Tucceri P. - Elettroottica 2008 - X Convegno Nazionale. 10/06 - 12/06 Fabrication of metallic nanopattern with interference lithography using a 46.9 nm laser. Milano
- Zuppella P. - Workshop di Ateneo sulle Nanotecnologie Interference Nanolithography by a soft X-ray laser beam - June 05, l'Aquila, Italy
- Zuppella P. - Meeting COST (European Cooperation in the field of Scientific and Technical Research) - Nanolithography by a soft X-ray laser beam - May 28-3 2008 Warsaw, Poland

References

[1] F.Bonfigli et al. High-resolution water window X-ray imaging of in vivo cells and their products using LiF crystal detector - MICROSCOPY RES. TECHNIQUE, 71-1, (2008)

[2] L.Reale et al. Mapping the intake of different elements in vegetal tissues by dual-energy X-ray imaging at DAFNE synchrotron light sourceMICROSCOPY RES .TECHNIQUE, 71-3, (2008)

[3] L.Reale et al. Qualitative detection of Mg content in a leaf of Hedera helix by using X-ray radiation from a laser plasma source - MICROSC RES TECHNIQUE, 71-6, (2008)

[4] C.Oliva et al. SNOM images of X-ray radiographs at nano-scale stored in a thin layer of lithium fluoride J .MICROSC-OXFORD, 229-3, (2008)

[5] L.Reale et al. X-ray Microscopy of Plant Cells by Using LiF Crystal as a Detector MICROSC RES TECHNIQUE, 71-12, (2008)

[6] L.Ottaviano et al. Fabrication of metallic micropatterns using table top extreme ultraviolet laser -PLASMA SOURCES SCI TECHNOL, 17-2, 024019 (2008)

[7] P.Parisse et al. Photoluminescence submicrometre spatial modulation of 6,13 pentacenequinone thin films - J PHYS-D-APPL PHYS, 41-11, 112003 (2008)

[8] L.Reale et al. X-ray microscopy of plant cells by using LiF crystal as detector - accepted by Microscopy Research and Technique

[9] L.Reale et al. Detection of lead in Zea Mais by dual energy X-ray microtomography at the SYRMEP beamline of ELETTRA Synchrotron and by AAS - submitted to Microscopy Research and technique

[10] L.Reale et al. Contact X-ray microscopy of cells Clamydomonas Reinhardtii, teh cyanobacteria Lptolyngbya VRUC 135 and a mouse macrophage cell line RAW 265.7 by using LiF crystal as a detector - to be submitted to MRT

[11] P.Zuppella et al. Spectral enhancement of Xe-based EUV discharge plasma source accepted by Plasma Sources Sci. and Tech.

[12] P.Zuppella et al. Large area 23 nm interference lithography using a table-top EUV laser - accepted by Nanotechnology

LASEX

Analysis and characterization of X-ray emission from plasma produced by a Nd-Glass laser on a Cu target.

L. Palladino[1,3], R. Gimenez De Lorenzo[1,3], G. Gualtieri[2], T. Limongi[1,2]

[1] *Physics Department of L'Aquila University*
[2] *Science and Biomedical Technology Department of L'Aquila University*
[3] *INFN, Laboratorio Nazionale del Gran Sasso, Assergi (AQ)*

1 Introduction

The activities in the year 2008 can be divided into three parts:

- Measurement and characterization of the X-rays beam emitted from the plasma.
- Realization of a mini-spectrometer and a mirror holder for plasma diagnostic.
- Development and construction of high voltage system: power supply circuit and interaction chamber.

In particular, we present an analysis of the soft X-rays emission produced by a Cu plasma, obtained focalizing a Nd:YAG/Glass laser at 532 nm, on a copper target. The laser pulse duration is 6 nsec and the laser shot energy range is 200 - 300 mJ. We measured the spectral X-rays emission for intensity I = 10^{12} W/cm^2, in the aluminum window at 73 eV with a harder X-rays tail around 400 eV, and the dependence of X-rays signal on the viewing angle.

2 Experimental results

2.1 Characterization of the soft X-rays emitted from plasma in the energy interval between about 70 eV and 1 keV.

In these measures the laser beam energy range from 200 to 300 mJ/shot, at 532 nm laser wavelength and 6 nsec pulse duration. The laser beam was focalized on a copper target. The best conditions of focus were obtained by varying the lens-target distance, and seeking the maximum of the X-rays detected signal by a solid state detector (PIN-diode) filtered

with an aluminum micro-foil of 3 microns thickness. We measured the diameter of craters, in the sequence, obtained by focusing the laser beam.

In figure 1 is shown the relation between the diameters of the craters with the lens-target working distance (the working distance is the distance between the physical end of the lens and the target). The analysis of these measures shows that the smallest size of the craters is 65 μm, which corresponds to a power density delivered on the target of about I = 10^{12} W/cm^2 and obtained with a working distance of 123.3 $\pm$ 0.1 mm. The figure 2 represents the X-rays intensity normalized to the diameter of the craters (nVsec/micron) versus lens-target working distance. We note that at the same working distance we obtain the conditions of maximum emission of the X-rays radiation.

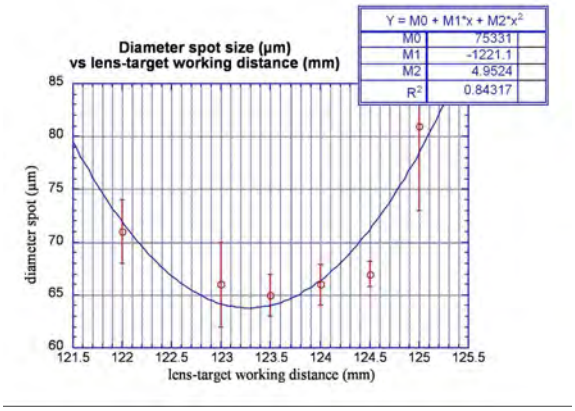

Figure 1: *Diameters of craters vs working distance between the lens and target.*

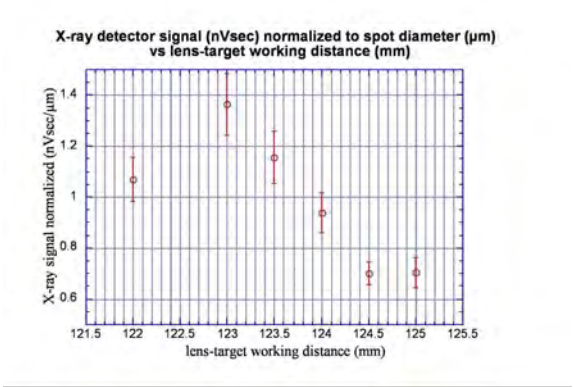

Figure 2: *X-rays intensity normalized to the diameter of the craters vs working distance*

A preliminary investigation of the energy spectrum of X-rays emitted by the plasma has been made measuring the intensity of the X-rays with a solid state detector (PIN-diode)

filtered with micro-foil aluminum of different thickness (1.6 μm, 2.4 μm, 3 μm, 3.8 μm, 4.6 μm, 6 μm and 7.6 μm). These measures are shown in figure 3, in which is represented the intensity of X-rays detected by the filtered PIN-diode (in nC) versus the micro-foil aluminum thickness.

In figure 3 we note that there are two linear slopes. One is associated at 500 eV and 73 eV (corresponding to an average linear absorption coefficient of 1.7745 μm^{-1}) with a ?E of about 10 eV (aluminum L-edge) and the other for photons with energy greater than 700 eV (corresponding to an average linear absorption coefficient of average 0.72413 μm^{-1}). In fact, as shown in figure 4, where the aluminum linear absorption versus of photon energy is represented, we note that the two average linear absorption coefficients of intercept in two different X-rays energy of 73 eV and 500 eV (red line in graph) and greater than 700 eV (green line in graph).

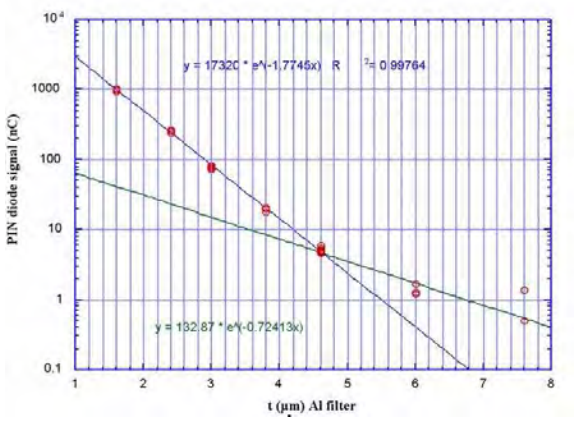

Figure 3: *X-rays intensity vs thicknesses of aluminum micro foil.*

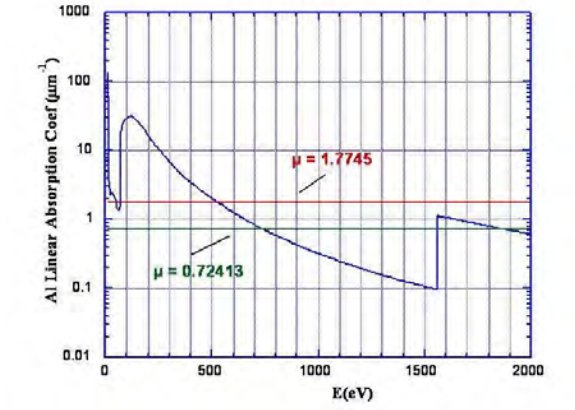

Figure 4: *Coefficient of linear absorption of aluminum as a function of photon energy. Shows the two average ratios discussed in the text.*

From these measures we can obtain an estimate of plasma temperature of about 50 eV, if we consider the plasma as a black body, or about 40 eV, if the plasma is not in thermodynamic equilibrium conditions and the estimate of the average ionization is +8. We have also measured and analyzed the angular emission of the X-rays. These measures, which have been obtained using a PIN-diode filtered with 3 μm of aluminum, are represented in figure 5.

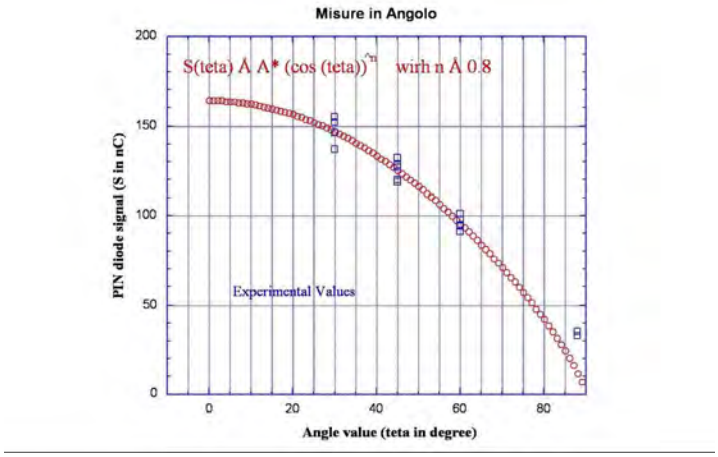

Figure 5: *X-rays intensity vs angle value formed by the normal to the surface of the target and the direction of the radiation.*

The best curve which fits the angular distribution data is the following:

$$A \times (\cos(\theta))^{0.8} \tag{1}$$

where θ is the angle formed by the normal to the surface of the target and the direction of the radiation X and A=163.

All these measures have been done with the bars of Nd Glass not intact due to the cracks present in the glass matrix, which have reduced the energy of the laser beam to about 1/3 of its initial value. In figure 6 are shown the initial profiles (a) and current (b) of the laser beam after the last stage of amplification. The circle of diameter 25 mm, indicates the size of the beam.

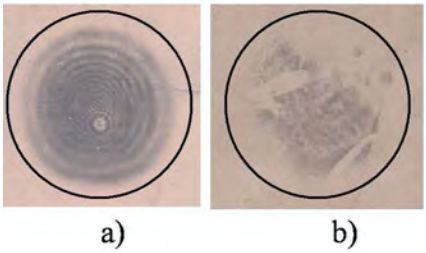

Figure 6: *Current profile (b) of the laser beam after the last amplifier and the initial profile (a). The circle indicates the diameter of the beam (25 mm).*

The characterization of the X-rays source will be complemented with other types of target (mylar, yttrium, aluminum) and at different energy laser beam.

2.2 Realization of a mini-spectrometer and a mirror holder for plasma diagnostic.

To improve the characterization and use of the X-rays beam we have designed and built a mirror holder and a mini-spectrometer. This mirror holder can be used with a copper mirror (see figure 7). It has an accuracy in the rotation angle of 1/10 of degree, and it is placed in the interaction chamber (see figure 8) in radial position. In this mode it is possible to select an X-rays beam in an energy interval defined by the copper reflection curve at a due grazing incident angle.

Figure 7: *Current profile (b) of the laser beam after the last amplifier and the initial profile (a). The circle indicates the diameter of the beam (25 mm).*

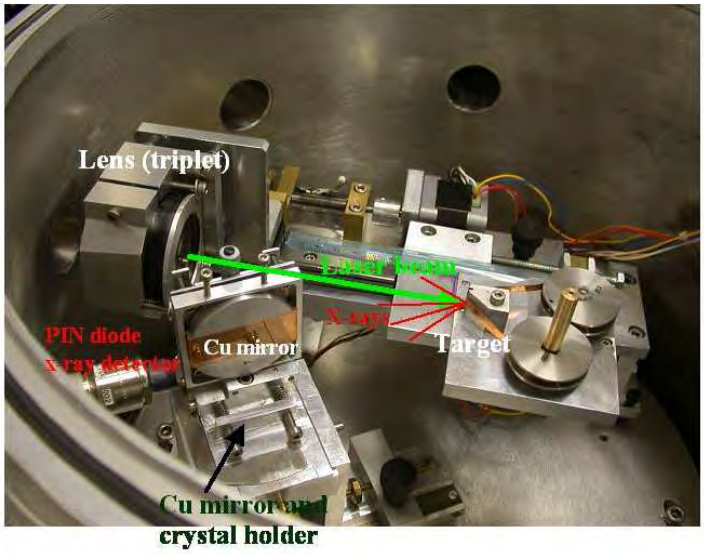

Figure 8: *Interaction chamber and where the mirror holder is placed.*

In figures 9 and 10 we shown the mechanical assembly, the geometry and operation principle of mini-spectrometer. The size of the long side is 11 cm. This spectrometer work in dispersive energy mode with crystals of KAP (2d = 26 ang) or ADP (2d = 10 ang) and use a photographic film as X-ray detector.

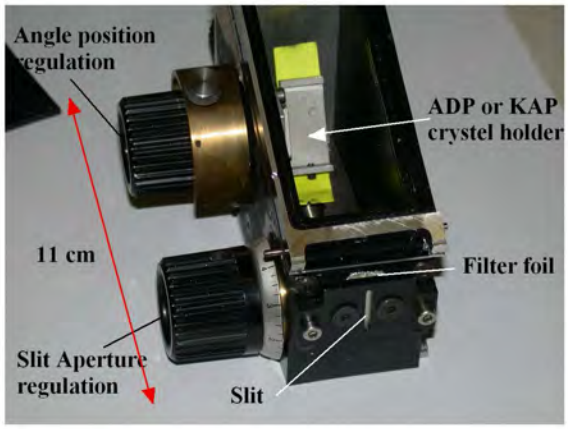

Figure 9: *Mini-spectrometer work in dispersive energy mode.*

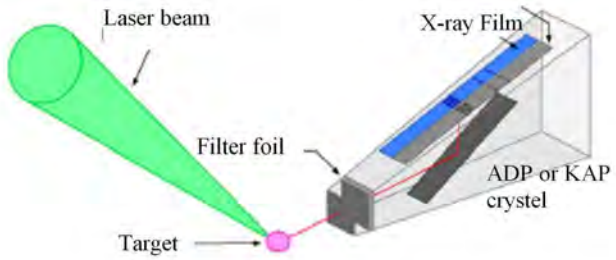

Figure 10: *Geometry and operation principle of mini-spectrometer.*

2.3 Development and construction of high voltage system: power supply circuit and interaction chamber.

We have critically reconsidered, respect to the original project, the interaction chamber and the charge/discharge circuit. For the production of hard X-rays, the application of high voltage, in the interaction chamber, have induced to put outside the interaction chamber the movements of the target and the focusing lens of the laser beam. In fact, the target is wrapped like a ring around negative electrode (cathode) and its rotation is transmitted from a magnetic coupled motor, placed outside the interaction chamber. In figure 11 is shown the final drawings of the internal and external of the interaction chamber. The dimensions of the diameter and the height of the chamber are respectively 40 cm and 43 cm.

The high voltage discharge circuit system is based on an LC inverter with 1.5 μF value of the main capacitor. With this solution, the voltage input is doubled in output. The max output voltage we can reach is 80 kV.

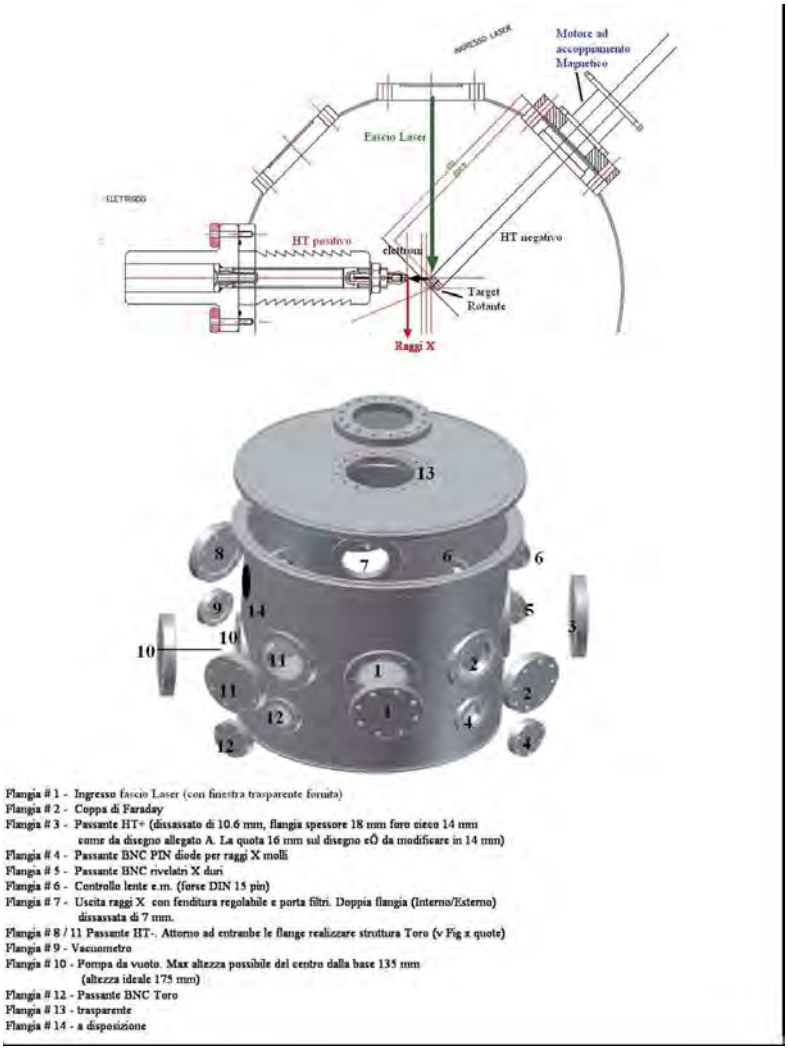

Figure 11: *Executive drawings (internal and external) interaction chamber for hard X-rays production.*

3 Acknowledgements

We would like to thank Prof. E. Coccia Director of Gran Sasso National Laboratories of INFN and Prof. S. Santucci Director of Physics Department of L'Aquila University for supporting us. This work is financially supported by INFN, LASEX experiment.

PULEX and CODA

Influence of environment radiation background on biochemistry and biology of cultured cells and on their response to genotoxic agents

F. Antonelli[1], M. Belli[1], M. Pinto[1], O. Sapora[1], E. Sorrentino[1], G. Simone[1], M. A. Tabocchini[1], F. Amicarelli[2], M. C. Carbone[2], L. Conti Devirgiliis [2], M. Balata[3], L. Ioannucci[3], S. Nisi[3], L. Satta[4]

[1]*Istituto Superiore di Sanità, Technology and Health Department, and INFN-Roma1 Gr. coll. Sanità, 00161 Roma, Italy*
[2]*Department of Basic and Applied Biology, L'Aquila University*
[3]*INFN - Gran Sasso National Laboratory*
[4]*INFN - Frascati National Laboratory*

1 Introduction

All humans receive some radiation exposure, both from natural sources, such as cosmic rays and radioactive decay products of radon gas, and from man-made sources, as in diagnostic radiology. In spite of the many epidemiological and experimental studies carried out for more than one century, there is no firm scientific knowledge on the health effects of exposures of human beings to ionising radiation at low dose and low dose-rate. The current view is that even at low doses the reaction of cells and tissues is more complex than previously known. Examples of phenomena that may have a role in determining the dose-response relationship are: i) adaptive response; ii) genomic instability; iii) low-dose hypersensitivity; iv) the occurrence of bystander effects in cell populations (see, for reviews, [1, 2, 3, 4] respectively).

Adaptive response refers to the ability of cells that were pre-exposed to low doses of radiation or chemical mutagenic agents to acquire resistance to moderate or high doses of the same or a different agent. Adaptive responses were observed in several systems in response to a number of different cytotoxic agents [5]. The first experiments on the induction of adaptation by low, chronic doses of ionizing radiation were carried out on human lymphocytes exposed to low concentration of radioactive thymidine [6].

However, few data exist about adaptive effects after exposure to very low doses and low dose-rates [7]. Environmental background radiation represents a source of chronic low

dose rate exposure to a genotoxic agent and may be acting as an ubiquitous adaptive agent. To clarify this aspect it is essential to evaluate the risk of chronic occupational radiation exposure, as well as to understand the role of environmental background radiation in the evolution of life on Earth.

The Gran Sasso National Laboratory (LNGS) of the Italian Institute for Nuclear Physics (INFN) located under the Gran Sasso mountain offers a unique opportunity to investigate whether a significant reduction in the background radiation exposure level can influence the susceptibility of cells to damage induced by acute exposures to genotoxic agents. The laboratory is covered by at least 1,400 m of over-lying rock, for an excellent shielding against cosmic rays and neutrons. Fluence is in fact reduced by a factor of 10^6 for cosmic rays [8] and by a factor of 10^3 for neutrons [9].

1.1 The PULEX experiment

The aim of the PULEX experiments was to understand if there exists a measurable effect, in terms of adaptation, of the natural background radiation on living matter. The first experiment, or rather a feasibility study was performed on yeast cells. It was found that after more than 100 generations cells grown inside the Gran Sasso Laboratory in a low background radiation environment were less efficient in repairing acute damage by genotoxic agents than those cultured in the external laboratory at the Genetic Laboratory of the Rome University "La Sapienza ", in a "normal" background radiation environment [10].

In the second experiment hamster cells of the V79 strain were employed, and we addressed several biological end-points. Differences between the internal and the external cultures (settled at the Physics Laboratory of the Istituto Superiore di Sanità, ISS, in Rome) were observed and were interpreted, again, considering the occurrence of an adaptive response due to variations of the natural background radiation [11]. However, the possibility could not be excluded that, after many generations (9 months correspond to roughly 540 cell duplications), clones having different characteristics have been selected in the two cultures, independently of the different radiation background.

Therefore we decided to perform a third experiment, PULEX-III, [12] on the same V79 cells, with two independent cultures growing both inside the Gran Sasso Laboratory and in the external laboratory. Furthermore, to reduce margins for errors, the external laboratory was installed at the Chemical Department building of the LNGS outside the tunnel. The constant presence of the same operators for the manipulation of the biological samples was a crucial point for the quality of such a critical experiment. However, this arrangement reduced the ratio of external/internal radiation background, since the gamma contribution at the LNGS external laboratory was found to be less than at the ISS in Rome, and the radon concentration was found to be approximately the same in the external and in the underground laboratories.

Duplicate and independent cultures of chinese Hamster V79 cells, grown in both the external laboratory at LNGS (cultures A and B) and in the underground laboratory under the tunnel (cultures C and D) were monitored for 10 months. Apart the radiation background, all other parameters, such as culture medium, serum, buffers, plastics, etc., were kept identical (i.e., prepared in the same way from the same batch) for all the

cultures. The γ-ray dose rate was 40.1 $\pm$ 4.2 nGy/h in the external laboratory and 4.3 $\pm$ 0.9 nGy/h in the underground laboratory; cosmic radiation contribution to the dose was negligible into the underground laboratory and equal to about 30 nGy/h into the external one [13]. The radon concentration in both laboratories was about 5 Bq/m^3 corresponding to a calculated dose-rate to the cells of 0.17 a nGy/h. If the background radiation acts as a priming dose eliciting an adaptive response subsequent to a challenging dose, the behaviour of the two cultures should differ as time goes by, at least for some biological end-points.

Among the assays performed, measurement of mutation induced by X-rays showed that V79 cells cultured for long time under reduced background radiation conditions became more sensitive, and antioxydant enzymes determination showed they are less protected against ROS produced by ionizing radiation, compared to the parallel external cultures. These features, which are mutually consistent, were found after 10 months but not after 3 months of culture. Other assays (micronulei induction after 1 Gy X-rays and apoptosis induced by cycloheximide) did not give consistent indications, although we never found opposite results, i.e., it never happened that cells cultured under the Gran Sasso tunnel exhibited a greater resistance with respect to those grown in the external laboratory.

The value of the "positive" results obtained from PULEX-III is higher than those from previous experiments, thanks to its design which involved pairs of cultures. This makes very unlikely that the observations are due to the random selection of mutants with such properties capable to mimic the loss of an adaptive response after 10 months inside the tunnel, since this should occur in both sister cultures. In effect, if one assumes that the mutation frequency in V79 cell cultures is of the order of $10^{-4} \div 10^{-5}$ for a given genetic locus, and that it is sufficient one mutated locus for giving the features observed (this is clearly an overestimation), the probability of observing the same mutant in two independent cultures is very small, of the order of $10^{-8} \div 10^{-10}$.

Overall, the results obtained from PULEX-III reinforce the hypothesis suggested by our previous studies that the background radiation induces an adaptive response in living matter. In effect, we observed that the underground cultures are less protected against ionizing radiation. This can be explained by the loss of the adaptive response gained in the presence of the "normal" background.

1.2 The CODA experiment

In order to give a more firm support to this conclusion, we decided to extract the cells grown under the Gran Sasso tunnel and to culture them in the external laboratory, together with those already there, to check if, in the presence of the "normal" background radiation, they will be able to recover the "lost" adaptive response. This experiment, which should be the last in the series, has been named CODA, and has been approved and financed by INFN. The four cultures, A & B (always maintained in "normal" background radiation conditions) and C & D (always maintained in low background radiation conditions) are being cultured together since a few months in the external LNGS laboratory. At the very beginning the cells were tested for mutation induction by X rays at the *hprt* genetic locus, and the previous results were confirmed. We plan to periodically perform tests on mutation induction by X-rays and on antioxidant enzyme activity, namely

superoxide dismutase (SOD), catalase (CAT) and selenium-dependent glutathione peroxidase (GPx), on the four cultures to check if, as a function of time, their behaviour will come to be similar.

2 Acknowledgements

The authors are grateful to Prof. V. Tombolini and to the technical staff at the Ospedale San Salvatore, Coppito, L'Aquila, for allowing irradiations of biological samples at the 6 MV linear accelerator.

References

[1] Wolff S. The adaptive response in radiobiology: evolving insights and implications. Environ Health Perspect 1(1998) 06 Suppl 1: 277-283

[2] Bavestock K. Radiation-induced genomic instability: a paradigm-breaking phenomenon and its relevance to environmentally induced cancer. Mutat Res (2000) 454: 89-10

[3] Joiner MC, Marples B, Lambin P, Short SC, Turesson I. Low-dose hypersensitivity: current status and possible mechanisms. Int J Radiat Oncol Biol Phys (2001) 49: 379-389

[4] Mothersill C, Seymur C. Radiation-induced bystander effects: past history and future directions. Radiat Res (2001) 155:759-767

[5] Wolff S. Is Radiation all bad? The search for adaptation. Radiat Res (1992) 131:117-123

[6] Olivieri G, Bodycote J, Wolff S. Adaptive response of human lymphocytes to low concentrations of radioactive thymidine. Science (1984) 223 (4636):594-597

[7] Elmore E, Lao XY, Kapadia R, Giedzinski E, Limoli C, Redpath JL. Low doses of very low-dose-rate low-LET radiation suppress radiation-induced neoplastic transformation in vitro and induce an adaptive response. Radiat Res (2008) 169 (3):311-8.

[8] Belli P, Bernabei R, D'Angelo S, De Pascale M, Paoluzi L, Santonico R, et al. Deep underground neutron flux measurement with large BF3 counters. Nuovo Cimento A (1989) 101:959-966.

[9] Rindi A, Celani F, Lindozzi M, Miozzi S. Underground neutron flux measurement. Nucl Inst Meth A (1998)272:871-874

[10] Satta L, Augusti-Tocco G, Ceccarelli R, Esposito A, Fiore M, Paggi P, Poggesi I, Ricordy R, Scarsella G, Cundari E. Low environmental radiation background impairs biological defence of the yeast Saccharomyces cerevisiae to chemical radiomimetic agents. Mutat Res (1995) 347 (3-4):129-33

[11] Satta L, Antonelli F, Belli M, Sapora O, Simone G, Sorrentino E, Tabocchini MA, Amicarelli F, Ara C, Cer MP, Colafarina S, Conti Devirgiliis L, De Marco A, Balata M, Falgiani A, Nisi S. Influence of a low background radiation environment on biochemical and biological responses in V79 cells. Radiat Environ Biophys (2002) 41 (3):217-24

[12] Antonelli F, Belli M, Sapora O, Simone G, Sorrentino E, Tabocchini MA, Conti Devirgiliis L, Carbone C, Balata M, Ioannucci L, Nisi S. PULEX LNGS Annual Report 2007, 229-235

[13] UNSCEAR 2000 Report, Sources, Annex E